Functional investigation of *Trypanosoma brucei* microtubule associated proteins and their role in cellular morphogenesis

Katie Towers

This thesis is submitted in partial fulfilment of the requirements for the degree of Doctor of Philosophy to

Lancaster University

September 2010

ProQuest LLC.
789 East Eisenhower Parkway
P.O. Box 1346
Ann Arbor, MI 48106 – 1346

Abstract

The *Trypanosoma brucei* cytoskeleton is generated by an elaborate array of subpellicular microtubules. This corset of microtubules requires extensive remodelling during cell growth and division. Microtubule nucleation/outgrowth and coordinated severing/re-establishment of inter-microtubule cross-links is orchestrated by microtubule associated proteins (MAPs). The *T. brucei* genome encodes a discrete set of trypanosomatid specific MAPs but functional data for most of these proteins is sparse.

Through bioinformatic analysis we have identified a novel trypanosomatid-specific protein (GB4L). GB4L has a functional role in trypanosome morphogenesis and microtubule organisation in the procyclic and bloodstream form of the parasite. RNAi ablation of GB4L causes a cytokinetic defect, as does depletion of TCP86 (another novel and trypanosomatid-specific MAP recently identified in the McKean laboratory). Electron microscopy was used to examine both the GB4L and TCP86 RNAi cell lines, demonstrating that the phenotypes observed after GB4L and TCP86 protein depletion are very distinct. However, in both cases protein depletion causes morphological abnormalities at the posterior end of cells.

ganisation of subpellicular microtubules was interrogated through localisation of canonical plus tip binding proteins (+TIPs) EB1 and XMAP215. Microtubule plus ends are organised in a highly reproducible pattern throughout the cell cycle. This organisation becomes disrupted when GB4L or TCP86 are depleted, showing that

GB4L and TCP86 play critical yet distinct roles in orchestrating cytoskeletal remodelling.

RNAi ablation of GB4L and TCP86 also has effects on other MAPs due the concerted roles these proteins play in cytoskeletal remodelling. Investigation into MAP interdependency relationships suggests that MAPs assemble as distinct complexes in a defined temporal order on subpellicular microtubules.

This work provides further insight into the complexities of trypanosome morphogenesis and indicates that disruption of critical MAP interactions could conceivably provide valid targets for the development of novel chemotherapeutic strategies against human and animal trypanosomiasis.

Acknowledgements

I wish to thank my supervisor, Paul McKean for all the support, guidance, ideas and opportunities he has provided throughout my time at Lancaster. I am grateful to past and present members of the McKean laboratory, with a special thanks to Emma Shawcross for all her help in the lab and her ongoing friendship.

Thank you to those from the Gull laboratory who shared time and knowledge contributing to this thesis; particularly Keith Gull for his support and discussions, Mike Shaw for his electron microscopy expertise, Steve Kelly and Bill Wickstead for helping with the bioinformatics.

I am endlessly grateful to Mike Cundell for his help in the lab, his patience when proof-reading and for keeping me going.

Thanks to my closest friends, Laura, Lou, Jan and Liz, a special thanks to Claire Dixon, you all got me through the harder times and are responsible for some of the best!

Loving thanks to my family, my parents Shirley and Kim Towers and brother Ryan without the enormous amounts of support and encouragement they offer I would be lost.

This project was funded by the Faculty of Science and Technology and the School of Health and Medicine at Lancaster University, the financial support they provided is greatly appreciated.

Declaration

I declare that this thesis was composed by myself and has not been submitted in substantially the same form for the award of a higher degree elsewhere.

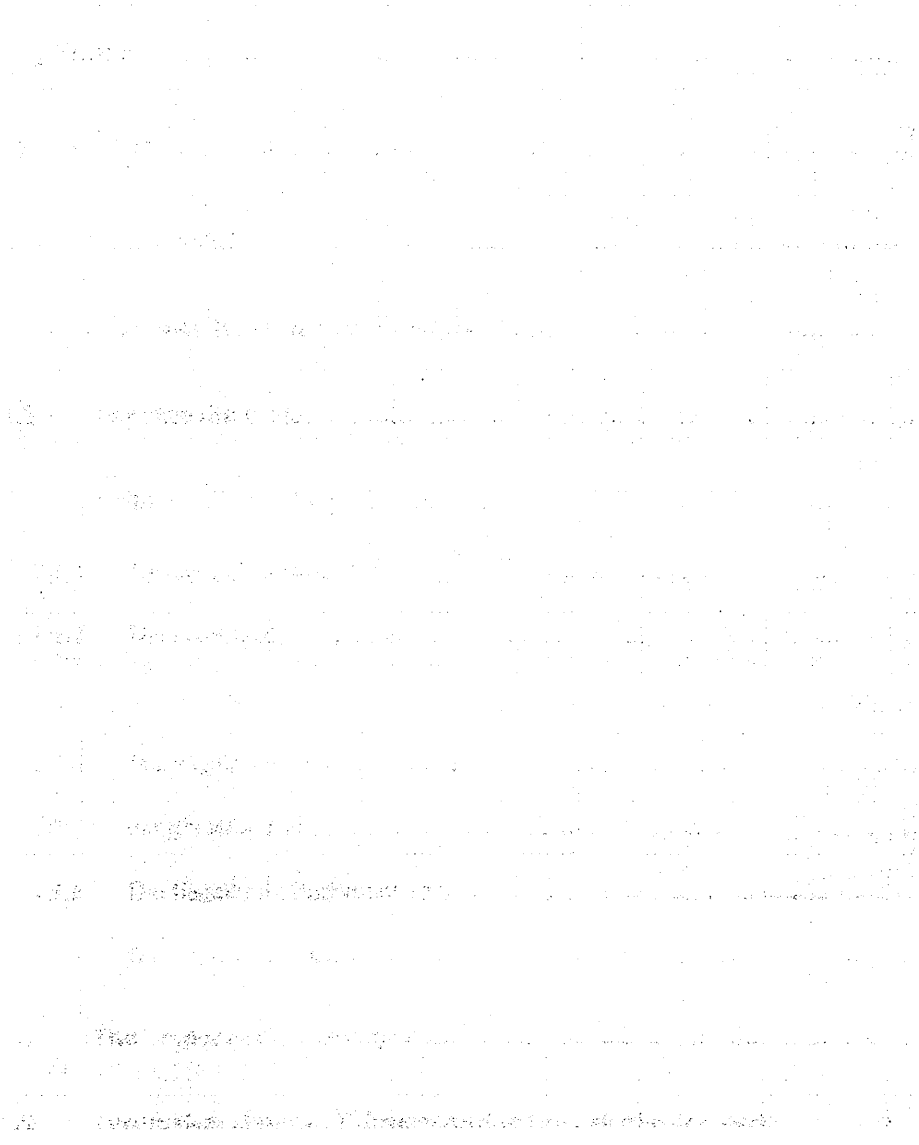

Table of Contents

List of Figures

List of Tables

Abbreviations

APC	Adenomatous polyposis coli
APR	Apical polar ring
APS	Ammonium persulphate
BLAST	Basic local alignment tool
BSA	Bovine serum albumin
BSF	Bloodstream form
bp	Base pair
CAP-Gly	Cytoskeletal associated protein-glycine rich
CCD	Charged coupled device
CDK	Cyclin dependent kinase
CHO-K1	Chinese hamster ovary-K1
CLASPs	CLIP-associating proteins
CLIPs	Cytoplasmic linker proteins
CPC	Chromosomal passenger complex
CRK	Cyclin related kinase
CYC	Cyclin
DAPI	4', 6-diamidino-2-phenylindole
DNA	Deoxyribonucleic acid
EDTA	Ethylene diamine tetra-acetic acid
EGTA	Ethylene glycol tetra-acetic acid
EB	End binding
EBH	End binding homology
EM	Electron microscopy
ER	Endoplasmic reticulum
FAZ	Flagellum attachment zone
FC	Flagella connector
FITC	Fluorescein-5-isothiocyanate
G418	G418 disulphide

GDP	Guanosine diphosphate
GFP	Green fluorescent protein
GTP	Guanosine triphosphate
γTuRC	Gamma tubulin ring complex
γTuSC	Gamma tubulin small complex
HAT	Human African trypanosomiasis
HRP	Horse radish peroxidase
IFT	Intraflagellar transport
kb	Kilobase
kDa	Kilo-dalton
LB	Luria broth
MAP	Microtubule associated protein
MT	Microtubule
MTOC	Microtubule organising centre
MtQ	Microtubule quartet
MW	Molecular weight
NF	New flagellum
NIMA	Never in mitosis gene A
OF	Old flagellum
PBS	Phosphate buffered saline
PCF	Procyclic form
PCR	Polymerase chain reaction
PEME	Pipes, EDTA, $MgCL_2$, EGTA
PFR	Paraflagella rod
PTM	Post translational modification
PPB	Preprophase band
RNA	Ribonucleic acid
RNAi	RNA interference
SDS	sodium dodecyl sulphate
SDS-PAGE	sodium dodecyl sulphate polyacrylamide gel electrophoresis

SEM	Scanning electron microscopy
SIF	Stumpy induction factor
TAC	Tripartite attachment complex
TAE	Tris(hydroxymethyl)aminomethane-acetate ethylenediaminetetraacetic acid
TbFP	*Trypanosoma brucei* flagella proteome
TBS	Tris buffered saline
TCP	Trypanosome cortex protein
TEM	Transmission electron microscopy
+TIP	Plus end tracking protein
TOG	Tumour overexpressed gene
Tris	Tris(hydroxymethyl)aminomethane
VSG	Variant surface glycoprotein
WCB	Whole cell body
WHO	World Health Organisation
WT	Wild type
YFP	Yellow fluorescent protein
ZMG	Zimmerman's postfusion medium

Chapter 1 Introduction

1.1 The Parasite, *Trypanosoma brucei*

Trypanosoma brucei, a species of parasitic protist belonging to the order Kinetoplastida diverged from the main eukaryotic lineage 900 million years ago (Douzery *et al*, 2004). The parasite is the causative agent of the cattle wasting disease N'gana, and Human African Trypanosomiasis (HAT). HAT more commonly referred to as African sleeping sickness causes approximately 50,000 deaths per annum (WHO, 2006). However, less than 12,000 cases are reported each year making HAT one of the most neglected tropical diseases (Brun *et al*, 2010). *T. brucei* was first identified by Sir David Bruce in 1895, however trypanosomiasis is an ancient scourge, and symptoms of the disease in cattle are described on papyrus written by ancient Egyptians dating from the 2nd millennium BC (Steverding, 2008). Today it is recognised as the most economically important disease constraint of livestock productivity in Africa causing estimated losses of over 5 Billion US dollars per annum (Taylor & Mertens, 1999), significantly contributing to the poverty of afflicted areas.

HAT is prevalent in 36 countries in sub-Saharan Africa and has a devastating effect on human health, it is always fatal when untreated, and currently the only treatment available is chemotherapy. Many of the drugs available have high levels of toxicity are outdated and/or resistance to them is widespread. The first effective drug, Suramin, was developed in 1916 and is still in use today (Steverding, 2010). There is an urgent need to develop new treatment strategies for the treatment of HAT. Studying *T. brucei* at the molecular level exposes novel drug targets and identifies

candidate proteins which could act as disease markers for the development of sensitive and specific test to aid in the diagnosis and management of HAT.

1.2 Parasite life cycle

The *T. brucei* life cycle involves the alternation between an insect vector (the tsetse fly) and a mammalian host and the parasite must adapt its cellular morphology and biology to survive and replicate within these different environments. As such cells at different life cycle stages have distinct morphologies, different organelle positioning and can often be distinguished by the length of the flagellum (Vickerman, 1985). Figure 1.1 is a cartoon representation of the life cycle showing the main developmental stages found in the mammalian host and insect vector. The slender bloodstream form (BSF) and the procyclic form (PCF) isolated from the fly's mid-gut are coloured blue on the diagram. These forms of the parasite are routinely cultured in the laboratory and are therefore most relevant to this thesis. Proliferative forms such as the BSF and PCF are associated with establishing a parasite population in a new environment whereas non-proliferative stages, such as the stumpy form in the bloodstream or the metacyclic form in the fly, are associated with major transitions between environments (Fenn & Matthews, 2007).

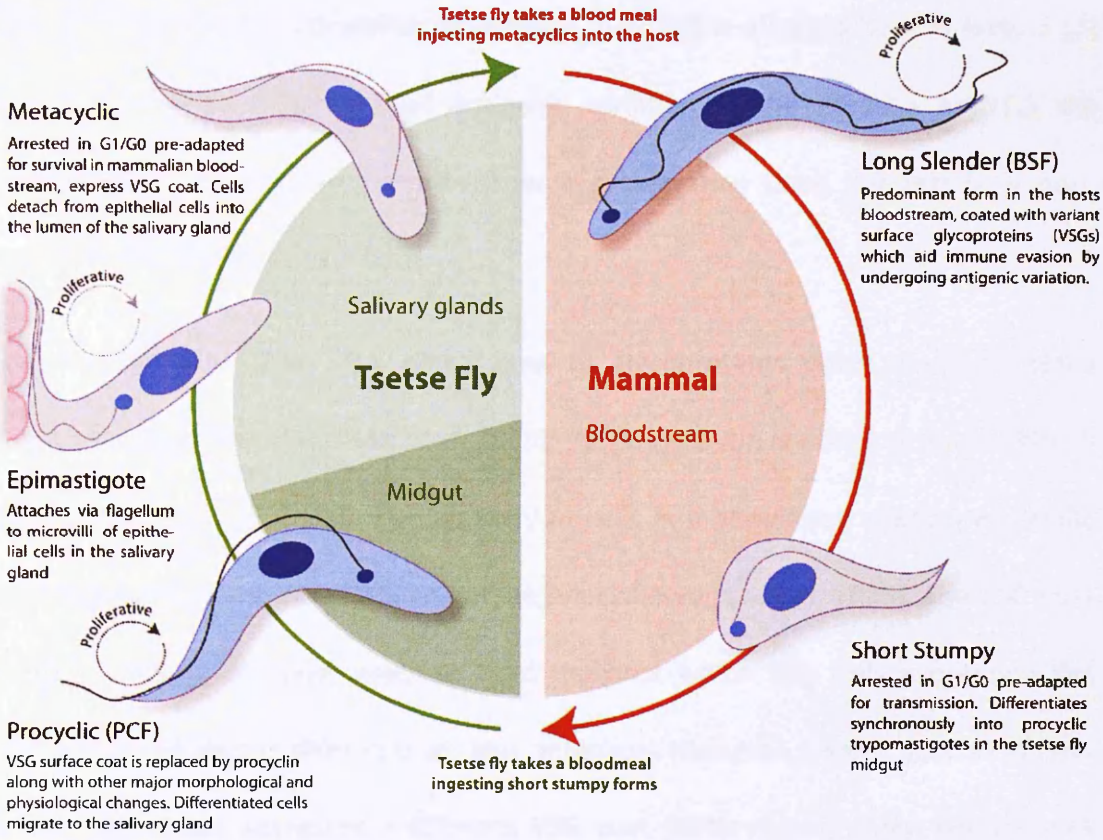

Figure 1.1 Simplified diagram of the life cycle of *T. brucei*

Cartoon describing the life cycle of *T. brucei* showing the main developmental stages of the parasite in the tsetse fly and the mammalian host: Cells coloured blue are the forms most relevant to this thesis, they are readily cultured *in vitro* and are genetically tractable.

Trypanosomes can infect their hosts very efficiently; given the right conditions a single bite from an infected fly can cause infection in a mammal (Thuita *et al*, 2008). Such a bite deposits metacyclic trypanosomes into the dermal connective tissue of the mammal where they differentiate into the long slender form and multiply by binary fission. They traverse capillary walls, enter the bloodstream and eventually access the brain and spinal fluid. The population in the host bloodstream is pleomorphic with a number of morphologically different forms existing at any one time. The two morphological extremes are the long slender form and the short stumpy form, the slender form predominates in the population (Matthews, 2005).

The level of parasitaemia within an infected mammal is affected by two factors (1) the host immune response and antigenic variation of the parasite and (2) the differentiation rate of the parasite from a proliferative (long slender) to a non-proliferative (short stumpy) form.

(1) The BSF is covered in a dense coat of glycoproteins called variant surface glycoproteins (VSGs) (Morrison *et al*, 2009); VSG expression is essential for viability in the BSF (Smith *et al*, 2009). The majority of cells in a population express a specific VSG type and are known as the homotype (Van Meirvenne *et al*, 1975). The VSG coat evokes a strong immune response from the host which kills cells expressing the homotype causing the disease to go into remission. However, a small portion of cells in the population expresses a different VSG coat (heterotypes) these heterotypes survive the host's immune attack and multiply during disease remission to give rise to a new wave of parasitaemia (Taylor & Rudenko, 2006).

(2) At peak parasitaemia long slender forms differentiate into short stumpy forms as a result of quorum sensing. The transition occurs in response to an uncharacterised parasite derived signalling factor known as the stumpy induction factor (SIF) (Vassella *et al*, 1997). The stumpy form is non-proliferative and is arrested in the cell cycle at G_1/G_0. Differentiation from slender to stumpy form is irreversible and stumpy forms are destined for transmission or death by apoptosis (reviewed by Duszenko *et al*, 2006).

Progression from slender to stumpy form requires a number of changes in cellular physiology and morphology. These changes are made to prepare the cell for the transition from mammalian bloodstream to tsetse fly midgut. Pre-adaption requires:

A remodelling of the cytoskeleton, and changes in the machinery required for energy metabolism (reviewed by Matthews, 2005).

Differentiation from long slender BSF into the pre-adapted short stumpy BSF is undertaken for two purposes;

(1) Uniform cell cycle arrest at G_1/G_0 ensures that upon transmission the parasite can synchronously re-enter the cell cycle and differentiate into the PCF. Additionally, energy for the process of differentiation can be readily generated by machinery prepared prior to transmission.

(2) Setting aside a portion of the population in a non-proliferating form allows maintenance of high levels of parasitaemia whilst prolonging host survival, therefore increasing chances of transmission (Matthews & Gull, 1994a) (reviewed by Matthews, 2005).

When infected blood is ingested by the tsetse fly it is taken in to the mid-gut where stumpy forms differentiate synchronously into the PCF (Ziegelbauer *et al*, 1990). A family of surface carboxylate-transporters called PAD proteins (proteins associated with differentiation) have recently been identified as markers for transmission-competent stumpy forms. PAD proteins convey the signal for stumpy to procyclic differentiation in the tsetse fly (Dean *et al*, 2009).

Differentiation from stumpy form to PCF is accompanied by a loss of the VSG coat which is quickly replaced by a procyclin coat. Unlike the VSG coat expressed by the BSF the procyclin coat is not essential for parasite survival but offers some protection against proteases within the tsetse mid-gut (Vassella *et al*, 2009).

The PCF has an increased cell body length, enhanced mitochondrion structure (van Hellemond *et al*, 2005) and the kinetoplast (a specialised organelle containing the mitochondrial DNA, discussed in section 1.3) is re-positioned closer to the nucleus in a sub-terminal position (Matthews *et al*, 1995). These changes take between 48 and 72 hours to complete and occur in the fly's mid-gut accompanied by cellular proliferation (Vickerman, 1985).

From the fly's mid-gut the parasites migrate to the salivary glands of the fly where cells undergo another gross morphological change to become epimastigotes. Differentiation from procyclic trypomastigotes to epimastigotes occurs in proliferating cells as a result of asymmetric division (Sharma *et al*, 2008). In epimastigotes the kinetoplast is re-positioned anterior to the nucleus and parasites attach to the microvilli of the epithelial cells in the salivary gland via their flagellum, whilst attached these cells proliferate and differentiate into metacyclic trypomastigotes (Van Den Abbeele *et al*, 1999).

Metacyclics are functionally equivalent to the bloodstream stumpy form; they do not proliferate and are pre-adapted for transmission into the next environment, in this case the mammalian bloodstream. Pre-adaption involves:

(1) Repositioning of the kinetoplast posterior to the nucleus.

(2) Mitochondrion repression, the organelle takes on a simple tubular form and relevant respiratory changes are made to pre-adapt the trypanosome to the changes in metabolism that it will encounter in the mammalian bloodstream (van Hellemond *et al*, 2005).

(3) Expression of a VSG surface coat.

The success of *T. brucei* as a parasite is largely due to its ability to transmit non-proliferative, pre-adapted cells into the host/vector. Progression through the life cycle is therefore intimately linked with cell cycle regulation as life cycle and cell cycle need to be co-ordinated. For example the stumpy form is arrested at a G_0/G_1 stage of the cell cycle and is receptive to signals for differentiation (Dean *et al*, 2009). Experiments using established markers for both cell cycle progression and differentiation show that upon release from cell cycle arrest cells progress through a normal cell cycle albeit at a slower rate. Progression through this first cell cycle coincides with a number of differentiation markers including; replacement of the VSG coat with procyclin, and the expression of the cytoskeletal protein CAP5.5 which is strictly stage specific and expressed in the PCF but not the BSF (reviewed in Hendriks *et al*, 2000).

Before reviewing the current knowledge of molecular mechanisms which govern the cell cycle in trypanosomes it is important to understand the basic architecture of the cell. As described earlier, morphological differences exist between the life cycle stages however the PCF of the parasite provides a paradigm for general trypanosome cell morphology and this form is described in the following section.

1.3 Cellular Morphology

Trypanosomes have a streamlined, vermiform shape, tapering from the middle of the cell out towards the poles. The anterior and posterior ends of the cell are defined with reference to the direction of cell movement. The majority of organelles are positioned towards the posterior pole of the cell. Figure 1.2 is a cartoon of a PCF

trypanosome in G_1; many aspects of the *T. brucei* cell are classically eukaryotic. For example, the cell possesses a nucleus contained within a nuclear envelope, as well as a cytoskeleton and endomembrane system which includes a plasma membrane, endoplasmic reticulum, Golgi apparatus, lysosomes, and vesicles. Alongside these characteristics the cell has some unusual features common to kinetoplastids. For example, glycolytic processes are confined to a specialised organelle called the glycosome (Opperdoes & Borst, 1977; Sommer & Wang, 1994). Also, rather than possessing hundreds of individual mitochondria as most eukaryotes do, *T. brucei* has a single elongated mitochondrion the genome of which is concentrated in an organelle called the kinetoplast. The kinetoplast is connected by unilateral kinetoplast filaments to the mitochondrial membrane and is also attached to the basal body by a transmembrane structure called the tripartite attachment complex (TAC) (Ogbadoyi *et al*, 2003). This interconnectivity allows the kinetoplast to maintain its position relative to the mitochondrion and the basal body.

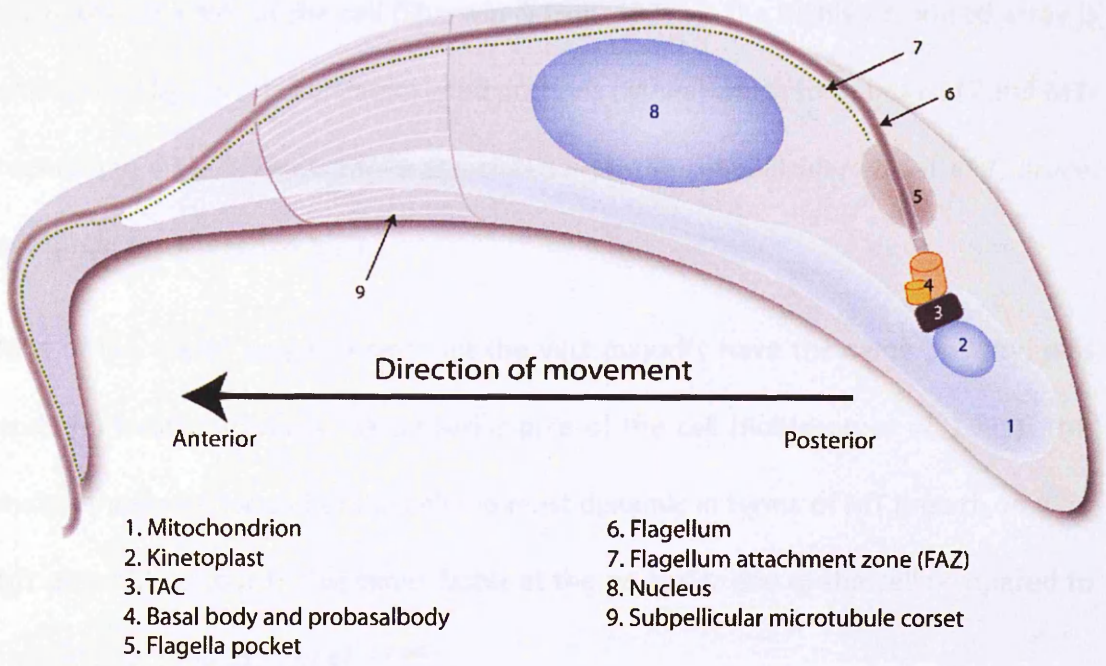

1. Mitochondrion
2. Kinetoplast
3. TAC
4. Basal body and probasalbody
5. Flagella pocket
6. Flagellum
7. Flagellum attachment zone (FAZ)
8. Nucleus
9. Subpellicular microtubule corset

Figure 1.2 Cartoon showing the cellular morphology of a procyclic form *T. brucei* cell

The trypanosome cell in G_1 possesses a single large mitochondrion (1), A Kinetoplast containing the mitochondrial DNA (2) which is attached to the basal body (4) via the tripartite attachment complex (TAC) (3). The flagellum (6) extends from the mature basal body (4) exiting the cell via the flagella pocket (5) the only site of endo/exocytosis in the cell. The flagellum (6) is attached to the cell body via the flagellum attachment zone or FAZ (7). The cellular DNA is contained in a nucleus (8). The vermiform shape of the cell is maintained by a highly organised microtubule based cytoskeleton which underlies the plasma membrane, called the subpellicular corset (9). The direction of cell movement is indicated, the cell swims with its flagellum leading, anterior and posterior ends are defined by this directionality of movement.

1.3.1 The subpellicular corset

The characteristic vermiform morphology of the cell is maintained by an arrangement of highly stable and organised microtubules (MTs) which lie just beneath the plasma membrane forming the subpellicular corset (Angelopoulos, 1970). The subpellicular corset (Figure 1.2 (9)) is composed of in excess of 100 MTs which are spaced regularly between 18 and 22nm apart and follow a helical pattern

along the long axis of the cell (Sherwin & Gull, 1989b). The highly organised array is maintained by microtubule associated proteins (MAPs) which form inter-MT and MT-membrane cross bridges. MAPs associated with the subpellicular corset in *T. brucei* are discussed in section 1.10.

MTs of the corset vary in length but the vast majority have the same polarity, plus ends (+) located towards the posterior pole of the cell (Robinson *et al*, 1995). This makes the posterior end of the cell the most dynamic in terms of MT growth, *in vitro* MT assembly is four to five times faster at the posterior end of the cell compared to the anterior (Robinson *et al*, 1995).

The corset in trypanosomes is extremely stable and remains intact throughout the cell cycle, changes in morphology are achieved by intercalation of new MTs between old ones without disassembly of the existing array (Sherwin & Gull, 1989a). Nucleation and growth of new MTs in the corset is discussed below in section 1.6.1.

Similarly to trypanosomes, Apicomplexa, a group of protozoan parasites including *Toxoplasma* and *Plasmodium* (causative agents of toxoplasmosis and malaria respectively) possess a subpellicular array of MTs. The Apicomplexan MT array is spirally arranged and confers an elongated shape to the parasite (Morrissette & Sibley, 2002). MTs radiate out, with their growing plus ends distal to a structure known as the apical polar ring (APR), a circular microtubule organising centre (MTOC) unique to apicomplexans (Morrissette & Sibley, 2002). In the trypanosome a MTOC resembling the APR has not been identified, suggesting nucleation of the subpellicular corset MTs occurs through different means this is discussed further in section 1.6.1.

1.3.2 The basal body

The basal body (Figure 1.2(4)) is an MTOC with numerous roles, from orchestrating mitochondrial DNA (kinetoplast) segregation to nucleating growth of the new flagellum and serving as a platform for recruitment of intraflagellar transport proteins (IFT) (Robinson & Gull, 1991; McKean *et al*, 2003; Davidge *et al*, 2006). The basal body in *T. brucei* conforms to the eukaryotic model of centriole/basal body structure, essentially being a cylindrical structure consisting of nine MT triplets (containing A, B, and C tubules). Early in G_1 phase *T. brucei* has a single mature basal body associated with a flagellum flanked by an immature basal body (pro-basal body) which elongates and matures during G_1 of the cell cycle (McKean, 2003). Growth of the new flagellum initiates when this pro-basal body has matured and subsequently two new pro-basal bodies are formed, each of which associate with a mature basal body. A recent study employing electron tomography has revealed that the new basal body rotates around the old basal body from an anterior to a posterior position as the new flagellum is forming. This process facilitates flagella pocket division and may have implications for kinetoplast segregation (Lacomble *et al*, 2010). When the cell divides the recently matured basal body with the newly formed flagellum and associated pro-basal body are inherited by the daughter cell (Woodward & Gull, 1990).

1.3.3 The flagellum

The flagellum (Figure 1.2(6)) exits the cell via the flagella pocket (Figure 1.2(5)) close to the posterior pole (the flagella pocket has been recently reviewed by Field & Carrington, 2009). It remains attached to the cell body and follows a left-handed helical path to the anterior pole where its distal end extends a short way beyond the

anterior tip of the cell. The primary function of the flagellum is motility; migration from the tsetse fly gut to the salivary glands is crucial for life cycle progression and is mediated by the flagellum (for a review of the flagellum see Vaughan, 2010). Trypanosomes, swim with the flagellum leading, their unusual corkscrew swimming style is generated by the flagellum beating from tip to base as opposed to the conventional undulating wave propagated from base to the tip, as seen in mammalian sperm (Kinukawa *et al*, 2005).

The flagellum of *T. brucei* consists of 3 major structures;

(1) The axoneme

(2) The paraflagella rod (PFR)

(3) The flagellum attachment zone (FAZ)

These structures are shown in Figure 1.3. In the PCF there is a fourth feature, the flagella connector (FC), this is a structure built during the cell cycle and as such is not shown in either Figure 1.2 or Figure 1.3. The four key components of the flagellum are discussed below.

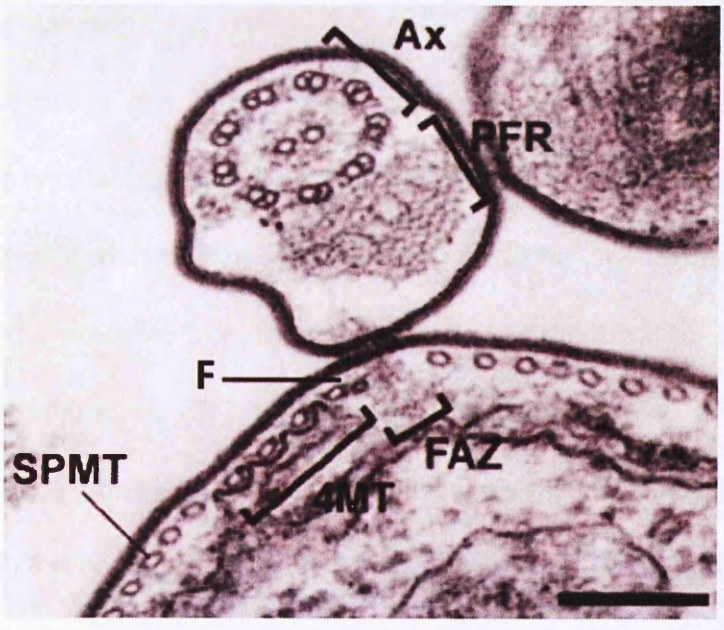

Figure 1.3 The *T. brucei* flagellum

Thin-section TEM of the BSF showing the key structures of the flagellum in *T. brucei* including a membrane bound axoneme (Ax) and associated paraflagella rod (PFR) which are attached to the main cell body by the flagellum attachment zone (FAZ) characterised by a wider space between subpellicular microtubules (SPMTs) where a cytoplasmic filament (F) is found. The filament lies next to the microtubule quartet (4MT). Scale bar = 2μm, image adapted from (Hammarton TC, 2007).

1.3.4 The flagellar axoneme

The axoneme is a cylindrical, MT based structure formed from nine outer doublets surrounding a central pair at the core. This 9 + 2 arrangement is highly conserved and is found within cilia and flagella of many eukaryotic cells. The axoneme extends from the basal body and contains numerous sub-structures which can be visualised in transmission electron microscopy (TEM) cross sections of the flagellum, including radial spokes, nexin (or interdoublet) bridges and the outer and inner dynein arms (Ralston & Hill, 2008).

1.3.5 Paraflagellar rod

Kinetoplastid protozoa like *T. brucei* possess a unique extra-axonemal structure called the paraflagellar rod (PFR) which in TEM cross sections has a lattice like structure with thin and thick filaments (Bastin *et al*, 1998) (see Figure 1.3). The PFR runs alongside the axoneme from the flagella pocket to the distal tip and is required for motility (Santrich *et al*, 1997; Bastin *et al*, 1998) and also acts as a scaffold for recruiting signalling molecules and metabolic enzymes (Ridgley *et al*, 2000; Pullen *et al*, 2004). The PFR is composed of three zones, the proximal, intermediate and distal domains with reference to their proximity to the axoneme. The proximal domain is linked to MTs of the axoneme by electron dense filaments on outer doublets 4 to 7 (Farina *et al*, 1986).

1.3.6 The flagellum attachment zone

The regular spacing of the corset is disrupted at one point where there is a large spacing between MTs; this is the site of the flagellum attachment zone (FAZ). The FAZ is composed of two elements:

(1) A cytoplasmic filament positioned between the two widely spaced corset MTs

(2) The microtubule quartet (MtQ), located to the left of the filament when the cell is viewed from the posterior end

The FAZ filament runs from the basal body area to the anterior tip of the cell and couples the cytoplasmic side of the flagellum to the cell body membrane by a series of regularly spaced electron-dense cross-links (Gull, 1999). The MtQ is nucleated close to the basal body and are the only MTs to underlie the membrane of the flagellar pocket. They have opposite polarity to the other MTs in the cortex, have a

higher resistance to depolymerisation at high salt concentrations and are invariantly associated with smooth endoplasmic reticulum (Vickerman, 1969; Sherwin & Gull, 1989b). The FAZ filament assembly lags slightly behind new flagellum growth 'stitching' the new flagellum on to the cell body as it is synthesised (Kohl *et al*, 1999).

1.3.7 The flagella connector

The flagella connector (FC) maintains the distal tip of the new flagellum in contact with the side of the old flagellum as the new flagellum grows (Moreira-Leite *et al*, 2001). There is no evidence for a similar structure at the tip of the old flagellum, this structure has not been observed in the BSF or any other flagellates (Moreira-Leite *et al*, 2001). The FC is produced early in G_1 of the cell cycle, it is found within the flagella pocket before the new flagellum emerges and proceeds to guide the new flagellum growth along the old flagellum throughout the cell cycle (Moreira-Leite *et al*, 2001; Briggs *et al*, 2004).

Very little is known about how this structure moves, the movement could be active as a result of + end directed MT motors such as kinesins (Briggs *et al*, 2004). Passive migration of the FC driven by new flagellum extension effectively pushing the FC along the old flagellum is unlikely. RNAi ablation of the IFT protein *Tb*CHE2 inhibits axoneme extension, regardless of this the cells still form an FC and the flagellar membrane still extends from the flagellar pocket, apparently pulled up the length of the old flagellum by the FC (Davidge *et al*, 2006). The FC migrates along the old flagellum until it reaches a 'stop point' at approximately 60% the length of the old flagellum where its progression halts. Anchorage of the FC at this point results in translation of new flagellum growth into a force which drives migration of the basal

bodies (Absalon *et al*, 2007). The connection between flagella is removed before the cell completes cytokinesis, the mechanism of FC disassembly is unknown, but the timing appears to be variable (Briggs *et al*, 2004).

1.4 The Trypanosome cell cycle

During the cell cycle single copy organelles such as the kinetoplast, mitochondrion, nucleus and flagellum are duplicated and segregated and the cytoskeleton is remodelled to produce two viable cells. The *T. brucei* cell cycle must be tightly regulated in both a temporal and spatial sense to enable faithful cell division. The following section describes the sequence of cytological changes observed during the cell cycle and the molecular mechanisms known to control progression through the division cycle.

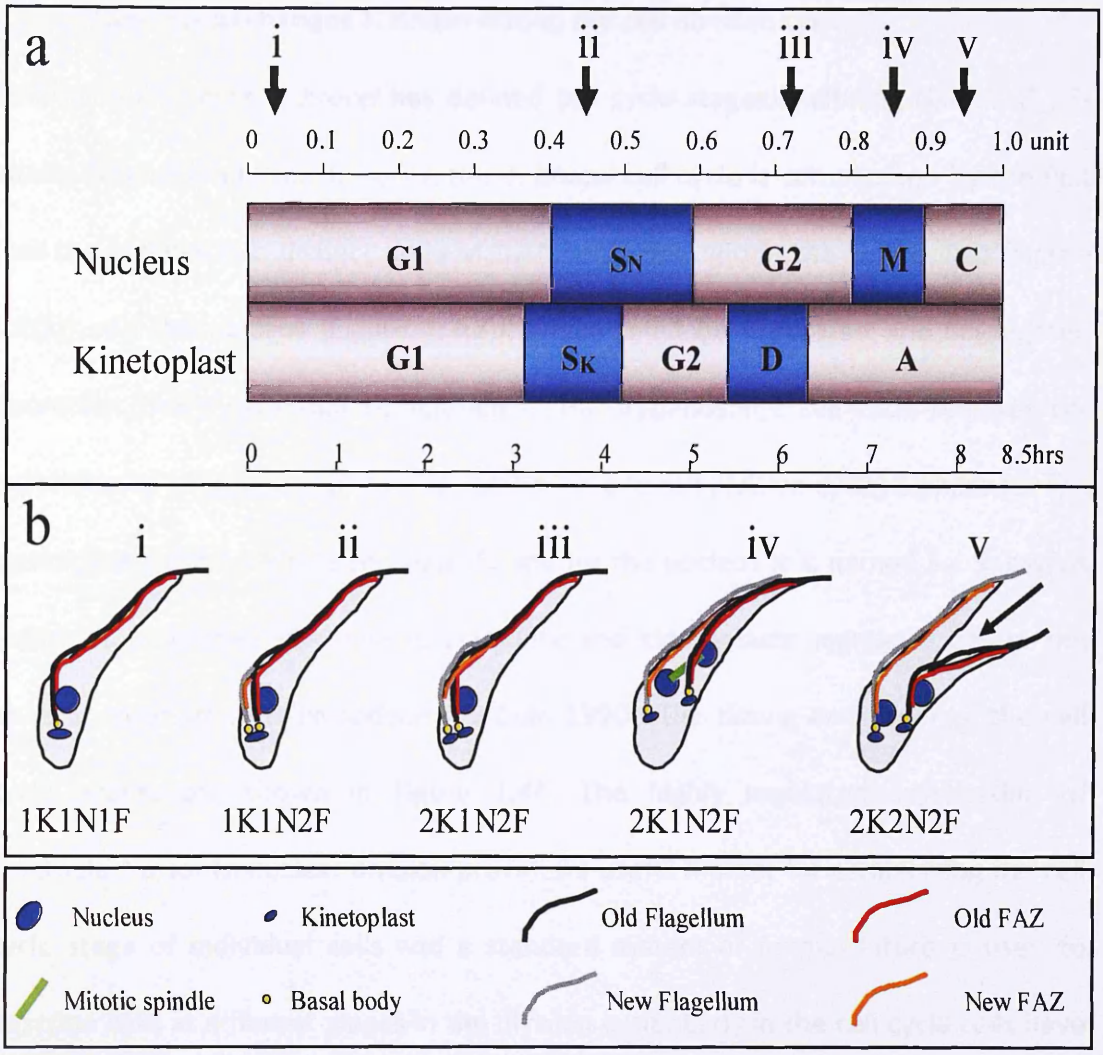

Figure 1.4 The major morphological events of the *T. brucei* cell cycle

Diagram describing the PCF cell cycle **(a)** the trypanosome cell cycle requires the co-ordination of nuclear and kinetoplast replication and segregation. This means G_1 phase is followed by two S-phases kinetoplast replication (S_K) and Nuclear S-phase (S_N). S_K starts before S_N and is considerably shorter in duration. This means kinetoplasts segregate (D) before nuclear mitosis begins (M). Kinetoplast segregation is followed by basal body separation, due to their physical attachment to the basal bodies kinetoplasts are further separated during this phase, this is therefore termed the 'apportioning' phase (A). Cell cycle duration for exponentially growing wild type PCF trypanosomes is 8.5 h. (b) Schematic representations of trypanosome cells at different stages of the cell cycle, i) a 1K1N1F cell from G_1, ii) a 1K1N2F cell during S_K/S_N probasal body has matured and the new flagellum is extending, iii) a 2K1N2F cell in G_2 phase for the nuclear cycle and is in the process of dividing the kinetoplasts, iv) A 2K1N2F cell undergoing nuclear mitosis, v) a 2K2N2F cell undergoing cytokinesis, the black arrow indicates the direction and position of the cleavage furrow (taken from McKean, 2003).

1.5 Cytological changes *T. brucei* during the cell division cycle

As in all eukaryotes *T. brucei* has defined cell cycle stages, including G_0 and G_1, S-phase, G_2 and M phase. However, the *T. brucei* cell cycle is complicated by the fact that the cell has two distinct units of DNA contained within the kinetoplast (Figure 1.2(2)) and the nucleus (Figure 1.2(8)), which must be replicated and segregated discretely. This means that completion of the trypanosome cell cycle requires co-ordination of two periods of DNA replication in one cell division cycle. S phase for the kinetoplast genome is referred to as S_k and for the nucleus it is named S_N. S_k begins before S_N and takes less time to complete and kinetoplasts segregate before the nucleus enters mitosis (Woodward & Gull, 1990). The timing and order of the cell cycle events are shown in Figure 1.4A. The highly regulated segregation of kinetoplast prior to nuclear division provides a useful marker for establishing the cell cycle stage of individual cells and a standard system of nomenclature is used to describe cells at different stages in the division cycle. Early in the cell cycle cells have a single nucleus and a single kinetoplast and are referred to as 1K1N. Once the kinetoplast DNA has duplicated and segregated to form a second kinetoplast, the cells are known as 2K1N, they then enter mitosis and once completed the cell is called a 2K2N. This cell undergoes cytokinesis forming two 1K1N daughter cells.

Figure 1.4B shows how cell morphology changes at each stage in the cell cycle. In G_1 the very first indication of cell cycle progression is the maturation of the pro-basal body, when this structure is fully matured the cell is capable of building a new flagellum alongside the old one, this new flagellum is physically attached to the old flagellum by a transmembrane junction called the flagella connector (FC) (Briggs *et al*, 2004). The FC guides flagellum growth along the path laid out by the old flagellum

as the cell progresses through the cell cycle. Once the pro-basal body has elongated and matured and the growth of a new flagellum has initiated, new pro-basal bodies form alongside both of the mature basal bodies (Lacomble *et al*, 2010). As a result of this, when the cell eventually divides, both products of division inherit one mature basal body and one pro-basal body. Following basal body duplication the Golgi apparatus duplicates (He *et al*, 2004) and then S-phase begins with S_K commencing before S_N (as described earlier).

Throughout the cell cycle the new flagellum extends and in the PCF new flagellum growth is accompanied by migration of the flagella connector (FC) towards the distal tip of the old flagellum (Moreira-Leite *et al*, 2001) (described in section 1.3.7). Upon reaching the 'stop point' basal bodies are driven apart by the force of the growing new flagellum (Absalon *et al*, 2007), the segregation of basal bodies is essential for kinetoplast segregation (Robinson & Gull, 1991) the two processes are coupled due to the physical connection between basal body and kinetoplast via the TAC (Figure 1.2(3)) (Ogbadoyi *et al*, 2003). Once kinetoplasts have segregated the cell forms an intra-nuclear spindle and undergoes nuclear mitosis with the nuclear envelope remaining intact (closed mitosis) throughout the whole process (Ogbadoyi *et al*, 2000). Once all organelles have been duplicated cleavage furrow ingression initiates at the anterior pole of the cell, its progress is unidirectional towards the posterior pole between the old and the new flagellum (cytokinesis is discussed in section 1.5.2). The molecular controls which govern the cell cycle are discussed in the following section.

1.5.1 Molecular control of the *T. brucei* cell division cycle

All eukaryotic systems rely on a tightly controlled cell cycle in order to maintain genomic stability and normal cell morphology. The cell cycle is driven by proteins called cyclin-dependent kinases (CDKs) and their binding partners the cyclins. In the fission yeast *Schizosaccharomyces pombe* there is a single CDK named Cdc2, the Cdc2 homologue in the budding yeast *Saccharomyces cerevisiae* is named Cdc28. By binding to different cyclins this kinase controls progression from G_1 to S phase and from G_2 to M phase. The *T. brucei* genome encodes eleven Cdc2 related kinases (CRKs 1-4 and CRK6-12) and ten cyclins (CYC 2-11). This is an unusually large number for a unicellular organism; this may reflect (1) the challenges of co-ordinating the replication and segregation of two discrete units of DNA and/or (2) the requirement to alter cell cycle dynamics at different life cycle stages.

In support of the latter, fundamental differences between PCF and BSF cell cycle regulation exist. For example, RNAi ablation of the cyclin CYC6 in the PCF blocks mitosis but not cytokinesis resulting in a population of non-viable cells which consists of anucleate cytoplasts termed zoids (1K0N) and cells containing a single kinetoplast and a single nucleus in which DNA is replicated but does not segregate (1K1N*). However, in the BSF both mitosis and cytokinesis are inhibited (Hammarton *et al*, 2003a). Whilst confirming that differences in cell cycle regulation exist between life cycle stages this experiment also shows that PCF trypanosomes are capable of undergoing cytokinesis without successfully completing mitosis. A similar observation has been made in studies using the drug aphidicolin, an inhibitor of nuclear S-phase and the anti-MT agent rhizoxin which inhibits mitosis. Cells treated with these agents do not complete mitosis but proceed through cytokinesis resulting

in the production of zoids showing that PCF cytokinesis is not reliant upon nuclear DNA synthesis or mitosis (Ploubidou *et al*, 1999). In most eukaryotic systems important control mechanisms exist to prevent cells from undergoing cytokinesis when there is a failure in completion of mitosis. The importance of such a control is demonstrated by *cut* mutants in *S. pombe* in which cell separation becomes uncoupled from nuclear division and cytokinesis proceeds with lethal results (Hirano *et al*, 1986).

Trypanosome cyclins can be classified by their sequence similarity to known cyclins in other systems; these include (1) cyclin PHO80, (2) B type cyclins and (3) transcriptional cyclins (Hammarton *et al*, 2004).

(1) The *T. brucei* CYC2 has homology to the cyclin PHO80 from the budding yeast *S. cerevisiae* (Van Hellemond *et al*, 2000). Five other *T. brucei* cyclins are classed as 'CYC2-like' including, CYC4, CYC5, CYC7, CYC10 and CYC11. In *S. cerevisiae* the PHO80 subfamily of cyclins complex with the CDK PHO85 and primarily regulate responses to environmental conditions (Measday *et al*, 1997). For example, the Pho80p-Pho85p cyclin-CDK complex regulates the response to phosphate limitation (Kaffman *et al*, 1994). Whilst a similar role in regulating nutrient metabolism cannot be ruled out for the *T. brucei* PHO80 homologues, RNA interference (RNAi) mediated ablation of CYC2 shows that it has a role in cell cycle progression as it is essential for the G_1/S phase transition in both the BSF and PCF (Li & Wang, 2003; Hammarton *et al*, 2004). It is also worth noting that despite the homology of these cyclins, trypanosome PHO80-like cyclins could not complement the function of PHO80 in yeast (Gourguechon *et al*, 2007).

In the PCF, RNAi depletion of CYC2 results in cell cycle arrest in G_1 phase and a 'nozzle' cellular morphology due to a MT mediated extension of the posterior end of the cell (Hammarton *et al*, 2004). CYC is suggested to play an auxiliary role in regulating cell cycle progression from G_1/S phase as RNAi ablation of this protein led to a ~50% reduction in growth rate compared to wild type cells. Depletion of CYC5, 7, 10 and 11 causes no apparent changes in growth rate so to date their function remains unknown (Li & Wang, 2003)

(2) In *S. cerevisiae* the B-type cyclins drive the cell cycle from S-phase to mitosis (Kuntzel *et al*, 1996). Three B-type cyclins have been identified in *T. brucei* CYC3, CYC6 and CYC8 (or CYCB1-B3). A study carried out by Li *et.al* (2003) employed RNAi to investigate the function of the *T. brucei* B-type cyclins. They found that CYC6/B2 is essential for cell cycle progression, RNAi mediated knockdown lead to almost 90% of cells arresting in G_2. CYC8/B3 accelerates progression through G_2/M but is not essential for cell cycle progression and no growth phenotype was observed upon RNAi ablation of CYC3/B1, suggesting this cyclin is not involved in cell cycle regulation (Li & Wang, 2003).

(3) The *T. brucei* CYC9 has homology to cyclin C, it has been suggested that CYC9 may play a role in transcriptional regulation. Functional characterisation is yet to be carried out for this cyclin (Hammarton *et al*, 2003b).

RNAi has also been applied to the *T. brucei* CRKs and the outcomes of these experiments have implicated CRK1 in the G_1/S passage and CRK3 in the G_2/M transition (Tu & Wang, 2004). In the PCF RNAi knockdown of CRK2, 4 and 6 had no effect on cell cycle progression; however, double knockdowns of CRK1 plus CRK2, 4

or 6 resulted in an increase in G_1–arrested cells (Tu & Wang, 2004). This suggests CRK2, 4 and 6 function (along with CRK1) in regulation of the G_1/S transition (Tu & Wang, 2004). The CRK1+CRK2 RNAi double knockdown resulted in an abnormal cellular morphology where cells arrested in G_1 had elongated posterior ends composed of newly synthesised MTs similar to the nozzle phenotype observed when the cyclin CYC2 is ablated by RNAi (Hammarton *et al*, 2004). Unusually, some of these elongated posterior ends were bifurcated (Tu & Wang, 2005). It has since been established that CRK2 plays the major role in morphological maintenance in a CYC2 dependent manner (Tu & Wang, 2005). These results show that posterior end morphogenesis and cytoskeletal remodelling is coupled to the cell cycle at the G_1/S transition at least in the PCF (Tu & Wang, 2005).

Understanding of the functional interactions between cyclins and CDKs is far from complete. To summarise our current understanding, CYC2 interacts with CRK1 to control transition through the G_1/S checkpoint (Tu & Wang, 2004) and the CYC2-CRK2 complex functions at G_1/S to control cellular morphogenesis in the PCF (Van Hellemond *et al*, 2000; Hammarton *et al*, 2004; Gourguechon *et al*, 2007). The CYC6-CRK3 complex controls the passage through G_2/M in both BSF and PCF (Tu & Wang, 2004). Recently CYC6 was shown to associate with CRK9 and regulate the G_2/M phase transition in the PCF. In CRK9 depleted cells mitotic arrest is accompanied by a lack of basal body segregation and inhibition of cytokinesis. This is abnormal in the PCF as cells which fail to undergo mitosis often continue through the cell cycle and progress through cytokinesis to produce a population of anucleate zoids (Gourguechon & Wang, 2009). As described earlier with the CYC6 RNAi cell line (Hammarton *et al*, 2003a) and rhizoxin treated cells (Ploubidou *et al*, 1999).

Knockdown of CRK9 in the BSF has no effect on mitosis or cytokinesis reflecting once again that different controls function in different lifecycle stages.

1.5.2 Cytokinesis

Cytokinesis is the final stage of the cell cycle and involves the partitioning and separation of a mother cell to yield two viable daughters. Different organisms have evolved different approaches, in animal and fungal cells cytokinesis is driven by the centripetal contraction of an actomyosin ring (comprised of F-actin, class II myosin and numerous other proteins) that is embedded in the plasma membrane at the division site. Ring contraction generates the cleavage furrow and is coupled to new plasma membrane (and in yeast, cell wall) synthesis leading to a physical separation of mother and daughter cell cytoplasm (Balasubramanian *et al*, 2004). In plant cells a MT and F-actin-based structure called the phragmoplast forms between segregated chromosomes after mitosis. This structure recruits vesicles necessary for cell wall synthesis and expands centrifugally towards the cell cortex where it fuses to produce two cells (Barr & Gruneberg, 2007). Trypanosomes and plants lack an actomyosin ring as they diverged before cells had evolved this cytokinetic mechanism (Pollard & Wu, 2010). As such they lack homologues of septins, type-II myosins, and IQGAP (Van Damme *et al*, 2004; Hammarton *et al*, 2007b) which are conserved in animal and fungal cells and function in regulating actomyosin ring assembly (Guertin *et al*, 2002). Despite the lack of an actomyosin ring plants still require actin for cytokinesis (Van Damme *et al*, 2004). In contrast division in *T. brucei* is unidirectional initiating near the anterior end of the cell and progressing longitudinally towards the posterior, and actin is not required for cytokinesis (Garcia-Salcedo *et al*, 2004).

Regardless of these different approaches cytokinesis in eukaryotes can be subdivided in to four major steps:

(1) Division site selection

(2) The initiation of cytokinesis

(3) Cleavage furrow progression

(4) Abscission

1.5.3 Division site selection

The mechanisms employed to select a division site for cytokinesis vary widely between organisms. Selection of the division site in animal cells takes place during anaphase and is directed by the mitotic apparatus. In *S. pombe* it is dependent upon the position of the pre-mitotic nucleus and as such it is selected during G_2 phase of the cell cycle whereas in *S. cerevisiae* it is determined in G_1 based on the positioning of the previous division site, the future site of cytokinesis is marked by the bud neck. In plants the division site is selected early in mitosis, the nucleus is positioned centrally in the cell in a MT based process and a ring structure of MTs and F-actin called the pre-prophase band (PPB) forms in the plasma membrane, with the PPB marking the future cleavage plane (Guertin *et al*, 2002).

In *T. brucei* the FAZ is believed to regulate the position and the direction of the cleavage plane (Robinson *et al*, 1995). Evidence to substantiate this idea comes from targeted depletion of specific proteins in the RNAi studies described below:

Intra-flagella transport (IFT) proteins - in the absence of IFT, cells are unable to build a full length flagellum. In these cells the cleavage furrow initiates closer to the

posterior end of the cell, resulting in a shortening of the overall cell length and implicating the anterior tip of the new flagellum as the site of cleavage furrow initiation. Intriguingly at later time points short rounded non-flagellated cells occur, the existence of such cells cannot be explained if the flagellum is responsible for determining the site of initiation. Upon further investigation these non flagellated cells were found to possess a short FAZ, suggesting that the FAZ normally associated with the new flagellum is the critical determinant for positioning of the division site (Kohl *et al*, 2003).

FAZ1 - a component of the FAZ filament was discovered in a screen using L3B2 a FAZ filament specific monoclonal antibody (Kohl *et al*, 1999; Vaughan *et al*, 2008). FAZ1 is a large repeat containing protein which has orthologues in other trypanosome species. RNAi ablation of FAZ1 in the PCF leads to an increase in zoids due to a mispositioned cleavage furrow, supporting previous suggestions that the FAZ is the critical determinant for cleavage site selection (Sherwin & Gull, 1989b). At later time points the ability to divide is further compromised and multinucleate cells (>2K2N) accumulate. These defects are a result of disorganised FAZ formation leading to the production of an unstable FAZ rather than complete absence of the structure. The gap in the corset which normally accommodates the FAZ filament is unusually large and the association between the MtQ and the smooth endoplasmic reticulum is abnormal or completely absent. Flagellum growth is not affected but in most cases the flagellum 'loops' away from the mid region of the cell or becomes completely detached (Vaughan *et al*, 2008).

The flagellum adhesion glycoprotein 1 (FLA1) - has also been localised by immunofluorescence to the FAZ region of *T. brucei*. Knockdown of FLA1 by RNAi in the PCF results in flagella detachment (Moreira-Leite *et al*, 2001; LaCount *et al*, 2002). These FLA1 depleted cells are also unable to initiate cytokinesis and become fat and rounded, they re-enter the cell cycle and eventually contain multiple nuclei and kinetoplasts (LaCount *et al*, 2002). In *T. cruzi* the homolog of FLA1 (GP72) localizes to the junction between the flagella and the cell body, *T. cruzi* GP72 null mutants have completely detached flagella but are still capable of dividing (Cooper *et al*, 1993). In an attempt to rescue FLA1 knockdown cells through expression of *T.cruzi* GP72 this study rather unexpectedly found that expression of GP72 in the absence of FLA1 RNAi caused complete flagella detachment. The authors suggest this is because GP72 dominantly interferes with the *T. brucei* flagellum attachment in the PCF (LaCount *et al*, 2002). Furthermore, the flagella detachment caused by GP72 expression did not cause cytokinesis inhibition suggesting that flagella attachment is not essential for cell division (LaCount *et al*, 2002). This implicates FLA1 in two discrete processes in *T. brucei* (1) flagella attachment and (2) initiation of cytokinesis.

1.5.4 Initiation of furrow ingression

All organisms must co-ordinate the initiation of cytokinesis with chromosome segregation. In *T. brucei* the exact mechanisms orchestrating this are currently unknown. However, some conserved and other unique aspects of cytokinesis regulation have been discovered through studies targeting proteins that function in cytokinesis in other systems for RNAi ablation.

Aurora kinases are highly conserved proteins amongst eukaryotes with essential roles in cytokinesis and chromosome/spindle dynamics during mitosis (Carmena & Earnshaw, 2003). Mammals have three Aurora kinases A, B, and C whilst *S. cerevisiae* has a single essential Aurora kinase, Ipl1 (Carmena & Earnshaw, 2003). Three Aurora kinase homologues have been identified in the *T. brucei* genome (TbAUK1-3) but only TbAUK1 is essential for cell growth (Tu *et al*, 2006). TbAUK1 is closely related to Ipl1 and the mammalian Aurora B kinase and is required for spindle formation, chromosome segregation and cytokinesis in both PCF and BSF (Li & Wang, 2006; Tu *et al*, 2006). The RNAi mediated depletion of TbAUK1 in the PCF results in a G_2/M cell cycle arrest. Kinetoplasts/basal bodies segregate as in wild type cells but mitosis and cytokinesis is blocked. Moreover, further rounds of kinetoplast/basal body duplication and segregation are inhibited (Tu *et al*, 2006). This is in contrast to cells treated with rhizoxin or depleted of the mitotic cyclin CYC6, which undergo kinetoplast duplication/segregation and cytokinesis in the absence of mitosis leading to the production of anucleate zoids (Ploubidou *et al*, 1999; Hammarton *et al*, 2003a). This data suggests that kinetoplast duplication/segregation drives cytokinesis in the PCF and shows that TbAUK1 has an essential role in initiating cytokinesis in *T. brucei* (Tu *et al*, 2006).

The phenotype resulting from TbAUK1 RNAi ablation in the BSF differs to that observed in the PCF. In both cases mitosis and cytokinesis are inhibited, however in the BSF nuclear DNA synthesis continues despite a lack of chromosome segregation. The kinetoplast cycle continues and further rounds of organelle replication are completed producing polyploid cells with multiple kinetoplasts, basal bodies and flagella (Li & Wang, 2006). This suggests that re-entry into S-phase is controlled

differently between life cycle stages. TbAUK1 also regulates posterior end morphology, in the BSF normal cellular architecture is lost upon RNAi mediated ablation of TbAUK1 and excessive MT synthesis is observed at the posterior end (Li & Wang, 2006).

In mammalian cells aurora kinase B is the core enzymatic sub-unit of the chromosomal passenger complex (CPC) which consists of aurora kinase B and three non-enzymatic components (survivin, borealin and INCENP). The CPC has a dynamic localisation pattern and is involved in many functions related to chromosome and tubulin dynamics during mitosis, it is also essential for completion of cytokinesis in eukaryotes (Ruchaud *et al*, 2007). Similarly, TbAUK1 functions in mitosis, is essential for cytokinesis and has a dynamic localisation pattern reflecting that of mammalian CPCs (Li & Wang, 2006). This suggests that TbAUK1 also functions as part of a CPC. However, *T. brucei* lacks homologues of the characteristic eukaryotic CPC components. Instead the *T. brucei* genome encodes two novel CPC's, TbCPC1 and TbCPC2. The complex of TbAUK1, TbCPC1 and TbCPC2 localises to the nucleus in G2, then to the spindle mid-zone at anaphase. It then relocates to the mid-point of the cell on its dorsal side before moving to the position where the anterior end of the daughter cell is tethered to the mother cell (this is the site where division will begin) and then moving towards the posterior end of the cell at the head of the cleavage furrow (Li *et al*, 2008a; Li *et al*, 2008b). The authors suggest that this relocation to the division site is involved in initiating cleavage furrow ingression. Furthermore, movement of the CPC with the cleavage furrow towards the posterior pole of the cell suggests it may also function to guide and/or sustain cleavage furrow ingression (Kumar & Wang, 2006; Umeyama & Wang, 2008).

Polo kinases are highly conserved serine/threonine kinases which are characterised by the presence of two C-terminal domains called polo box domains which mediate interactions with target proteins (Archambault & Glover, 2009). Polo kinases such as Cdc5p in *S. cerevisiae* play a pivotal role at several cell cycle stages (Archambault & Glover, 2009) including:

(1) Entry into M phase

(2) The metaphase/anaphase transition

(3) Mitotic exit

(4) The initiation of cytokinesis

The *T. brucei* polo-like kinase (TbPLK) has structural and functional homology to the *S. cerevisiae* protein Cdc5p (Kumar & Wang, 2006). When the TbPLK gene was introduced into a temperature sensitive *cdc5-1* mutant it was capable of complementing lost functions (Kumar & Wang, 2006). However, in the PCF TbPLK has a more limited function as it only functions in initiation of cytokinesis. It is interesting to note that few homologues to substrates of Cdc5 in *S. pombe* have been identified in the *T. brucei* genome (Umeyama & Wang, 2008).

Two independent studies have carried out RNAi ablation of TbPLK with differing results. Studies carried out in the Wang laboratory concluded that PLK is required for the initiation of cytokinesis in the PCF, as they recorded that upon TbPLK depletion nuclear divisions and multiplications of kinetoplast, basal body, and flagellum continued but cell division was blocked. The result was an increase in cells with multiple nuclei, kinetoplasts, basal bodies, and flagella (Kumar & Wang, 2006).

However, studies by Hammarton demonstrated that a role for TbPLK in basal body duplication in the PCF rather than cytokinesis initiation (Hammarton *et al*, 2007a). This study also showed that TbPLK is required for cleavage furrow ingression but not initiation of cytokinesis in the BSF (Hammarton *et al*, 2007a). Although this study could not rule out a function in cytokinesis initiation, the authors suggest that the defect in cytokinesis initiation observed when TbPLK is ablated is a downstream effect of an initial defect in basal body duplication.

There are also conflicting reports for the localisation of TbPLK in the PCF, initially TbPLK was localised by C-terminal HA-epitope tagging at a midpoint on the dorsal side of the cell coinciding with the FAZ, and the anterior tip of the cell. The localisation of TbPLK-3HA was also observed on membrane extracted cytoskeletons (Kumar & Wang, 2006). A second independent study employing an N-terminal TY1 tagged version of TbPLK, showed a punctate cytoplasmic localisation (Hammarton *et al*, 2007a). A third group used affinity-purified antibodies raised against TbPLK and found TbPLK localised at the growing tip of the new FAZ (de Graffenried *et al*, 2008), a similar localisation to the original observation made by Kumar and Wang (2006).

This controversy prompted the Wang laboratory to re-examine their previous localisation and confirm their initial observation showing that the HA-tagged TbPLK is found at a single localisation at the dorsal mid-point of the cell in association with the FAZ in both PCF and BSF trypanosomes (Umeyama & Wang, 2008). TbPLK is expressed late in S-phase and disappears rapidly before the initiation of cytokinesis (Umeyama & Wang, 2008). This coincides with the translocation of CPC to its position at the dorsal mid-point of the cell. It was postulated that recruitment of the CPC to

the site of cleavage furrow initiation may depend on the *T. brucei* homologue of polo kinase (TbPLK) (Umeyama & Wang, 2008).

It has recently been shown that direct recruitment of the CPC by TbPLK is unlikely since TbPLK dissociates from the FAZ into the cytoplasm before the translocation of TbAUK from the dorsal mid-zone to its position at the FAZ (Li *et al*, 2010). Also inhibition of TbPLK in late S-phase allows cells to continue through one complete cell cycle. These cells accurately complete cytokinesis once before it is completely inhibited in the second cell cycle. However, cells treated with the same PLK inhibitor in G1, or prior to TbPLK expression in S-phase, do not undergo cytokinesis at all and essentially generate the same phenotype as seen in when TbPLK is depleted by RNAi. This suggests that TbPLK affects cell cycle progression indirectly most likely by phosphorylating an unknown substrate early in S-phase (Li *et al*, 2010).

The GTPase Arl2 (ADP-ribosylation factor-like 2) regulates MT biogenesis in a variety of systems. Alp41 the Arl2 homologue in *S. pombe* regulates MT architecture, when Alp41 is mutated cells possess short MTs and defects in cell division and cytokinesis are observed (Radcliffe *et al*, 2000). RNAi mediated ablation of the Arl2 homologue in *C. elegans* causes defects in the organization of embryonic MTs (Antoshechkin & Han, 2002). A recent study has implicated the trypanosome homologue of Arl2 in cleavage furrow formation. When Arl2 is depleted by RNAi in the BSF, very few cells can be found with cleavage furrows. Where furrows are present their progression is attenuated in the early stages, and cells accumulate as multinucleates. The authors suggest that Arl2 effects cleavage furrow formation due to disruption of MT dynamics (Price *et al*, 2010b). TEM analysis showed that the FAZ and the

subpellicular MTs were intact and organised as normal. However the study found that RNAi depletion of Arl2 leads to a loss of acetylated α-tubulin (a post translational modification which is discussed in section 1.6.3).

1.5.5 Progression of the cleavage furrow

The CPC complex described earlier is localised to the point of cleavage furrow initiation and is thought to play a role in directing the cleavage furrow ingression (Li *et al*, 2008a). Other proteins required for cleavage furrow ingression, have been identified through RNAi. Characteristically, upon depletion of these proteins the cell initiates cytokinesis but then fails to complete cell division as ingression of the cleavage furrow arrests. An example of this stalled cleavage phenotype is seen when the *T. brucei* polo kinase (TbPLK) is depleted in the BSF (Hammarton *et al*, 2007a). Other proteins implicated in cleavage furrow progression in *T. brucei* include MOB1, PK53, TRACK, SPT2 and DLP; these are discussed in detail below.

MOB1 - RNAi ablation of MOB1 in the BSF initially causes an increase in the number of post mitotic (2K2N) cells, followed by slow cleavage furrow ingression (Hammarton *et al*, 2005). The delay in cleavage furrow progression means that cells often re-enter the cell cycle and re-replicate their DNA before completing cytokinesis, at later time-points this leads to a general deregulation of the cell cycle. Unlike TbPLK no effects on basal body segregation were noted when MOB1 was depleted (Hammarton *et al*, 2005). Effects of MOB1 depletion in the PCF are more subtle, no increase in ploidy was detected but in some cases the furrow became mispositioned resulting in zoid production. Despite a conserved role for MOB1 in

mitotic exit in other systems no function in mitosis was found in *T. brucei* (Hammarton *et al*, 2005).

MOB proteins in other eukaryotes are co-activators of NDR (nuclear Dbf2-related) kinases which are essential regulators of mitosis and growth/development in many organisms (Hergovich *et al*, 2008). TbMOB1 was shown to form a complex with the NDR kinase TbPK50 in the PCF (Hammarton *et al*, 2005). PK50 is a functional homologue of Orb6 one of the two NDR kinases found in *S. pombe,* Orb6 is involved in regulation of cell morphology, polarity and division (Garcia-Salcedo *et al*, 2002).

It is tempting to suggest that the coupling of MOB1 to a cell polarity controlling NDR kinase could regulate the positioning of the cleavage furrow and its polarised progression from anterior to posterior of the cell. However in a more recent study the interaction between PK50 and MOB1 could not be confirmed (Ma *et al*, 2010). The study showed that the two *T. brucei* NDR kinases (PK50 and PK53) were active in the absence of MOB1 in both life cycle stages and no interaction with MOB1 was detected in either case (Ma *et al*, 2010). It is possible that *T. brucei* NDR kinases are regulated by a different mechanism than in other eukaryotic systems.

The NDR kinases PK50 and PK53 - The effects of PK50 and PK53 depletion were studied in the BSF and each kinase was found to be essential for viability with growth defects quickly observed upon induction of RNAi (Ma *et al*, 2010). In both cases there was an initial increase in the number of 2K2N cells in the population indicating a defect in cytokinesis. Interestingly the proteins appear to function during different phases of cytokinesis; depletion of PK50 causes a delay in cytokinesis initiation whereas reduced PK53 expression causes a later cell cycle block during cleavage

furrow ingression. This data suggests that the kinases may act in a cytokinesis signalling pathway in a sequential manner (Ma *et al*, 2010).

TRACK - The *T.brucei* Receptor for Activated C Kinase (TRACK) is also implicated in cleavage furrow progression. RACK proteins are important for recruiting signal proteins to specific sites in the cell, providing spatial organisation for many signalling processes including those involved in cell growth and morphology (McCahill *et al*, 2002). TRACK is found in the cytoplasm and is expressed in all life cycle forms; its expression restores growth in *S. pombe cpc2-* (RACK1 homologue) cells. In the PCF, TRACK is required for the progression of the cleavage furrow beyond the midpoint of the cell (Rothberg *et al*, 2006). When its expression is reduced cells undergo multiple rounds of partial cytokinesis, similar to the phenotype seen in the MOB1 depleted BSF (Hammarton *et al*, 2005). These partially cleaved cells re-enter the cell cycle and in many cases progress at different rates despite sharing cytoplasm (Rothberg *et al*, 2006). In some cases the cleavage furrow is mispositioned leading to zoid formation. In the BSF TRACK appears to be essential for the initiation of cytokinesis rather than cleavage furrow ingression, as RNAi depletion of TRACK causes cell division to stall in a post-mitotic stage. As seen in many other cell lines, stalled cytokinesis does not prevent re-entry into the cell cycle and leads to the formation of large polyploid cells (Rothberg *et al*, 2006).

SPT2 - A very similar phenotype is generated upon RNAi ablation of serine palmitoyltransferase 2 (SPT2). SPT2 functions in the sphingolipid biosynthesis pathway, SPT activity and sphingolipid biosynthesis is essential in humans and yeast. Sphingolipids play important roles in membrane architecture and

endocytosis/exocytosis as well as being second messengers in the regulation of many processes including cell growth and cell cycle progression (Hannun & Obeid, 2008). In the PCF of *T. brucei* SPT2 ablation causes a block in cytokinesis, an increase in 2K2N cells which appear to be paused mid-way through cleavage ingression. In some cases the growing new flagellum becomes detached at the anterior tip or across partial/full length of the cell body; this in part may explain the cleavage furrow defect. In some cells cytokinesis does not initiate and the flagella pocket fails to divide after the new flagellum has been nucleated and although basal bodies duplicate they fail to segregate producing a cell with a 1K2N2F configuration (Fridberg *et al*, 2008). Defects in vesicular trafficking only emerge after prolonged induction of the RNAi ablation of SPT2 and the effects seen are mild. The study showed that in the PCF sphingolipids are not essential for exocytosis or maintenance of lipid rafts. However, the BSF shows greater sensitivity to sphingolipid depletion, the integrity of lipid rafts is lost when SPT2 was depleted in this life cycle form (Fridberg *et al*, 2008).

Dynamin like proteins (DLPs) – DLPs are large modular GTPases which function in organelle division, and endo/exocytosis. The *T. brucei* genome encodes a single DLP which regulates mitochondrial membrane division (Morgan *et al*, 2004). RNAi ablation of TbDLP leads to inhibition of mitochondrial fission and cells accumulate at the 2K2N stage indicating a block of cytokinesis, 75% of the cells stalled at this cell cycle stage had a nucleus-kinetoplast-kinetoplast-nucleus (NKKN) configuration which is normally adopted by cells in the final stages of cytokinesis and corresponds to two daughter cells laying opposed to one another attached at their posterior poles (Chanez *et al*, 2006). These cells do not re-enter the cell cycle and large multinucleate cells do not accumulate (Chanez *et al*, 2006). This study showed that

RNAi depletion of TbDLP in the PCF caused deficient endocytosis but went on to prove that this is not the reason for the stall in cleavage furrow ingression. Clathrin and dynamin are the key components of the clathrin-mediated endocytosis pathway; RNAi depletion of clathrin in the PCF causes a reduction in endocytosis and reduced population growth as cells die as a result, however there was no evidence of a specific cytokinesis defect (Chanez *et al*, 2006). This suggests that the cytokinetic defect observed when dynamin is depleted by RNAi in the PCF is not related to the defect in endocytosis but may be linked to defective mitochondrial fission. The authors suggest the existence of a novel cell cycle checkpoint in the PCF which ensures cytokinesis is initiated only once the single mitochondrion has replicated and undergone fission.

1.5.6 Abscission

Once the cleavage furrow has traversed the length of the cell the two cells remain attached at the posterior end and the final stage of cytokinesis is to sever this linkage in a controlled manner to form two independent cells. Very little is known about the molecular mechanisms of abscission in *T. brucei,* and no proteins which play a direct role in this process have been identified. It appears that flagella motility is essential for abscission in the PCF, four independent motility mutants resulting from RNAi mediated ablation of axonemal proteins RSP3, PF16, and PF20 and the PFR protein PFR2 caused a loss of flagellar motility followed by a cell division defect where cells remain attached by their extreme posterior ends and form multinucleate 'clusters' in culture (Ralston *et al*, 2006). Gentle agitation of cultures had a compensatory effect on the cells which had lost motility, and prevented the formation of such clusters suggesting the mechanical force provided by the beating flagellum is not essential for

cell viability but is required for abscission to occur in the PCF (Ralston *et al*, 2006). In contrast to the PCF, compromised flagellar motility in the BSF is lethal and no cleavage furrow ingression is observed suggesting that flagellum function is essential in this life cycle stage (Broadhead *et al*, 2006).

For trypanosomes to successfully complete the four steps of cytokinesis described above it is fundamental that the elaborate array of subpellicular MTs is extensively remodelled. Before describing our current knowledge of how the trypanosome cell orchestrates this process. Some general aspects of MTs will be discussed in the following section.

1.6 Microtubules

Generally the eukaryotic cytoskeleton is divided into three filament classes, MTs, intermediate filaments and actin microfilaments. An interesting observation drawn from the Tritryp genome sequencing projects is the apparent lack of any homologues to known intermediate filament proteins (Berriman *et al*, 2005). Coupled with this, *in silico* studies show trypanosomes have a reduced dependence on the acto-myosin network in comparison to other eukaryotes (Berriman *et al*, 2005). Reduced dependence upon these two key cytoskeletal components means they are highly dependent upon a MT-based cytoskeleton.

Microtubules are hollow cylinders 25 nm in diameter, formed from heterodimers of α and β tubulin (Weisenberg *et al*, 1968). α/β-tubulin subunits are incorporated longitudinally into protofilaments which associate laterally to form a MT. The head-to-tail organisation of α/β heterodimers in protofilaments confers a polarity to the MT; the α-tubulin monomer is exposed at the minus end of the MT and the β tubulin

monomer at the plus end. Plus and minus refers to the growth rate of the MT which is fastest at the plus end.

A MT is a dynamic structure which elongates and shrinks, most growth takes place at the plus end of MTs as the minus end is often associated with a MTOC. Furthermore, polymerisation of free minus ends has never been observed in any cell type or in MTs which were assembled in cytoplasmic extracts (Dammermann *et al*, 2003) (the cycle of MT growth and shrinkage is shown in Figure 1.5). The energy required to drive MT elongation comes from the hydrolysis of GTP which occurs as part of a cycle (Howard & Hyman, 2003). Both α and β tubulin contain a GTP binding site, GTP binds to α tubulin irreversibly and is not hydrolysed, however, the GTP bound to the β tubulin is hydrolysed to GDP. This hydrolysis is coupled to MT polymerization, the GTP bound β -subunit is exposed at the plus end of the MT and when the new α/β tubulin dimer arrives at the plus end key residues in the incoming α –tubulin interact with the GTP bound to the receiving β-tubulin subunit and it is consequently hydrolysed (Nogales *et al*, 1999). The resulting GDP is then buried by the docking of the incoming α/β-subunit and is therefore non-exchangeable (Nogales *et al*, 1999). Since MT growth is accompanied by the hydrolysis of GTP the majority of the MT possesses GDP bound β -tubulin.

MTs with GTP bound subunits at their ends are stable and serve as primers for polymerisation, the loss of this 'GTP-cap' through dissociation or hydrolysis exposes underlying GDP subunits and results in destabilisation of the MT lattice often resulting in depolymerisation (Drechsel & Kirschner, 1994). Destabilisation is the result of a conformational change which occurs in the tubulin subunit when GTP is

hydrolysed (Howard & Hyman, 2003). When β-tubulin is bound to GTP, the dimer has a straight conformation which aids MT extension, when incorporated into protofilament it becomes even straighter, whereas the GDP bound dimer has a curvature which weakens lateral interactions promoting depolymerisation (Rice *et al*, 2008). As a result the plus ends of MTs are structurally different when growing or shrinking. Growing plus ends of MTs possess a two-dimensional sheet of protofilaments with strong lateral interactions which eventually cause the sheet to fold round and form a MT (Chretien *et al*, 1995). When the sheet closes up it creates a seam in the MT lattice (Kikkawa *et al*, 1994). Shrinking plus ends of MTs appear frayed as protofilaments peel apart and curl away from the MT promoting the loss of tubulin subunits (Howard & Hyman, 2003).

Microtubules oscillate between growing and shrinking states in a process known as dynamic instability (Mitchison & Kirschner, 1984). This behaviour is essential for MT function and is modulated by the rate of polymerisation and GTP hydrolysis and an array of MAPs (Akhmanova & Steinmetz, 2008). MAPs will be discussed in detail in section 1.8 .

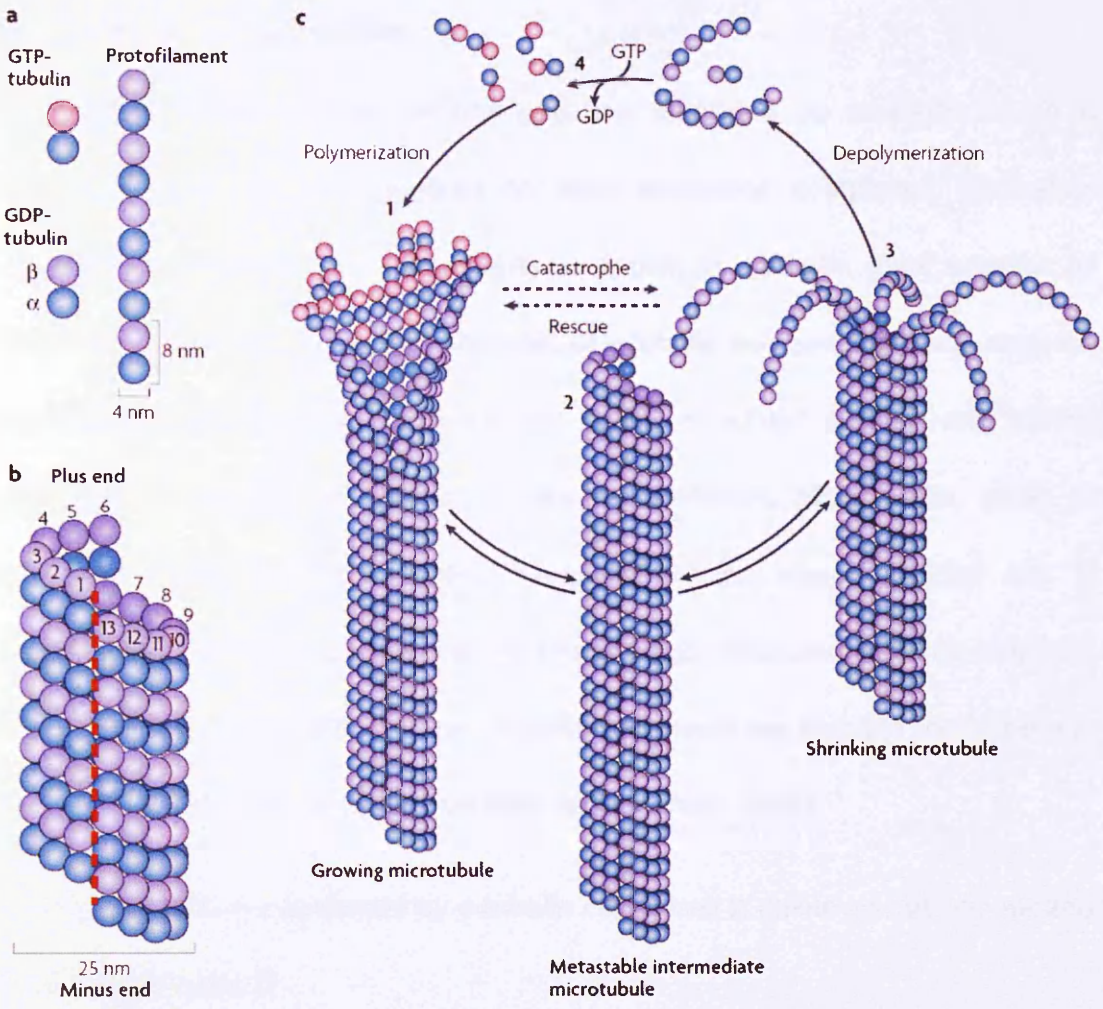

Figure 1.5 Microtubule structure and dynamic instability

Figure adapted from (Akhmanova & Steinmetz, 2008) a) Microtubules are composed α/β tubulin heterodimers that align head-to-tail forming protofilaments (b) 13 protofilaments associate laterally to form the wall of the microtubule. Microtubules are polar structures with β tubulin exposed at their plus ends and α- tubulin exposed at the minus end. A longitudinal seam forms in the lattice where α and β – subunits interact laterally (red dashed line). (c)The polymerisation/depolymerisation cycle: 1) Polymerization is initiated from a pool of GTP-bound tubulin subunits. GTP hydrolysis occurs shortly after incorporation, promoted by the addition of the next incoming subunit. Growing microtubule sheets are maintained by a 'cap' of tubulin-GTP. 2) Closure of the sheet into a tube generates a metastable microtubule, which can pause, undergo further growth or switch to the depolymerisation. 3) A shrinking microtubules are characterised by frayed protofilament structures at the plus end. 4) Soluble tubulin heterodimers are free to exchange GDP with GTP and the cycle can begin again.

1.6.1 Microtubule nucleation

Microtubules originate from MTOCs and are nucleated by γ-tubulin which is associated with accessory proteins to form nucleation complexes. Nucleation complexes can take the form of a tetramer known as γ-tubulin small complex (γ-TuSC) which is composed of two molecules of γ-tubulin and two additional proteins, or a ring structure composed of multiple copies of γ-TuSC proteins and several additional proteins (γ-TuRC) (Raynaud-Messina & Merdes, 2007; Wade, 2009). In mammals there are five γ-tubulin complex proteins named GCP2-6 but in trypanosomes and yeast only homologues to GCP2 (Spc97p) and GCP3 (Spc98p) are found (Hammarton TC, 2007). These γ-tubulin complexes are found in the cytoplasm as well as bound to MTOCs (Raynaud-Messina & Merdes, 2007).

Exactly how MTs are nucleated by γ-tubulin complexes is unknown but two models have been proposed:

(1) The template model-proposes that the γ-tubulins found in the nucleation complexes interact laterally and associate with the α-tubulin longitudinally at the minus end of the MT. Providing a platform so that elongation can occur, in this case the number of protofilaments in the MT is determined by the number of γ-tubulin subunits in the nucleation complex (Zheng *et al*, 1995).

(2) The protofilament model, in which γ-tubulins of the nucleation complex interact with each other longitudinally. The nucleation complex unwinds and forms the first protofilament of the MT and α/β-tubulins associate laterally forming a sheet which eventually closes into a MT (Erickson, 2000).

A recent study employing cryo-electron microscopy in *S. cerevisiae* has shown when γ-TuSC are stabilised by the protein Spc110 (normally found in the *S. cerevisiae* MTOC the spindle pole body) they assemble into well-ordered helical filaments with 13 γ-tubulins per turn. This correlates with the average number of protofilaments in a MT. The model also showed that γ-tubulin and α -tubulin subunits are most likely to associate longitudinally. Taken together this data provides convincing evidence in favour of the template model for MT assembly (Kollman *et al*, 2010).

In trypanosomes depletion of γ-tubulin by RNAi impedes the formation of central pair MTs in the axoneme causing paralysis of the new flagellum. Formation of outer doublet MT is unaffected suggesting their nucleation is independent of γ-tubulin and requires only the template provided by the basal body rather than *de novo* recruitment of γ-tubulin (McKean *et al*, 2003). At later stages induced cells accumulated large nuclei indicating a failure of mitosis, possibly related to defects in the intranuclear spindle. This phenotype was not studied extensively and no comment was made about the effects of γ-tubulin depletion on the structure of the subpellicular corset, as the primary focus of the experiment was to investigate effects of γ-tubulin depletion on flagella biogenesis.

1.6.2 Other proteins implicated in microtubule nucleation

MAPs also play important roles in the nucleation of MTs. For example, the MAPs Mto1 and Mto2 play an important role in MT dependent MT nucleation in *S. pombe* (Janson *et al*, 2005). Mto1p and mto2p form a complex and recruit γ-tubulin complexes to existing MTs (Janson *et al*, 2005; Samejima *et al*, 2005). This is required for MT nucleation during interphase and results in the formation of MT bundles

(Janson *et al*, 2005). MT dependent MT nucleation has also been observed in plant cells where MTs have been observed branching off pre-existing cortical MTs with γ-tubulin found at the branch point (Murata *et al*, 2005). XMAP215 a highly conserved MAP first identified in *Xenopus* can nucleate MTs in pure α and β-tubulin solutions, and depletion of this protein from *Xenopus* egg extracts impairs MT nucleation (Popov *et al*, 2002).

1.6.3 Microtubule post translational modifications

α and β tubulin sub-units which form MTs are targets for multiple post-translational modifications (PTMs), and in *T. brucei,* which expresses identical α/β tubulin isotypes, these modifications are the sole source of variation in MTs (McKean *et al*, 2001). Differential modification of MTs through PTMs may be important in regulating MAP interactions. In eukaryotes PTMs can include acetylation, detyrosination/tyrosination, glutamylation and glycylation. Acetylation and detyrosination/tyrosination and their relevance in terms of protein-MT interactions are discussed below.

Acetylation - is a common PTM occurring on α-tubulin, it is the addition of an acetyl group to the lysine residue at position 40 (Hammond *et al*, 2008). This reversible modification is widespread and found on many different isotypes of α-tubulin in diverse organisms from protists such as *Trypanosoma* (Sasse & Gull, 1988) and *Chlamydomonas* (L'Hernault & Rosenbaum, 1983) to mammals (L'Hernault & Rosenbaum, 1983; Cambray-Deakin & Burgoyne, 1987; Sasse & Gull, 1988). Acetylation is carried out by the enzyme acetyltransferase after α-tubulin is assembled into the MT. As such the extent of acetylation on a MT reflects the length

of time its sub-units have been available as substrates, acetylation is therefore generally associated with stable MTs such as those of the axoneme (Maruta *et al*, 1986). However, in trypanosomes this PTM is detected on the short-lived MTs of the mitotic spindle proving an exception to this rule (Sasse & Gull, 1988). Little is known about how tubulin acetylation affects the function of MTs but in CAD cells which are used as a model of primary neurites in mammals Kinesin-1 (a motor protein involved in transporting cargo along MTs) appears to bind preferentially to acetylated tubulin (Reed *et al*, 2006). However it has recently been shown that hyper-acetylation of MTs does not cause mis-localisation of Kinesin-1 suggesting that other PTMs may have a role in selective localisation of this protein (Hammond *et al*, 2010).

The detyrosination/tyrosination cycle - occurs in numerous eukaryotes including humans, plants and trypanosomes (Preston *et al*, 1979; Wehland *et al*, 1984; Sasse & Gull, 1988). The C-terminal tyrosine of α-tubulin is a targeted for removal by a carboxypeptidase enzyme once the α-tubulin has been incorporated into a MT. When the microtubule depolymerises and releases the detyrosinated α-tubulin, a tyrosine residue can be replaced by a tubulin tyrosine ligase, thus creating a tubulin tyrosination cycle (Idriss, 2000).

The detyrosination/tyrosination cycle functions in regulating the interaction between MTs and MT binding proteins (Hammond *et al*, 2008). The motor protein Kinesin-1 binds preferentially to detyrosinated MTs rather than tyrosinated tubulin (Liao & Gundersen, 1998). Furthermore a study in *S. cerevisiae* has implicated tyrosinated tubulin in the recruitment of certain plus end binding proteins (+TIPs) to MTs (+TIPs are MT binding proteins which associate with the growing plus end of the MT, they

are discussed in section 1.8). *S. cerevisiae* encode a C-terminal phenylalanine (Glu-Phe) which is analogous to the C-terminal tyrosine (Glu-Tyr) found in other eukaryotes (Badin-Larcon *et al*, 2004). Expression of an α-tubulin mutant lacking the C-terminal phenylalanine (resembling detyrosinated tubulin) led to the mis-localisation of Bik1p, the yeast ortholog of the mammalian +TIP CLIP170 (Badin-Larcon *et al*, 2004). The antibody YL1/2 detects tyrosinated tubulin (Kilmartin *et al*, 1982) and as such can be used as a robust marker for newly polymerised MTs. This antibody has been employed during the course of this thesis and has previously been used effectively to study MT assembly in the subpellicular corset of *T. brucei* through the cell cycle (Sherwin & Gull, 1989a).

1.7 Cytoskeletal remodelling during the cell cycle, visualised by YL1/2

Immunogold using YL1/2 labelling of whole mount cytoskeletons defined three broad patterns of MT assembly and insertion into the corset during the cell cycle (Sherwin & Gull, 1989a).

(1) Early in the cell cycle (G_1) 94% of the MT ends in the corset are positive for YL1/2 and are therefore growing. The posterior end of the cell is heavily labelled with YL1/2; additionally new ends of MTs are seen invading the existing array in the central region of the cell. Raising the possibility that both ends of a single MT may be labelled with YL1/2 indicating that two end assembly of the MT polymer may be occurring at this stage (Sherwin & Gull, 1989a).

(2) In cells immediately prior to, and during, mitosis far fewer MT ends are YL1/2 positive (20%) suggesting that MT growth is reduced compared to the cells in G_1.

(3) Cells late in the cell cycle, from anaphase through to completion of cytokinesis had more YL1/2 labelled MT ends than the previous category (64%) but not as many as the cells in G_1. Moreover, these cells contained a new 'type' of MT not observed in earlier cytoskeletons. In the central portion of the cytoskeleton, short MTs labelled with YL1/2 over their whole length were observed. These short MTs were not associated with either end of the cell or any visible structure and are assembled laterally between older and longer MTs of the corset (Sherwin & Gull, 1989a).

Inter-digitation of these short MTs explains how the inter-MT distance of the subpellicular array can remain the same despite the cell being broader in the central portion and tapering towards either end. Exactly how these short MTs are nucleated and the mechanisms governing temporal and spatial control of MT growth through the cell cycle are unknown; however MAPs are highly likely to be involved in processes.

Lateral insertion of new MTs between older MTs of the corset suggests that the cytoskeleton of *T. brucei* is inherited in a semi-conservative manner (Sherwin & Gull, 1989a). This process which demands extensive cytoskeletal remodelling including MT nucleation/outgrowth and coordinated severing/re-establishment of inter- MT (and inter-membrane) cross-links, processes which will be performed by MAPs.

1.8 Microtubule associated proteins

MAPs directly or indirectly regulate the organisation of MTs, their polymerisation/depolymerisation dynamics and transport along MTs. They are a diverse group of proteins whose activities cover a wide range of regulatory processes. MAPs can be classified into three distinct sub-groups:

(1) Microtubule motor proteins, kinesin and dynein motors move along MTs transporting cargo using the energy they produce from ATP hydrolysis (Hirokawa *et al*, 2009). They are employed by cells for many different processes e.g. the intraflagellar transport (IFT) system in *T. brucei* which is required for the formation of the flagellum (Absalon *et al*, 2008).

(2) Structural MAPs, bind along the length of the MT and are generally associated with stable MT populations e.g. the vertebrate proteins tau and MAP2 which are found in neurones and are characterized by their ability to bind and stabilize MTs (Dehmelt & Halpain, 2005).

(3) The +TIPs which are associated with the growing plus end of MTs, these proteins are described in the following section.

1.9 Plus end tracking proteins

Plus end tracking proteins (+TIPs) are a disparate group of evolutionarily conserved microtubule-associated proteins that specifically accumulate at the ends of growing MTs (reviewed in Akhmanova & Steinmetz, 2008). They are involved in mediating cellular architecture, chromosome segregation, cell polarization and migration, organelle transport, and intracellular signalling (Honnappa *et al*, 2009). CLIP170 was the first +TIP to be discovered; GFP-CLIP170 was described as a 'cellular firework' due to its comet-like appearance caused by a dynamic 'treadmilling' of the protein at MT plus ends (Rickard & Kreis, 1990; Perez *et al*, 1999). Since this discovery many more proteins with the same localisation pattern have been observed. Whilst most +TIPs can directly bind to MTs, there are many examples where interdependency interactions exist between +TIPs allowing complexes to form at MT plus ends (Su *et*

al, 1995; Busch & Brunner, 2004; Akhmanova & Hoogenraad, 2005; Lansbergen & Akhmanova, 2006). +TIPs can be categorised into 4 discrete groups (Slep, 2010).

(1) EB1 family members

(2) CAP-Gly domain-containing proteins

(3) SxIP motif containing proteins

(4) TOG domain-containing proteins

1.9.1 EB1 family

End binding 1 (EB1) proteins are small (approximately 35 kDa) and are characterised by their domain architecture. The C-terminus contains an end-binding homology (EBH) motif which interacts with SxIP motif containing +TIPs (discussed later) (Honnappa *et al*, 2005; Slep *et al*, 2005) and a coiled-coil domain which allows EB1 monomers to dimerise (Honnappa *et al*, 2005). At the C-terminus of EB1 is a EEY/F motif which is the target of the CAP-Gly family of +TIPS (Akhmanova & Steinmetz, 2008). The N-terminus contains a calponin homology (CH) domain which interacts with MTs (Gimona *et al*, 2002). Since its discovery many interactions between EB1 and other +TIPs have been identified resulting in EB1 being deemed the 'master regulator of dynamic +TIP interaction networks at growing MT ends (Honnappa *et al*, 2009).

EB1 was first identified by a yeast two hybrid screen searching for proteins which interact with the human tumour suppressor protein, adenomatous polyposis coli (APC) (Su *et al*, 1995). EB1 homologues have since been identified in most organisms explored to date (Tirnauer & Bierer, 2000), the yeast homologues are Mal3p (*S.*

pombe) (Beinhauer *et al*, 1997) and Bim1p (*S. cerevisiae*) (Tirnauer *et al*, 1999). In *Arabidopsis thaliana* there are three EB1 homologues AtEB1a, AtEB1b and AtEB1c (Chan *et al*, 2003). An EB1 homologue is found in the *T. brucei* genome but it is not conserved in closely related *Leishmania* suggesting that +TIP interactions are mediated by an alternative protein/proteins in this organism (Hammarton TC, 2007).

EB1 influences dynamic instability in MTs, usually with a stabilising function which promotes growth (Akhmanova & Hoogenraad, 2005). Immuno-depletion and protein addition experiments in *Xenopus* egg extracts show that EB1 decreases catastrophes and increases rescues and polymerization rate (Tirnauer *et al*, 2002). Localisation experiments carried out in the same study show EB1 at the plus end of the MT and along the length of the MT wall. EB1 staining on the MT wall remained static ruling out the possibility that it is transported along MTs to the plus end, furthermore tubulin monomers did not co-immuno-precipitate with EB1 suggesting that it does not co-polymerise with tubulin, leading the authors to postulate that EB1 has two distinct binding patterns, one at the MT wall and the other at the plus end where EB1 recognises some property of the polymerising MT (Tirnauer *et al*, 2002). A more recent study shows that *Mal3p* the EB1 homologue in *S. pombe* aligns along the MT lattice seam as well as accumulating at the plus ends (Sandblad *et al*, 2006). The authors suggest that *Mal3p* is acting to re-enforce lateral protofilament interactions and 'clamp' the seam together. This work also showed that *Mal3p* promotes sheet closure into the tubular form in dynamic MTs. In *Chlamydomonas reinhardtii* EB1 (CrEB1) localises to the flagella tip as well as at discrete spots in the cytoplasm where it is thought to be binding to cytoplasmic MT plus ends (Pedersen *et al*, 2003). In contrast to the studies described above CrEB1 is seen associated to growing, stable

and shrinking MTs showing that, at least in some organisms, EB1 is not just associated with polymerisation.

The interaction between EB1 and the tumour suppressor APC (Su *et al*, 1995) is required for APC localisation to the growing tip of MTs (Askham *et al*, 2000). This interaction plays an important role in MT-based cell polarity in mammalian cells (Slep *et al*, 2005). An analogous situation is observed in *S. cerevisiae* as the polarity determinant *Kar9p* associates with *Bim1p* (EB1 homologue) and as a consequence of this interaction MTs are targeted to the cell cortex (Miller *et al*, 2000). APC and *Kar9p* are SxIP motif containing proteins which interact with the EBH domain of EB1 this family are further discussed below.

1.9.2 SxIP motif containing proteins

A proline/serine-rich region containing a short conserved motif known as the SxIP motif has been identified in a large and diverse group of +TIPs. The SxIP motif interacts with the EBH domain at the C-terminus of EB proteins and targets proteins to the plus end of MTs in an EB1 dependent manner (Honnappa *et al*, 2009). Representatives of this diverse group include, mammalian APC and Kar9 in *S. cerevisiae* (discussed above), the mammalian spectraplakin MACF (microtubule-actin cross-linking factor), the drosophila homologue Shot (Slep *et al*, 2005), the human transmembrane protein STIM1 (stromal interaction molecule -1) (Grigoriev *et al*, 2008) and the human mitotic centromere associated kinesin (MCAK) (Honnappa *et al*, 2009), a recognised MT depolymerase known to destabilise the MT plus-ends (Desai *et al*, 1999).

1.9.3 CAP-Gly domain-containing proteins

CAP-Gly proteins contain a conserved domain of approximately 80 residues called the cytoskeletal associated protein-glycine rich (CAP-Gly) domain at their N-termini. CAP-Gly domains can be found in single or multiple copies and mediate interactions with tubulin and EB proteins (Steinmetz & Akhmanova, 2008). The CAP-Gly domain interacts with the C-terminal EEY/F motif of EB proteins (Weisbrich *et al*, 2007). Examples from this family include the mammalian cytoplasmic linker proteins (CLIPs), CLIP -170 and its neuronal paralog CLIP-115 (Schuyler & Pellman, 2001). A number of CAP-Gly proteins (including CLIP-170 and CLIP-115) bind more efficiently to tyrosinated MTs (Peris *et al*, 2006). However the tyrosination state does not influence the binding of EB1. This demonstrates that MT tyrosination, at least in part, regulates the interaction between CAP-Gly proteins and MTs. There is no evidence from the genome analysis that CLIPs or CLIP-associating proteins (CLASPs) are conserved in *T. brucei* (Hammarton TC, 2007).

1.9.4 TOG domain-containing proteins

TOG domains are a tubulin binding domain discovered in the human MAP chTOG (colonic and hepatic tumour-over expressed gene) (Charrasse *et al*, 1995). chTOG is homologous to XMAP215 (Charrasse *et al*, 1998), a 215kDa protein purified from *Xenopus* eggs which promotes MT growth at the plus-end (Gard & Kirschner, 1987) and tracks the tips of growing and shrinking MTs (Brouhard *et al*, 2008). Homologues to XMAP215/chTOG have since been identified in a vast range of organisms. XMAP215 family members have been implicated in organising cortical MTs in *Dictyostelium* (Hestermann & Graf, 2004) and *Arabodopsis* (Whittington *et al*, 2001). In *S. cerevisiae* Stu2p the XMAP215 homologue promotes spindle elongation during

anaphase (Severin *et al*, 2001). Both XMAP215 (Al-Bassam *et al*, 2006) and Stu2p (Severin *et al*, 2001) bind tubulin dimers with 1:1 stoichiometry. In both cases the binding of tubulin induces a conformational change and XMAP215/Stu2p close up around the tubulin dimer. A model has been suggested based on results from *in vitro* studies, that XMAP215 is a 'processive polymerase' which catalyses multiple rounds of tubulin subunit addition (Brouhard *et al*, 2008). This is achieved without energy consumption by stabilizing an intermediate state, preventing tubulin diffusing away and increasing the probability that it will become bound and incorporated into the lattice. In the absence of soluble tubulin XMAP215 can act in reverse and catalyze depolymerisation (Brouhard *et al*, 2008). The activity of XMAP215 may differ *in vivo* as it is known to interact with other MAPs which may mediate its behaviour (van der Vaart *et al*, 2009).

Whilst the *T. brucei* genome encodes a homologue of the highly conserved MAP EB1 and a member of the XMAP215/TOG family, there are few examples of other well characterised and conserved proteins from other systems. For example there is no evidence that *T. brucei* possesses a homologue to the MAP tau, or the cytoplasmic linker proteins (CLIPs) or their associated proteins (CLASPs) (Berriman *et al*, 2005). A number of trypanosome specific MAPs have been identified and these are discussed in the following section.

1.10 Microtubule associated proteins associated with the *T. brucei* subpellicular corset

The highly organised subpellicular corset of MTs is maintained by proteins which form inter-MT cross bridges and in some cases cross-link the MTs and the plasma

membrane. To date a number of MAPs associated with the corset MTs have been identified in *T. brucei*, including GB4, WCB, MARP1 and 2, I/6, CAP5.5, CAP17 and CAP15 (Rindisbacher *et al*, 1993; Affolter *et al*, 1994; Detmer *et al*, 1997; Hertz-Fowler *et al*, 2001; Vedrenne *et al*, 2002; Baines & Gull, 2008). These proteins are found exclusively in trypanosomes, they co-purify with tubulin and in some cases where RNAi cell lines have been generated, ablation leads to disruption of the normally highly organised subpellicular microtubules. Some of these proteins localise to specific poles of the cell and some are known to be expressed in specific life stages (Vedrenne *et al*, 2002; Olego-Fernandez *et al*, 2009). Studies of these critical proteins are limited mostly to the PCF and have generally been carried out in isolation leaving many questions unanswered regarding roles in other life cycle stages and also the existence of functional interactions between distinct proteins. This section describes the current knowledge available for *T. brucei* MAPs.

1.10.1 WCB

WCB so called as it is localised to the whole cell body of *T. brucei* is closely linked to the MTs of the subpellicular corset but is excluded from the flagella and mitotic spindle. Immunogold studies show that the protein is found on the exterior side of the corset MTs in close proximity to the plasma membrane (Woods *et al*, 1992). It is expressed in both the BSF and the PCF but characterisation of this protein has only been carried out in the PCF. RNAi mediated ablation of WCB resulted in cells with enlarged and rounded posterior ends and the generation of large numbers of anucleate zoids and multinucleate cells indicative of problems during cytokinesis (Baines & Gull, 2008). Indirect immunofluorescence experiments show that upon RNAi mediated ablation WCB is lost initially from the more dynamic posterior end of

the cell but is retained on MTs at the anterior, evidence of a stable association with MTs (Baines & Gull, 2008). Where WCB remains associated with MTs the corset is regularly organised. In contrast ultrastructural observations indicated that loss of WCB protein results in a loosening of the connection between the subpellicular MTs and the overlying plasma membrane, which leads to blebbing of plasma membrane from the cell surface. A loss of general overall integrity of the subpellicular corset is also observed with loss of regular spacing and organisation. During detergent extraction microtubules of the subpellicular corset splay apart at the posterior end indicating that the robust connection that previously held the posterior end of the cell together is lost following WCB ablation. WCB possesses a C2 domain at its N-terminus, and while many C2 domain containing proteins interact with membranes (Cho & Stahelin, 2006), it remains unknown whether WCB interacts directly or indirectly with the plasma membrane.

1.10.2 CAP5.5

CAP5.5 is expressed only in the PCF (Matthews & Gull, 1994b; Hertz-Fowler *et al*, 2001) it localises to MTs of the subpellicular corset (Hertz-Fowler *et al*, 2001). Unlike many other MAPs, CAP5.5 does not contain any repetitive elements, however the N-terminus of CAP5.5 contains motifs that allow for modification by myristoylation and palmitoylation, both these modifications are known to target proteins to membranes (Resh, 1999), suggesting CAP5.5 may associate with the plasma membrane (Hertz-Fowler *et al*, 2001).

CAP5.5 is a member of a diverse family of calpain-like proteins found in *T. brucei*. Calpains are calcium-dependent cysteine proteases with essential roles in signal

transduction, cytoskeletal remodelling and differentiation. In animals and plants calpains play important roles in development (Goll *et al*, 2003; Croall & Ersfeld, 2007). *T. brucei* has an extended calpain-related gene family, expressing more calpain related proteins (CALPs) than most other organisms. It is unlikely that all TbCALPs function as cysteine proteases as the putative active site in most cases lacks the essential catalytic triad (C-H-N) suggesting these proteins have evolved a species specific function (Ersfeld *et al*, 2005). In CAP5.5 only one of the amino acids of the catalytic triad is conserved (S-Y-N) (Hertz-Fowler *et al*, 2001) and the protein appears to have evolved an alternate function in regulation of cytoskeletal organisation (Olego-Fernandez *et al*, 2009).

The first visible phenotype following RNAi depletion of CAP5.5 in the PCF is the loss of protein from the posterior end of the cell (similar to that seen in the WCB cell line described above) this corresponds temporally to nuclear mispositioning in 2K2N cells indicative of organelle segregation defects (Olego-Fernandez *et al*, 2009). There is an increase in zoids and 1K2N cells in the population, progeny resulting from an aberrant cytokinesis event. Whether zoid formation is a consequence of miss-localised organelles or a direct result of aberrant cleavage furrow ingression is unknown but after 48 hours of induction multinucleates possess multiple stalled cleavage furrows. TEM analysis shows inter-MT spacing in the subpellicular corset is disrupted and bundles of MTs are visible beneath the plasma membrane.

This study confirmed that CAP5.5 function is limited to the PCF but identified a paralog, CAP5.5V which plays an analogous role to CAP5.5 in the BSF (Olego-Fernandez *et al*, 2009). This study did not determine if CAP5.5/CAP5.5V function as

proteases however the authors suggest these proteins may be required to severe inter-MT cross bridges and that CAP5.5/CAP5.5V ablation impedes the ability of new MTs to interdigitate into the existing subpellicular corset leading to a loss of organisation and resulting in severe cytokinetic defects (Olego-Fernandez *et al*, 2009).

1.10.3 CAP17 and CAP15

CAP17 and CAP15 are another example of related proteins with stage specific expression. CAP17 (a 17kDa protein) is found only in the PCF, whereas CAP15 (15kDa) is constitutively expressed but is ten-fold more abundant in the BSF. The proteins are very closely related, they have 49% sequence identity, differing due to a hydrophobic domain at the C-terminus of CAP17. As with CAP5.5, these proteins do not contain repeat regions like many other MAPS but co-fractionate with tubulin suggesting they associate with MTs. Immunofluorescence analysis has shown that CAP17 and CAP15 proteins localise specifically to the less dynamic anterior part of the subpellicular corset (Vedrenne *et al*, 2002). Over expression of the CAPs in the PCF results in the proteins being detected over the entire cytoskeleton rather than just the anterior end. This leads to organelle mispositioning and the formation of multinucleate cells and anucleate zoids. Cells also have difficulties in promoting kinetoplast segregation despite the presence of two flagella and two basal bodies (Vedrenne *et al*, 2002).

Both proteins were independently expressed in CHO-K1 and HeLa cells and in all cases colocalised with MT networks. CAP15 expression in CHO-K1 cells caused MTs to become insensitive to nocodazole treatment (a drug which inhibits MT formation)

suggesting reduced MT turnover in the presence of CAP15. Furthermore in HeLa cells both CAPs prevented MT depolymerisation in the presence of nocodazole and MT networks became resistant to cold where they would normally rapidly depolymerise. It is suggested that since CAP15 and 17 are MT stabilizers mis-localisation to the posterior end of the cell when over expressed prevents essential cytoskeletal remodelling during cytokinesis (Vedrenne *et al*, 2002).

1.10.4 GB4

In contrast to CAP17 and CAP15, the MAP GB4 is localised specifically to the posterior end of the trypanosome cell. It is proposed to form a cap structure which stabilises MTs at the posterior pole (Rindisbacher *et al*, 1993). Sequence analysis predicted that the gene for GB4 encodes a very large, highly repetitive protein, with a predicted mass of 928.3 kDa (GeneDB accession number Tb09.160.1200). Each repeat is 200 amino acids long with a calculated molecular weight of 22.6 kDa (Rindisbacher *et al*, 1993). Immunoblotting experiments using an anti-GB4 antibody identified a 28kDa protein which corresponds roughly with the size of a single repeat unit from the protein suggesting that GB4 undergoes rapid proteolytic processing *in vivo*. GB4 is conserved in all *T. brucei* subspecies and orthologs have since been identified in *T. cruzi* and *L. major* (Berriman *et al*, 2005) but it is not conserved amongst other eukaryotes. Immunofluorescence localised GB4 to a single narrowly defined spot at the posterior end of cells and in some cases a ring like structure was observed at the posterior pole of the cell. This localisation was not affected when cells were detergent extracted and so a role for GB4 in capping and stabilizing MT plus ends was suggested (Rindisbacher *et al*, 1993).

1.10.5 I/6

Immunogold electron microscopy localised the protein I/6 to the MT cross links of the subpellicular corset (Detmer *et al*, 1997). In view of this, it has been suggested that I/6 is a MT cross linker found in the PCF and BSF. I/6 is a highly repetitive protein which is recognised by host autoimmune antibodies very early after infection (Detmer *et al*, 1997). Interestingly amongst the other prominent antigens detected early in an infection are the proteins MARP1 and 2 which are also MAPs (Affolter *et al*, 1994).

1.10.6 MARP1 and MARP2

Microtubule Associated Repetitive Proteins (MARP) 1 and 2 were first identified in the salt soluble fraction when purifying *T. brucei* cytoskeletons, as a 320kDa protein (p320) confirmation of cytoskeletal association came from the p320 specific antibody which localised the protein to the corset (Schneider *et al*, 1988). They are closely related proteins which share a repetitive region that consists of a highly conserved (50% sequence identity/similarity) 38 amino acid repeat unit (Affolter *et al*, 1994). The repetitive domains of MARP1 can bind pig brain MTs which are already saturated with endogenous MAPs, this suggests that MARP-1 binds to tubulin at an alternative domain to ones used by the major brain MAPs such as tau and MAP2 (Hemphill *et al*, 1992). There is a gradient of identity between MARP 1 and 2 which is low at the N-terminus no-similarity) and increases towards the C-terminus (>95% similarity). The C-terminal domain is rich in S/T residues, contains many (putative) phosphorylation sites and can interact with MTs in a high affinity detergent resistant manner. Affolter *et al.* (1994) suggest that the globular C-terminal domain serves as an anchor which can bind to MTs; this association is regulated by phosphorylation events. The central

repeat domain then stabilizes MTs by interacting with up to 100 tubulin dimers over a 500 nm stretch along a protofilament (Affolter *et al*, 1994).

1.10.7 p15

A trypanosome specific MAP with a molecular weight of approximately 15kDa was isolated using a tubulin affinity column and named p15A. Immuno-electron microscopy localised this protein exclusively to the MTs of the corset and the p15A specific antibody co-localised with anti-tubulin antibodies (Balaban & Goldman, 1992). Sequence analysis shows that p15A contains 16 almost identical tandem repeats containing positively charged and hydrophobic amino acids. The authors suggest that the protein contains hydrophobic domains capable of interacting with phospholipids whilst the positively charged amino acids interact with tubulin. The study confirms that p15A binds tubulin and phospholipids *in vitro*, implicating it in the formation of cross-links between MTs of the corset and the plasma membrane (Rasooly & Balaban, 2002).

1.10.8 P52

A 52kDa protein co-purifies with subpellicular microtubules and was shown to bind tubulin specifically. Addition of this protein to calf brain tubulin in the presence of taxol and GTP caused MT bundling. The MTs were held together by regular cross-bridges at 7.2 nm apart which corresponds to one per tubulin dimer (Balaban *et al*, 1989). The spacing between MTs within the bundles was reminiscent of that seen between corset MTs. This MT bundling only occurred if p52 was added before tubulin had polymerised, when added to MTs already formed in the presence of

endogenous MAPs no bundling was observed. The explanation for this was that the site that p52 binds was occupied by an endogenous MAP.

1.11 Remaining questions relating to the *T. brucei* subpellicular corset and associated MAPs

The subpellicular corset is generated by an elaborate array of subpellicular microtubules and requires extensive remodelling, involving MT nucleation/outgrowth and coordinated severing/re-establishment of inter-MT cross-links during cell growth and division. Cytoskeletal remodelling is fundamentally important for trypanosome cell survival, however little is understood about how the process is orchestrated. As such, several important questions remain to be answered:

Firstly, how are subpellicular MTs nucleated? In *T. brucei* the nucleation of MTs in the corset occurs in the absence of a defined MTOC such as the APR which nucleates the subpellicular corset of apicomplexans (Morrissette & Sibley, 2002) (see section 1.3.1). γ-tubulin, (which serves as a marker for MTOCs (Scott *et al*, 1997) discussed in section 1.6.1) is detected by immunofluorescence analysis as low level fluorescence in a punctate distribution over the whole cell body (Scott *et al*, 1997). It remains to be determined whether this γ-tubulin is involved in nucleating new MTs in the corset (Scott *et al*, 1997).

Secondly, MAPs play critical roles in cytoskeletal remodelling, section 1.10 lists the MAPs currently know to associate with the *T. brucei* subpellicular corset. Little is known about the specific functions of individual MAPs or how they are targeted to MTs of the subpellicular corset.

Thirdly, some MAPs have a restricted spatial distribution within the trypanosome cell, e.g. GB4 which is found only at the posterior pole in the PCF (Rindisbacher *et al*, 1993) and CAP15/17 which are restricted to the anterior end of the cell (Vedrenne *et al*, 2002). What influences the spatial distribution of MAPs? And does the distinct spatial distribution of MAPs play a role in establishing cellular polarity?

Fourthly, why are some MAPs expressed in a stage specific manner? CAP5.5 is only expressed in the PCF and its paralogue CAP5.5*V* which carries out an analogous role in the BSF (Olego-Fernandez *et al*, 2009) Also, CAP17 and CAP15 are differentially expressed in the PCF and BSF of the parasite (Vedrenne *et al*, 2002). The selectable advantage of differential protein expression between life cycle stages remains to be understood. Oleg-Fernandez *et al*. (2009) suggest it may reflect the parasites need to fine tune protein requirements between morphologically distinct life cycle forms.

Fifthly, Do MAPs interact to form functional complex(es)? To date MAPs have been studied in isolation, as such, much remains to be uncovered about the co-ordinated roles of MAPs on the cytoskeleton. How do these interactions occur, i.e. what domains are involved? Is there a defined temporal order for association? And, what is the functional significance of these interactions?

1.12 Initial aims and objectives of this thesis

The work described in this thesis aimed to advance the current knowledge of *T. brucei* MAPs and their role(s) in cytoskeletal remodelling specifically by:

(1) Identifying additional MAPs which may function in organising the MTs of subpellicular corset (Chapter 3).

(2) Further characterising TCP86 a MAP recently identified in the McKean laboratory (Chapter 4).

(3) Investigating the function of previously published MAPs by applying RNAi techniques to proteins which were published before RNAi techniques were available (Chapter 5).

(4) To investigate interdependency between identified *T. brucei* MAPs, thus building towards a functional interactome (Chapter 5).

(5) To understand the role(s) of MAPs in remodelling the MTs of the subpellicular corset throughout the cell cycle (Chapter 6).

Chapter 2 Materials and Methods

2.1 Chemicals and Reagents

Chemicals were bought from the following suppliers:

Melford Laboratories

Agarose, dithiothreitol (DTT), ethylenediaminetetraacetic acid (EDTA), glycerol, glycine, LB agar, LB broth, piperazine-N, N-bis-2-ethanesulfonic acid (Pipes), phleomycin, potassium chloride, sodium chloride, sodium dodecyl sulphate (SDS), Tris base and isopropyl-beta-D-thiogalactopyranoside (IPTG).

Sigma-Aldrich

Ampicillin, acetic acid, ammonium persulphate (APS), acetone, acrylamide, bromophenol blue, CHAPS, C7BZ0, coomassie brilliant blue G250 and R250, chloroform, deoxyribonuclease, doxycyclin, E64d protease inhibitor, heat inactivated foetal bovine serum, hemin, hydrochloric acid, imidazole, iodoacetamide, magnesium acetate, potassium hydrogen phosphate, poly-L-lysine, phleomycin, phosphoric acid, sodium carbonate, sodium citrate, sodium hydroxide, sodium fluoride, sodium orthovanadate, tween 20, triton X-100.

Duchefa Biochemica

LB broth and LB agar

Biorad

Precision Plus (all blue) Pre-stained Protein Standards

Fluka Biochemika

Nonidet P-40 (NP-40)

Invitrogen

Blasticidin, HMI-9, SDM-79, Trizol

Fisher Scientific

Calcium acetate, ethanol, ethidium bromide, methanol, magnesium choloride, magnesium sulphate, propylene glycol, thiourea.

Fermentas

Restriction enzymes and their buffers

Agar Scientific

Gluteraldehyde

BDH

Bovine serum albumin (BSA), ethyleneglycol tetraacetic acid (EGTA) and paraformadehyde

PAA Laboratories

Foetal calf serum (FCS) and hygromycin B

GIBCO

Geneticin G418

Arcos Organics

Orange G

Formedium

Glucose

Vector Laboratories

Vectashield with 4, 6 diamidino-2-phenylindole (DAPI)

Promega

T4 DNA Ligase and buffer, pGEMT-Easy vector system

Abgene

High fidelity PCR mix

Scharfe systems

Casyton solution and Casy clean

Calibiochem

Focus protease inhibitors

2.2 Buffers and Media

2.2.1 Buffers and solutions

- Blocking buffer for slides: 1% BSA in PBS-Tween 20 (0.05%)
- Standard Blocking buffer for immunoblotting: 0.05% Tween 20 and 5% skimmed milk powder in TBS, pH7.4

- 5x DNA loading buffer: 0.25% bromophenol blue, 50mM EDTA, 46% glycerol
- EM fixative solution: 2.5% glutaraldehyde, 2% paraformadehyde and 0.1% picric acid in 100mM phosphate (pH 7.0)
- LB media: 20g LB low salt broth containing 10g tryptone, 5g yeast extract and 5g sodium chloride (Duchefa)
- PEME buffer: 100 mM Pipes 2mM EGTA, 0.1 mM EDTA and 1 mM $MgSO_4$
- PBS (10x stock): 1.5 M NaCl, 25 mM KCl, 0.1 M of Na_2HPO_4 and 17.5 mM KH_2PO_4, pH to 7.4 with HCL
- 2x SDS gel loading buffer: 100 mM Tris-HCL (pH6.8), 200 mM DTT, 4% SDS, 0.2% bromophenol blue, 20% glycerol
- SDS running buffer: 3.02g Tris, 18.8g glycine and 5ml 20% SDS per litre
- 20xSSC 3 M sodium chloride and 300 mM trisodium citrate. pH to 7.0 with HCl
- TAE buffer: 0.04M Tris-acetate, 0.001M EDTA, (pH8)
- TBE (5x stock) 0.445 M Tris, 0.445 M boric acid and 0.01 M EDTA
- TBS 10x stock 1.5 M NaCl, 25 mM KCl, 0.5 M Tris. pH to 7.4 with HCL
- TGF1: 30 Mm KAc, 100 mM RbCl, 10mM $CaCl_2$, 50 mM $MnCl_2$, 15% v/v glycerol, complete volume using dH_20 and pH to 5.8 using Acetic acid before filter sterilizing
- TGF2: 10 mM MOPs, 75 mM $CaCl_2$, 10 mM RbCl, 15% v/v glycerol, complete volume using dH_20 and pH to 6.5 using Sodium Hydroxide before filter sterilizing
- Transfer buffer for Western blotting: 25 mM Tris base, 0.2M glycine and 20% methanol
- Wash buffer for Western blotting: 0.05% Tween 20 in 1x TBS

- ZMG (Zimmerman's post fusion medium): 132 mM NaCl, 8 mM Na_2HPO_4, 0.5 mM Mg Acetate, 0.09 mM Ca acetate, pH 7.0

2.2.2 Antibiotic solutions

Table 2.1: Antibiotic solutions

Antibiotic	Working concentration (µg/ml)	Stock solution (mg/ml)
Ampicillin	100	100
Blasticidin	5	5
Doxycyclin	1	1
G418	2	2
Hygromycin	20	20
Phleomycin	7.5	7.5

2.2.3 Antibodies

Table 2.2: Primary antibodies used for western blotting

Antibody	Specificity	Animal	Dilution
KMX1	β-tubulin	Mouse IgG	1:500
TCP86 polyclonal	TCP86	Rabbit	1:1000
WCB	WCB	Mouse	1:2
CAP5.5	CAP5.5	Mouse	1:50

Table 2.3: Secondary antibodies used for western blotting

Antibody	Animal	Dilution
Anti-mouse HRP conjugate	Goat	1:80,000
Anti-rabbit HRP conjugate	Goat	1:3000

Table 2.4: Primary antibodies used for immunofluorescence

Antibody	Specificity	Animal	Dilution
ROD1	PFR	Mouse IgM	1:5
L6B3	FAZ filament	Mouse IgM	Neat
L8C4	PFR	Mouse IgG	1:10
BBA4	*T. brucei* basal bodies	Mouse IgM	1:50
YL1/2	Tyrosinated α-tubulin	Rat IgG	1:50
CAP5.5	CAP5.5	Mouse IgG	1:10
TCP86	TCP86	Mouse IgG	1:100
WCB	WCB	Mouse IgG	1:2
TAT1	α-tubulin	Mouse IgG	1:2000
NUP1	Nuclear membrane	Mouse IgG	1:200

Table 2.5: Secondary antibodies used for immunofluorescence

Antibody	Animal	Dilution
Anti-rat IgG FITC conjugate	Rabbit	1:200
Anti-mouse IgG FITC conjugate	Goat	1:200
Anti-mouse IgG Rhodamine conjugate	Goat	1:200
Anti-mouse IgM Rhodamine conjugate	Goat	1:200

2.3 Molecular Biology

2.3.1 Oligonucleotides

Primers were designed for the amplification of specific regions of *T. brucei* genes by PCR. Primers were designed to contain the relevant restriction enzyme sites for ligation into specific vectors (vector maps are shown in section 2.3.2) either p2T7-177 for RNAi (Wickstead *et al* 2002) or PET-GFP for GFP tagging (Kelly *et al* 2007).

2.3.1.1 RNAi primers

RNAi primers were designed using the website RNAIt (Redmond *et al*, 2003) and then ordered from Invitrogen. Each forward primer contains an *Xho*1 site and each reverse primer contains a *Bam*H1 site to allow for ligation into the p2T7-177 vector.

Table 2.6: Sequences of primers used for RNA interference screen of proteins identified by HMM.

Table shows the gene name, accession number, sequence of the forward and reverse primers used for PCR amplification of products and the expected size of the PCR product. Restriction sites are underlined and highlighted in bold.

Gene	Forward Primer (5'-3')	Reverse Primer (5'-3')	Fragment size (bp)
Tb927.7.3330	CAC**CTCGAG**CCACAGAACACACCGAAATG	CAC**GGATCC**CCTTCTCGTCCAACTCAAGC	414
Tb927.5.1120	CAC**CTCGAG**AGTTTGTTGCAGTTGGG	CAC**GGATCC**CCTTCAGTTCTTGCTCCAGG	423
Tb10.389.0100	CAC**CTCGAG**GGGAGTGTGTGAAGGACG	CAC**GGATCC**GCGCGATATGGGTAAGTG	483
Tb09.160.1110	CAC**CTCGAG**CTGTCACCGTGCTGAAG	CAC**GGATCC**AGCGATGAAGTTCTCGG	427
Tb09.160.1100	CAC**CTCGAG**TCCTTTTCTGGATCGAATGG	CAC**GGATCC**GTGGATAAAGGGCAACGG	445
Tb927.7.4270	CAC**CTCGAG**GTGCAACGGAATGGAAG	CAC**GGATCC**AAGGATGATTGGCATTGC	418
Tb10.70.7280	CAC**CTCGAG**GAACTTGAAAGAACGCTGGC	CAC**GGATCC**CAACTGGTGGAGGACAAGG	540
Tb09.211.1910	CAC**CTCGAG**GTTTCCAAGGGGAAATGGAT	CAC**GGATCC**ATCCCATTCATCGCTTTCAG	411
Tb927.4.2060	CAC**CTCGAG**GCAGAACTGGAGGCAGAAAC	CAC**GGATCC**TCGCCGTTAGTAGCTTCGTT	428
Tb10.70.7320	CAC**CTCGAG**GCATGAAAACGATGCTCTGA	CAC**GGATCC**TCGCCGTTAGTAGCTTCGTT	548

Table 2.7: Sequences of primers used for RNA interference of *T. brucei* MAPs

Table shows the gene name, accession number, sequence of the forward and reverse primers used for PCR amplification of products and the expected size of the PCR product. Restriction sites are underlined and highlighted in bold.

Gene	Forward Primer (5'-3')	Reverse Primer (5'-3')	Fragment size (bp)
GB4 (Tb09.160.1200)	CAC**CTCGAG**GATCGTGAAGGGTTGGAGAA	CAC**GGATCC**GATCCCAGTCATCTCCCTCA	586
GB4L (Tb927.2.5760)	CAC**CTCGAG**AGGCCTTTTACGGTGATGTG	CAC**GGATCC**GTCGCAGACGTCAAGATTCA	463
CAP5.5 (Tb927.4.3950)	CAC**CTCGAG**TACCGTGGGAAGAAGTGGAC	CAC**GGATCC**CTGGCGCTCCAGTAAAGTTC	567
MARP1/ MARP2 (Tb10.406.0560/Tb10.406.0650)	CAC**CTCGAG**TATAAGCGTGATGTGCTCCG	CAC**GGATCC**CCTGATAAACCTGTTGCGGT	597
I/6 (A and B) (Tb927.7.3440/Tb927.7.3450)	CAC**CTCGAG**GAAAAGCGGTGCTTCAAGAG	CAC**GGATCC**CTTCTTCACCATACAGCGCA	400
CAP15 (Tb11.01.3805)	CAC**CTCGAG**CGGAAGCAAAACATGGACTT	CAC**GGATCC**TAGAGGGTTTCTTCCCCCTC	286
CAP17 (Tb11.01.7880)	CAC**CTCGAG**AAACATGGACCTCTTCACCG	CAC**GGATCC**CCGCAATGTCTCCAATTTTT	229
WCB (Tb927.7.3550)	CAC**CTCGAG**GTGGTGTGCTGTGTCTGCTT	CAC**GGATCC**CGGTCTGTCAGGTTGAGTCC	505
EB1 (Tb09.160.1440)	CAC**CTCGAG**GGCCTTGGTGATGTGCTTAT	CAC**GGATCC**GGGGACTGTTGCGTAGCTCC	573

2.3.1.2 Primers designed to create GFP fusions of *T. brucei* MAPs

To epitope tag proteins at the C terminus, primer pairs were designed to amplify a 200bp product located at the C-terminus end of the ORF. This product was designed to lack a stop codon and contain the appropriate restriction sites, each forward ORF primer contains a site for *Xba*1 and the reverse ORF primer contains a site for *Xho*1. A second set of primers were designed to amplify the first 200bp of the 3' untranslated region (UTR) immediately following the ORF sequence the forward primer in this case contains an *Xho*1 site and the reverse UTR primer contains a *Bam*H1.

To fuse GFP to the N terminus a pair of primers was designed to amplify a product corresponding to the last 200bp of the 5'UTR, the forward primer in this case contains a *Hind*III restriction site and each reverse UTR primer contains an *Xho*1 site. Another primer pair was designed to amplify 200bp located at the N terminus of the ORF in this case the forward primer contains an *Xho*1 site and the reverse primer contains a site for *Spe*1. This combination of restriction sites allows the products to be cloned into the plasmid vector. The primers described above allow proteins to be endogenously tagged with GFP and expressed at near physiological levels.

Gene	C/N Terminus	UTR Primers (5'-3')	ORF Primers (5'-3')
MARP1	C	F:CGC**AAGCTT**AATATTTGAGAAGCGGTATTTTCC R: CGC**CTCGAG**CAGCACGTGCCAGTAGTCG	F:CGC**CTCGAG**CCGCGCATAGAGATTTCAAGGC R:CGC**ACTAGT**CACCTTGCGACCCGAGTGATTAACG
I/6	C	F: CGC**AAGCTT**ACGGATCTGGAATGGGTGG R: CGC**CTCGAG**CGACAAGTACGCAACCCACG	F:CGC**CTCGAG**CGCACTGGACTTGGGTAACCGGGG R:CGC**ACTAGT**CAACTCTGCCTCTTCATCTGCTTCC
CAP17	C	F:CGC**AAGCTT**TGTAATCTTTTAAAATGCTGAAGGG R: CGC**CTCGAG**CCGAGACGCTCGATTTAAGGTAC	F:CGC**CTCGAG**GGCGGAAAAGGACGTAAAGGCG R: CGC**ACTCGT**TGATGTTTGAGCGGGCCCATTCG
MARP1	N	F: CGC**CTCGAG**CCTTCCACAAGGAACTGTG R: CGC**GGATCC**CCTTCCTTTGGTATTTTTGATTCC	F: CGC**TCTAGA**ATGCCTGGCACAAAGGGATTAGAAGC R:CGC**CTCGAG**GGGATCAACATGACGAGGGCCCGTTAC
CAP15	N	F: CGC**CTCGAG**GGCCTTCTGCTTCTCCAGGC R: CGC**GGATCC**GCTGAGGCTCGTATTGAAAG	F: CGC**TCTAGA**ATGGACCGGA GACTCATCGAAATGC R:CGC**CTCGAG**GGCCTTCTGCTTCTCCAGGC
EB1	N	F: CTG**CTCGAG**CGAAATGTTGTAGGCGG R: CTG**GGATCC**CGGTAACGATAATAACGGG	F: CTG**TCTAGA**ATGGACCATCGCAATACCC R: CTG**CTCGAG**ACGGAAGCATCTGCGGAAGC
GB4	N	F: CTCT**CTAGAA**TGATGCAAGAGAGAACGTTAACG R: CTC**CTCGAG**CGCAGCATAGCGCCTCTCTCCC	F: CTC**CTCGGA**CCGAAGTTCCAAGGAGTGG R: CTC**GGATCC**GTGAAATGCCTTTACCG
GB4L	N	F: CTC**TCTAGAA**TGGGTGAAGCAGATGCGCC R: CTC**CTCGAG**CCAACCTCACGAACGATGC	F: CTC**CTCGAG**GCCCCTCATCGTAGATTTTAG R: CTC**GGATCC**GCCAGATCCCCCAGAAAACTG

Table 2.8: Sequences for primers used for cloning into pETGFPblast.

Table shows the gene, whether primers are designed to tag the N or the C terminus, the sequence of primers and the restriction sites incorporated into the design (shown in bold.

2.3.1.3 Sequencing primers

For sequencing PCR products that had been cloned into pGEMT-Easy vector M13F and M13R primers were used.

M13 Forward 5'-3' CGCCAGGGTTTTCCCAGTCACGAC

M13 Reverse 5'-3' TCACACAGGAAACAGCTATGAC

2.3.2 Plasmids

All PCR products were first cloned into Promega's pGEMT-Easy vector (Figure 2.1) this allowed for sequencing before being sub-cloning into either p2T7-177 (Figure 2.2) or PEnT6B-G (Figure 2.3).

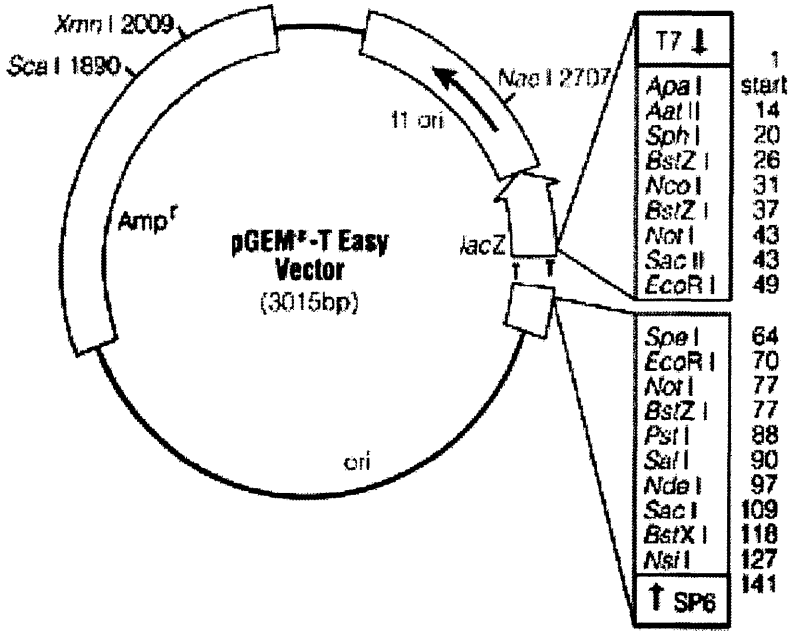

Figure 2.1 The pGEMT-Easy cloning vector

(Promega technical manual 2009)

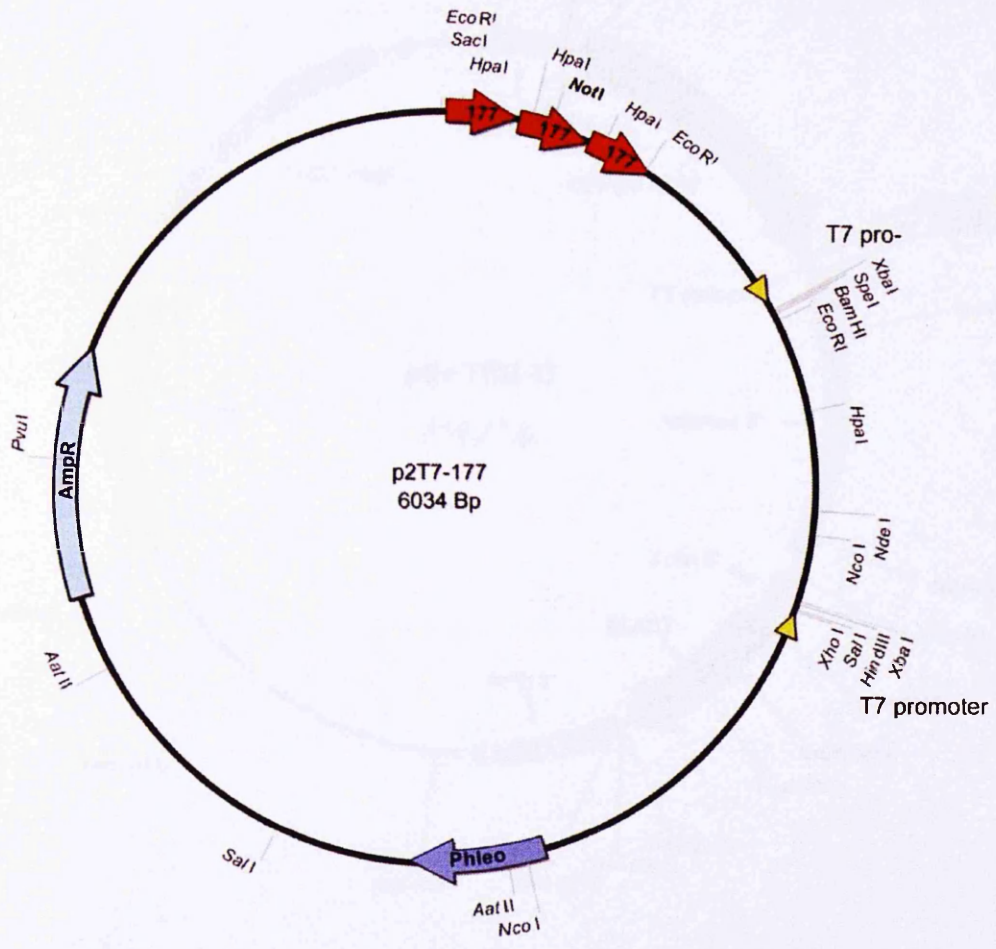

Figure 2.2 The P2T7-177 cloning vector

(Wickstead *et al* 2002)

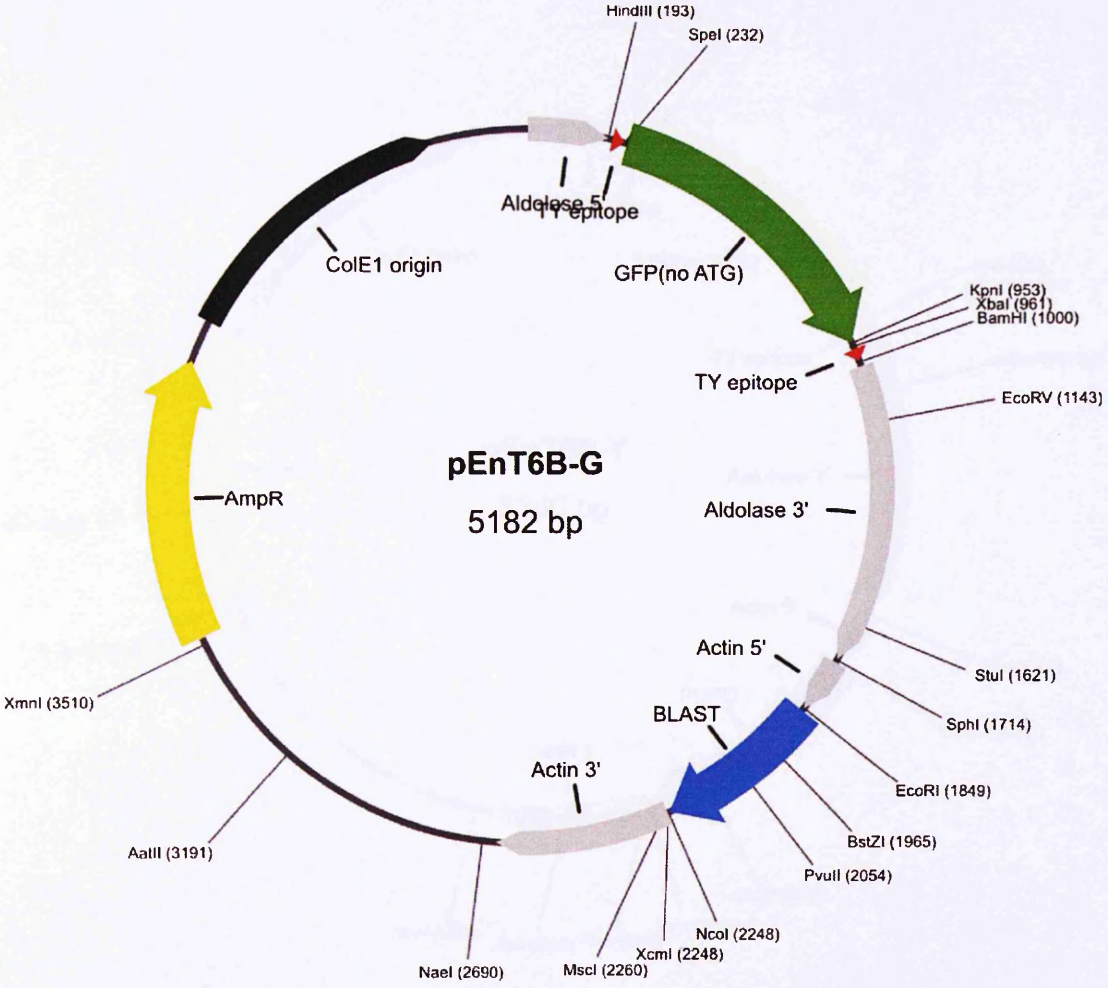

Figure 2.3 The PEnT6B-G cloning vector used for endogenous GFP tagging

(Kelly *et al.* 2007)

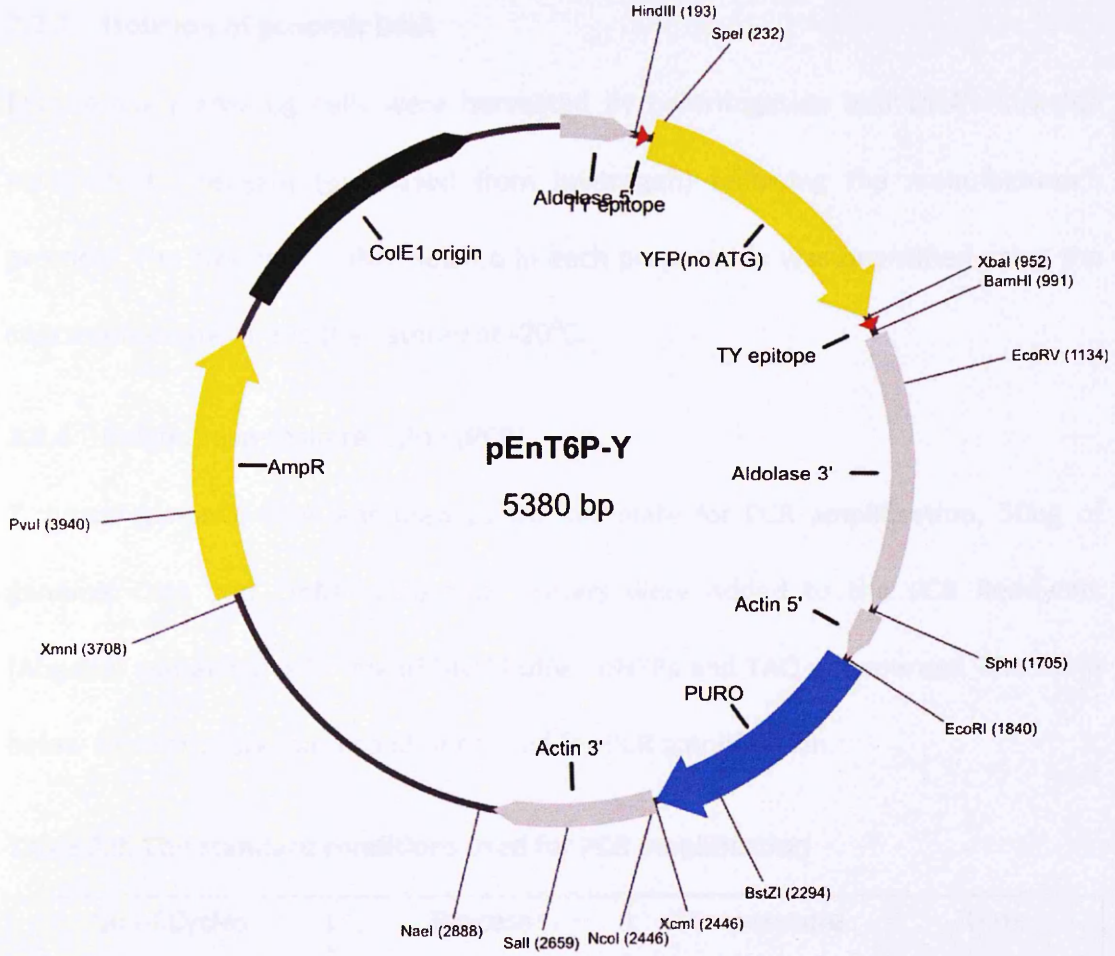

Figure 2.4 The PEnT6P-Y cloning vector used for endogenous YFP tagging

(Kelly *et al.* 2007)

2.3.3 Isolation of genomic DNA

Exponentially growing cells were harvested by centrifugation and DNA extracted using TRIZOL reagent (purchased from Invitrogen) following the manufacturer's protocol. The amount of DNA isolated in each preparation was quantified using the spectrophotometer and then stored at -20°C.

2.3.4 Polymerase chain reaction (PCR)

T. brucei genomic DNA was used as the template for PCR amplification, 50ng of genomic DNA and 1mM of specific primers were added to the PCR Reddymix (Abgene) containing a 2x mix of Mg^{2+} buffer, dNTPs and TAQ polymerase. The table below shows the standard conditions used for PCR amplification.

Table 2.9. The standard conditions used for PCR amplification

No of Cycles	Process	Temperature	Time
1	Initial Denaturation	94°C	2 minutes
25	Denaturation	94°C	30 seconds
	Annealing	55°C	30 seconds
	Extension	72°C	30 seconds
1	Final Extension	72°C	5 minutes

The annealing temperature was altered at times to temperatures ranging from 50 to 62°C to allow for the different melting temperature of the primers thus allowing optimal amplification of different genes.

2.3.5 Agarose Gel Electrophoresis

PCR products were loaded onto 0.8-2% (w/v) agarose gels made up in TAE buffer containing 0.5 μg/ml ethidium bromide, the percentage of the gel was altered

according to the expected size of the DNA fragment. Also loaded onto the gel was 5µl of Trackit 1Kb DNA ladder (Promega). Gels were run at 70V for 40 minutes and visualised using a UV transilluminator.

2.3.6 Purification of PCR products

PCR products were then purified using a PCR purification kit (Qiagen) according to the manufacturer's instructions and quantified by absorbance at 260 and 280 nm using a UV spectrophotometer (Eppendorf).

2.3.7 Ligation of DNA inserts into pGEMT-Easy

All PCR products were ligated into pGEMT-Easy vector for sequencing before sub-cloning into the desired final vector. The purified PCR product was mixed with 50ng of pGEMT-Easy in a 3:1 insert: vector ratio as directed by the Promega technical handbook the reaction also contained T4 DNA ligase and 2 x ligase buffer. A control was always prepared in exactly the same way where the PCR product was replaced with water. The reactions were left for one hour at room temperature before being transformed into DH5α competent cells.

2.3.8 Preparation of competent bacterial cells for transformations

All transformations were carried out using DH5α *Escherichia coli* cells; chemically competent cells were prepared as follows. -80°C glycerol stocks were streaked onto an LB agar plate and grown overnight at 37°C. Individual colonies were grown overnight in 5mls LB broth at 37°C in a shaking incubator at 225RPM, 50mls of LB broth was inoculated with 1ml of this overnight culture and incubated at 37°C shaking at 225RPM measuring the OD600 at regular intervals until the reading was between 0.4-0.5. The cells were transferred to pre-chilled falcon tubes, incubated on

ice for 10 minutes and centrifuged at 2000g for 5 minutes at 4°C on the Sanyo Harrier 18/80 centrifuge using a 43124-141 swing bucket rotor. Cells were then resuspended in 20mls of ice cold TFG1 buffer (see list of buffers) and incubated on ice for 15 minutes before harvesting at 2000g for 5 minutes at 4°C. Cells were resuspended gently in 2mls of ice cold TFG2 and incubated on ice for between 15 and 60 minutes. Then cells were aliquoted into 1.5ml tubes and snap frozen in liquid nitrogen.

2.3.9 Bacterial transformation and screening of clones containing plasmid DNA

Transformation of DH5α cells with DNA was carried out by gently mixing ligation reactions with an aliquot of competent cells then incubating on ice for 30 minutes. Cells were heat shocked at 42°C for 40 seconds, then recovered on ice for 2 minutes. 800µl of LB broth was added and the cells were incubated at 37°C and for 90 minutes shaking at 225RPM, before being spread onto agar plates containing ampicillin for plasmid selection and incubated overnight at 37°C.

Colonies were selected from the agar plates and grown overnight at 37°C in LB broth containing Ampicillin. The bacterial culture was harvested by centrifugation and plasmid DNA was isolated using Qiagen plasmid purification kits based on sodium acetate precipitation of plasmid DNA, in accordance with manufacturers' instructions. To check for the presence of the insert restriction digests were carried out.

2.3.10 Restriction digests

Restriction digests were set up with appropriate restriction enzymes following manufacturer's instructions for optimal conditions. Digests were loaded onto a 1%

(w/v) agarose gel made up in TAE buffer containing 0.5 µg/ml ethidium bromide and visualised using a UV transilluminator.

2.3.11 Sequencing

DNA from colonies containing the correct sized DNA fragment was sent for sequencing at Geneservice (Nottingham) using M13 forward and reverse primers.

2.3.12 Gel extraction of DNA fragments

DNA fragments were separated on a 1% gel by agarose gel electrophoresis; the gel was stained with 0.5 µg/ml ethidium bromide solution for 10 minutes. The desired fragments were excised with single-edged razor blades (SLS) whilst observing the gel on a UV transilluminator. DNA was purified using a gel extraction kit (Qiagen) according to the manufacturers' instructions. Once purified the DNA concentration was quantified by absorbance at 260 and 280nm using a UV spectrophotometer (Eppendorf) before being ligated into the desired vector.

2.3.13 Ligation into p2T7-177

The purified DNA insert was added to a reaction mix containing 50ng of linearised vector, rapid ligase buffer and T4 DNA ligase, a 3:1 ratio of insert: vector was always used. This reaction was mixed and incubated for 5 minutes on the bench before being transformed into *E.coli* DH5α competent cells as described earlier.

2.3.14 Ligation into pEnT6B-G

Both the purified UTR and ORF sequences were simultaneously ligated into the pEnT6B-G vector in a 3-way reaction (see Figure 2.5). The orientation and the specificity of the overhangs ensured that both sequences were ligated into the vector in the correct orientation.

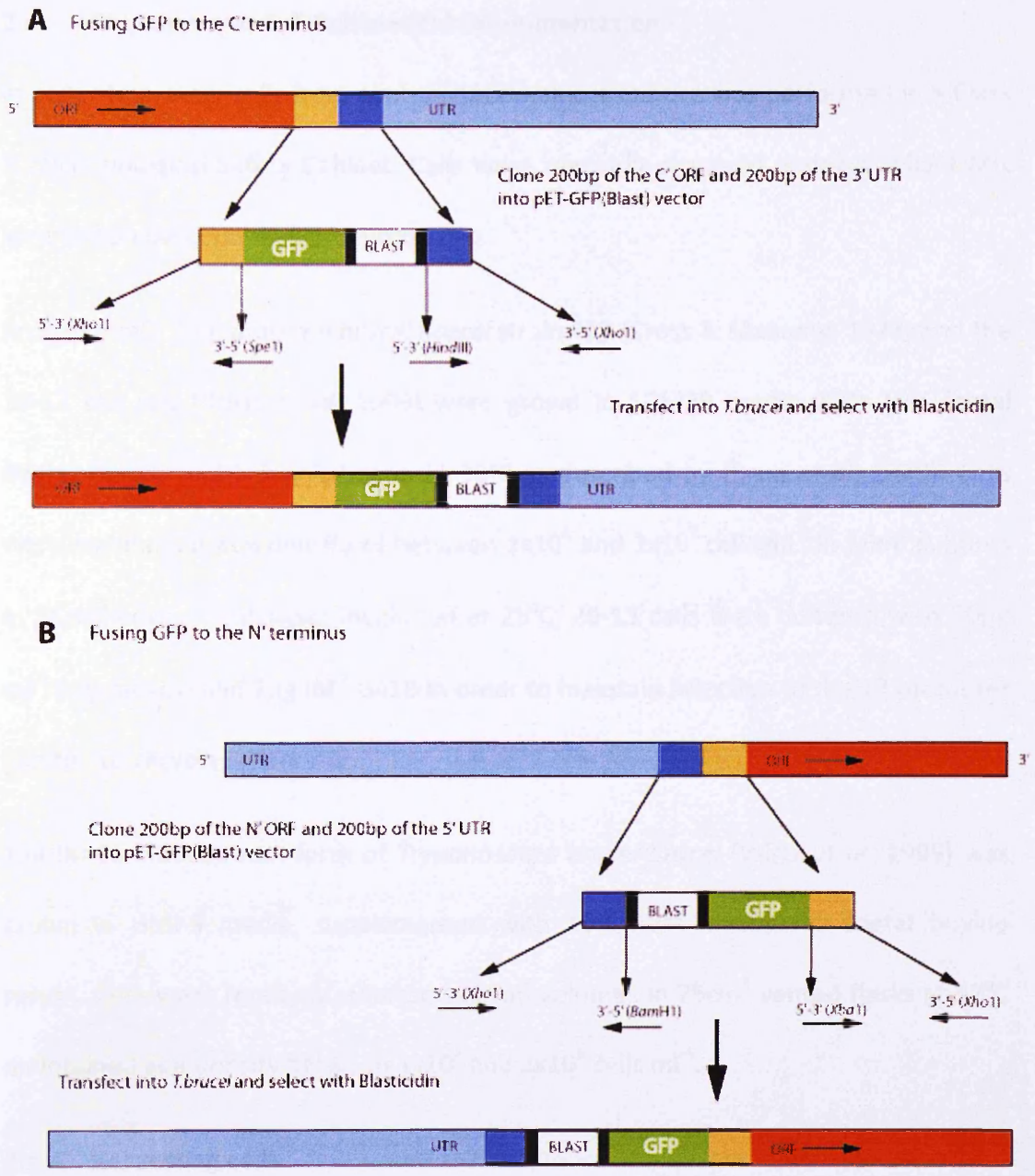

Figure 2.5 Diagram showing insertion of PEnT6B-GFP at either the N or C terminus

Position of the gene is shown in orange and the untranslated region is shown in blue, restriction sites used for ligation are shown.

2.4 Trypanosome Cell Culture and Experimentation

In order to protect cells from contamination all cell culture was performed in a Class II Microbiological Safety Cabinet. Cells were regularly observed under a Leica DMIL inverted phase contrast light microscope.

Procyclic cells *Trypanosoma brucei brucei* strain 427 (Cross & Manning, 1973) and the 29-13 cell line (Wirtz *et al*, 1999) were grown in SDM79 media with 10% foetal bovine serum and 7.5mg/L hemin at 28°C as described by (Brun *et al*, 1979). Cells were maintained at a density of between $1x10^6$ and $1x10^7$ cells ml^{-1} in 10ml cultures in $25cm^3$ closed vent flasks incubated at 28°C, 29-13 cells were cultured with 20μg ml^{-1} hygromycin and 2μg ml^{-1} G418 in order to maintain selection of the T7 promoter and the tetracycine repressor.

The 90-13 bloodstream form of *Trypanosoma brucei brucei* (Wirtz *et al*, 1999) was grown in HMI-9 media, supplemented with 15% heat inactivated foetal bovine serum. Cells were routinely cultured in 10ml volumes in $25cm^3$ vented flasks at 37°C maintained at a density between $1x10^4$ and $2x10^6$ cells ml^{-1}.

2.4.1 Harvesting cells

Cells were harvested by centrifugation at 2000g for 10 minutes using a Sanyo Harrier 18/80 centrifuge with a 43124-141 swing bucket rotor, unless other conditions are specified.

2.4.2 Freezing and storage

Samples could be stored by freezing at -80°C for up to a month, for long term storage cell lines were transferred from -80°C storage into liquid nitrogen. A 'healthy' 10ml

mid-log culture (approx $2x10^6$ cells ml^{-1}) was harvested by centrifugation, all but 0.5ml of the supernatant was removed, the cell pellet was resuspended and 0.5ml of freezing mix (consisting of the relevant media containing 14% glycerol) was added (total 1ml). The culture was then transferred to a cryotube (Corning) and frozen at -80°C. For longer term storage cells were transferred to liquid nitrogen after a period of a month at -80°C.

2.4.3 Cell counting

Trypanosome cells were counted using the Casy cell counter (Schärfe systems), which gives an accurate count of cell number, cell size and percentage of viable cells. 20µl of cell culture was added to 10mls Casyton solution in a Casy cup; this was mixed by inversion and placed under the capillary for measurement. Cells were also counted using a haemocytometer on the Leica DMIL inverted phase contrast light microscope by settling 10µl of cells onto a haemocytometer slide.

2.4.4 Linearisation of plasmid DNA

3-10µg of plasmid containing the desired insert was digested using the enzyme *Not*1 (p2T7177, pEnT6B-Y) or *Xho1* (pEnT6B-G) for between 90 minutes and 4 hours at 37°C, to check that linearization was complete, 1µl of the restriction digest was run on a 1% agarose gel containing ethidium bromide. Digested DNA was purified using a Qiagen PCR purification kit according to the manufacturers' instructions and eluted from the purification column in 50µl of ddH_20.

2.4.5 Transfection of trypanosomes

In order to protect cells from contamination this procedure was performed in a class II microbiological safety cabinet with exception for the electroporation which took

place outside of the microbiological safety cabinet but within sealed and sterile cuvettes.

T. brucei (29-13 or 90-13) cells were grown to a density of $5x10^6$ cells ml^{-1} for PCF and $2x10^6$ cells ml^{-1} for BSF and harvested by centrifugation. The supernatant was carefully removed and approximately $3x10^7$ cells resuspended in 0.5mls of ZMG for each transfection. 3-10μg of linearised DNA in 50μl of sterile ddH_20 was added to a 0.4cm electroporation cuvette; 0.5mls of cells were transferred into each electroporation cuvette and mixed carefully with the DNA (or 50μl of ddH_20 as a negative control). Cells were subjected to one round of 3 unipolar pulses of 1700V for 100μs, 200ms interval in the ECM 830 Electro Square Porator (BTX). The cells were then placed in a flask containing pre-warmed media, PCF were recovered in 10ml of SDM-79 and BSF were recovered in 25ml of HMI-9 overnight. A negative control was always set up; 50μl of sterile ddH_20 was added to a cuvette in place of linearised DNA. This control was included to ensure that there was sufficient selection of trypanosomes containing the drug resistance marker.

The following day cells were put onto antibiotic selection using relevant antibiotics (20μg/ml hygromycin, 7.5μg/ml phleomycin and 2μg/ml G418 for RNAi cell lines or 5μg/ml blasticidin for GFP cell lines and 5μg/ml puromycin). Antibiotic resistant cells became confluent after approximately 2 weeks, and resistant cultures were expanded until they were healthy and ready for experimentation.

2.4.6 Induction of RNA interference

T. brucei p2T7-177 cell lines were screened for a phenotype by adding doxycycline to a final concentration of 1μg ml^{-1}, to induce production of dsRNA and RNA

interference. PCF cultures were diluted back to $1x10^6$ ml^{-1} and fresh doxycycline was added daily, BSF cultures were diluted back to $1x10^5$ ml^{-1}.

2.4.7 Growth curves

A healthy mid-log culture was counted using the Casy cell counter and 20 mls of cells at a concentration of 1x 10^6 cells ml^{-1} for PCF and $1x10^5$ ml^{-1} for BSF prepared. This was split to form two 10ml cultures which were counted again to ensure each was at 1x 10^6 cells ml^{-1} (PCF) $1x10^5$ ml^{-1} (BSF). 1µg ml^{-1} of doxycycline was added to one of these cultures to start the expression of the inducible vector, the other remained un-induced. Cultures were diluted to $1x10^6$ (PCF) or $1x10^5$ (BSF) cells ml^{-1} every 24 hours. Cells were counted using the Casy© counter at the same time the next day and subsequently diluted to 1x 10^6 (PCF) or $1x10^5$ (BSF) cells ml^{-1}. Growth curves were maintained for a maximum of 10 days.

2.4.8 Preparation of cells for flow cytometry

Between 5x 10^6 and 1x 10^7 cells per sample to be analysed were harvested then washed in 1XPBS and the centrifugation step was repeated. The supernatant was removed and the cells were then resuspended in 10 ml of 70% methanol in PBS. Cells were fixed for either 2 hours at room temperature or overnight at 4˚C (at this point cells could be stored for up to 4 weeks at 4˚C). Immediately prior to analysis cells were harvested at 1500g for 10 minutes at 4˚C then the supernatant was carefully removed by pipetting to avoid disturbing the pellet. The cells were washed in 5ml PBS and centrifuged at 1500g for 10 minutes at 4˚C before removing the supernatant carefully. The remaining pellet was resuspended in 2mls of PBS containing propidium iodide and RNAse both at 10µg/ml. Samples were incubated for 1 hour at 37˚C

before being analysed on the BD Biosciences FACsCanto II flow cytometer using the BDFACsDiva software.

2.5 Microscopy

2.5.1 Preparing slides for immunofluorescence - procyclic form trypanosomes

To prepare slides for immunofluorescence 1ml of a healthy mid-log procyclic trypanosome culture was centrifuged at 800g for 5 minutes, the pellet was resuspended in 1ml of PBS and centrifuged at 800g for 5 minutes the supernatant was removed and cells were resuspended in PBS to a concentration of approximately $8x10^6$ cells ml^{-1} 50µl of this suspension was placed onto an uncoated glass slide until the cells settled (approx 5 minutes); note that for Delta Vision microscopy cells were settled onto glass cover slips. Slides or cover slips were put into a copling jar containing ice-cold methanol for 20 minutes at –20˚C, for storage slides could be placed in methanol and placed in the –20˚C freezer.

2.5.2 Preparing slides for immunofluorescence - bloodstream form trypanosomes

Star Frost silan coated slides (Knittel Glaser) prepared immediately before use by treatment with 5% glutaradehyde in ddH_20 for 15 minutes before being washed twice in ddH_20 and air dried. 1ml of a healthy mid-log BSF trypanosome culture was centrifuged at 800g for 5 minutes; the pellet was resuspended in 1ml of PBS and centrifuged at 800g for 5 minutes then the supernatant was removed, the cells were washed in this way a total of three times to ensure all media was removed. Cells were resuspended in PBS to a concentration of approximately $8x10^6$ cells ml^{-1} and 50µl of this suspension was placed onto the pre-treated slide until the cells settled (approx 10 minutes). Slides were put into a copling jar containing ice-cold methanol

for 20 minutes at –20°C, for storage slides could be placed in methanol and placed in the –20°C freezer.

To prepare PCF or BSF cytoskeletons, once cells had settled onto the glass slide, PBS containing 0.05% NP-40 was applied to the slide for between 30-60 seconds before the slide was placed in methanol.

2.5.3 Immunofluorescence

Following incubation in methanol slides were rehydrated in PBS for 30 minutes and then placed in a humidity chamber. A blocking solution was applied for 1 hour; the primary antibody was diluted in blocking buffer and applied for 1 hour at room temperature. Slides were washed in wash buffer 3 times for 5 minutes. Following this the cells were exposed to the secondary antibody diluted in blocking buffer for 1 hour at room temperature. Slides were washed 3 times for 5 minutes in wash buffer then mounted using Vectashield mounting medium (Vector laboratories) with DAPI. Slides were sealed with nail varnish and then viewed on either the Leica DM RXA2 epifluorescence microscope with fluorescence (Leica Imaging) or the DeltaVision core epifluorescence microscope (Applied Precision). All images were captured using a charged coupled device (CCD) camera and the brightness/contrast adjustments were made using Adobe Photoshop© (Adobe Systems Inc.)

2.5.4 Double-labelling with antibodies of the same isotype

Following methanol fixation and rehydration in PBS as described earlier, slides were incubated with the first primary antibody (targeting the smaller or less abundant protein first) for 30 minutes, then washed 5 times for 5 minutes in PBS. Slides were then incubated with the FITC conjugated secondary antibody diluted in PBS for 30

minutes. Slides were washed again 5 times for 5 minutes in PBS then incubated with a neat non-relevant monoclonal antibody of the same isotype as the two antibodies of interest. PBS washes were repeated then the cells were exposed to the second primary antibody diluted in PBS, for 30 minutes. The 5 minute washes in PBS were repeated and the slides were then incubated with the TRITC conjugated secondary antibody for 30 minutes, the washes were repeated for a final time before the slides were mounted using Vectashield mounting medium (Vector laboratories) with DAPI. Slides were sealed with nail varnish and then viewed on the Leica DM RXA2 light microscope with fluorescence (Leica Imaging). All images were taken using a charged coupled device (CCD) camera and brightness/contrast adjustments made using Adobe Photoshop© (Adobe Systems Inc.).

2.5.5 Scanning electron microscopy

10mls trypanosomes at a density of ~2-6 x10^6 were centrifuged at 500g for 5 minutes and washed in 10mls PBS. Live cells were allowed to settle for 10 minutes on 13mm glass coverslips positioned in a 24 well plate. Cells were fixed using 1ml EM fixative solution. After fixation the samples were rinsed three times with dd$H_2$0 and dehydrated through a series containing 10, 20, 30, 50, 70, 90 and 95% ethanol for 15 minutes each time, then placed in 100% ethanol 3 times for 30 minutes each time. Samples were critically point-dried and after drying the coverslips were mounted onto stubs and sputter coated with a 20nm thick layer of gold. Alternatively, cells were fixed by adding 0.5 ml of 25% glutaraldehyde to 5 ml of cells in culture media at ambient temperature. The cells were fixed for 3-16 hours, washed twice with PBS and aliquots deposited on clean 13 mm silane (3 aminopropyltriethoxysilane)-coated coverslips (Buechi & Baechi, 1979). The cells were allowed 30 minutes to attach to

the glass after which they were rinsed three times with ddH_20, dehydrated through a series of 10, 20, 30, 50, 70, 90 and 95% ethanol for 15 minutes each time and then critically point-dried. After sputter coating with gold the samples were examined in a JOEL JSM 6390 scanning electron microscope. (Sample preparation was performed by Mike Shaw, University of Oxford).

2.5.6 Transmission electron microscopy

For TEM analysis cells were initially fixed by adding 1ml of 25% glutaraldehyde to 9ml of cells in culture media at ambient temperature. After 5 minutes the cells were gently centrifuged (500g for 3 minutes) and then transferred into EM fixative. The cells were centrifuged at 16000g in an Eppendorf microcentrifuge at room temperature. Fresh fixative was added and fixation continued for 2-24 hours at 4°C. The pellet was washed in 200 mM phosphate buffer before the samples were post-fixed in 1% osmium in 100mM phosphate (pH 7.0) for 1.5 hours at 4°C, the pellet was then washed five times in ddH_20 and en bloc stained with 2% aqueous uranyl acetate for 2 hours at 4°C in the dark. The pellet was then washed briefly in ddH_20 and dehydrated through 30, 50, 70 and 90% ethanol before being placed in 100% ethanol three times for 30 minutes each time. Samples were treated with propylene oxide twice for 15 minutes each time and then embedded in Agar 100 epoxy resin (Agar Scientific). This was achieved by treatment with a 2:1 mix of propylene oxide:resin for 1 hour then treatment with 1:1 propylene oxide:resin for 1 hour and finally treatment with a 1:2 mix of propylene oxide:resin for 1 hour. Resin blocks were polymerised for 12 -24 hours at 60-70°C then ultrathin (~70 nm thick) sections were cut. These sections were double stained with uranyl acetate and lead citrate and

examined in a FEI Technai 12 electron microscope. (Sample preparation was performed by Mike Shaw, University of Oxford).

2.5.7 Protein preparation from *T. brucei* cultures

2.5.7.1 Whole cell preparation

Cells were centrifuged and washed in PBS. Cells were centrifuged again and the pellet resuspended in hot (100°C) SDS loading buffer (50 µl of SDS loading buffer per $2x10^7$ cells). The sample was then heated in a heat block (100°C) for 5 minutes before being loaded onto an acrylamide gel or stored at -80°C.

2.5.7.2 Cytoskeleton preparation

Cells were harvested as described above however once the cells had been washed in PBS, the pellet was resuspended in PEME containing 1% NP40. Following centrifugation at 1500g for 10 minutes and removal of the supernatant (containing the soluble fraction), the pellet was resupended in hot SDS loading buffer as described above.

2.5.7.3 Acetone precipitation for protein concentration

The supernatant resulting from the detergent extracted cells contains detergent soluble trypanosome proteins were concentrated by acetone precipitation. Acetone was cooled to -20°C and 4x the sample volume added directly to the sample and mixed thoroughly before being incubated for 60 minutes at -20°C then centrifuged at maximum speed in a microcentrifuge for 10 minutes. The supernatant was discarded and the tube left open under a fume hood to allow any remaining acetone to evaporate. The remaining pellet was resuspended in SDS loading buffer.

2.5.8 Polyacrylamide Gel Electrophoresis (PAGE)

Protein samples were separated on polyacrylamide gels using the BioRad minigel system, using either 10%, 12% or 15% polyacrylamide minigels. Protein samples were heated for 5 minutes in a heat block (100°C) before pulse centrifuging then loaded alongside Precision Protein standards (Biorad). Electrophoresis was carried out at room temperature at 120V.

2.5.9 Western blotting

Protein samples separated by SDS-PAGE were transferred from the polyacrylamide gel onto Hybond P nitrocellulose membrane (Amersham Biosciences) for 40 minutes at 10V in transfer buffer using a semi-dry transfer cell (Biorad). The membrane was then washed in ddH_2O before being incubated on a shaker in blocking buffer for 1 hour. Membranes were then incubated with the primary antibody (diluted accordingly in blocking buffer see Table 2.2) for 2 hours at room temperature before being washed twice for 5 minutes in TBS. Secondary antibody (diluted in blocking buffer see Table 2.3) was washed over the membrane for 1 hour at room temperature and the membrane was then washed three more times with TBS. Results were visualised using the ECL-Plus western blotting detection reagent (Amersham Biosciences) and on the Compact x4 developer (Xograph Imaging Systems) using Hyperfilm ECL (Amersham Biosciences).

2.6 Bioinformatics

2.6.1 Hidden markov model

An iterative profile-based search was performed using the *Trypanosoma brucei* GB4 (Accession number Tb09.160.1200) predicted protein sequence. To initiate this

search, the protein sequence was converted to a hidden-Markov model using the hmmer program (Eddy *et al* 1998) built using the '-s' option which permits the identification of the single best local hit in any given sequence. This model was then used to search a set of 32 eukaryotic genomes listed in Table 2.10. The resultant hits were filtered based on an e-value threshold of $1X10^{-10}$. The region of each sequence which was identified by the HMM was extracted and aligned using MAFFT E-INS-i (Katoh *et al* 2005) and columns within the alignment that contained more than 50% gaps were removed to prevent acid insertions biasing the models. These gap-parsed alignments were then further parsed for with > 95% identity to any other sequence within the alignment. This step was done to prevent biasing of the HMM towards any particular group of sequences which may be overrepresented in the alignment due to the presence of paralogues. This gap and identity-parsed alignment was then used to generate the HMM for the next round of searches. This search was terminated after 8 iterations when no further hits passing the e-value threshold could be identified.

To increase the diversity of the motif multiple local hits to any given sequence were permitted by taking the final alignment from the above search procedure and using it to build a HMM using the '-f' option. Using this method we identified 196 examples of this motif each passing an e-value threshold of $1X10^{-10}$ after three iterations.

Table 2.10: Genomes searched by HMM

Organism	Source	Version	Web reference
Arabidopsis thaliana	TIGR	-	www.arabidopsis.org/
Aureococcus anophagefferens	JGI	-	http://www.jgi.doe.gov/
Batrachochytrium dendrobatidis	Broad institute	-	http://www.broad.mit.edu/
Caenorhabditis elegans	C. elegans Sequencing Consortium	WS150	www.wormbase.org/
Chlamydomonas reinhardtii	JGI	v3.0	www.chlamy.org/
Coprinus cinereus	Broad institute	1	http://www.broad.mit.edu/
Cryptosporidium parvum	MRC Laboratory of Molecular Biology	3.3	cryptodb.org/cryptodb/
Cyanidioschyzon merolae	National Institute of Genetics, Japan	-	merolae.biol.s.u-tokyo.ac.jp/
Dictyostelium discoideum	The Dictyostelium discoideum Sequencing Consortium	Primary	dictybase.org/
Drosophila melanogaster	The FlyBase Consortium/Berkeley Drosophila Genome Project/Celera Genomics	BDGP4.2	www.ebi.ac.uk/ensembl/
Emiliania Huxleyi	JGI	-	http://www.jgi.doe.gov/
Giardia lamblia	Marine Biological Laboratory	-	www.mbl.edu/Giardia/
Homo sapiens	ENSEMBL	NCBI 36	www.ebi.ac.uk/ensembl/
Leishmania major	Friedlin Consortium	v5	www.genedb.org/
Micromonas pusilla	Micromonas Genome Consortium	-	http://www.jgi.doe.gov/
Naegleria gruberi	JGI	V1.0	http://www.jgi.doe.gov/
Phaeodactylum tricornutum	JGI	V2.0	http://www.jgi.doe.gov/
Phycomyces blakesleeanus	JGI	-	http://www.jgi.doe.gov/
Phytophthora ramorum	JGI	-	http://www.jgi.doe.gov/
Physcomitrella patens	JGI	-	http://www.jgi.doe.gov/
Plasmodium falciparum	geneDB	3D7 v2.1.1	www.genedb.org/
Saccharomyces cerevisiae	ENSEMBL	SGD1	www.ebi.ac.uk/ensembl/
Selaginella moellendorffii	JGI	-	http://www.jgi.doe.gov/
Tetrahymena thermophila	TGD	Predic-tions_Aug_2004	www.ciliate.org/
Thalassiosira pseudonana	JGI	V3.0	http://www.jgi.doe.gov/
Theileria annulata	Sanger Institute	-	www.genedb.org/
Toxoplasma gondii	TIGR	V4.1	http://www.toxodb.org/
Trichoplax adhaerens	JGI	-	http://www.jgi.doe.gov/
Trichomonas vaginalis	TIGR	20050331	http://www.tigr.org/
Trypanosoma brucei	TIGR & Sanger Institute	v4	www.genedb.org/
Ustilago maydis	Broad institute, Bayer CropScience, Exelixis	-	http://www.broad.mit.edu/

Chapter 3 An RNAi screen identifies a protein essential for cytokinesis

3.1 Introduction

Trypanosome cortex protein 86 (TCP86) is a novel MAP recently identified in the McKean laboratory. TCP86 associates with subpellicular corset MTs over the entire cell body, and RNAi mediated ablation causes a cytokinetic defect where asymmetrical division leads to the production of non-viable anucleate zoids and multinucleate progeny (Shawcross, 2008). Bioinformatic analysis shows that TCP86 shares a region of homology with GB4 (Shawcross, 2008) a *T. brucei* MAP which also localises to the subpellicular MTs (Rindisbacher *et al*, 1993). To investigate if the sequence homology between these MAPs is shared by any other proteins a Hidden Markov model (HMM) was built based upon this region of homologous sequence between GB4 and TCP86; for the purpose of this thesis this sequence has been named the GB4 motif. The HMM was employed to search 32 eukaryotic genomes and consequently identified thirty six proteins which possess the GB4 motif, all of these proteins were from trypanosomatid species, including 17 from *T. brucei.* To establish whether the GB4 motif proteins play a role in cellular morphogenesis an RNAi screen was carried out in *T. brucei* procyclic form (PCF) cells. RNAi mediated ablation of one of the proteins identified by the HMM, which we have designated GB4-Like (GB4L), causes a severe defect in cytokinesis. The phenotype observed upon RNAi mediated ablation of GB4L was further characterised and is described in detail in this chapter.

Additionally, this chapter provides evidence that TCP86 and GB4L are essential for viability in the BSF, and that RNAi depletion of TCP86 and GB4L in this life cycle form leads to phenotypes similar to those seen in the PCF.

3.2 TCP86 shares homology with the microtubule associated protein GB4

Homology between TCP86 and GB4 was first identified in a BlastP search which defined two regions of homology between the proteins (Shawcross, 2008). Figure 3.1 shows that one of these regions is approximately 350 amino acids in length and is positioned close to the N-terminus in both GB4 and TCP86. This region shares 21% identity and 41% similarity and has homology with dynein heavy chain proteins from many different organisms, including *T. brucei, C. elegans* and *Homo sapiens*. The second region is a shorter sequence of 110 amino acids found once in TCP86 close to the C-terminus. This sequence is repeated 38 times in GB4 and as such has been named the GB4 motif. The GB4 motif has 25% identity and 45% similarity to the 110 amino acid sequence found in TCP86 and similar sequences of amino acids are found in a number of kinesin or putative kinesin-like proteins. When the GB4 motif amino acid sequence was analysed by BlastP, all hits with an e-value of less than 1 were trypanosomatid; this suggests that the GB4 motif is specific to trypanosomes.

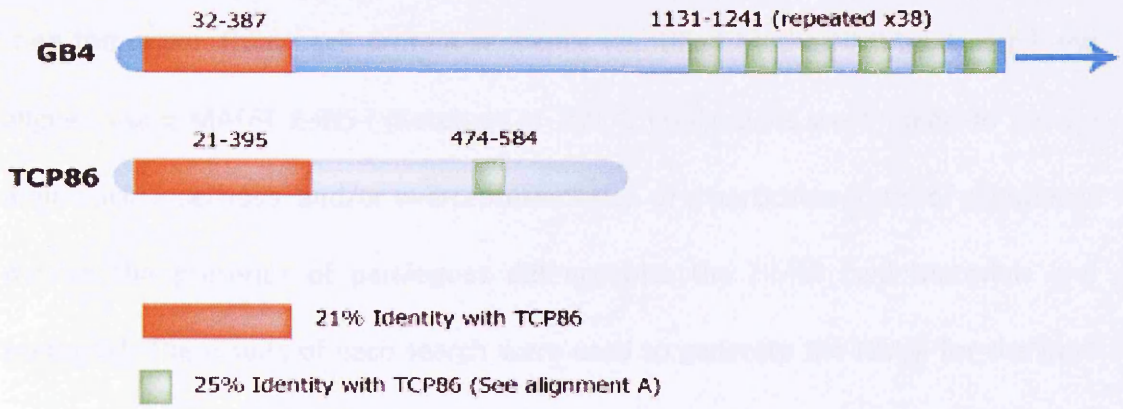

Figure 3.1 The microtubule binding proteins GB4 and TCP86 share regions of homology.

A cartoon showing the regions in both proteins where amino acid sequence is conserved (Adapted from Shawcross, (2008).

3.3 Generation of a Hidden Markov Model (HMM) for the GB4 motif

To establish if this sequence is trypanosomatid specific and identify any further proteins which share the GB4 motif the amino acid sequence was used to initiate an iterative profile based search. This bioinformatic analysis was carried out in collaboration with Dr Steven Kelly and Dr Bill Wickstead (Sir William Dunn School of Pathology, University of Oxford). The GB4 motif sequence was converted to a Hidden Markov model (HMM) using the HMMER program (Eddy *et al* 1998) this model was designed to identify the single best local hit in any given sequence. The HMM was used to search 32 eukaryotic genomes including, *Arabidopsis thaliana, C. elegans, Drosophila melanogaster, H. sapiens, S. cerevisiae, L. major* and *T. brucei* genomes; for the full list of genomes see Materials and Methods

.

The results from this search were filtered, based on an e-value threshold of $1x10^{-10}$, then the region from each protein sequence identified by the HMM extracted and aligned using MAFFT E-INS-i (Katoh *et al* 2005). Precautions were taken to ensure amino acid insertions, and/or overrepresentation of a particular group of sequences due to the presence of paralogues did not bias the HMM (see Materials and Methods). The results of each search were used to generate the HMM for the next round of searches and therefore refine the motif, after 8 iterations the search was terminated as no further hits passed the set e-value threshold. This initial HMM search generated a list of 36 proteins all of which were found in either *T. brucei* or *L. major,* there were no hits from other organisms which passed the e-value threshold; this result indicated the identification a trypanosomatid specific motif (to view the alignment file for the 36 identified proteins see supplementary Figure 8.1).

To assess if any of the proteins identified by this search possess multiple motifs the final motif from the original search was taken and a new HMM built which allowed multiple local hits in any given sequence. This method identified 206 examples of the motif, all within the same 36 proteins identified in the first screen (to view these alignments see supplementary Figure 8.2). The results of this expanded HMM did not include any non-trypanosomatid sequences thus confirming the trypanosomatid-specific nature of this motif.

3.4 Conservation of amino acids in the GB4 motif

In order to visualise the result of the HMM screen the 206 examples of the GB4 motif were aligned and a sequence logo was plotted (Figure 3.2) this graphically represents the conservation of amino acids in each position (or column) of the multiple

alignment. The total stack height represents the relative entropy and the height of each letter in the stack is proportional to its frequency at the position. Apart from a very highly conserved tryptophan residue at position 15 of the motif the sequence logo shows that the 196 motifs identified by the HMM are quite variable. The motif has a hydrophobic nature, there are numerous hydrophobic residues such as valine, leucine, and phenylalanine which are reasonably well conserved along the length of the sequence. Conservation of amino acids is reduced near the end of the sequence from amino acid 91 onwards so the logo was trimmed down to the tyrosine at position 90. The trimmed logo is shown in Figure 8.3. The HMM was run again using this logo, and the same 36 proteins were identified.

The 36 proteins identified by the HMM are listed in Table 3.1; if the protein is annotated in GeneDB it is highlighted (yellow –*L. major*, blue-*T. brucei*) and the name is given in brackets. Also shown is the number of repeats identified in each protein; the majority of the proteins have a single copy of the motif. However, 77 repeats were identified in GB4, this is more than the 38 repeats originally identified by BlastP; these additions are truncated versions of the repeat.

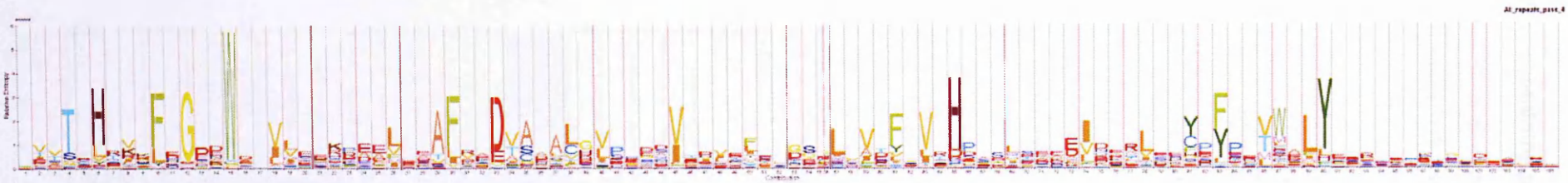

Figure 3.2 The GB4 motif amino acid sequence logo

Sequence logo constructed using the alignment of the 196 motifs identified by the HMM search, each column represents the position of each amino acid in the motif. The height of each letter represents the degree of conservation; tall letters show positions of highly conserved amino acids within the motif. The GB4 motif has a number of highly conserved residues interspersed by divergent regions. The motif is particularly degenerate in the final 16 amino acid positions at the C-terminus.

Table 3.1 GB4 Motif containing proteins identified by the HMM search

Accession numbers from GeneDB of the proteins identified and the number of motifs found within each of the proteins. Proteins which are annotated on GeneDB are highlighted *L. major* (yellow) *T. brucei* (blue) and listed with their name.

Accession Number	Number of motifs
Tb09.160.1200 (GB4)	77
LmjF33.3070	34
LmjF26.1950 (GB4)	21
Tb927.2.5760	17
Tb927.5.1120	10
LmjF34.2530	5
LmjF33.3060	5
Tb927.7.3330	4
LmjF18.0770	3
LmjF22.1320	2
Tb927.4.3740 (FAZ1)	2
LmjF34.0690	2
Tb09.211.1910	1
Tb927.4.2060	1
LmjF14.1120 (Kinesin k39)	1
LmjF09.0800 (Kinetoplast associated protein -like protein)_	1
LmjF21.1240	1
Tb10.70.7320	1
LmjF26.1990	1
LmjF22.1330	1
LmjF26.2160	1
Tb09.160.1160 (TCP86)	1
Tb09.160.1180 (TCP66)	1
LmjF26.1980	1
Tb10.70.7280	1
LmjF26.1960	1
Tb10.389.0100	1
Tb09.160.1110	1
Tb09.160.1100	1
LmjF25.1060	1
LmjF34.2570	1
LmjF34.0680	1
Tb927.7.4270	1
Tb927.2.5860	1
Tb927.2.5870	1
LmjF21.1220	1

Of the seven GB4 motif proteins annotated in GeneDB, three are from *L. major*. These include; (1) The GB4 homolog (LmjF26.1950) with 21 repeats of the motif, (2) A putative kinesin (K39, accession number LmjF14.1120) which has a single GB4 motif, (note that the function of this protein as a kinesin has not been experimentally proven but is inferred from its homology to K39 in *L. chagasi*), (3) An uncharacterised protein, LmjF09.0800 which is annotated as a hypothetical kinetoplast associated protein due to its homology to an annotated protein in *T. cruzi* (GeneDB).

As expected the GB4 motif is identified in the *T. brucei* proteins TCP86 (Tb09.11.1160) and a closely related protein, TCP66 (Tb09.160.1180); a shorter isoform of TCP86 previously described by Shawcross (2008). Additionally the HMM identified 2 copies of the GB4 motif in the protein FAZ1 (Tb927.4.3740); a highly repetitive protein required for the assembly of the FAZ. A complete GB4 motif is located towards the C terminus of the protein and a more degenerate 50 amino acid sequence close to the N terminus (see Figure 3.4). Upon RNAi mediated ablation of FAZ1 in the PCF, FAZ assembly is compromised and flagellum detachment occurs, resulting in cytokinetic defects (Vaughan *et al*, 2008). All the other proteins identified by the HMM search are novel and uncharacterised.

Figure 3.3 and Figure 3.4 are schematic diagrams showing the relative length of each GB4 motif containing protein (grey line) and the position of the GB4 motifs (purple boxes). In many cases proteins contain a truncated version of the motif; these are represented by incomplete boxes.

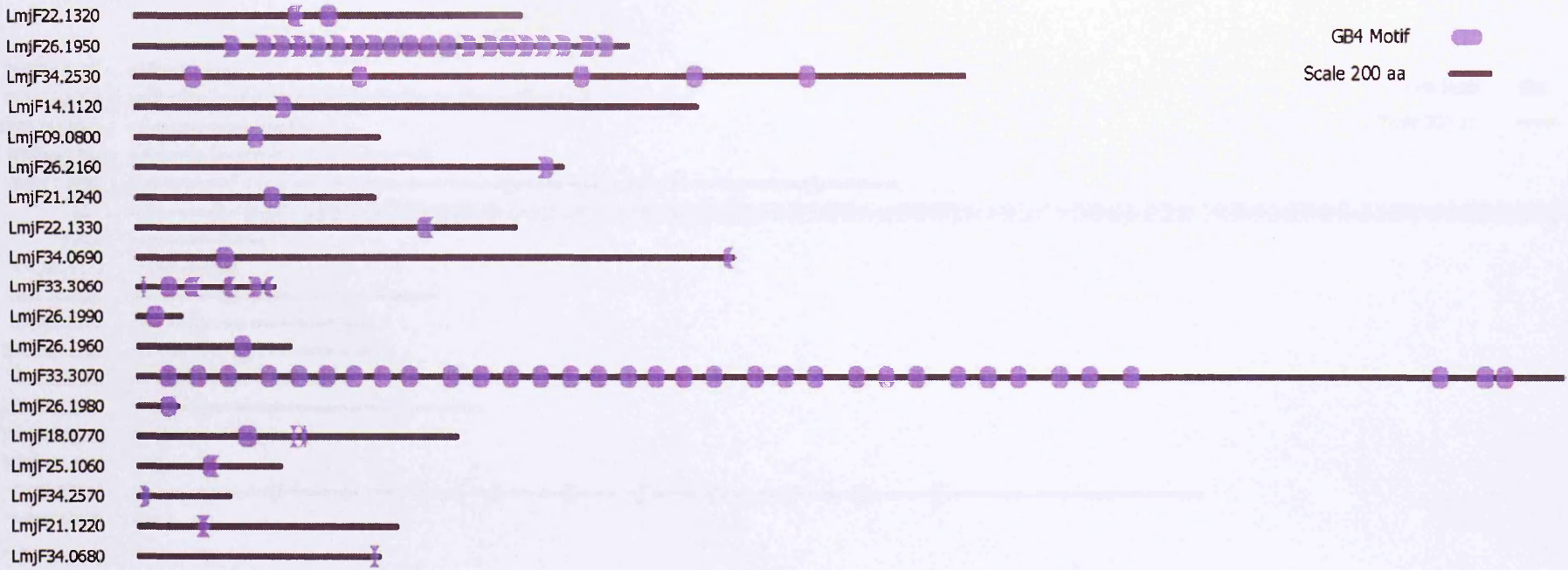

Figure 3.3 Position of the GB4 Motifs in *L. major* proteins identified by HMM

The 19 proteins which were identified by the HMM in *L major*, GB4 motif represented in purple, protein length shown in grey, GeneDB accession numbers for each protein on the left. Some proteins contain multiple repeats of the sequence; in many cases the motif is truncated (incomplete purple boxes).

Figure 3.4 Position of GB4 Motifs in *T. brucei* proteins identified HMM

The 17 proteins identified by the HMM in *T. brucei* including GB4 and TCP86, the GB4 motif is represented in purple, protein length shown in grey, GeneDB accession numbers or names of proteins on the left. Some proteins contain multiple repeats of the sequence; in many cases the motif is truncated (incomplete purple boxes).

Many of the GB4 motif-containing proteins are novel and so their function(s) have yet to be established. The identification of conserved domains (in addition to the GB4 motif) may point towards the role of these proteins and so all proteins were screened against the Pfam database using a program designed by Dr Bill Wickstead (Sir William Dunn School of Pathology, University of Oxford). The results of this search are shown in Figure 3.5 (*L. major* proteins) and in Figure 3.6 (*T. brucei* proteins).

Additional conserved domains with diverse functions were identified in 7 out of the 36 GB4 motif containing proteins. In *L. major*, 4 of the 19 proteins have additional domains defined by Pfam (Figure 3.5). Two proteins contain multiple repeats of a CAST (cytomatrix at the active zone (CAZ)- associated structural protein) domain which is implicated in determining the site of synaptic vesicle fusion in mammals. Intriguingly one of these CAST domain containing proteins (LmjF34.0690) also contains an ERM domain (ezrin, moesin, and radixin domain) which is found in a number of cytoskeletal associated proteins and is believed to function in cytoskeleton-plasma membrane cross-linking. This suggests that Lmj34.0690 may function as a MT binding protein which functions at the subpellicular corset-plasma membrane interface. The same protein also has a Cenp-F_leu_zip domain, Cenp-F is a MT-binding protein that associates with the centromere-kinetochore complex. LmjF14.1120 is the putative kinesin (K39) described earlier, this search identified a kinesin domain, shared by MT-based kinesin motors as well as multiple repeats of the CAST domain. Finally, LmjF21.1240 contains two truncated WD40 domains, repeats of this domain often serve as a platform for protein-protein interactions and are found in proteins with a variety of functions (Li & Roberts, 2001).

In *T. brucei* 3 proteins have additional conserved domains Tb10.70.7320 has two truncated WD40 repeats and Tb927.5.1120 has 10 regularly spaced truncated repeats of the GB4 motif each repeat is associated with a truncated phage fiber-2 domain. Tb927.7.4270 has a Tweety domain close to the C-terminus; Tweety domains are associated with transmembrane proteins (Campbell *et al*, 2000).

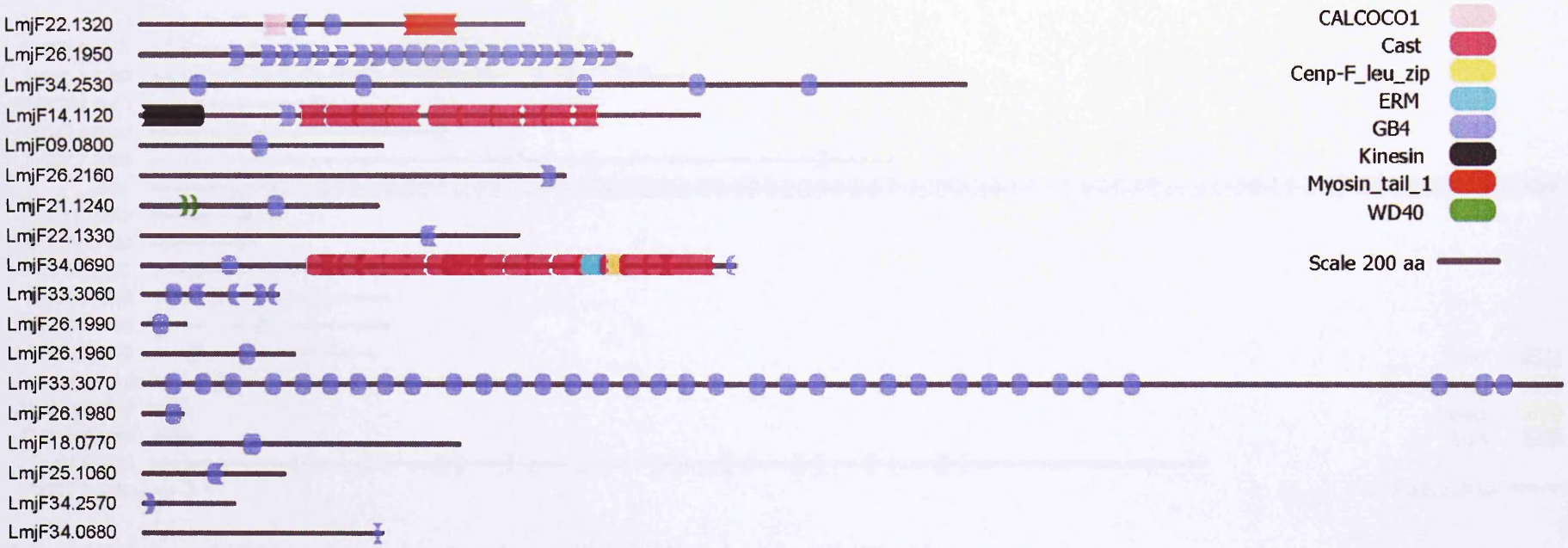

Figure 3.5 *L. major* GB4 motif proteins showing additional domains identified by Pfam

GB4 motif shown in purple other motifs identified by the Pfam database are marked in different colours, see the key. **CALCOCO1** - Calcium binding and coiled-coil domain, **Cast** - a domain belonging to a family of proteins involved in determining the site of synaptic vesicle fusion, **Cenp-F_leu_zip**-a domain containing Leucine-rich repeats found in the microtubule binding kinetochore protein Cenp-F. **ERM** (ezrin, radixin, moesin) domain - found in a number of cytoskeletal associated proteins involved in localising proteins to the plasma membrane, **Kinesin** - present in microtubule-based kinesin motors, **Myosin_tail_1** - found in the heavy chain of myosin motor protein. **WD40** - a domain found in proteins with a wide variety of functions, WD40 repeats often serve as platforms for protein-protein interactions. There is no obvious correlation between GB4 motif and other known domains.

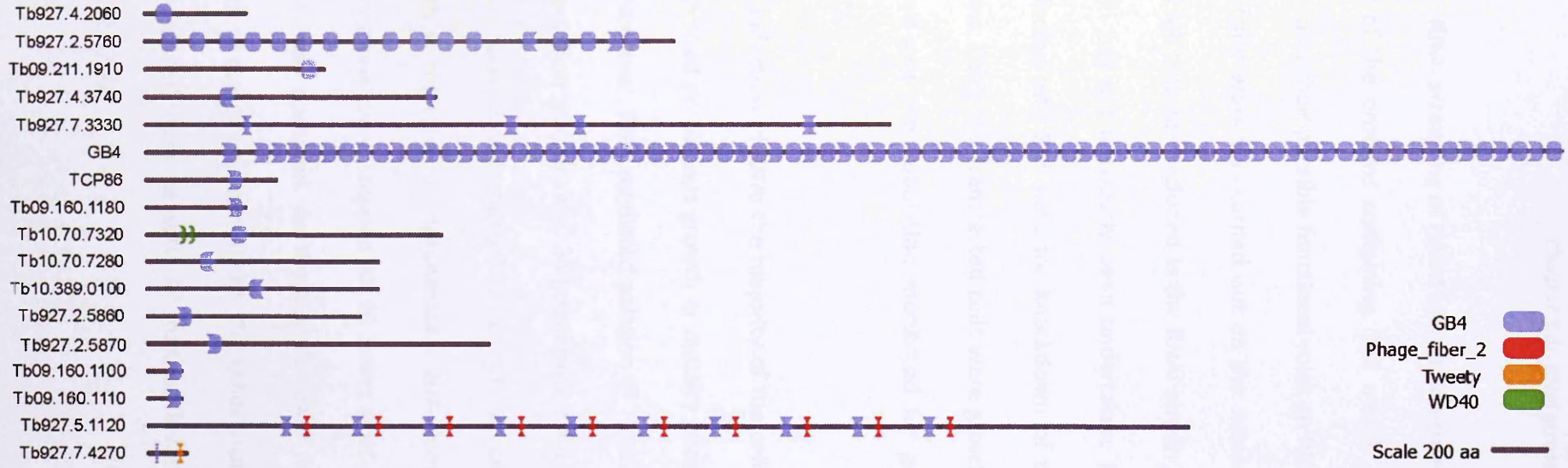

Figure 3.6 *T. brucei* GB4 motif proteins showing additional domains identified by Pfam

Only three proteins have additional domains none of these are complete, GB4 motifs are shown in purple, Pfam domains are shown in red, orange and green (see key). **Phage_fiber_2** - a repeat that is found in the tail fibres of phage, **Tweety** - found in transmembrane proteins, **WD40** - a domain found in proteins with a wide variety of functions, WD40 repeats often serve as platforms for protein-protein interactions. There is no correlation between the occurrence of the GB4 motif and the other domains identified by Pfam.

3.5 RNAi screening of HMM identified proteins

Many of the proteins containing GB4 motifs are uncharacterised and so to gain insight into their possible functional roles an RNAi screen was undertaken in the PCF (no further work was carried out on the subset of proteins identified in *L. major*). GB4 itself was also included in the RNAi screen as functional characterisation of this protein has not previously been undertaken. RNAi constructs were prepared and transfected into PCF cells for knockdown of the specific GB4 domain containing proteins. Once the transfected cells were growing well on drug selection, RNAi was induced and the population monitored for growth, morphology and/or motility defects.

Upon induction of RNAi the majority of the cell lines (including GB4) grew normally and showed no obvious growth or motility phenotypes (see growth curves in Figure 3.7). However, RNAi mediated ablation of Tb927.2.5760 led to a significant decrease in population growth rate. 24 hours post induction cell doubling time is reduced to approximately 50% compared to the non-induced control. After 72 hours population growth is reduced to approximately 20% compared to the non-induced control. Observations were stopped at 96 hours post induction as no further population growth was observed. As these preliminary results suggested that there was no growth or motility phenotype for the other proteins included in the screen, analysis of these cell lines ceased. All further investigation focused on characterising Tb927.2.5760.

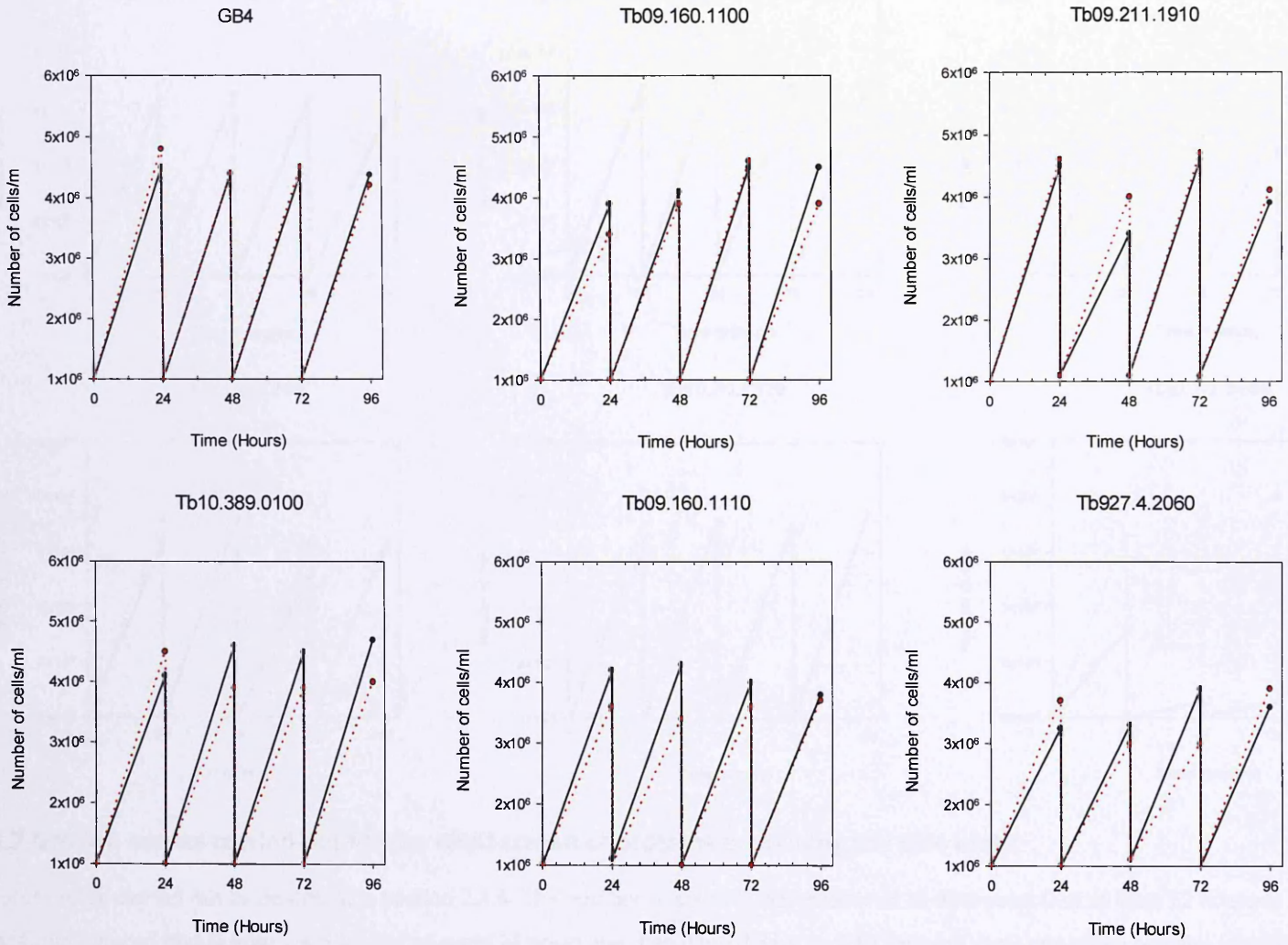
GB4
Tb09.160.1100
Tb09.211.1910
Tb10.389.0100
Tb09.160.1110
Tb927.4.2060
Number of cells/ml
Time (Hours)
6x10⁶
5x10⁶
4x10⁶
3x10⁶
2x10⁶
1x10⁶
0
24
48
72
96

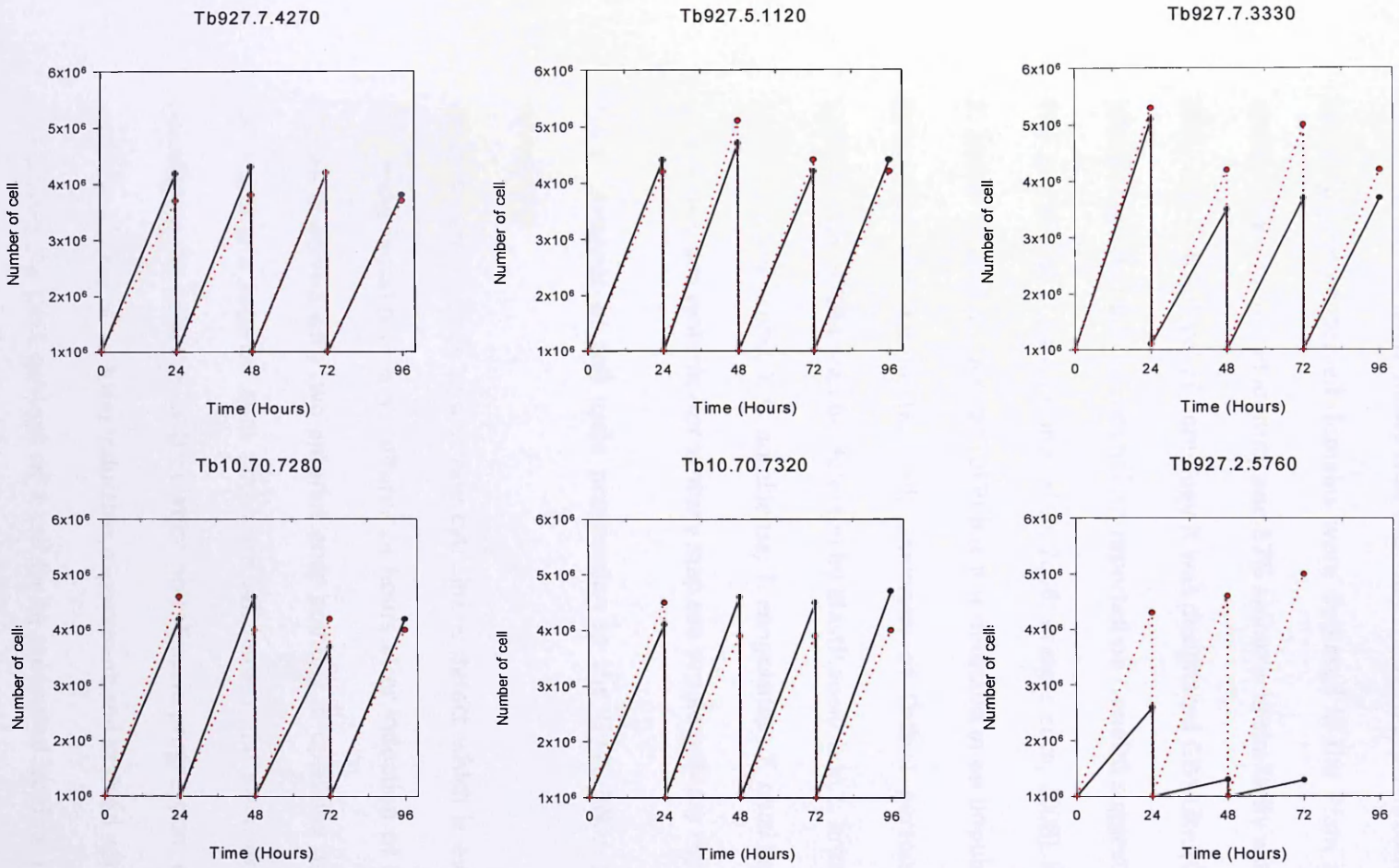

Figure 3.7 Growth curves carried out for the RNAi screen of proteins containing the GB4 motif

Growth curves were carried out as described in section 2.4.6. The number of cells/ml was measured at time point 0 to at least 72 hours as indicated on graphs. Induced and non-induced populations were measured every 24 hours and then diluted back to $1x10^6$ cells/ml. Only one of the proteins identified gave a phenotype (Tb927.2.5760), surprisingly GB4 ablation did not affect growth.

3.6 Further investigation of Tb927.2.5760 (GB4L)

Bioinformatic analysis shows that the Tb927.2.5760 protein contains 17 GB4 motifs; no additional conserved domains were detected in the Pfam screen. This protein shares 23% amino acid identity and 37% amino acid similarity with the *T. brucei* MAP GB4; due to this level of homology it was designated GB4-Like (GB4L). Gb4L is a 330 kDa protein that proteomic analysis reported on GeneDB suggests is expressed in the PCF and BSF of *T. brucei* (Jones *et al*, 2006; Bridges *et al*, 2008). It is not found in the *T. brucei* flagella proteome (TbFP) but it is detected in an unpublished PCF *T. brucei* cytoskeleton proteome (K. Gull, University of Oxford personal communication). Orthologues of GB4L can be detected by BlastP analysis in *L. braziliensis, L. infantum, L. major, L. mexicana, T. b. gambiense, T. congolense , T. cruzi* and *T. vivax*; all of the GB4L genes are syntenic (for synteny map see supplementary Figure 8.5).

3.6.1 Analysis of cell cycle progression in the GB4L RNAi cell line using flow cytometry

GB4L depletion leads to a severe cytokinetic defect which is evident when directly observing induced cells in culture. 24 hours after induction of RNAi, aberrant cells can be observed with two anterior ends pointing in opposing directions; other cells have multiple anterior ends and large cell bodies and swim erratically. To further investigate the effect of GB4L ablation on cell cycle progression, cells were harvested over the course of an RNAi induction experiment and stained with propidium iodide; this allows the DNA content of a cell to be measured by flow cytometry. The flow cytometer was set to measure the DNA content of 10,000 cells from the following cultures, non-induced population of cells (which would act as a control to determine

the normal distribution of cells before GB4L ablation), and 12, 24 and 48 hours post RNAi induction. The results of this analysis are shown in Figure 3.8.

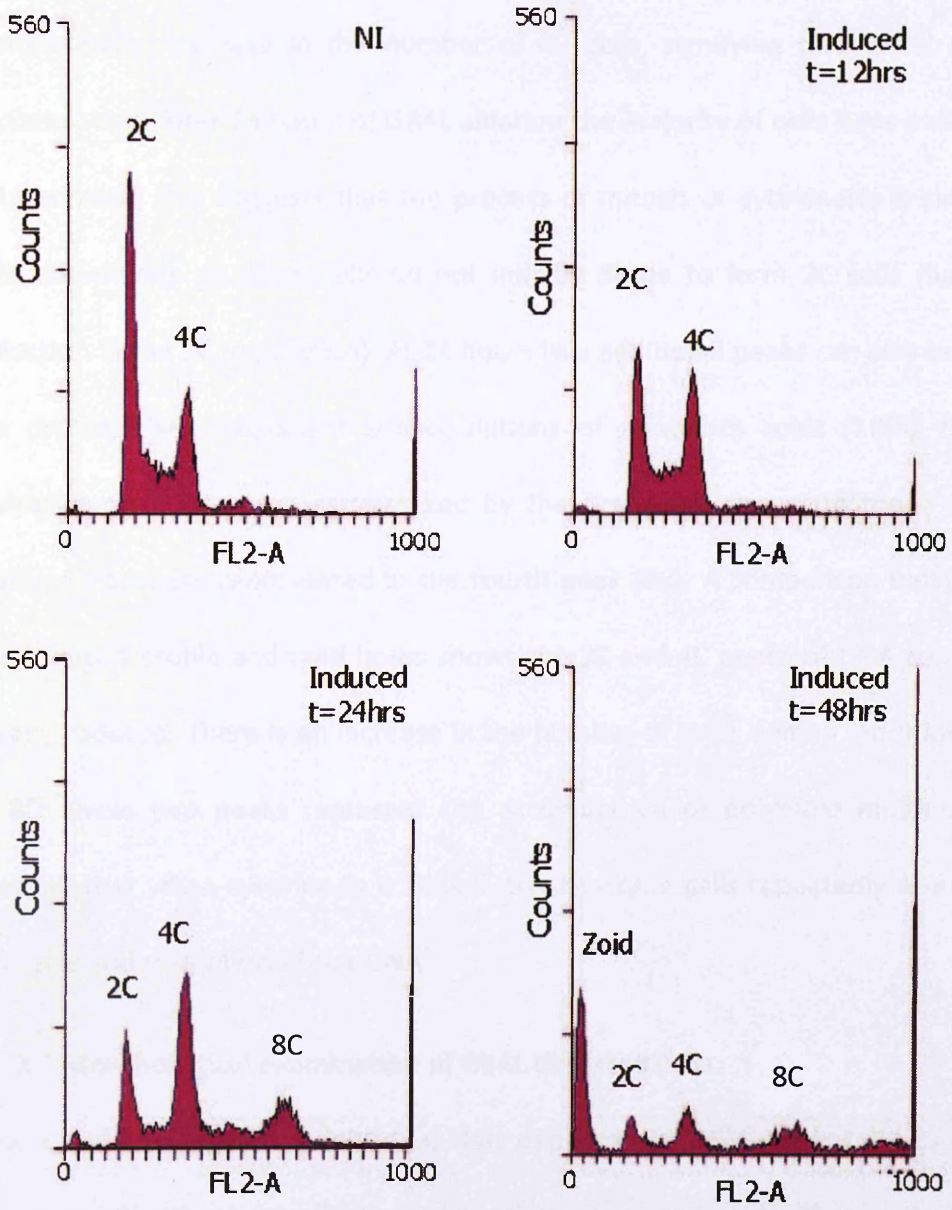

Figure 3.8 Flow cytometry analysis of the GB4L RNAi cell line

Cells from a GB4L RNAi induction time course were harvested and stained with propidium iodide in preparation for analysis by flow cytometry as described in section 2.4.8. Changes in ploidy were recorded over time, non-induced control (NI), 12, 24 and 48 hours post induction. The *x* axis shows fluorescence intensity in the FL2-A channel (propidium iodide). Ploidy of peaks is indicated. Analysis shows an increase in 2K2N cells and the development of subpopulations of anucleate zoids and multinucleates at 24 and 48 hours.

In the non-induced control cells, the flow cytometry profile shows that the majority of cells have a 2C (1K1N) DNA content, the second peak (4C) represents the 2K2N cells. After 12 hours of induction the number of 2C cells is reduced and there is a corresponding increase in the number of 4C cells, signifying that 2K2N cells are accumulating. After 24 hours of GB4L ablation the majority of cells have a 4C (2K2N) DNA content, this suggests that the process of mitosis or cytokinesis is stalled. 4C cells accumulate as these cells do not initially divide to form 2C cells (hence the reduction in the 2C population). At 24 hours two additional peaks can also be seen in the profile, these represent subpopulations of anucleate zoids (1K0N cell) and multinucleates. Zoids are represented by the first peak closest to the y axis and multinucleates are represented in the fourth peak (8C). A comparison between the non-induced profile and t=48 hours shows the 2C and 4C peaks of DNA content are greatly reduced. There is an increase in the number of zoids and an additional peak at 8C; these two peaks represent the accumulation of polyploid multinucleates, showing that when cytokinesis is stalled, trypanosome cells repeatedly re-enter the cell cycle and re-replicate their DNA.

3.6.2 Morphological examination of GB4L depleted cells

Flow cytometry analysis established that depletion of GB4L leads to a cytokinetic defect resulting in the production of multinucleates and zoids. These effects occur rapidly upon RNAi induction as the phenotype can be detected in live culture as early as 12 hours after the addition of doxycycline to the media. To investigate the consequences of GB4L depletion at a cellular level, cells were harvested every 12 hours over the course of an RNAi induction experiment and settled on to slides. Cell morphology was examined and the number, and intracellular positioning, of nuclei

and kinetoplasts assessed by DAPI staining. Cells were also examined by indirect immunofluorescence using antibodies against the basal bodies, FAZ and PFR to identify if there were any problems in organelle positioning.

3.6.3 Visualisation of kinetoplast and nuclear configuration using DAPI

Figure 3.9 shows the results of DAPI counts carried out on non-induced cells and cells from cultures at 24 and 48 hours post RNAi induction. As with the flow cytometry data, the most abundant sub-population of cells in the non-induced control are the 1K1N cells (which make up 80% of the population) this is followed by 2K1N (12%) and finally 2K2N (7%) at this time point there were no multinucleate or anucleate zoids observed. After 24 hours of GB4L depletion the observed cell types changed with the population of 2K2N cells increasing dramatically, consistent with the flow cytometry data shown in Figure 3.8. The largest sub-population is the 2K2N cells (47%) there are fewer 1K1N cells (19%) and there are additional sub-populations of multinucleates and zoids (6 and 18% respectively). The significant increase in the 2K2N sub-population, and the reduction in the number of cells at G1 (1K1N), points towards a stall in cytokinesis. After 48 hours of GB4L depletion the population of 1K1N shows a 100-fold reduction (from 80% in the non-induced culture to 0.8% after 48 hours), showing that very few cells successfully complete cytokinesis to produce viable daughter cells. At this time point 65% of the populations are multinucleated cells and 33% are zoids.

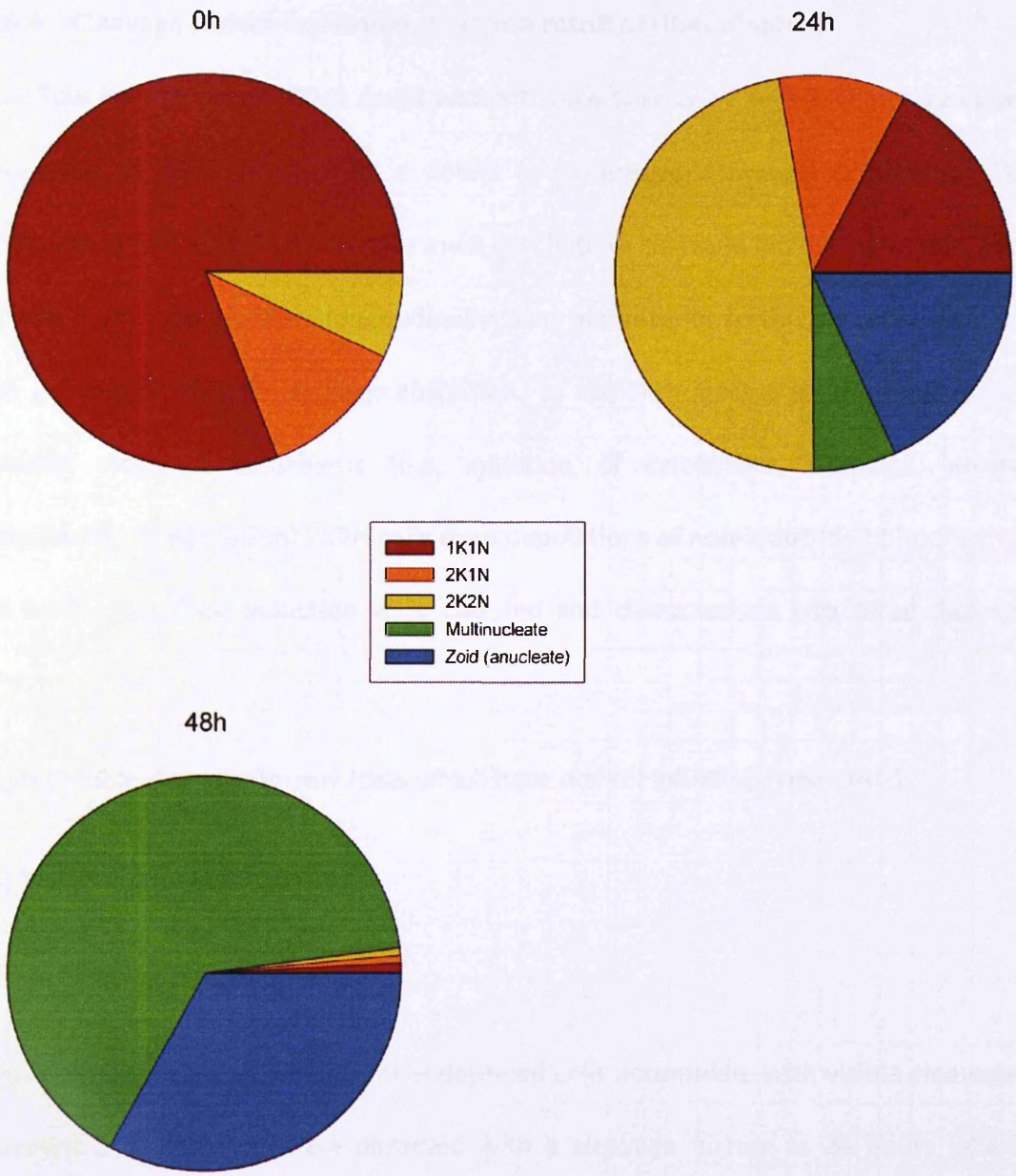

Figure 3.9 Pie charts showing kinetoplast and nuclear content in the GB4L RNAi cell line

Samples of non-induced cells and cells from cultures 24 and 48 hours post induction of GB4L RNAi ablation were settled onto slides (as described in section 2.5.1) and stained with DAPI to allow visualisation of the nuclei and kinetoplast configuration. 500 cells were counted for each time-point. Pie charts show the percentages of different cell types present at each time point. At 24 hours post-induction there is an increase in the number of cells with 2K2N content, a large reduction in the number of 1K1N cells and two sub-populations not observed in the non-induced culture have appeared, these populations represent multinucleate cells and anucleate zoids. At 48 hours the number of multinucleate and zoids has increased and these sub-populations account for the majority of the cells counted. Very few cells are observed with a normal nuclei/kinetoplast configuration.

3.6.4 Cleavage furrow ingression stalls as a result of GB4L ablation

The flow cytometry and DAPI count analysis show that 2K2N cells accumulate upon depletion of GB4L; suggesting a defect in progression through cytokinesis. To complete cytokinesis, *T. brucei* cells must first initiate cleavage furrow ingression, the furrow must then progress longitudinally from the anterior to the posterior pole of the cell and finally cells undergo abscission. To establish if GB4L ablation disrupts a specific stage of cytokinesis (e.g. initiation of cytokinesis, cleavage furrow progression or abscission) 2K2N cells from populations of non-induced, 12 hours and 24 hours post RNAi induction were counted and characterised into three distinct groups:

(1) No visible cleavage furrow (cells which have not yet initiated cytokinesis)

(2) Visible cleavage furrow and

(3) Undergoing abscission

Figure 3.10 shows that when GB4L is depleted cells accumulate with visible cleavage furrows: 50% more cells are observed with a cleavage furrow at 24 hours when compared to the non-induced control. This analysis shows that initiation of cytokinesis is not prevented by the ablation of GB4L and moreover that cells are capable of commencing cleavage furrow ingression. However, progression of the cleavage furrow is clearly disrupted and cells stall mid-way through cytokinesis with fewer cells reaching abscission.

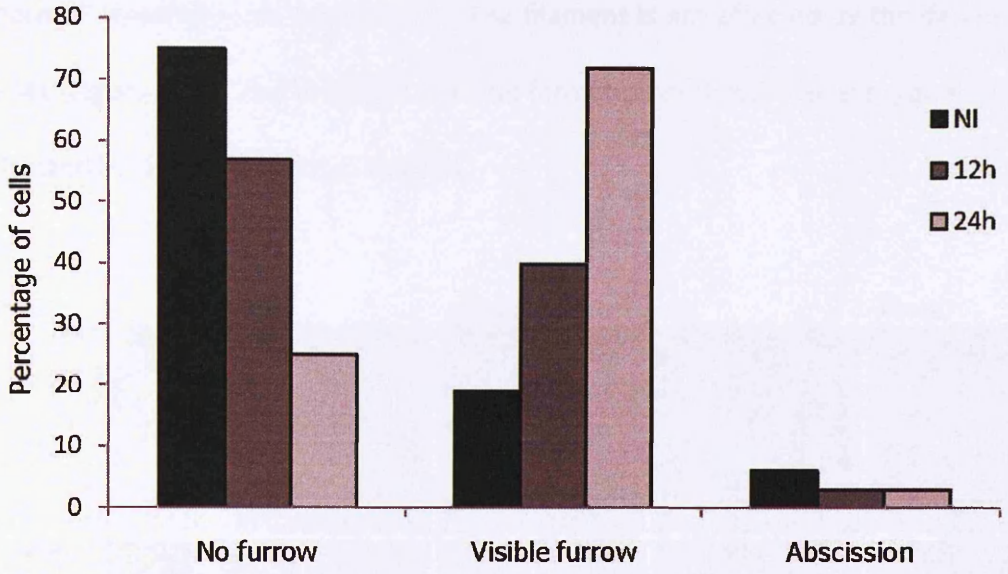

Figure 3.10 Characterisation of cytokinesis stage of 2K2N cells from GB4L RNAi cell line

Samples of non-induced (NI) cells and cells from cultures 12 and 24 hours post induction of GB4L RNAi ablation were settled onto slides (as described in section 2.5.1), stained with DAPI to allow visualisation of the nuclei and kinetoplast configuration. 200 2K2N cells from each time point were counted and classified into three distinct groups, those with no furrow, those with a visible furrow and those undergoing abscission. The graph shows that GB4L depleted cells are capable of initiating cytokinesis but cleavage furrow ingression is disrupted.

3.6.5 The formation of the flagellum, FAZ and basal bodies are not affected by GB4L ablation

Key organelles such as the basal bodies and the FAZ must be correctly formed and positioned to allow faithful cytokinesis. To investigate the possible cause of the cytokinetic defect observed in GB4L depleted cells, the PFR, which serves as a marker for the flagellum, and the FAZ and basal bodies were labelled with specific antibodies. The results of these indirect immunofluorescence assays are shown in Figure 3.11 and Figure 3.12. Although cells become progressively more abnormal with respect to morphology at later time points the immunofluorescence analysis shows that basal bodies have segregated and have nucleated new flagella of a

'normal' length (Figure 3.11) and the FAZ filament is not affected by the depletion of GB4L (Figure 3.12). This indicates that the formation of these critical organelles is not affected by the RNAi ablation of GB4L.

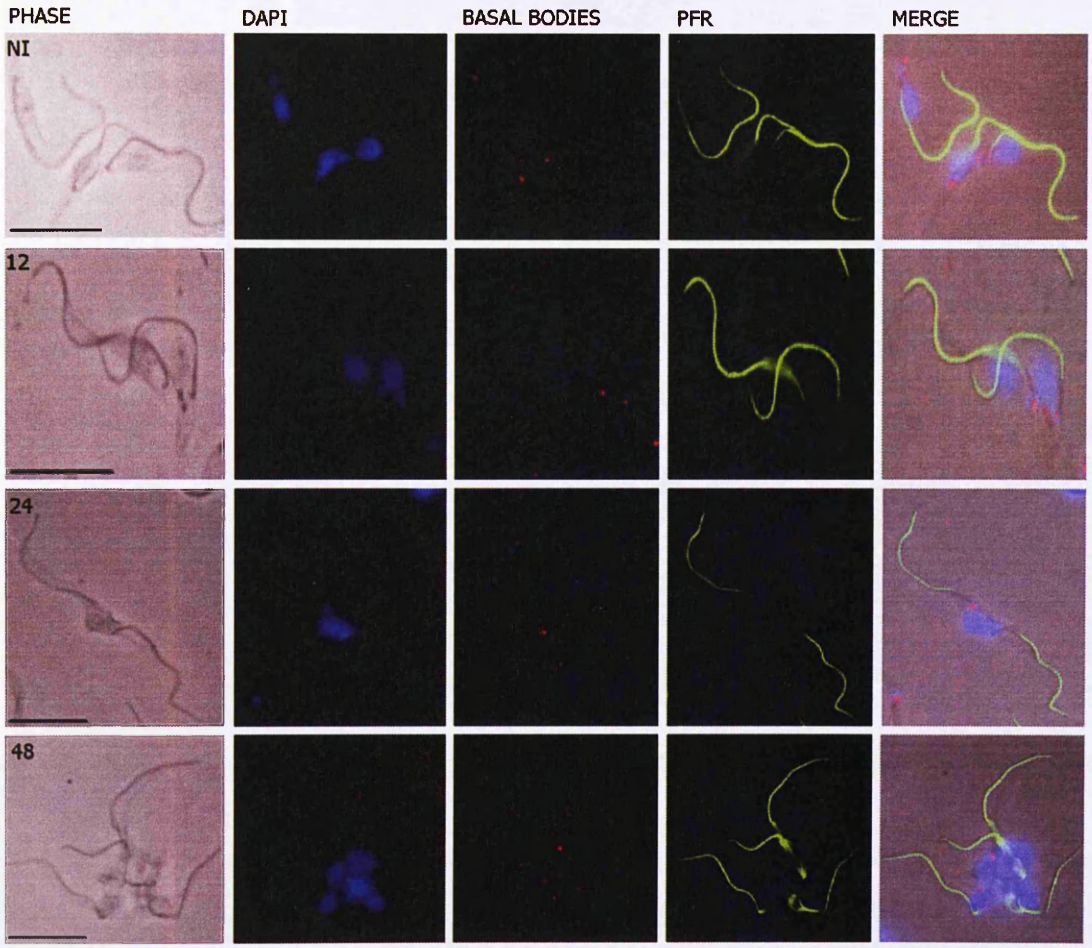

Figure 3.11 Immunofluorescence images showing the basal body and paraflagellar rod in the GB4L RNAi cell line

Samples of non-induced cells and cells from cultures 12, 24 and 48 hours after induction of GB4L RNAi ablation were settled onto slides (as described in section 2.5.1), and labelled with the antibodies L8C4 (green) and BBA4 (red) specific for the PFR and basal bodies respectively (dilutions used are given in section 2.2.3) and DAPI (blue). RNAi ablation of GB4L appears to have no affect on the positioning or formation of the PFR and basal bodies, even in cells with grossly abnormal morphology (scale bar = 10 μm).

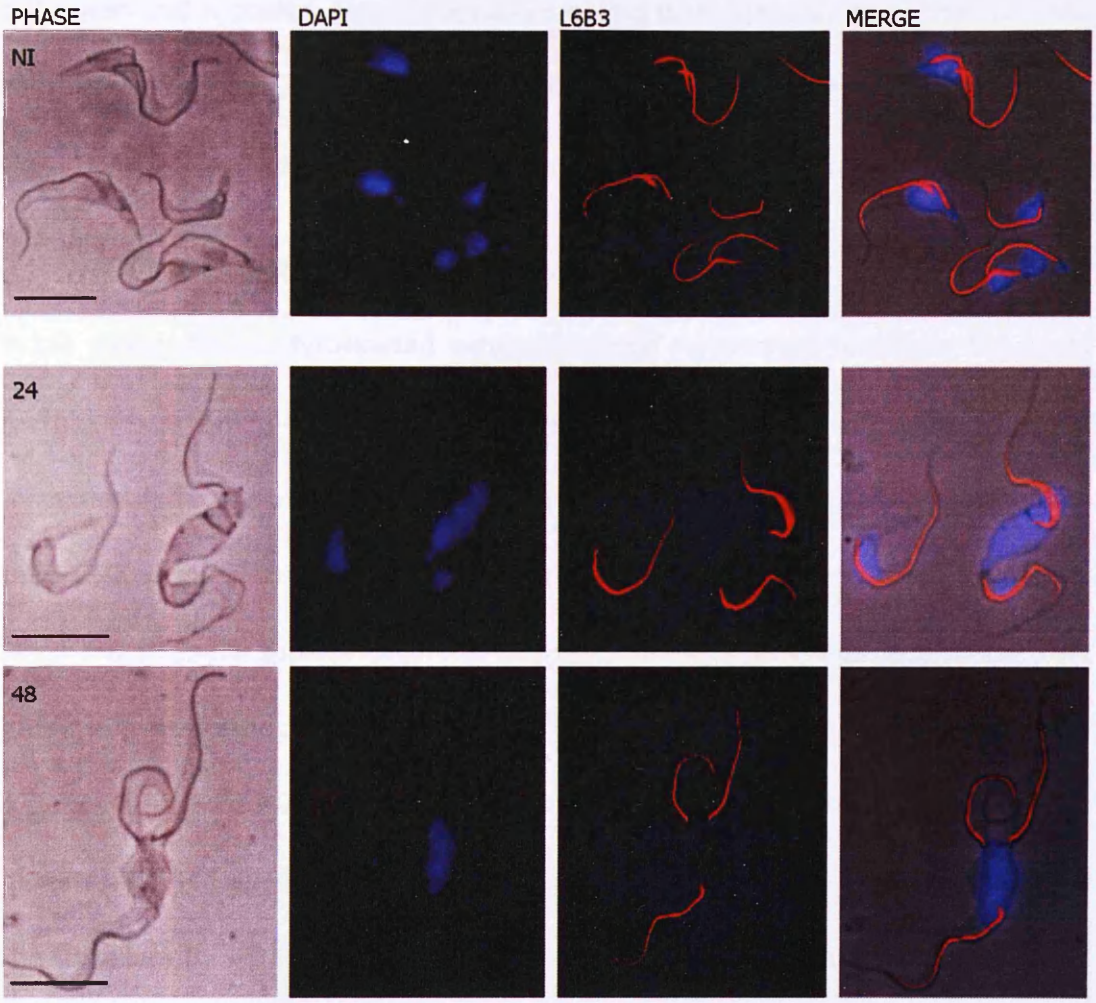

Figure 3.12 Immunofluorescence images showing the flagellum attachment zone in the GB4L RNAi cell line

Samples of non-induced cells and cells from cultures 24 and 48 hours after induction of GB4L RNAi ablation were settled onto slides (as described in section 2.5.1), and labelled with the antibody L6B3 specific for the FAZ filament (red) and DAPI (blue). RNAi ablation of GB4L appears to have no affect on the positioning or formation of the FAZ filament, even in cells with grossly abnormal morphology (scale bar = 10 μm).

3.7 Visualisation of new microtubule growth in GB4L depleted cells

After 12 hours of GB4L ablation cells are observed with two normal anterior ends which remain attached due to a stalling of cleavage furrow ingression. The presence of anterior ends which are apparently normal suggests that the cleavage furrow initiates correctly and makes accurate progress in the early stages of cytokinesis. It is upon reaching the posterior end of the cell that the cleavage furrow encounters

difficulties and is stalled. The consequence of this is the generation of characteristic cells referred to hereafter as 'push me-pull you' cells (by reference to the fictional creature in Dr Doolittle stories which has two heads at opposite ends of the body).

It is possible to visualise new MTs at the posterior pole of the cell using the antibody YL1/2 which detects tyrosinated α-tubulin. Once tyrosinated α-tubulin has been recruited to the MT polymer the C terminal tyrosine residue on α-tubulin is a target for removal, this process is time dependent and once the tyrosine residue is removed the YL1/2 signal is lost; this makes YL1/2 a useful marker for new MT formation. Since most tubulin growth occurs at the more dynamic posterior end of the cell, YL1/2 is a useful posterior end marker. The characteristic YL1/2 staining pattern includes a bright dot associated with the mature basal body. This is because YL1/2 detects a pool of unpolymerised tyrosinated α-tubulin waiting to be transported into the flagellum by IFT (Stephan *et al*, 2007). The α-tubulin detected by YL1/2 in this position is associated with transitional fibres of the mature basal body and is seen as either one or two bright dots depending on the stage of the cell cycle.

In wild type (Sherwin & Gull, 1989a) and GB4L non-induced populations YL1/2 has a distinctive staining pattern, 1K1N cells in G_1 have strong YL1/2 staining at the posterior end indicating that new MT growth is taking place at this stage. In 2K1N cells the staining of the posterior end is still present but has a reduced intensity and more staining is seen over the cell body as new MTs are intercalated into the existing corset to allow for an expansion in the cell diameter to accommodate duplicated organelles. Finally in 2K2N cells just prior to cytokinesis YL1/2 staining can be seen at the existing posterior end and in the region between the two separated nuclei which

will form a new posterior end (Figure 3.13). Thus YL1/2 labelling shows that new MTs are formed and grow in a manner which organises the subpellicular corset in preparation for cytokinesis.

In the GB4L RNAi induced cells YL1/2 staining is also evident in 1K1N and 2K1N cells indicating that new MTs are forming and being intercalated into the pre-existing corset. In the characteristic 'push-me-pull-you' 2K2N cells the YL1/2 staining pattern is different from that observed in a non-induced cell, a region of YL1/2 staining can be detected in between the two adjoined anterior ends in what appears to be a 'ridge' across the cell body; this is shown in Figure 3.13. This suggests that MT growth at the posterior end in these cells is disorganised and may explain why cleavage furrow progression has stalled.

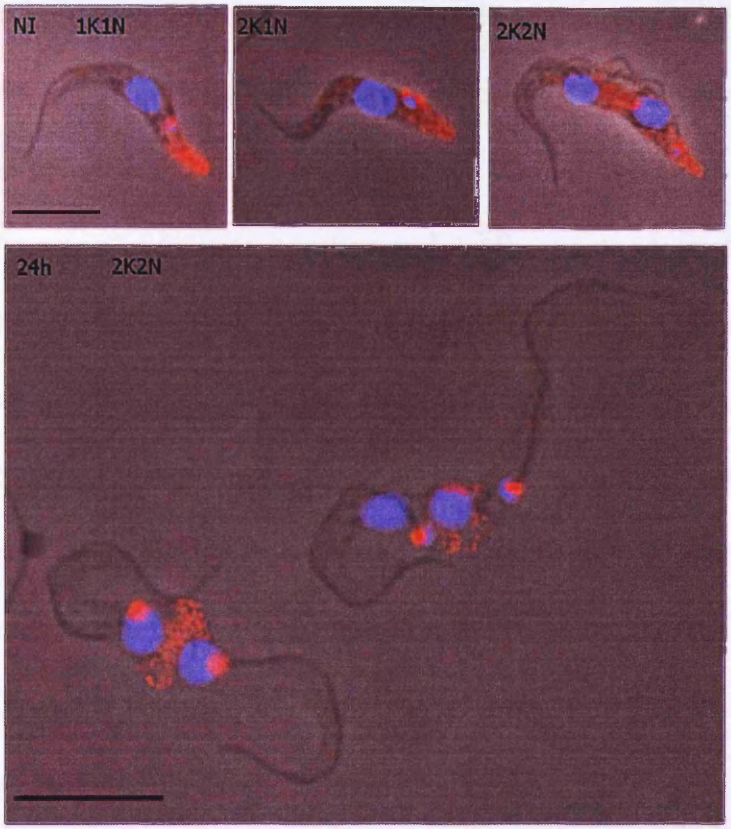

Figure 3.13 Immunofluorescence images showing sites of new microtubule formation in the GB4L RNAi cell line

Cells from a non-induced sample and a sample 24 hours after induction of GB4L RNAi were prepared for immunofluorescence as described in section 2.5.1, labelled with the antibody YL1/2 (for dilutions used see section 2.2.3) which detects tyrosinated α-tubulin and acts as a marker for new MTs. Top images show representative cells from a non-induced population; YL1/2 is detected at the posterior end and shows organised microtubule growth leading to the formation of two distinct posterior ends. Bottom, after 24 hours of GB4L depletion YL1/2 staining is concentrated in the region where the cleavage furrow has stalled (scale bar = 10μm).

3.8 Organelle positioning in GB4L depleted cells

Preliminary immunofluorescence experiments suggest that defective cytokinesis is not explained by aberrant formation of the FAZ filament, PFR (and therefore length of the flagella) or the basal bodies. There is evidence from the YL1/2 staining pattern to suggest that MT formation at the posterior end of the cell is disorganised.

Extension of the posterior end early in the cell cycle and intercalation of new MTs into the existing corset throughout the cell cycle are essential processes which enable the cell to grow and accommodate newly formed organelles. The relative positioning of organelles to one another and to the posterior end must adapt consistently throughout the cell cycle to ensure the cleavage furrow accurately divides the cell and faithfully partition duplicated organelles. The positioning of organelles within the cell and in relation to one another is highly co-ordinated and is in turn temporally and spatially co-ordinated with cytokinesis. To establish if there are abnormalities in spatial arrangement of organelles within GB4L depleted cells specific measurements were taken in non-induced cells and at 12 hours post RNAi induction; these measurements are shown in Figure 3.14.

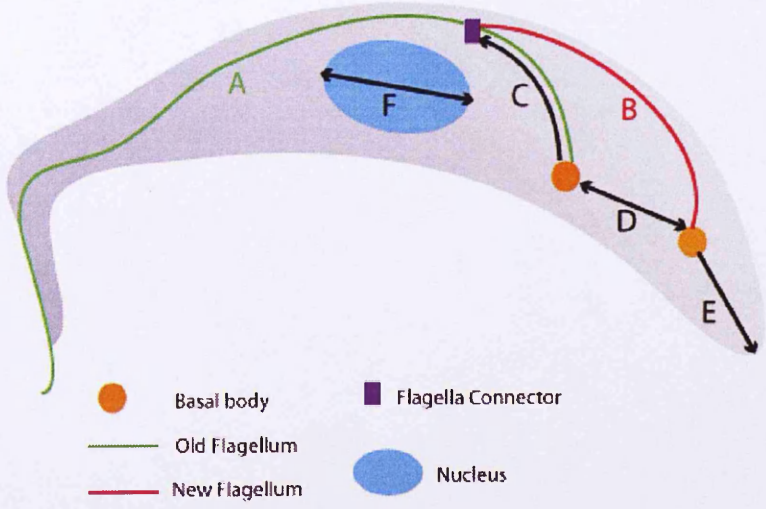

Figure 3.14 Cartoon showing the measurements taken for examining organelle positioning in RNAi cell lines

Cells were prepared for immunofluorescence (as described in section 2.5.1) and labelled with an anti-PFR antibody (L8C4) and an anti-basal body antibody (BBA4) (dilutions are shown in section 2.2.3) and stained with DAPI. This allows the following measurements to be carried out : A – length of old flagellum, B – length of new flagellum, C – FC migration, D – Inter-basal body distance, E distance from new basal body to posterior end of the cell and F – Inter-nuclear distance.

The 12 hour time point was selected in order to try and visualise the initial effects of reducing GB4L expression. To allow for variation in cell size the data is expressed as a ratio of old flagellum length as the old flagellum length is the only measurement which remains consistent through the cell cycle changing only due to variation in individual cell size rather than due to cell cycle events. As the new flagellum extends progressively throughout the cell cycle it is used as a temporal marker for cell cycle progression.

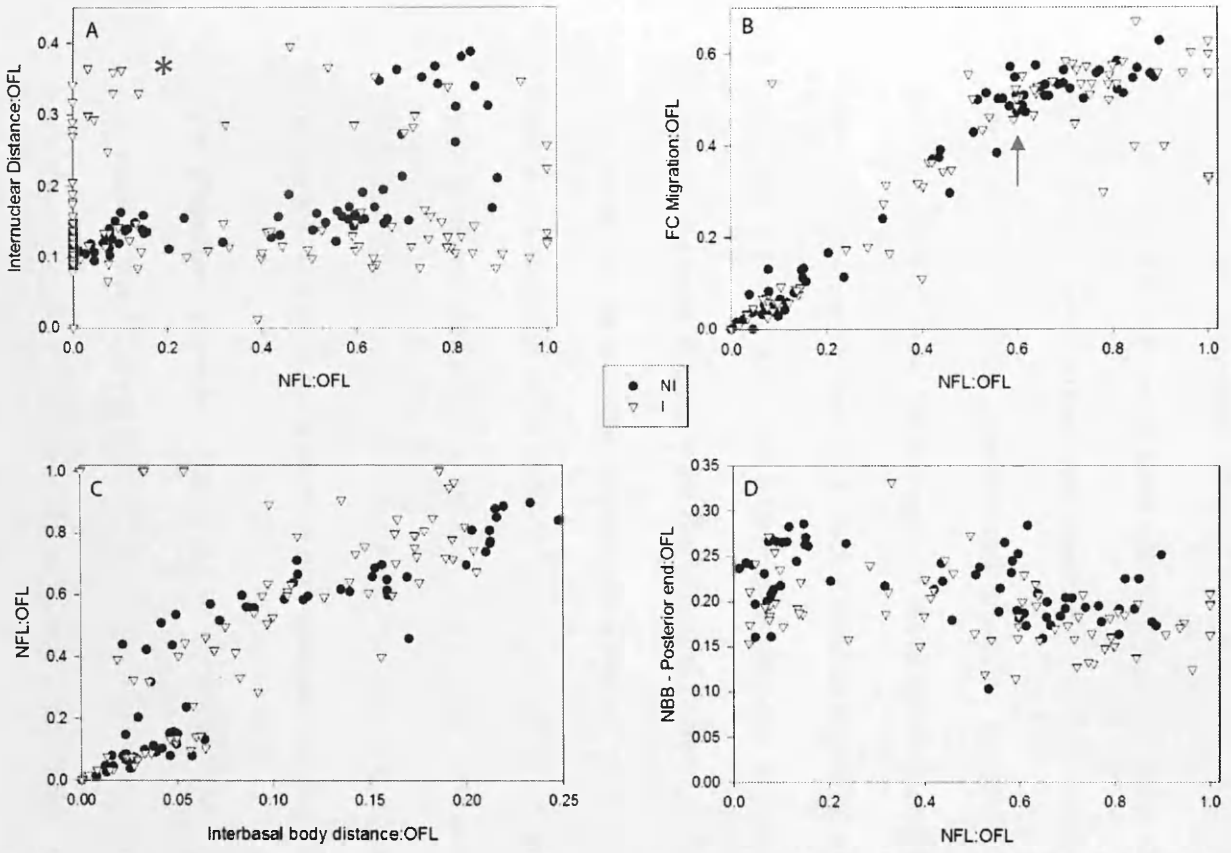

Figure 3.15. Graphs describing organelle positioning in the GB4L RNAi cell line

Cells from the GB4L RNAi cell line were induced and samples from a non-induced culture and a culture 12 hours after induction were settled onto slides as described in section 2.5.1. These cells were labelled for immunofluorescence with an anti-PFR antibody (L8C4) and an anti-basal body antibody (BBA4) and stained with DAPI. The position of key organelles was measured in relation to one another in 200 cells from each sample, as described in section 3.8. The asterisk in Graph A represents a subpopulation of induced cells where internuclear distance is high and the new flagellum is short this may represent a population of 1K2N cells. The arrow in Graph B indicates the inflexion point in the graph where FC migration reaches the 'stop' point.

Nuclear separation - The most intriguing observation arising from the measurement data is seen in Figure 3.15A which shows inter-nuclear distance plotted in relation to new flagellum growth. In the non-induced sample (black circles) as the new flagellum extends nuclear separation remains consistent this is because these measurement represent 1K1N cells which have not yet entered mitosis. Upon entering mitosis the nuclear diameter increases and eventually two nuclei form which move apart. The inflection point in the non-induced graph at approximately 0.6 (on the *X*-axis) indicates where nuclei have begun to move apart during mitosis. The induced cell line (white triangles) appears to lack a distinct inflection point. In some cells nuclei separate and have a normal internuclear distance at later stages in the cell cycle, however the general trend is for the internuclear distance to remain the same, nuclei separation may be restricted meaning they remain in closer proximity to one another than in non-induced cells. There is a subpopulation of cells shown top left of the graph (indicated with a blue asterix) which may represent 1K2N cells which have under gone cytokinesis and re-entered the cell cycle, these cells will have a large internuclear distance and a short or non-existent new flagellum.

New flagellum growth - Figure 3.15B describes the relationship between the migration of the FC along the old flagellum and the growth of the new flagellum; in both the induced and non-induced cells migration of the FC along the old flagellum and extension of the new flagellum is biphasic starting out as a linear relationship each extending progressively until reaching the 'stop' point (Davidge *et al*, 2006). The 'stop' point indicates where the FC migration along the old flagellum halts this is at approximately 0.5 on the y axis meaning the FC migrates approximately half way along the old flagellum before stopping (indicated on the graph by a blue arrow).

Once the FC has stopped migrating the new flagellum continues to grow to between 80-100% the length of the old flagellum, this growth is slower, approximately half the rate of that seen in cells earlier in the cell cycle. RNAi mediated ablation of GB4L does not appear to effect the growth of the new flagellum or the migration of the FC.

Basal body separation - Figure 3.15C shows basal body separation in relation to new flagellum growth. The non-induced cell measurements show that as the new flagellum extends and the cell progresses through the cell cycle, the interbasal body distance increases. This relationship is also biphasic, as initially interbasal body distance changes very little until the new flagellum has reached approximately half its final length (0.5) then basal body separation occurs. This shows that further growth of the new flagellum is translated into basal body migration. The non-induced cells show the same general trend.

Distance from the new basal body to the posterior end - Figure 3.15D describes the position of the new basal body in relation to the posterior as the new flagellum extends. The distance from new basal body to the posterior end of the cell is reduced slightly in the induced culture. However this reduction is consistent in all cell types and so suggests it is not cell cycle related.

Conclusions - the measurement data for the GB4L cell line shows that organelle positioning in the non-induced cells is as expected for wild type. The induced cell line follows the same general trend as the non-induced cells in most cases. However, points for the induced population are slightly more dispersed and nuclear separation appears to be restricted in some cells.

3.8.1 Effect of GB4L and TCP86 RNAi mediated ablation on growth of bloodstream form *T. brucei*.

Expression of TCP86 in BSF of *T. brucei* has been demonstrated experimentally by immunofluorescence and immunoblot analysis using a TCP86 specific polyclonal antibody (Shawcross, 2008). Immunofluorescence experiments showed TCP86 is found over the entire subpellicular corset, matching the localisation pattern seen in the PCF (Shawcross, 2008). Proteomic data also shows that GB4L and the previously published trypanosome MAP GB4 are expressed in the BSF (Bridges *et al*, 2008) and so to study the role of these proteins in the BSF of *T. brucei,* RNAi constructs were transfected into the 90-13 cell line (Wirtz *et al*, 1999) to enable inducible ablation in this life cycle stage.

Growth curves for these three RNAi cell lines are presented in Figure 3.16 and show that both GB4L and TCP86 are essential in the BSF since their ablation results in a marked reduction in population growth. GB4 is not essential in the BSF as the growth curve shows no effect on doubling time when this protein is ablated.

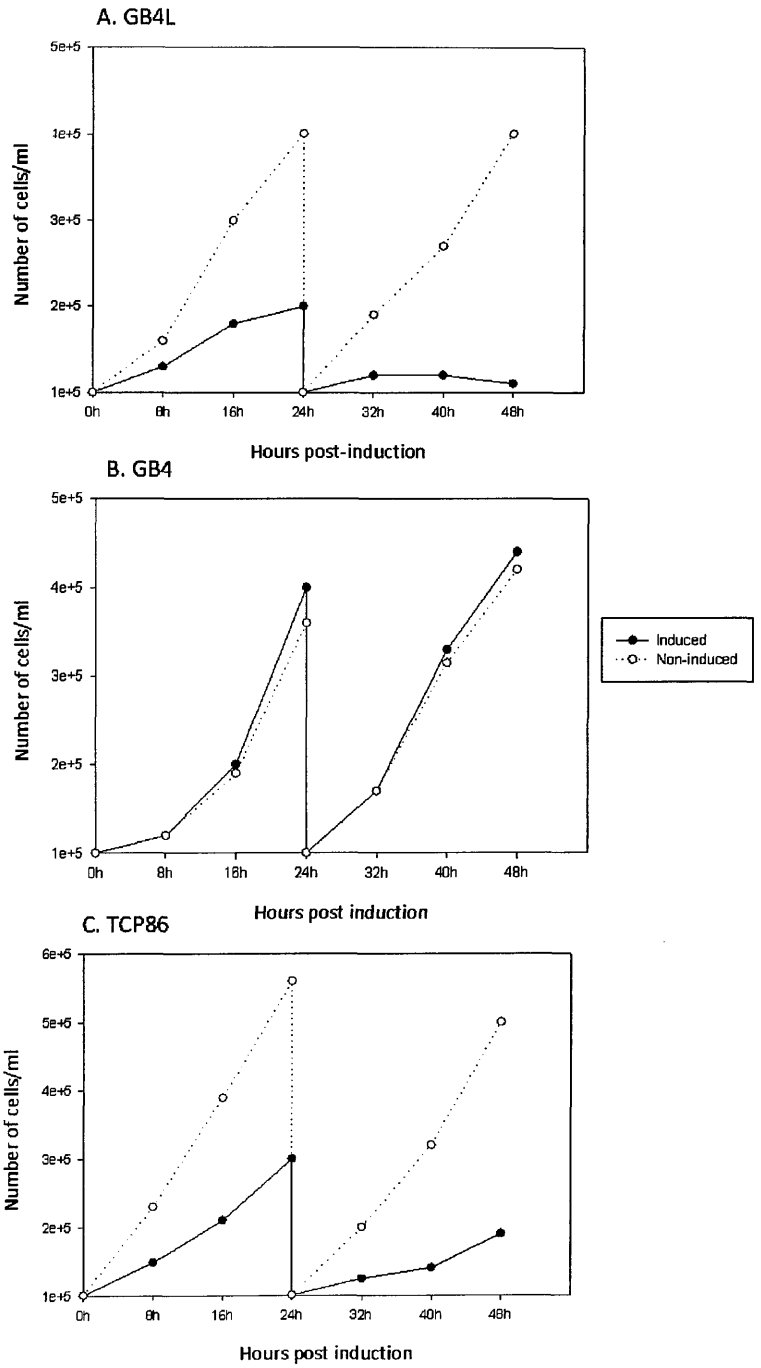

Figure 3.16 Growth curves showing effects of RNAi mediated ablation of GB4L, GB4 and TCP86 in the bloodstream form

RNAi ablation was induced by the addition of doxycyclin to culture medium containing RNAi cell lines at a concentration of $1x10^5$cells/ml (methods described in section 2.4.6). The induced and non-induced populations were measured every 24 hours and diluted back to $1x10^5$cells/ml, counts were continued for 48 hours GB4L and TCP86 show a growth defect when compared to the non-induced control, GB4 ablation has no affect on population growth over 48 hours.

Ablation of GB4L causes reduced growth from as early as 8 hours post induction, 16 hours after induction of GB4L RNAi the doubling time for the population is less than half that of the non-induced control, between 16 and 24 hours there is very little growth observed. The population showed no significant growth between 24 and 48 hours so analysis was stopped. Reduction of TCP86 expression has similar effects on the population, 8 hours after the induction of TCP86 RNAi cells grow at approximately half the rate of the non-induced control, there is still growth after 24 hours but it is severely reduced, a small amount of growth was recorded at the time points beyond 24 hours when compared with the non-induced cells but this growth was not significant and so measurements were stopped at 48 hours. The growth of the GB4 RNAi cell line varied little when compared to the non-induced control over the 48 hour time course; this suggests that GB4 is not essential for viability in the BSF.

To further investigate the effects that GB4L and TCP86 depletion have on the BSF, DAPI counts were carried out. DAPI counts allow the number of nuclei and kinetoplasts to be counted within each cell, the DNA content of the cell is a reliable indicator of the cell cycle stage and any abnormalities in kinetoplast or nuclei segregation or cytokinesis are easily detected by this method.

3.8.2 Visualisation of kinetoplast and nuclear configuration in the bloodstream GB4L RNAi cell line

DAPI counts for the GB4L BSF RNAi cell line are shown in Figure 3.17; counts were carried out on cells from cultures which were non-induced, 12, 24 and 48 hours post induction of RNAi. The counts reveal that at the 12 hour time point there is an

increase in the 2K2N sub-population coupled with a reduction in the number of 1K1N cells (Figure 3.17). This is similar to the observations in the PCF RNAi cell line and suggests a blockage in mitosis and/or cytokinesis. After 24 hours there is a profound increase in the number of multinucleates and zoids and by 48 hours the majority of the cells counted were multinucleates followed by zoids. Very few cells appear to be progressing through the cell cycle as normal this was expected after the results of the growth curve which showed no population growth at 48 hours post induction.

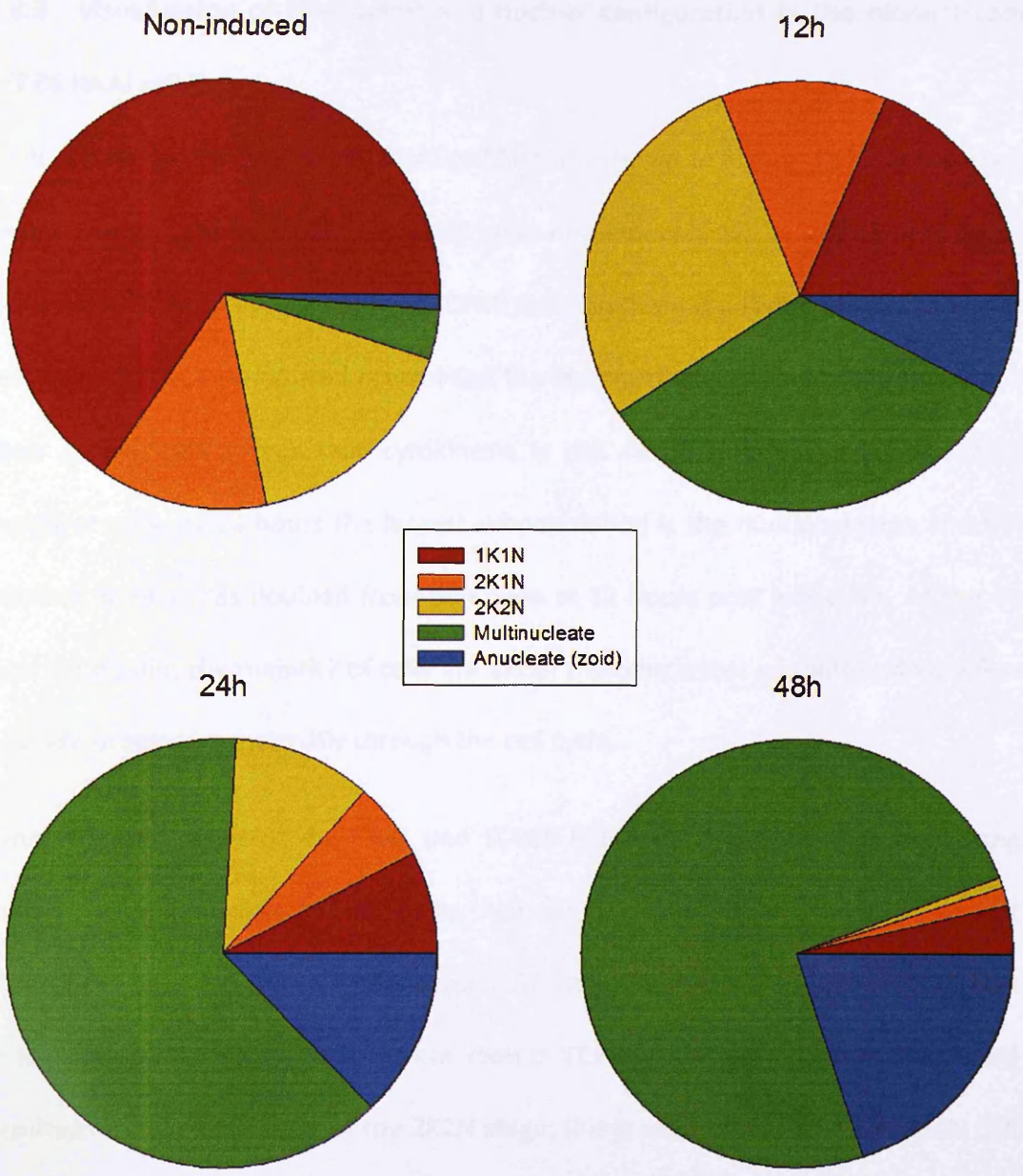

Figure 3.17 Pie charts showing the kinetoplast and nuclear content of the BSF GB4L RNAi cell line

The BSF GB4L RNAi cell line was induced and cells were harvested, settled onto slides and labelled with DAPI as described in section 2.2.3. 500 cells were classified by the number of kinetoplasts and nuclei they possessed. Samples were taken from a non-induced culture and cells which were 12, 24 and 48 hours post induction. Pie charts show a reduction of cells progressing through the cell cycle 'normally' and an initial increase in the 2K2N population (12 hours) before the majority of the population become multinucleates or zoids (24 – 48 hours).

3.8.3 Visualisation of kinetoplast and nuclear configuration in the bloodstream TCP86 RNAi cell line

DAPI counts for the TCP86 BSF RNAi cell line are shown in Figure 3.18 counts were carried out on cells from cultures which were non-induced, 12, 24 and 48 hours post induction of RNAi. After 12 hours of TCP86 ablation there is a reduction in 1K1N cells compared to the non-induced control and the multinucleate and zoid subpopulations have grown, this shows that cytokinesis is not faithfully producing two viable daughter cells. By 24 hours the largest subpopulation is the multinucleates and the number of zoids has doubled from that seen at 12 hours post induction. At the 48 hour time point the majority of cells are either multinucleates or zoids and very few cells are progressing normally through the cell cycle.

Whist the end result of the GB4L and TCP86 BSF RNAi is a population consisting mainly of multinucleates and zoids, the DAPI counts show some important differences between the two phenotypes. At 12 hours there is an increase in 2K2N cells in the GB4L cell line which is not seen in TCP86. This suggests that GB4L RNAi results in a stalled cell cycle at the 2K2N stage; this is seen in the PCF GB4L RNAi cell line where the cleavage furrow stalls and forms the 'push-me–pull-you' phenotype (see Figure 3.10 and Figure 3.13). The fact that this increase in 2K2N cells is not observed in either the PCF or the BSF TCP86 RNAi cell lines indicates that cells complete cytokinesis however the presence of zoids and multinucleates suggests there is a problem with cytokinesis.

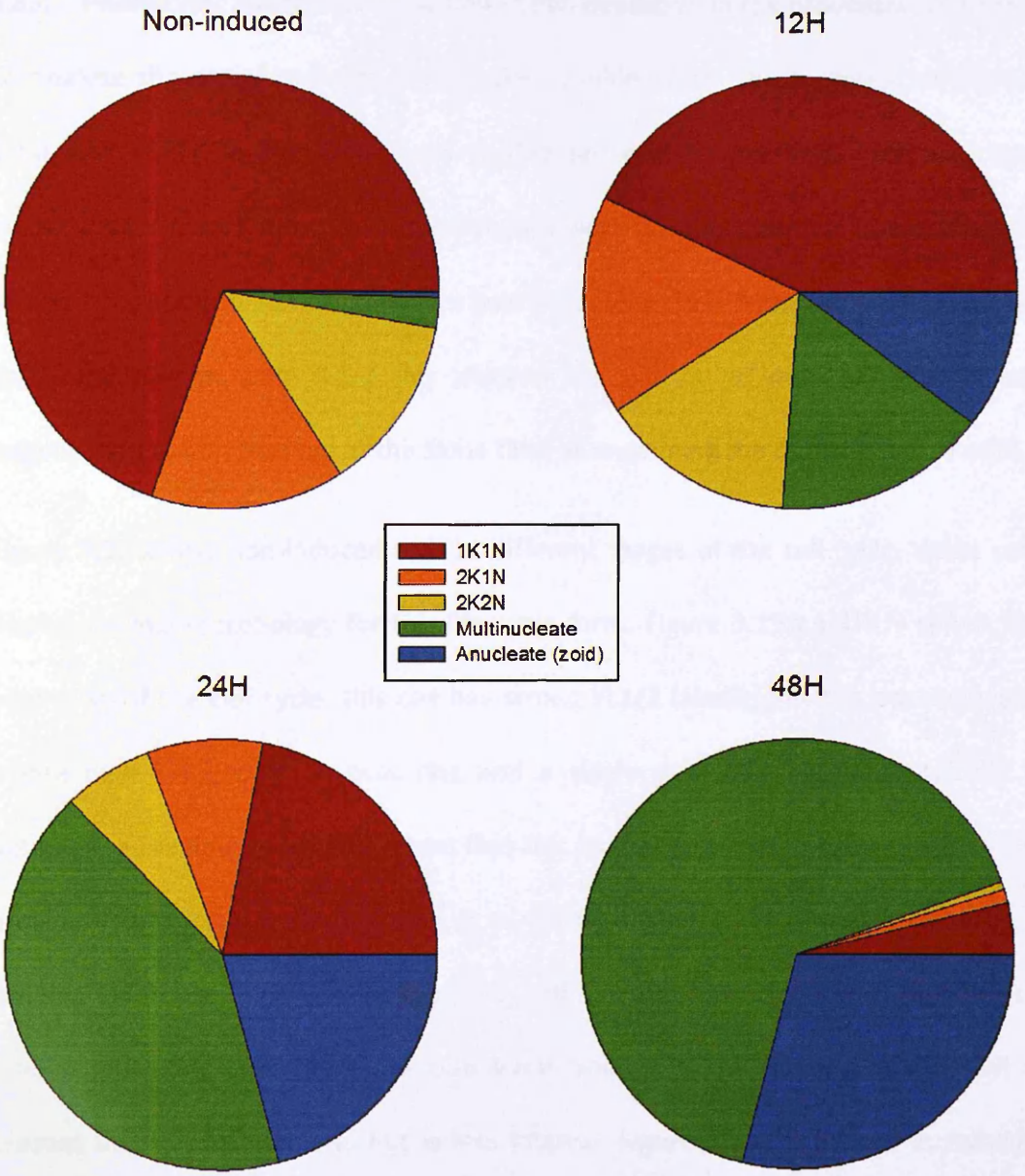

Figure 3.18 Pie charts showing the kinetoplast and nuclear content of the BSF TCP86 RNAi cell line

The BSF TCP86 RNAi cell line was induced and cells were harvested, settled onto slides and labelled with DAPI as described in section 2.2.3. 500 cells were classified by the number of kinetoplasts and nuclei they possessed. Samples were taken from a non-induced culture and cells which were 12, 24 and 48 hours post induction. Pie charts show a reduction of cells progressing through the cell cycle 'normally' and an increase in multinucleates and zoids over time.

3.8.4 Phenotypic analysis of GB4L and TCP86 depletion in the bloodstream form

To analyse the morphogenetic phenotypes resulting from the targeted ablation of GB4L and TCP86 in BSF, cells were settled on to slides for immunofluorescence analysis. Cells from a non-induced population were used as a control to compare the effects of protein depletion 24 hours post induction. Cells from the GB4L RNAi cell line were stained with YL1/2 this allowed the pattern of new MT growth and organisation to be observed at the same time as examining the morphology of cells.

Figure 3.19 shows non-induced cells at different stages of the cell cycle, these cells display normal morphology for this life cycle form. Figure 3.19A a 1K1N cell at the beginning of the cell cycle, this cell has strong YL1/2 labelling at the posterior end where new MT growth is occurring and a single pool of tyrosinated tubulin is detected, a previous study has shown that this pool of tyrosinated tubulin is found in proximity to a basal body (Stephan *et al*, 2007). Figure 3.19B shows a cell with a dividing kinetoplast and one nucleus, this cell has two distinct pools of tyrosinated tubulin indicating that there are two basal bodies; YL1/2 staining in this cell is present at the posterior end but is less intense. Figure 3.19C a 2K cell in mitosis; YL1/2 staining is reduced at the posterior end suggesting there is less new MT growth occurring in this region. YL1/2 staining is now seen diffusely over the entire cell body indicating that new MTs are being inserted into the corset to allow for circumferential growth of the cell. The next stage of the cell cycle is shown in Figure 3.19D this is a 2K2N cell, YL1/2 staining is still seen diffusely over the entire cell body but is more intense in the region between the two nuclei. In the BSF the new basal body is found much closer to the posterior end when compared to its position in the PCF; in the PCF cells adopt a K-N-K-N configuration of kinetoplast and nuclei before

they undergo cytokinesis. In the BSF cells maintains a K-K-N-N distribution of organelles (see Figure 3.19D and E). Cytokinesis in the BSF initiates at the anterior as in the PCF, in Figure 3.19E the cleavage furrow mid way through ingression and a patch of YL1/2 staining can be seen between the nuclei suggesting new MTs are being incorporated in this region as the cleavage furrow progresses.

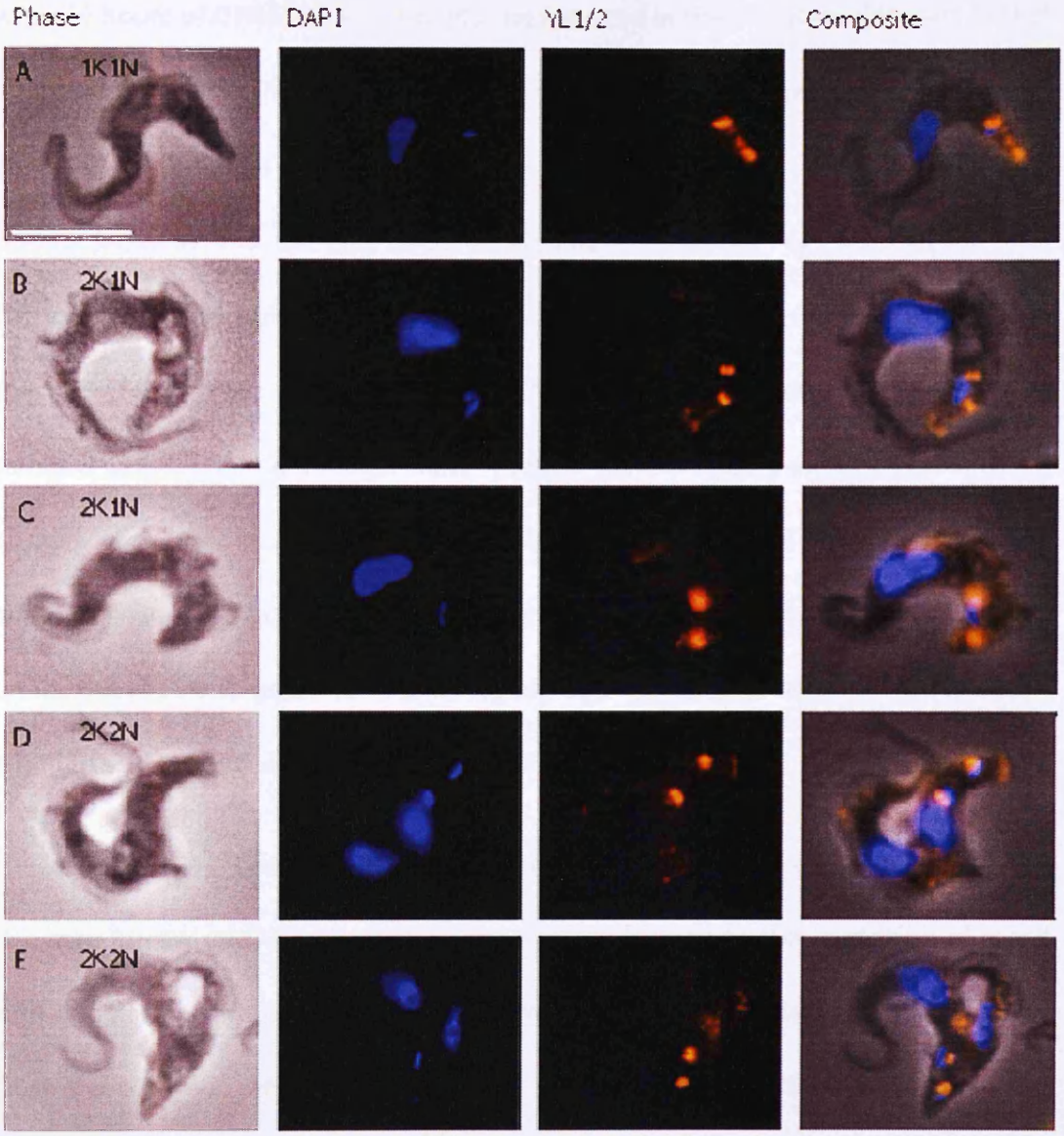

Figure 3.19 Immunofluorescence images of YL1/2 staining in non-induced cells from the BSF GB4L RNAi cell line

Non-induced cells from the BSF GB4L RNAi cell line were harvested for immunofluorescence analysis; slides were prepared as described in section 2.5.2. Cells were labelled with the antibody YL1/2 (orange) (dilutions used are shown in section 2.2.3) and DAPI (blue). Cells at progressively later stages of the cell cycle (A-E), from (A) 1K1N to (E) 2K2N cell undergoing cytokinesis, YL1/2 staining indicates where new MTs are growing. In the BSF the cell adopts a K-K-N-N configuration of kinetoplasts and nuclei rather than the K-N-K-N organisation seen in the PCF. The morphology of the cells at all cell cycle stages appears as wild type (scale bar = 10 μm).

After 24 hours of GB4L ablation the phenotype seen in the BSF is reminiscent of that observed in the PCF. Figure 3.20 shows the morphological abnormal cells which were observed at this time point. Figure 3.20A shows a 1K1N cell with a rounded and stumpy posterior end, this type of cell is often observed in the PCF RNAi cell line after 12 hours of RNAi ablation (see Figure 4.2F). The YL1/2 staining in Figure 3.20A suggests there is little new MT growth at the posterior end of this cell. Figure 3.20B shows a 1K1N cell with a longer more 'normal' cone shaped posterior end which is positive for YL1/2. Images C and D YL1/2 staining is seen more strongly on the cell body. This suggests that MT growth is disorganised as it is occurring all over the cell rather than being targeted to specific regions such as the area between the nuclei as it is in the non-induced cells seen in Figure 3.19E.

The most striking effect of the RNAi ablation in the PCF was the stalling of the cleavage furrow mid way through its progression leading to the formation of a cell with two normal anterior ends connected by a large cell body, such cells were named 'push-me-pull-you' cells and they are also seen as a result of GB4L ablation in the BSF. Examples of BSF 'push-me-pull-you' cells are shown in Figure 3.20C and D.

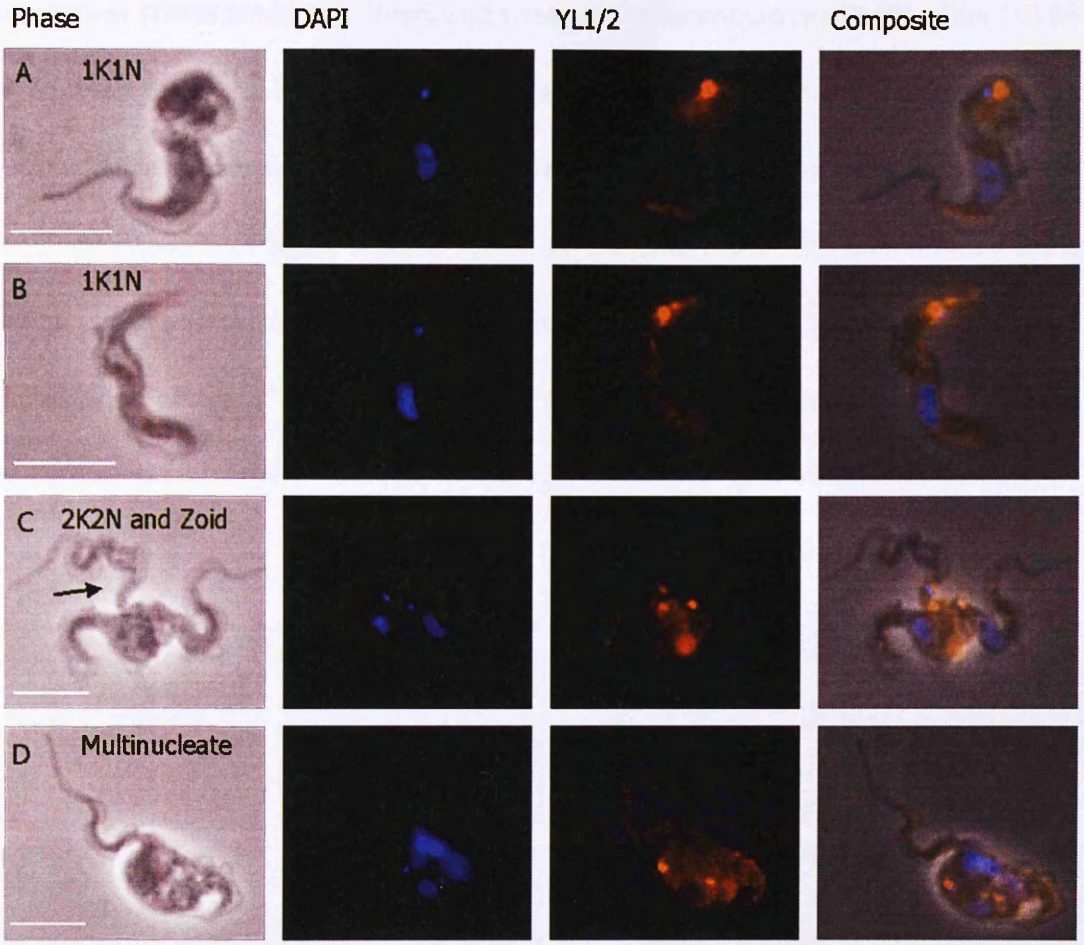

Figure 3.20 Immunofluorescence images of the BSF GB4L RNAi cell line 24 hours after induction of RNAi labelled with YL1/2

Cells from the BSF GB4L RNAi cell line were induced and harvested for immunofluorescence analysis 24 hours after induction slides were prepared as described in section 2.5.2. Cells were labelled with the antibody YL1/2 (orange) (dilutions used are shown in section 2.2.3) and DAPI (blue). A shows a 1K1N cell with a rounded posterior end, YL1/2 staining is not detected at the posterior end as in wild type. B is a 1K1N cell with a longer tapering posterior end which is YL1/2 positive. C and D show cells with a stalled cleavage furrow like those observed in the PCF. C shows a 2K2N 'push-me-pull-you' cell and a zoid (black arrow) and the cell in D is a multinucleate cell with a large cell body, some nuclei have not segregated and it is difficult to determine the number of nuclei by eye, two anterior ends are visible (scale bar = 10 μm).

To confirm TCP86 ablation by RNAi and to study the morphology of cells when TCP86 is depleted RNAi was induced and cells were settled onto slides from a non-induced culture, 12 and 24 hours post induction. These cells were labelled with the polyclonal antibody raised specifically against TCP86. Figure 3.21 shows the non-induced cells; TCP86 can be seen over the entire cell body in all cell cycle stages (Figure 3.21A shows an example of a 1K1N cell; Figure 3.21B shows a 2K2N cell). This labelling pattern seen in the BSF is identical to that seen in the PCF (Shawcross, 2008).

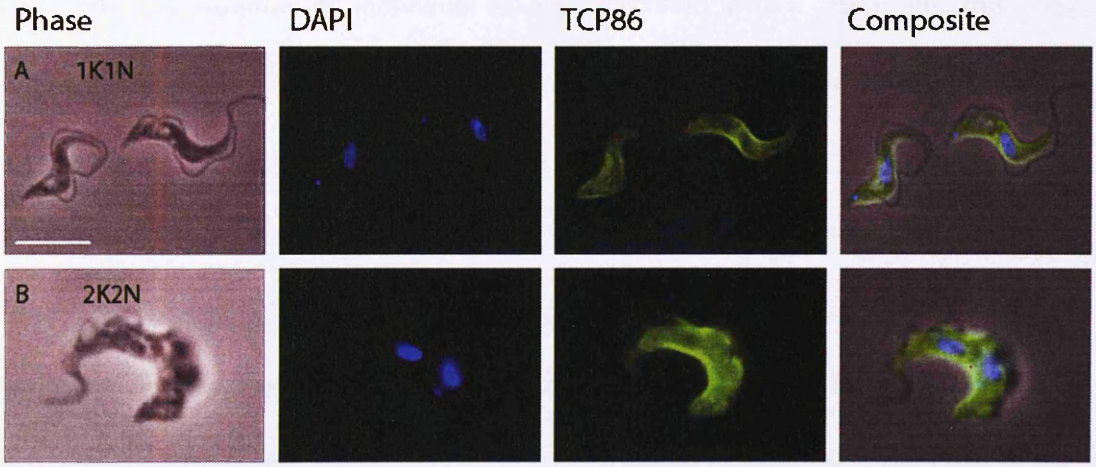

Figure 3.21 Immunofluorescence images of the BSF TCP86 RNAi cell line showing TCP86 localises over the whole cell in non-induced cells

Non-induced cells from the BSF TCP86 RNAi cell line were harvested for immunofluorescence analysis and slides were prepared as described in section 2.5.2. Cells were labelled with the anti TCP86 (green) antibody (dilutions used are shown in section 2.2.3) and DAPI (blue). A shows a 1K1N cell and B shows a 2K2N cell, both cells are positive for TCP86 over the entire cell body (scale bar = 10 μm).

Figure 3.22 shows the effects of TCP86 RNAi ablation 12 and 24 hours after induction of RNAi. Figure 3.22A - C show cells 12 hours post induction, A) a 1K1N cell B) a 2K1N cell and C) a 2K2N cell, none of these cells have TCP86 labelling on the new MTs of the posterior end. These results are in line with the observations made in the PCF

and suggest that TCP86 forms a stable association with MTs in the corset. When the cytoplasmic reserves of TCP86 are depleted there is little protein available to decorate new MTs and so the loss is most apparent at the posterior end which is where most new MT growth takes place.

Figure 3.22D - F are cells from a population 24 hours post induction of TCP86 ablation; these cells have reduced expression of TCP86 at the posterior end. All the cells shown are multinucleates, these cells have large nuclei and it is difficult to determine the number of individual nuclei contained within each cell, this may reflect a defect in mitosis. In all cases a cleavage furrow is present; in Figure 3.22D positioning of the cleavage furrow appears aberrant as the anterior ends produced from this furrow ingression are disproportionate. This sort of asymmetrical division is a characteristic of TCP86 ablation in the PCF and is implicated in the production of anucleate zoids and multinucleates (Shawcross, 2008). Figure 3.22E and F show two very abnormal cells, the cell in E has a number of nuclei positioned in the path of the cleavage furrow. The cell in F is close to abscission, if successful this will produce two cells of unequal size and abnormal morphology. The phenotype shown here in this BSF cell line is similar to that observed in the PCF by Shawcross (2008). In both cases TCP86 is lost initially from the posterior end of the cell and leads to aberrant asymmetrical cytokinesis.

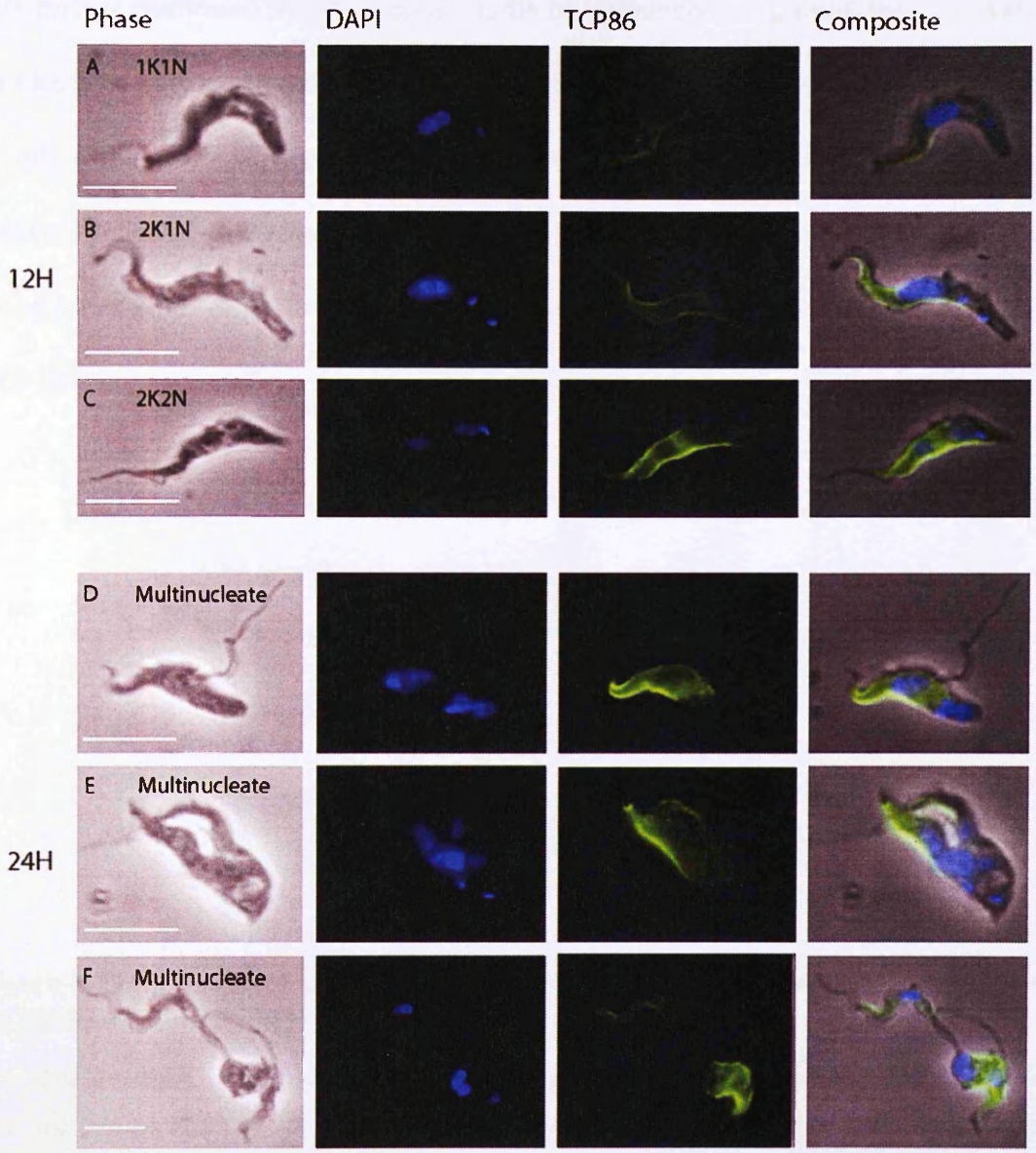

Figure 3.22 Immunofluorescence images of BSF cells showing reduction in expression of TCP86 12 and 24 hours after induction of RNAi

Cells from the BSF TCP86 RNAi cell line, at 12 and 24 hours post induction were harvested for immunofluorescence analysis and slides were prepared as described in section 2.5.2. Cells were labelled with the anti TCP86 (green) antibody (dilutions used are shown in section 2.2.3) and DAPI (blue). After RNAi mediated ablation TCP86 remains localised at the anterior end of the cell but is lost from the posterior end. Cells in D – F are multinucleated and show cytokinetic defects. Cells are undergoing asymmetrical division similar to that seen in the PCF (scale bar = 10μm).

We further confirmed the ablation of TCP86 by immunoblotting using the polyclonal antibody raised specifically against TCP86 (Figure 3.23). This antibody detects 2 bands at the molecular weights 110kDa and 86kDa in whole cell protein extracts. The 86kDa version of the protein is reduced over the RNAi time course but the 110kDa band is not affected. A similar observation was made when TCP86 was ablated in the PCF (Shawcross, 2008).

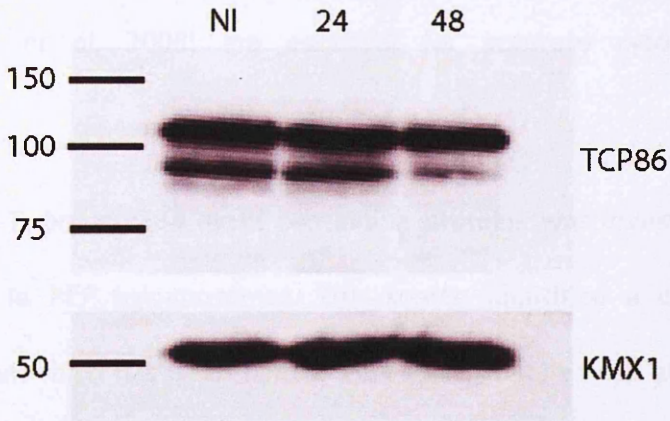

Figure 3.23 Immunoblot showing the reduction in TCP86 expression after induction of TCP86 RNAi in the BSF

The TCP86 RNAi cell line was induced and protein samples were collected from a non-induced culture (NI) and cultures at 24 and 48 hours post RNAi mediated ablation (as described in section 2.5.7.1). Whole cell extracts were separated by SDS-PAGE (whole cell protein extracts from $5x10^6$ cells loaded per lane), transferred to nitrocellulose membranes then probed with the TCP86 antibody (for dilution used see section 2.2.3). Membranes were then incubated with polyclonal-goat anti-rabbit HRP conjugated secondary antibody and the immobilised TCP86 antigens were detected by chemiluminescence. Immunoblots show the 110kDa band is stable whilst the 86kDa band appears reduced. The anti β-tubulin antibody KMX1 was used as a loading control.

3.9 Summary

Chapter 3 describes bioinformatics analysis which led to the identification of a trypanosomatid specific motif (GB4 motif) (the amino acid sequence logo is shown in Figure 8.3). This sequence is found in a total of 35 proteins, 17 of which are from *T. brucei.* Included in this family of *T. brucei* GB4 motif containing proteins are the MAPs GB4, TCP86 and TCP66 along with the flagellum attachment zone protein FAZ1. Two recent and independent studies have shown that TCP86 (Shawcross, 2008) and FAZ1 (Vaughan *et al*, 2008) are essential for accurate cytokinesis in PCF trypanosomes.

The function of *T. brucei* GB4 motif containing proteins was investigated through RNAi screening in PCF trypanosomes. This screen identified a protein with an essential function which has been named GB4-Like (GB4L) whose ablation leads to stalled cytokinesis. In the absence of cytokinesis GB4L depleted cells re-replicate their DNA and form multinucleate cells (Figure 3.8, Figure 3.9), as is well documented for many other PCF RNAi cell lines (Hammarton *et al*, 2005; Kumar & Wang, 2006; Rothberg *et al*, 2006). Intriguingly these cells successfully initiate cleavage furrow ingression but the furrow stalls mid-way through progression (Figure 3.10) resulting in a characteristic cell which possesses two apparently normal anterior ends associated with flagella, this cell type has been called a 'push-me-pull-you' cell. Repeated attempts at furrowing are made by these cells leading to the formation of cells with multiple anterior ends which project from a central cell body. Ablation of GB4L does not appear to affect the formation or organisation of key organelles such as the PFR, basal bodies (Figure 3.11) or the FAZ (Figure 3.12) however new MT growth at the posterior end appears to be disorganised (Figure 3.13)

Since GB4, GB4L and TCP86 are known to be expressed in the BSF from proteomic analysis (Bridges *et al*, 2008) RNAi cell lines were raised in the BSF to examine the function of these proteins in this life cycle stage. GB4 depletion did not affect growth of the BSF (Figure 3.16), showing that this protein is not essential in this life cycle stage and ruling out one hypothesis that GB4 and GB4L may exhibit stage specificity.

RNAi depletion of GB4L and TCP86 in the BSF caused growth defects (Figure 3.16) and the phenotypes observed when both GB4L and TCP86 were depleted in the BSF are similar to those seen in the PCF. DAPI counts in the BSF GB4L cell line show an accumulation of 2K2N cells which is followed by an increase in the number of multinucleates and zoids (Figure 3.17). GB4L ablation in the BSF leads to the accumulation of 'push-me-pull-you' cells with a stalled cleavage furrow (Figure 3.19) and YL1/2 staining suggests that this may be related to disorganisation of new MT growth (Figure 3.20).

When TCP86 is depleted by RNAi in the BSF it is initially lost from the posterior end of the cell (Figure 3.22) as observed in the PCF (Shawcross, 2008). This may be explained by the fact that the posterior end of the cell is composed of more new MTs which were formed after the reserve of TCP86 protein in the cytoplasm has been depleted, meaning no TCP86 is available to decorate these MTs. The fact that TCP86 remains associated with the MTs at the anterior end suggests that it associates stably with MTs with little turnover (as observed in the PCF) (Figure 3.22). DAPI counts show an increase in the number of zoids and multinucleates in equal numbers after 12 hours of depletion (Figure 3.18); this is due to asymmetrical division which produces 1K0N zoids and 1K2N multinucleate progeny parallel to that seen in the

PCF (Shawcross, 2008). Multinucleates then re-enter the cell cycle resulting in a population mainly consisting of multinucleates and zoids by 24 hours (Figure 3.18).

The next chapter looks at the PCF GB4L and TCP86 RNAi cell lines in greater detail employing electron microscopy to investigate cellular morphology and ultrastructure in an attempt to further understand the distinct cytokinetic defects observed in both of these cell lines.

Chapter 4 Further investigation of GB4L and TCP86

4.1 Introduction

This chapter describes further functional characterisation of the GB4L and TCP86 RNAi cell lines by scanning and transmission electron microscopy (SEM and TEM) approaches. SEM analysis, which allows the visualisation of cellular morphology at a high resolution, shows that RNAi ablation of GB4L or TCP86 causes distinct morphological abnormalities; particularly with respect to posterior end formation which ultimately leads to distinct cytokinetic defects. TEM analysis of intracellular ultrastructure shows that GB4L depletion results in aberrant FAZ formation and cells with supernumerary MTs within the cytoplasm. In contrast, RNAi ablation of TCP86 has no discernable effects on the organisation of the FAZ and/or subpellicular corset MTs.

4.2 Analysis of the GB4L RNAi cell line using scanning electron microscopy

4.2.1 Non-induced

Figure 4.1 shows non-induced cells with wild type morphologies; with panels A-E showing cells at progressively later stages in the cell cycle. For instance, the cells in Figure 4.1A are in G_1 of the cell cycle, as they each possess a single flagellum while in panel B a new flagellum has emerged from the flagella pocket (white arrow) revealing this cell to be further advanced through the cell division cycle. Figure 4.1C and D also show examples of cells with two flagella; the length of the new flagellum

indicates that these cells are at a later stage in the cell cycle. The cell shown in Figure 4.1E is in cytokinesis and the path of cleavage furrow ingression is clearly defined; the position of the cleavage furrow suggests that upon completion of cytokinesis both daughter cells will be of equal size with clearly defined posterior ends. In this cell the FC is no longer attaching the new flagellum to the old and there are two distinguishable anterior ends (white arrows).

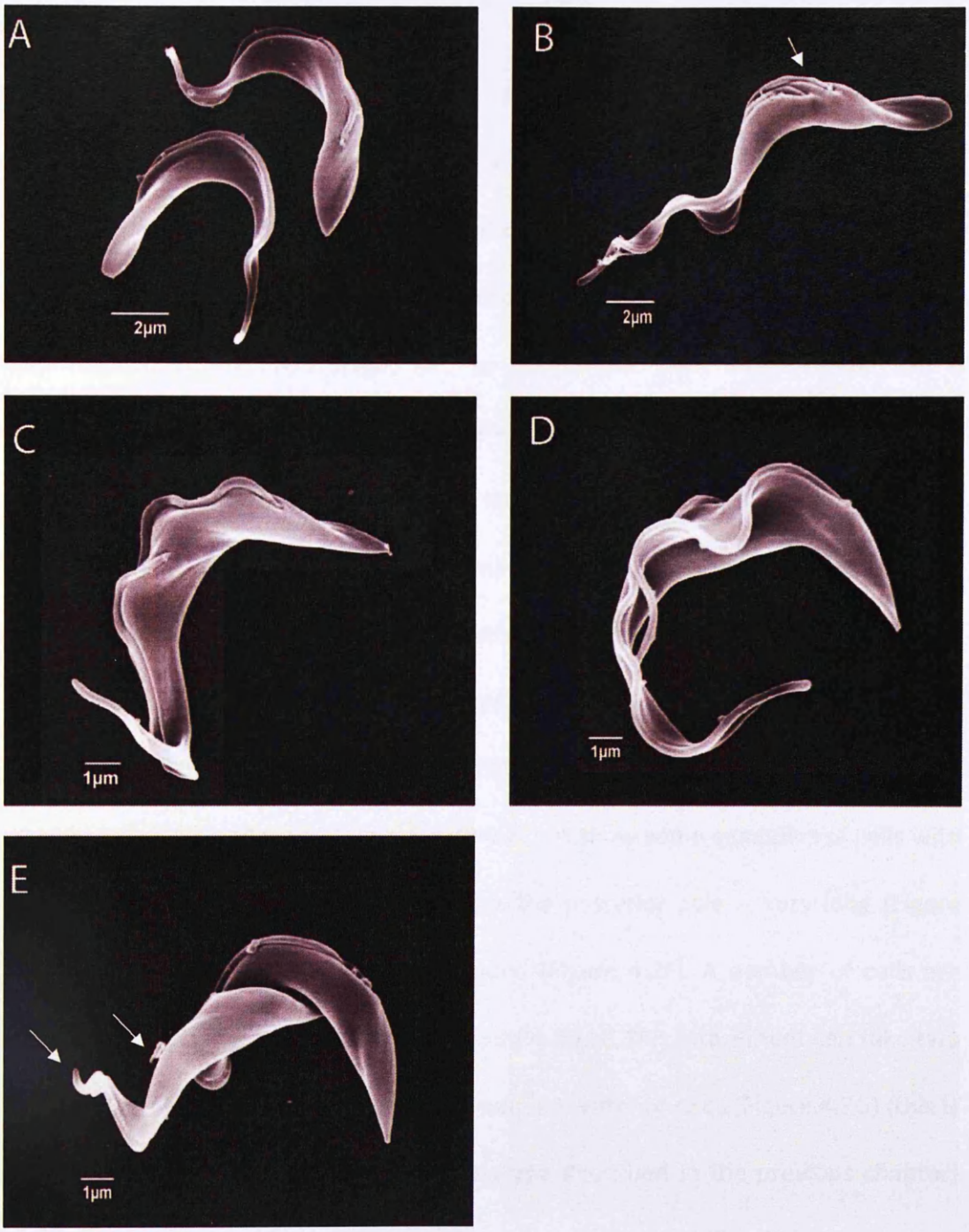

Figure 4.1 Scanning electron micrographs of the non-induced GB4L RNAi cell line at different stages of the cell cycle

Cells were prepared for SEM analysis as detailed in section 2.5.5, examples shown are representative cells from a non-induced culture. Cells did not show abnormal morphology at any cell cycle stage, A-E show cells at progressively later cell cycle stages from G_1 (A) to cytokinesis (E). White arrow in (B) indicates new flagellum; white arrows in (E) indicate two distinct anterior ends.

4.2.2 12 Hours post-induction

In contrast to the normal cell morphologies seen in non-induced cells (Figure 4.1A-E), cells taken from cultures 12 hours after the induction of GB4L RNAi show abnormal morphologies. The heterogeneity of morphological phenotype observed is likely to be a reflection of the fact that RNAi is induced in a population that is heterogeneous with respect to cell cycle stage; and so the output from an individual cell is dependent upon the stage in the cell cycle when GB4L protein expression is ablated. However, as the doubling time of this cell line exceeds 12 hours; it is safe to assume that the cells shown here have not completed more than one cell cycle under conditions of GB4L depletion. Representative cell types from the 12 hour induced sample are shown in Figure 4.2; a feature common to all these cell types is an apparent defect in posterior end formation. Figure 4.2A - D show cells at progressively later cell cycle stages, Figure 4.2E - H show some examples of cells with gross morphological defects. In some cases the posterior pole is very long (Figure 4.2E) while in others it is short and rounded (Figure 4.2F). A number of cells are found attached by their posterior ends (Figure 4.2G,H), this attachment can take two forms; (i) a 'plate' or 'ridge' structure between two anterior ends (Figure 4.2G) (this is the characteristic 'push-me-pull-you' phenotype described in the previous chapter) or (ii) cells can remain attached by a thin 'bridge' (Figure 4.2H). Cells which have failed to complete cytokinesis re-enter the cell cycle and appear as multiflagellated cells (Figure 4.2H). In all cases formation of the anterior end appears normal.

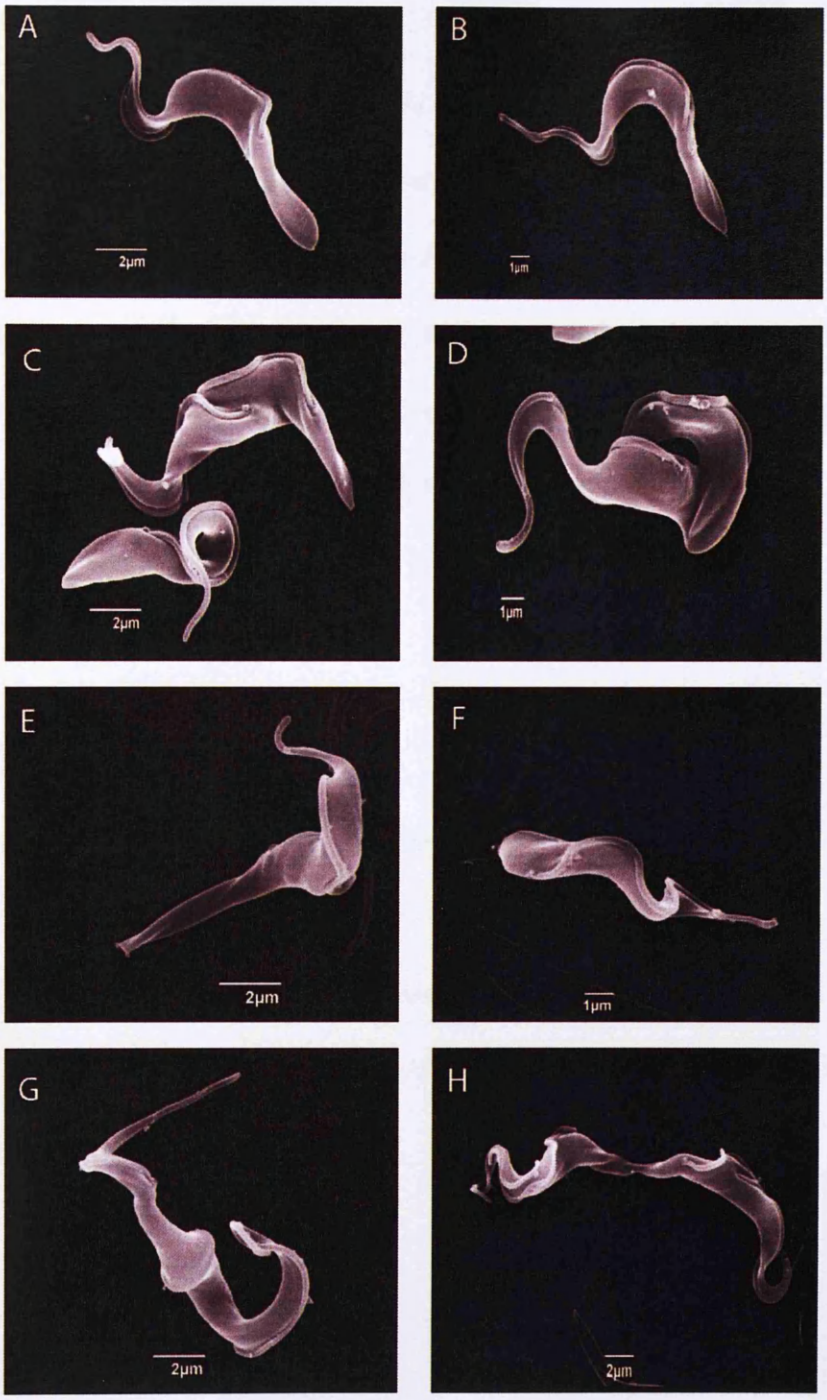

Figure 4.2 Scanning electron micrographs of the GB4L RNAi cell line 12 hours post induction

Cells were prepared for SEM analysis as detailed in section 2.5.5, examples shown are representative cells from a culture 12 hours post induction. A-D cells at progressively later stages of the cell cycle. Images E-H abnormal cell morphologies observed. Cell in image E has an elongated posterior end; cell in image F has a rounded posterior end. Cells shown in G and H are stalled in cytokinesis.

4.2.3 24 Hours post-induction

24 hours after the induction of GB4L RNAi very few cells progress through the cell cycle with a normal cell morphology. A large proportion of the cells appear to be stalled in cytokinesis with a 'push-me-pull-you' phenotype characterised by a 'ridge' between two apparently normal anterior ends (Figure 4.3A-C). These cells remain attached and re-enter the cell cycle; the product of this cell cycle is often a multinucleate cell with multiple anterior ends protruding from a large cell body (Figure 4.3D and E).

4.2.4 48 Hours post-induction

After 48 hours of GB4L depletion the majority of cells are multinucleates, shown in Figure 4.4. Cells at this time point are still unable to resolve the posterior end and have re-entered the cell cycle multiple times. Numerous attempts of cleavage furrow ingression have been made and reasonably normal anterior ends are still visible protruding from a large cell body.

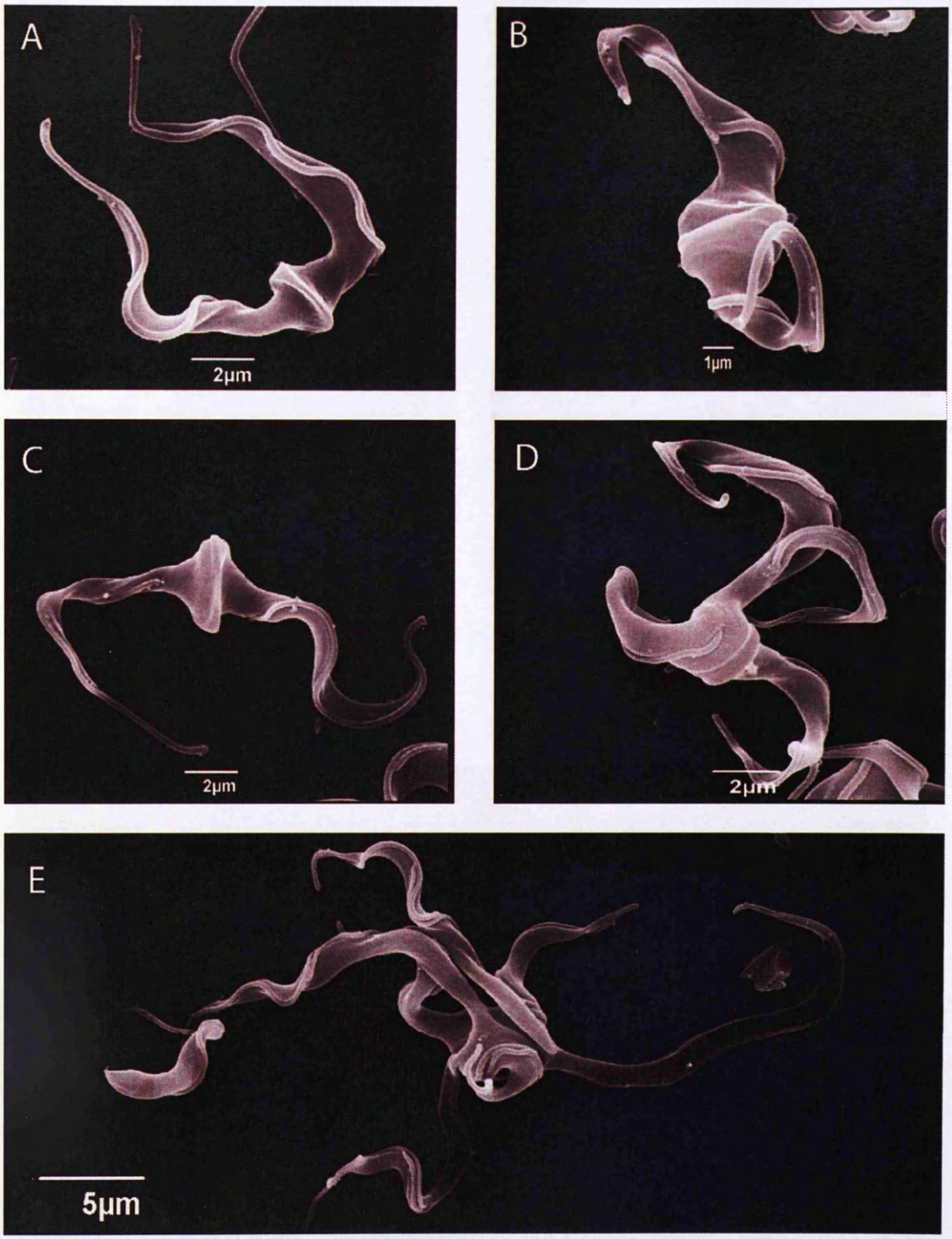

Figure 4.3 Scanning electron micrographs of the GB4L RNAi cell line 24 hours post induction

Cells were prepared for SEM analysis as detailed in section 2.5.5, examples shown are cells from a culture 24 hours post induction. Cells in A-C show the characteristic 'push-me-pull-you' phenotype with a ridge structure between the two joined posterior ends. Cells in D and E are multinucleates with multiple anterior ends protruding from a single cell body.

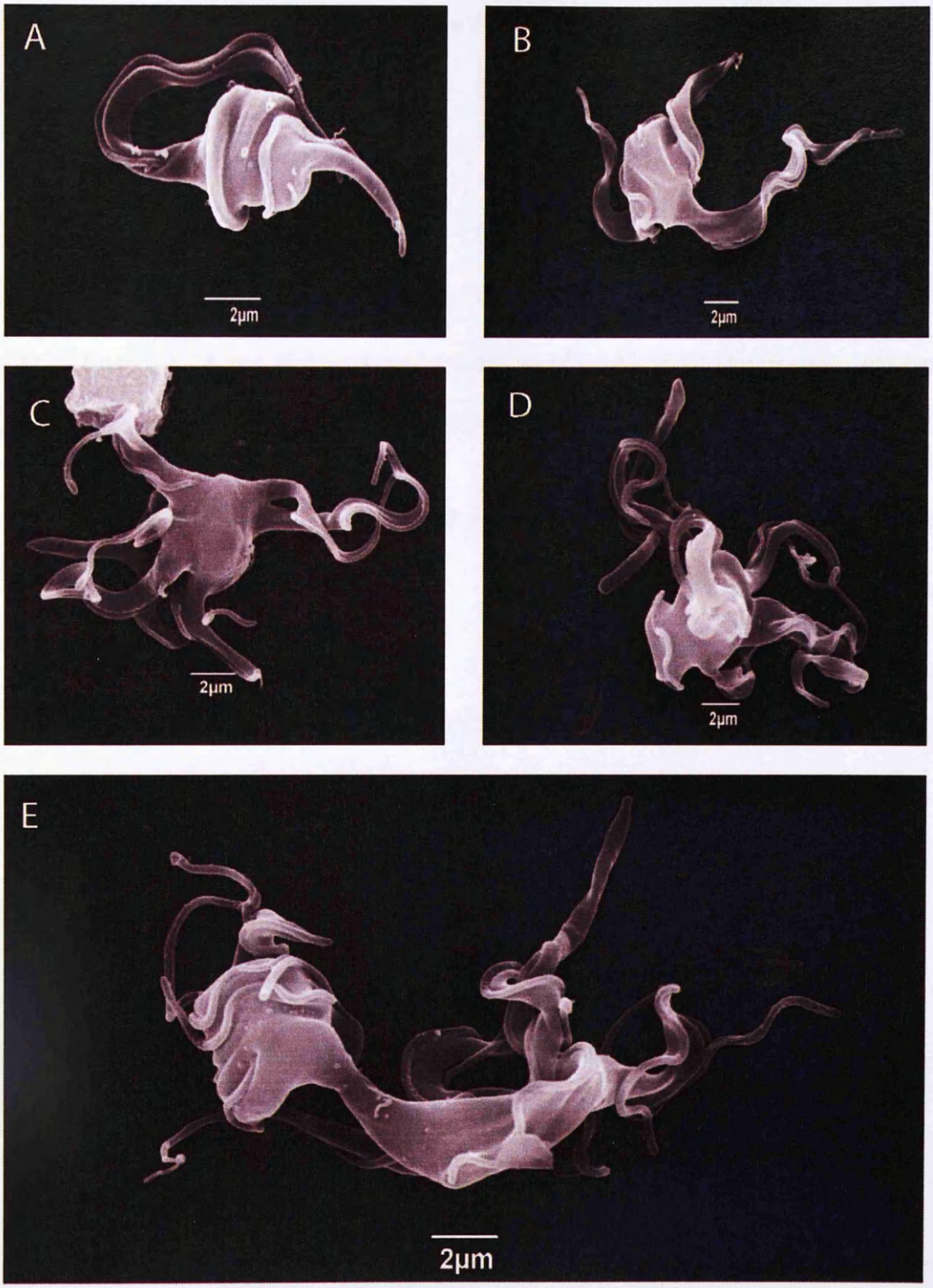

Figure 4.4 Scanning electron micrographs of the GB4L RNAi cell line 48 hours post induction

Cells were prepared for SEM analysis as detailed in section 2.5.5, examples shown are cells from a culture 48 hours post induction. The majority of cells are large multinucleates with multiple anterior ends projecting from a central 'cell body'.

4.3 Analysis of the GB4L RNAi cell line by transmission electron microscopy

Having used SEM to visualise the grossly abnormal cellular morphologies resulting from RNAi ablation of GB4L, transmission electron microscopy (TEM) analysis was undertaken to investigate any defects in ultrastructural organisation. The sections below present images of TEM cross-sections through non-induced cells and cells from cultures 12, 24 and 48 hours post induction of GB4L RNAi. The position of cross sections within the cell was established as follows (see Figure 4.5):

(i) **Anterior** - if they were small in diameter and possessed an axoneme associated with a PFR

(ii) **Mid-region** - if they were distinguished by a wider diameter, the presence of a nucleus and one or two axonemes

(iii) **Posterior** - if they were of small diameter and a flagellum was either absent (extreme posterior) or the section contained a kinetoplast and/or flagella pocket

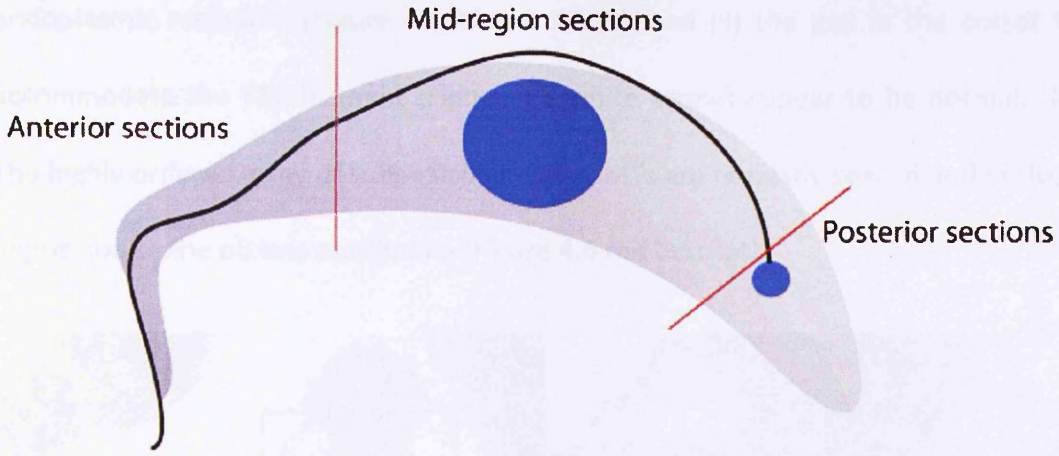

Figure 4.5 Cartoon to show how TEM sections were classified

TEM cross-sections presented are classified as the anterior end, the mid region and the posterior end of the cell. The cartoon shows how these regions were defined. Anterior sections can be identified by the presence of an external flagellum/flagella and a comparatively small diameter, mid-regions are identified by a larger diameter, external flagellum/flagella and/or the presence of a nucleus, and posterior end sections can easily be identified due to the smaller diameter, no associated flagellum and/or presence of a flagella pocket, basal body or kinetoplast.

Sections are viewed from the posterior end of the cell, with polarity determined by reference to the axial polarity of the outer MT doublets and associated dynein arms. This orientation of sections ensures that in biflagellate cells the new flagellum is always located to the left-hand side of the old flagellum (Davidge *et al*, 2006).

4.3.1 Non-induced

TEM analysis confirmed cells were normal prior to the induction of GB4L RNAi, with no discernable morphological abnormalities. However, given the ultrastructural abnormalities that are observed following GB4L RNAi induction (discussed in the following sections) it is particularly worth noting the following: (i) The organisation of the FAZ, which consists of a microtubule quartet (MtQ) and associated smooth

endoplasmic reticulum (Figure 4.6 blue bracket), and (ii) the gap in the corset to accommodate the FAZ filament (Figure 4.6 white arrow) appear to be normal. (iii) The highly ordered array of subpellicular corset MTs are regularly spaced and in close apposition to the plasma membrane (Figure 4.6 red bracket).

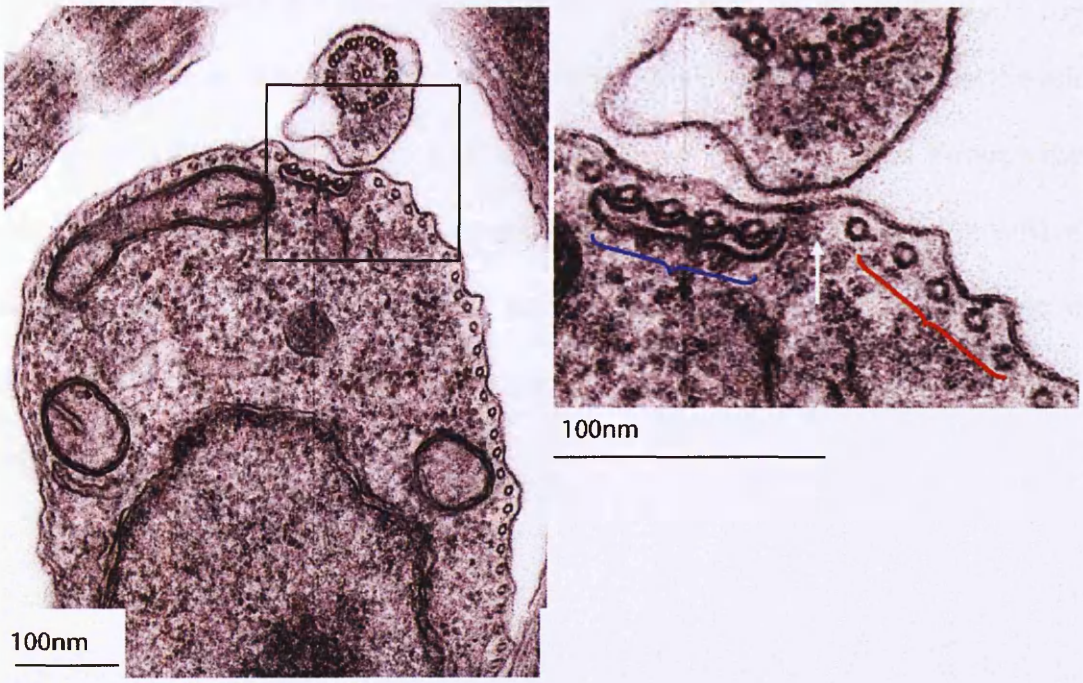

Figure 4.6 Transmission electron micrograph of a transverse section through a non-induced GB4L cell

Cells from a non-induced culture of the GB4L RNAi cell line were prepared as described in section 2.5.6. This is a section through the mid-region of a cell from a non-induced GB4L culture. Left, black box indicates the region magnified on the right. Blue bracket shows where the MtQ is located; microtubules are associated with smooth ER. White arrow, shows the wide space in between corset microtubules where the filament resides. Red brackets show the subpellicular corset microtubules which are located just beneath the plasma membrane with regular spacing as in wild type cells.

4.3.2 12 Hours post-induction

After 12 hours of GB4L ablation abnormities in FAZ formation were detected examples of this are shown in Figure 4.7. Figure 4.7A shows a transverse section through the anterior region of a cell, showing that axoneme and PFR morphology

appears normal, and moreover that MTs of the subpellicular corset are regularly spaced. However, it is noticeable that the smooth endoplasmic reticulum (ER), which normally associates with the MtQ of the FAZ, appears only to associate with two MTs. Figure 4.7B, shows another example of FAZ disruption, in this case in a section through a mid region of a cell. The smooth ER can be seen on both sides of the FAZ filament; an unusual configuration as it would normally be located only on the left side of the FAZ filament. Figure 4.7C, is another example of a section through the mid-region of a cell, the FAZ associated with the new flagellum (on the left) is abnormal, the arrow points to the FAZ filament and to the right of this is the gap in the corset MTs which is abnormally wide and filled with electron dense material (blue brackets).

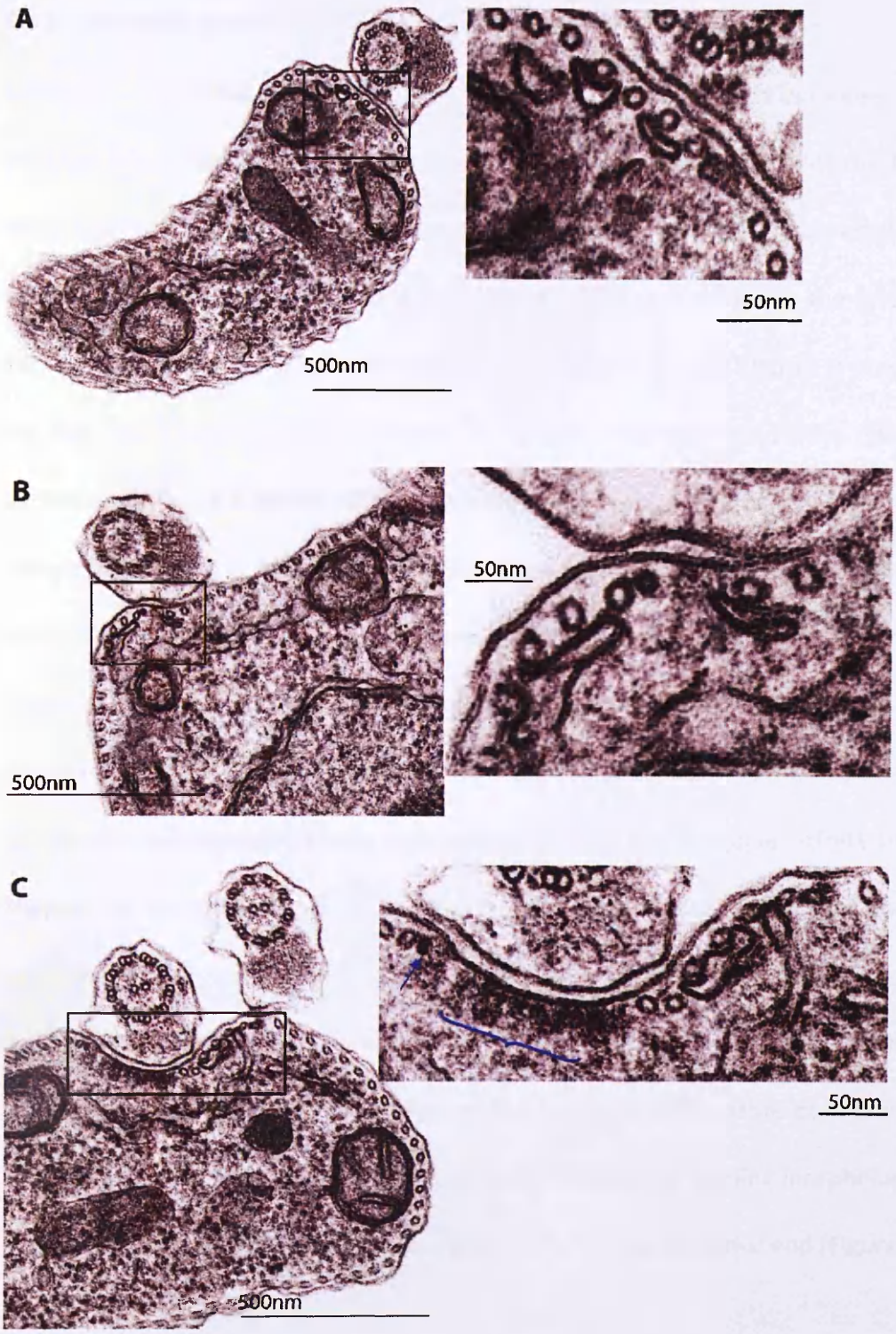

Figure 4.7 Transmission electron micrographs of transverse sections through cells 12 hours post induction of GB4L RNAi ablation

Cells from a culture 12 hours post induction of GB4L RNAi were prepared as described in section 2.5.6. Cells in A-C have a disrupted FAZ architecture. Boxed regions are zoomed in on the left. C, blue arrow indicates the FAZ filament; bracket indicates an abnormally large space in subpellicular MTs filled with electron dense material.

4.3.3 24 Hours post-induction

Anterior - Figure 4.8 shows a selection of TEM cross sections taken close to the anterior end of GB4L RNAi induced cells 24 hours post induction. Whilst the MTs of the subpellicular corset maintain an even spacing and remains closely apposed to the plasma membrane, in some regions additional MTs are present within the cytoplasm immediately beneath the subpellicular corset; indicated by blue arrows in images on the left. The boxed regions are shown at a higher magnification on the right with additional MTs highlighted with a blue asterisk. As seen in cells 12 hour post induction (Figure 4.7), the smooth ER associated with the MtQ is also disrupted at 24 hours (Figure 4.8A-C). However this phenotype appears more severe at 24 hours post induction, the smooth ER is seen associating with one, or a maximum of two, MTs compared to four MTs in wild-type and non-induced samples. Figure 4.8B shows that membrane also appears to have invaded the space in the MT corset where the FAZ filament is normally found. It is important to note that disruption of the FAZ architecture does not interfere with flagellum attachment as there was no increase in cells with detached flagella within the induced population compared with non-induced cells. Furthermore, the disrupted FAZ is clearly still capable of defining the plane of cleavage as cells initiate cleavage furrow ingression forming morphologically normal anterior ends before ingression stalls closer to the posterior end (Figure 3.11, Figure 3.12, and Figure 4.3).

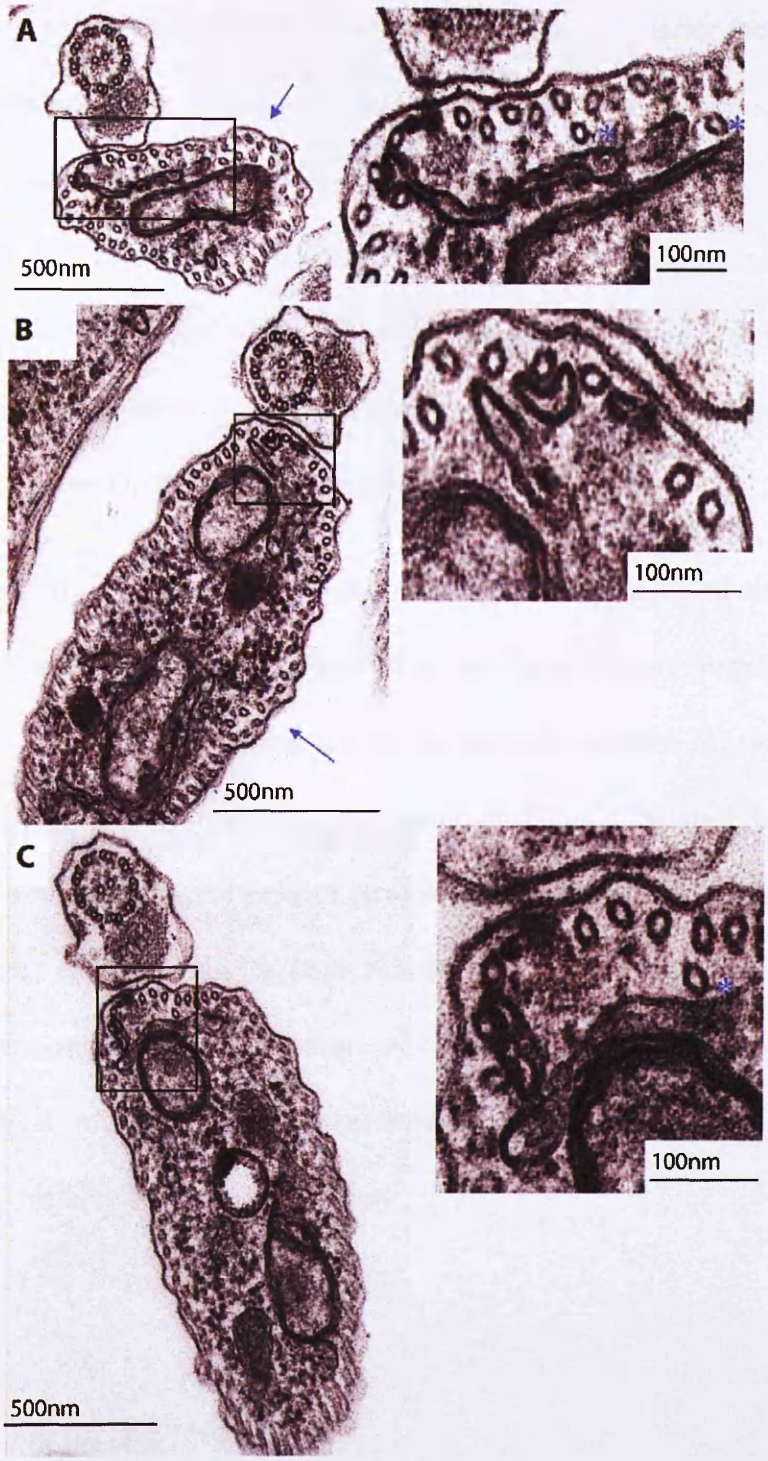

Figure 4.8 Transmission electron micrographs of transverse sections through cells 24 hours post induction of GB4L RNAi ablation (anterior)

Cells from a culture 24 hours post induction of GB4L RNAi were prepared as described in section 2.5.6. Sections taken through the anterior end of cells, black boxed regions are shown magnified on the right, sections have additional microtubules (indicated with blue arrows/asterisks) and the smooth ER associated with the MtQ is disrupted.

Mid-region - is shown in Figure 4.9, similarly to the 24 hour anterior sections (Figure 4.8) these sections taken through the mid-region of cells at 24 hours show some additional MTs and disruption of the smooth ER of the FAZ. Figure 4.9A, a 1F cell, the spacing of the MTs in the corset is maintained however a small number of additional MTs are apparent, the most obvious abnormality is seen in the FAZ where a MT associated with membrane is found within the cytoplasm, this is boxed off and shown at a higher magnification to the right.

Figure 4.9B is a 2F cell, the old flagellum is on the right and indicated with an O, the FAZ region appears normal and is magnified on the right. The new flagellum (N) is to the left of the old and has an abnormal FAZ. The normal organised subpellicular array of MTs in this region is disrupted and the smooth ER is not associated with the MtQ, there is only a small amount of smooth ER which is only loosely associated with MTs. This shows that when the old flagellum was forming (before the ablation of GB4L) the cell was capable of building a normal FAZ. In contrast, when the new flagellum was being built in GB4L depleted conditions; an abnormal FAZ was formed, supporting a role for GB4L in FAZ formation.

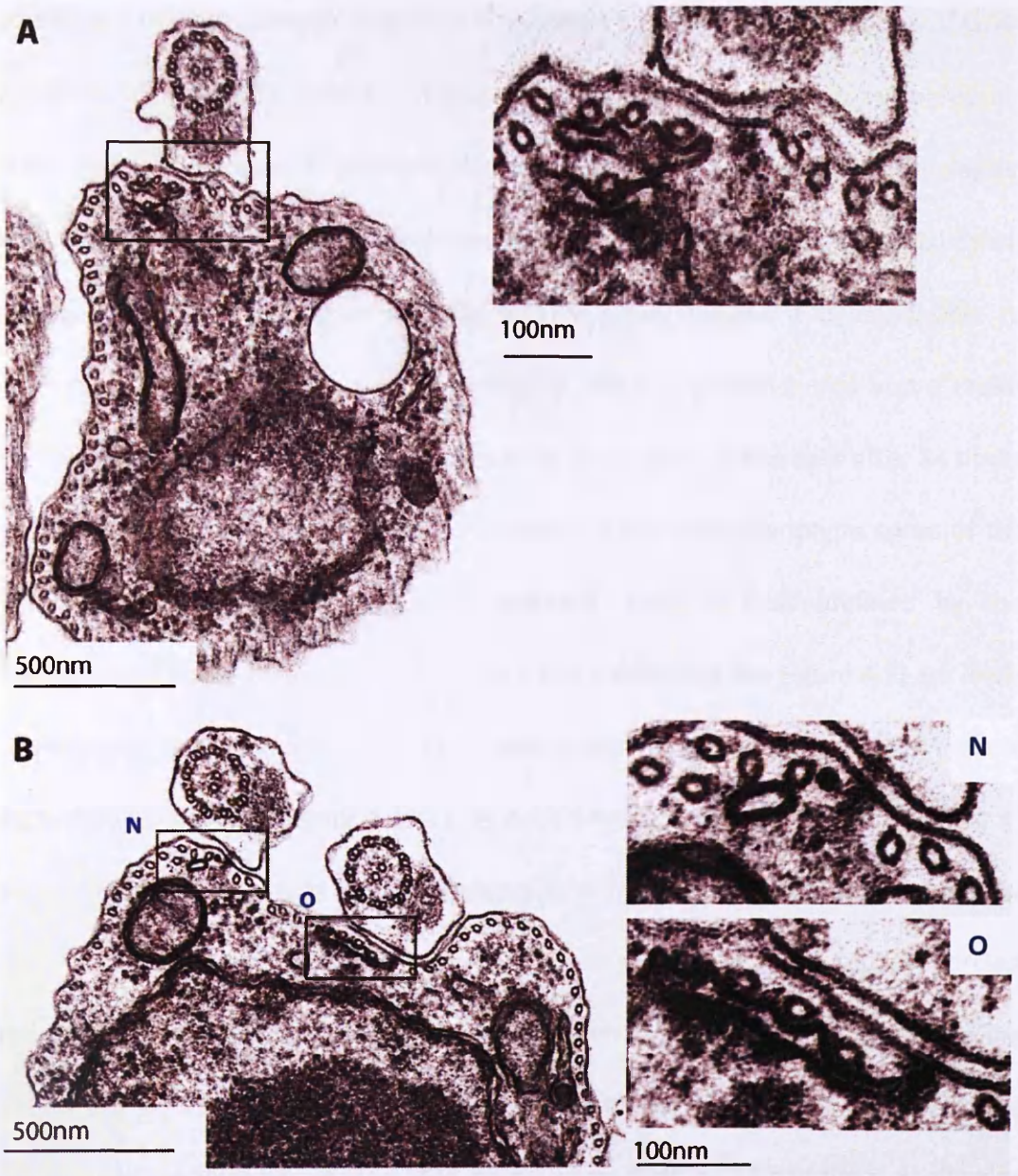

Figure 4.9 Transmission electron micrographs of transverse sections through cells 24 hours post induction of GB4L RNAi ablation (mid-region)

Cells from a culture 24 hours post induction of GB4L RNAi were prepared as described in section 2.5.6. Cell in A, has one flagellum and FAZ region shows a microtubule associated with the smooth ER within the cytoplasm. Cell in B, has two flagella, the smooth ER associated with FAZ of the old flagellum appears normal (O). In contrast the smooth ER associated with the FAZ of the new flagellum (N) is disrupted suggesting this phenotype occurs when cells attempt to build a new FAZ in the absence of GB4L.

Posterior - The SEM analysis described in section 4.2 confirmed that ablation of GB4L results in a cytokinetic defect and that in many cases cleavage furrow ingression stalls and cells take on a 'push-me-pull-you' phenotype (Figure 3.13). The region between the two joined cells (which would normally form the posterior ends) forms a ridge structure (see Figure 4.3A-C). In TEM cross-sections it is impossible to distinguish between a cross-section through a 'normal' posterior end and a cross-section through the 'ridge' structure. However, since many of the cells after 24 hours of GB4L RNAi induction have adopted a 'push-me-pull-you' phenotype some of the TEM cross-sections which represent 'posterior' ends of cells (defined by the possession of a flagella pocket or the absence of a flagellum see Figure 4.5) are likely to represent the ultrastructure of the 'ridge' region. Examples of these TEM cross-sections are shown in Figure 4.10A-C in each section there are a large number of supernumerary MTs which are disorganised in terms of orientation as some can be seen in transverse section whilst others are viewed in longitudinal section (circled red).This confirms earlier observations made by immunofluorescence analysis using YL1/2 (see Figure 3.13) which indicated that disorganised growth of new MTs was occurring in the ridge region. The TEM images show that the MTs of the subpellicular MTs remain in close apposition to the plasma membrane.

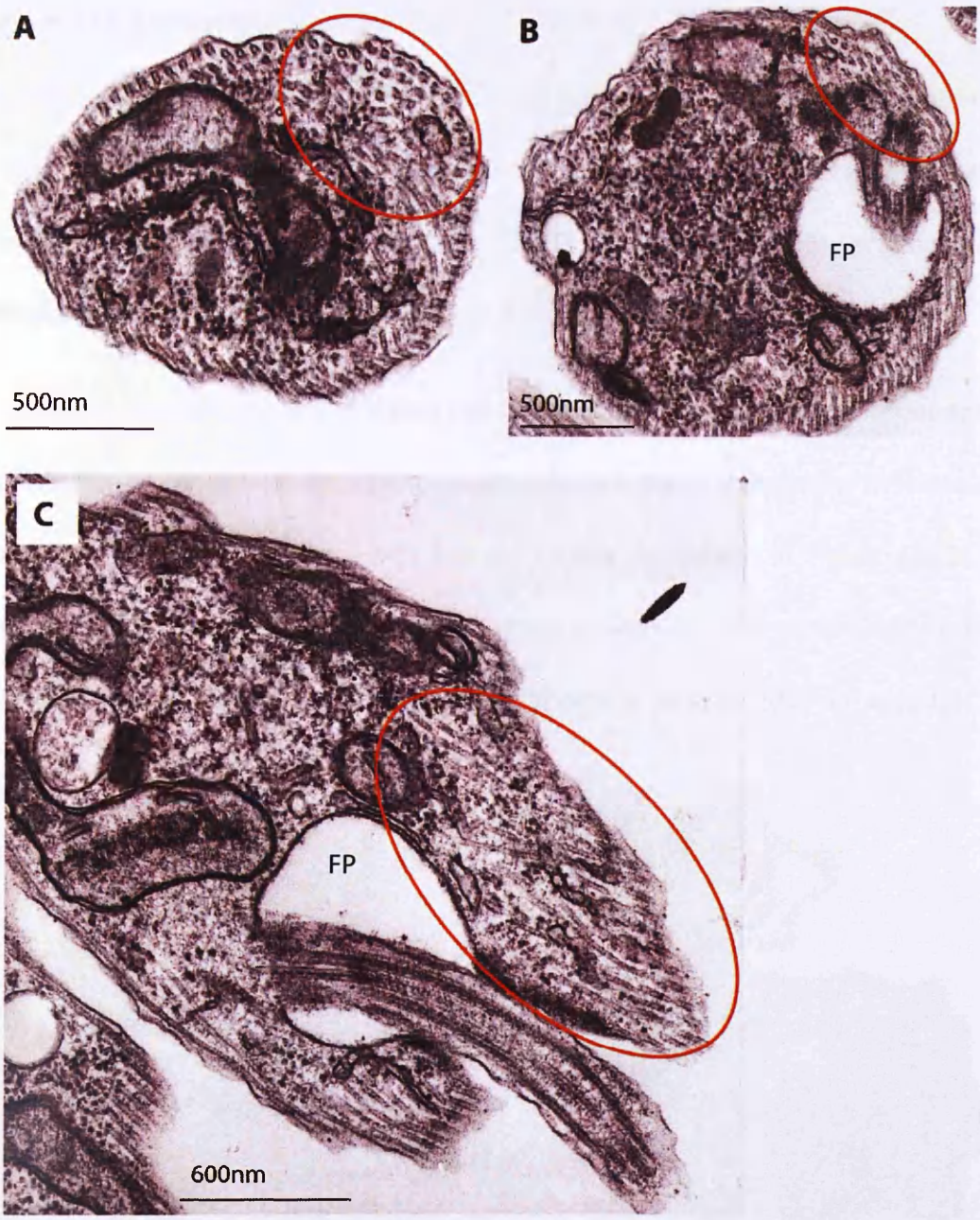

Figure 4.10 Transmission electron micrographs of sections through cells 24 hours post induction of GB4L RNAi ablation (posterior)

Cells from a culture 24 hours post induction of GB4L RNAi were prepared as described in section 2.5.6. Cell in A, possibly the 'ridge' region with many additional MTs seen in the cytoplasm (some of which are circled in red). Section B is through the flagella pocket (FP) there are many additional MTs in the cytoplasm (circled in red). Section C, a longitudinal section of the flagella pocket (FP), circled in red is a region of disorganised subpellicular MTs.

4.3.4 48 Hours post-induction

48 hours after the induction of GB4L ablation supernumerary MTs are present in the cytoplasm throughout the cell, this is a more severe phenotype than observed at 24 hours in which supernumerary cytoplasmic MTs were restricted to the sections taken through the posterior end of cells (Figure 4.10).

Anterior - Figure 4.11A and B shows transverse sections through the anterior end of two cells and in both images although spacing between subpellicular MTs remains uniform there are additional MTs present in the cytoplasm. In Figure 4.11B, the orientation of many supernumerary MTs is not uniform as while some clearly appear in transverse section others are blurred and appear to be in longitudinal section.

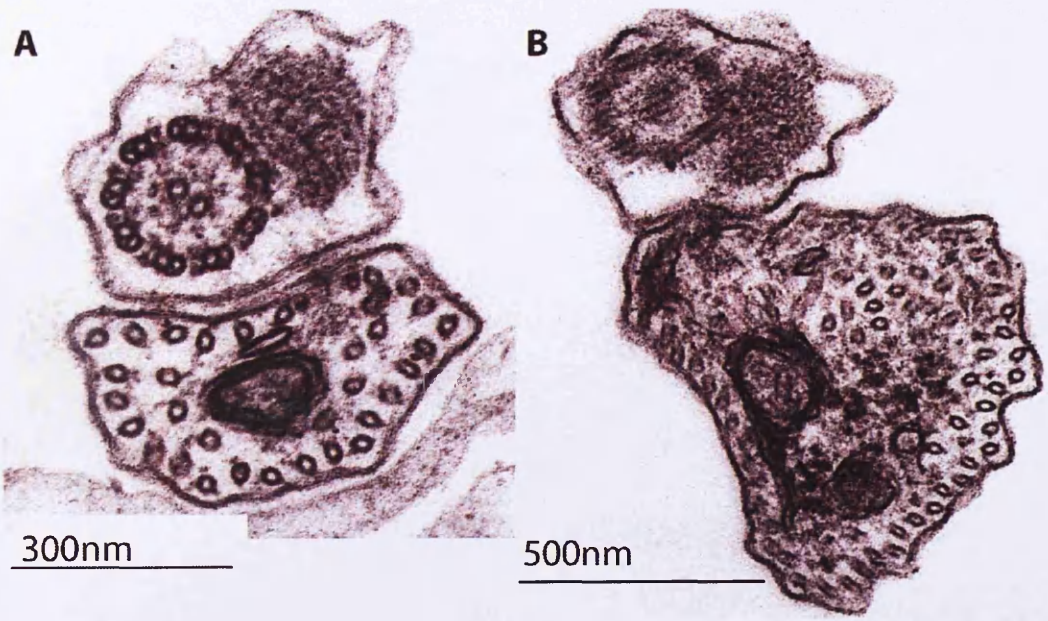

Figure 4.11 Transmission electron micrographs of transverse sections through cells 48 hours post induction of GB4L RNAi ablation (anterior)

Cells from a culture 48 hours post induction of GB4L RNAi were prepared as described in section 2.5.6. A and B are two examples of sections through the anterior end of cells which show many supernumerary microtubules in the cytoplasm, the cell in B shows supernumerary MTs are disorganised in terms of their orientation.

Mid-region - Figure 4.12A-C shows sections through the mid-region of cells 48 hours post GB4L ablation. As in earlier time points, cells exhibit abnormal FAZ architecture (Figure 4.12A-C boxed regions magnified on the right). Supernumerary MTs can be seen in the cytoplasm of all three cells this is especially pronounced in the cell shown in Figure 4.12B. Moreover, smooth ER was observed aberrantly associated with cytoplasmic MTs; normally in wild type/non-induced cells it is located just below the plasma membrane in association with the MtQ of the FAZ (Figure 1.3 and Figure 4.6). This phenotype is similar to the FAZ defects observed at 24 hours but appears more severe in cells at 48 hours after the induction of GB4L RNAi.

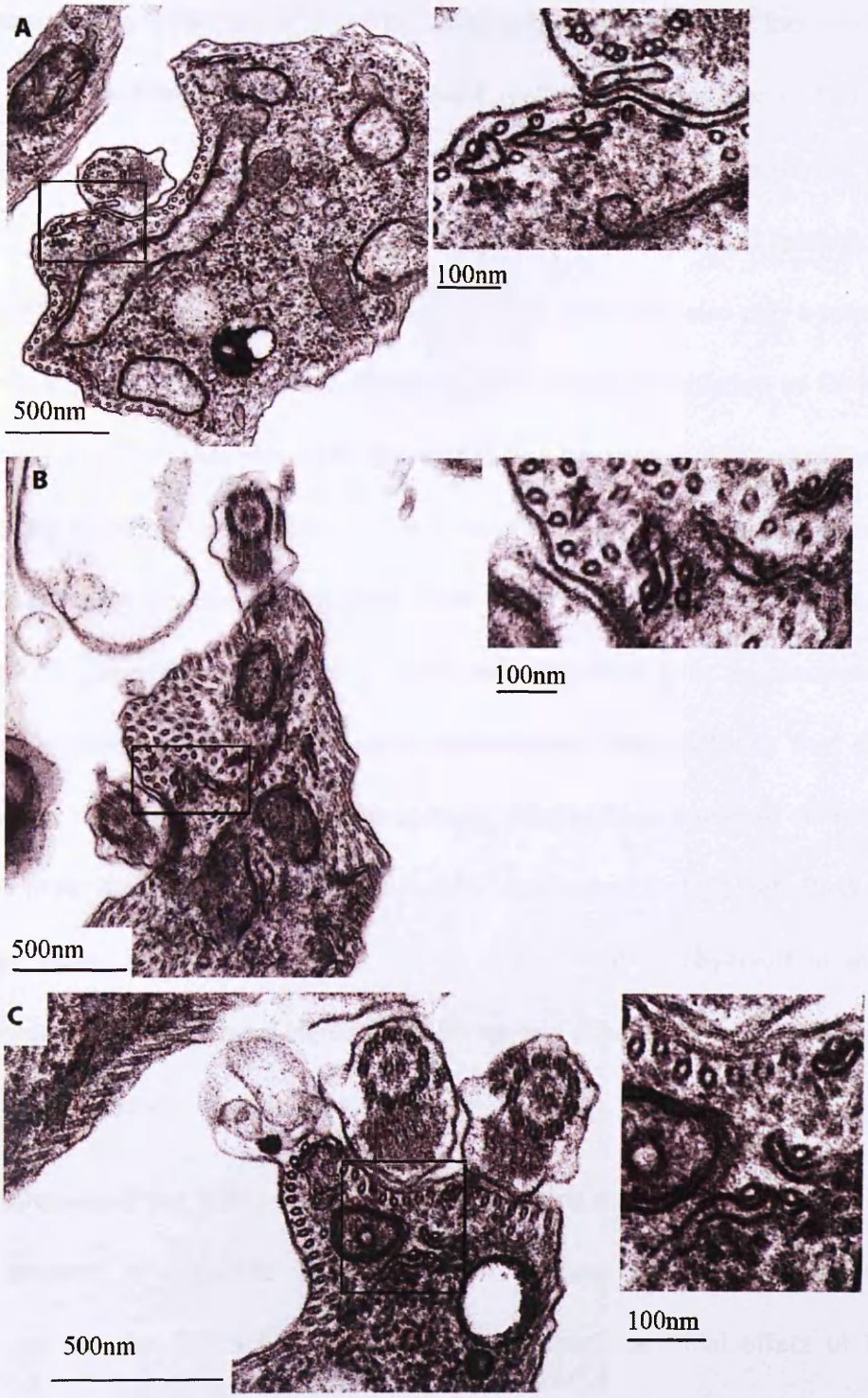

Figure 4.12 Transmission electron micrographs of transverse sections through cells 48 hours post induction of GB4L RNAi ablation (mid-region)

Cells from a culture 48 hours post induction of GB4L RNAi were prepared as described in section 2.5.6. Sections A-C show cells with disrupted FAZ regions (see magnified images on the right) also additional MTs can be seen beneath those of the subpellicular corset.

Conclusions - The TEM study on the GB4L RNAi cell line shows that at increasing time points post induction there is a progressive increase in the number and extent of supernumerary MTs. Initially these MTs are most apparent at the posterior end of the cell suggesting that the organisation and regulation of new MT growth is lost following GB4L ablation. TEM analysis suggests that GB4L may also play a role in the structural organisation of the FAZ. However, RNAi mediated ablation of GB4L does not disrupt the formation of the FAZ filament as this structure is often seen clearly at all time points in sections from anterior through to posterior of the cell. In some cases cells which possess two flagella have an old flagellum with a normal FAZ morphology (formed pre-induction), and a new flagellum with an abnormal FAZ (formed post-induction) this observation corroborates the hypothesis that GB4L is required for normal FAZ formation. Intriguingly, despite these apparent disturbances the two main functions of the FAZ (1) flagella attachment and (2) definition of the cleavage plane are unaffected. No flagella detachment is observed in induced cultures and cleavage furrow ingression initiates and produces two morphologically normal anterior ends.

4.4 Analysis of the TCP86 RNAi cell line by scanning electron microscopy

Measurements of organelle positioning and immunofluorescence experiments carried out on the TCP86 RNAi cell line suggest that the initial effect of TCP86 depletion is an elongation of the posterior end of the cell, which ultimately leads to a defect in cytokinesis. Cells undergo asymmetrical division resulting in the production of anucleate zoids and multinucleate 1K2N cells (Shawcross, 2008). To further investigate the effects of TCP86 ablation SEM analysis was carried out; the results of this analysis are presented below.

Non-induced cells from the TCP86 RNAi cell line were initially examined and shown to have wild type morphology (see supplementary Figure 8.6).

4.4.1 12 Hours post-induction

After 12 hours of TCP86 RNAi induction, cells early in the cell cycle have an elongated posterior end indicated by the white arrows in Figure 4.13A-C. Later in the cell cycle, cells undergo aberrant cytokinesis in which cells divide asymmetrically resulting in a much smaller daughter cell indicated with asterisks in Figure 4.13E and F. DAPI counts indicate that these smaller cells are often an anucleate zoid, and the larger cells have a 1K2N DNA content (Shawcross, 2008).

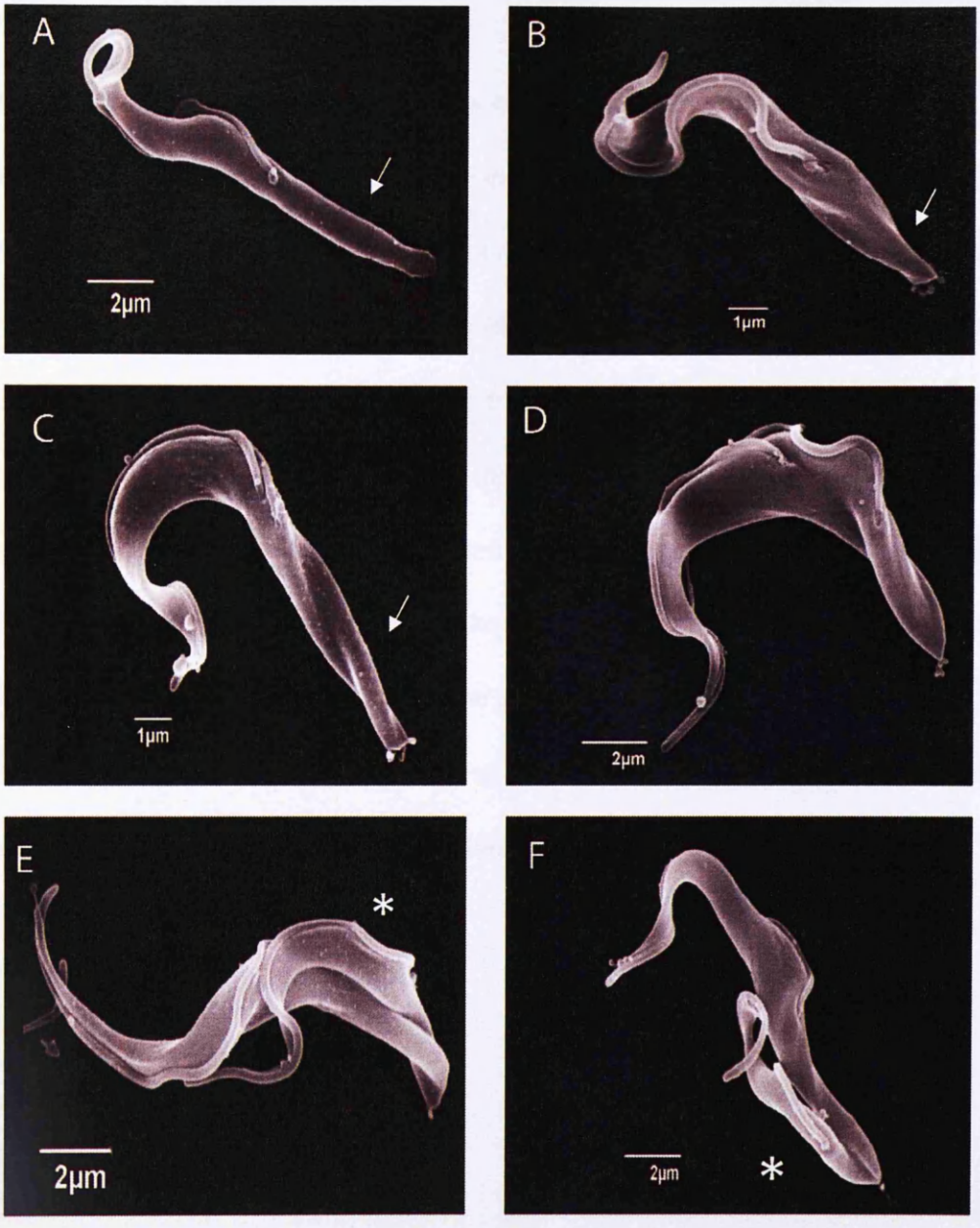

Figure 4.13 Scanning electron micrographs of the TCP86 RNAi cell line 12 hours post induction

Cells prepared for SEM analysis as detailed in section 2.5.5, examples shown are from a population 12 hours after induction of TCP86 RNAi. Cells in A-C show early stages of the cell cycle with abnormally long posterior ends (indicated with arrows), cell in D a later cell cycle stage (possibly mitosis). Cells in E and F have a cleavage furrow, these cells are undergoing aberrant cytokinesis; this asymmetrical division will result in progeny of unequal size. The small daughter cell is indicated with an asterisk and probably represents a zoid containing only a kinetoplast. The large daughter cell is likely to represent a multinucleate containing 1K2N.

4.5 24 Hours post-induction

After 24 hours, TCP86 RNAi induced cells can still be seen with elongated posterior ends (Figure 4.14A and B), and most cytokinetic events are asymmetric. Figure 4.14C-F show examples of cells in which the cleavage furrow has sufficiently progressed to indicate that the products of cytokinesis will be asymmetric. Whilst it is impossible to ascertain the DNA content of these cells from the SEM data, previous DAPI counts (Shawcross, 2008), show there is a large increase in zoids and multinucleates at this time point. This suggests that the asymmetrical division observed by SEM results in a smaller cell which contains a kinetoplast but does not possess a nucleus (a zoid) and a larger cell which contains two nuclei and a kinetoplast (a multinucleate). The small cells shown in Figure 4.14G and H are also likely to represent zoids; it is noticeable that some of these zoids have extremely long posterior ends (Figure 4.14H).

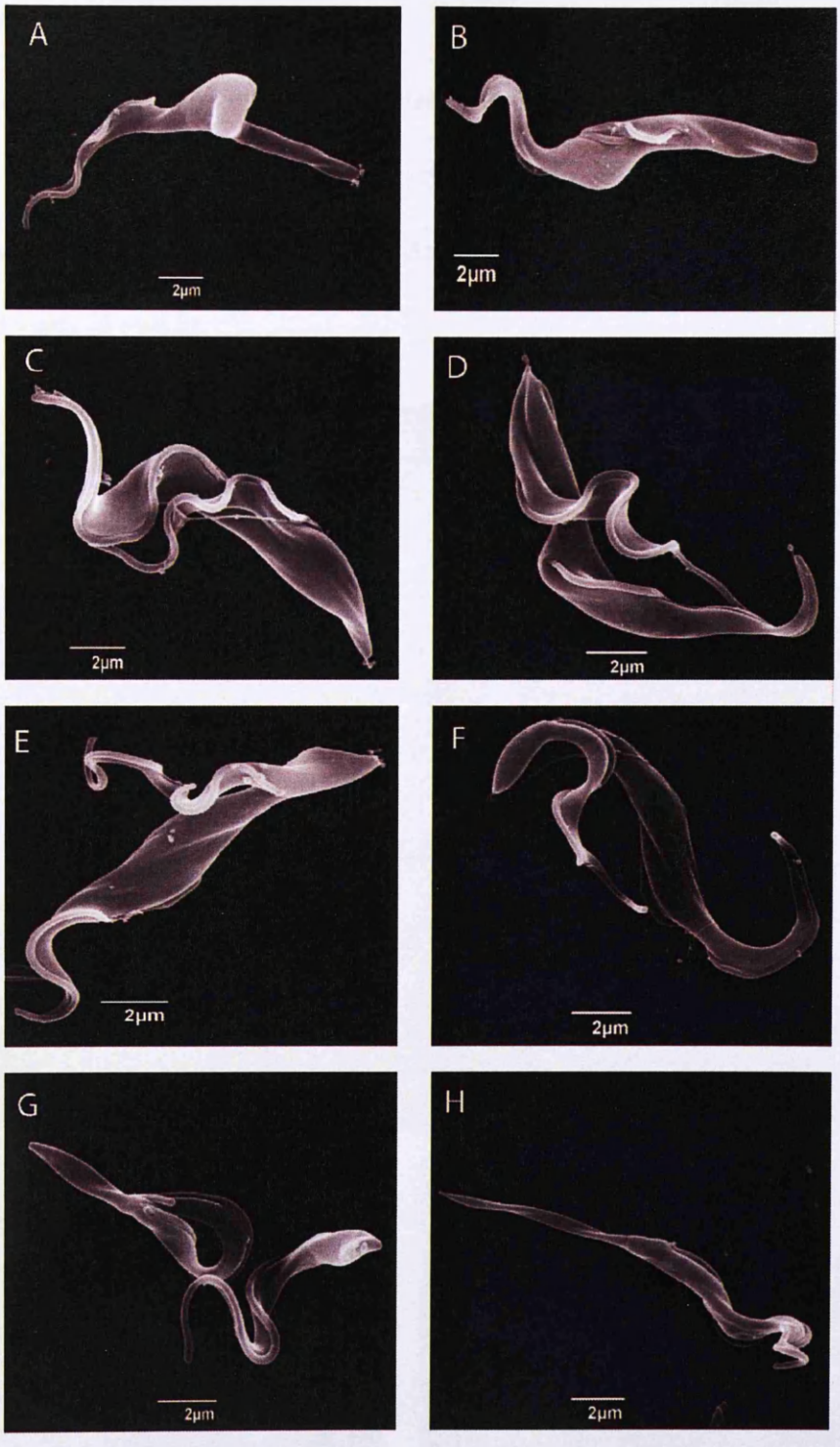

Figure 4.14 Scanning electron micrographs of the TCP86 RNAi cell line 24 hours post induction

Cells prepared for SEM analysis as detailed in section 2.5.5, examples shown are representative cells from a population 24 hours after induction of TCP86 RNAi. Cells shown in A and B have an elongated posterior end, cells in C-F are undergoing asymmetrical division, and cells in G and H probably represent zoids.

4.5.1 48 Hours post-induction

After 48 hours the majority of TCP86 ablated cells are multinucleates or zoids, and very few cells progress through the cell cycle with a normal morphology (Shawcross, 2008). Figure 4.15 shows a large multinucleate (A) and two smaller cells which likely represent zoids (B and C).

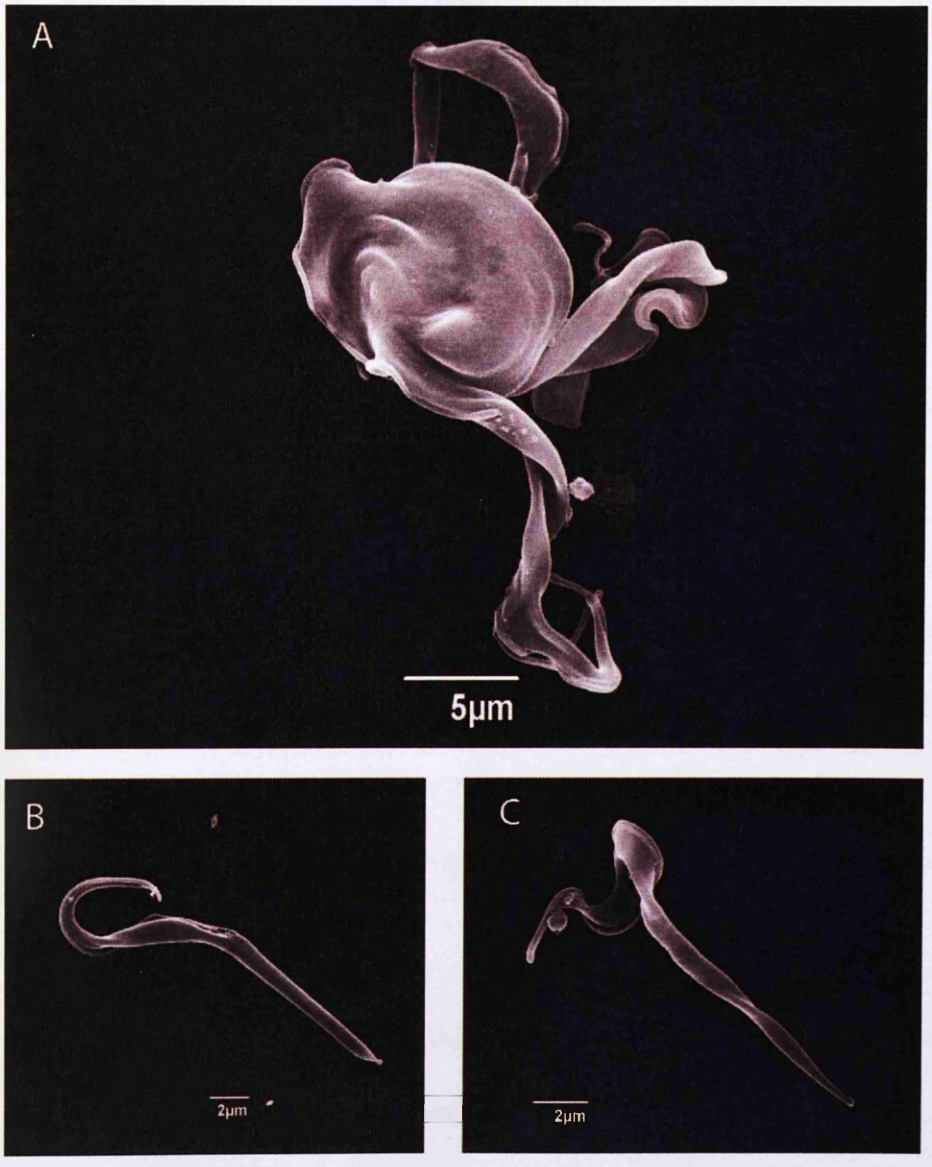

Figure 4.15 Scanning electron micrographs of the TCP86 RNAi cell line 48 hours post induction

Cells were prepared for SEM analysis as detailed in section 2.5.5, examples shown are cells from a population 48 hours post induction of TCP86 RNAi. Cell in (A) is a multinucleate, (B) and (C) are zoids.

Whilst the effects of TCP86 ablation have been extensively studied, and the phenotype observed upon RNAi ablation characterised (Shawcross, 2008), the reason why TCP86 depletion leads to asymmetric division is unknown. TCP86 is localised to the subpellicular corset, including the MTQ of the FAZ (Shawcross, 2008). Immunofluorescence experiments to investigate the integrity of the FAZ in TCP86 depleted cells indicated that FAZ formation is apparently normal and ruled out mis-positioned or defective FAZ formation as the cause of asymmetric division (Shawcross, 2008). To further investigate the TCP86 RNAi phenotype TEM analysis was undertaken on the TCP86 RNAi cell line.

4.6 Analysis of the TCP86 RNAi cell line by transmission electron microscopy

The TEM analysis particularly focused on (1) the organisation of the subpellicular corset, and (2) the organisation of the FAZ. However, since an independent study localised TCP86 (known to this group as NOP86) to the nucleolus and suggested that RNAi mediated ablation of TCP86 causes a defect in mitotic progression (Boucher *et al,* 2007); TEM analysis also focussed on the ultrastructure of the nucleus and mitotic spindle. Cells were harvested for TEM analysis from a non-induced culture and from cultures 12, 24 and 48 hours post induction. The results of this investigation are presented below.

Before examining the effects of TCP86 depletion, the ultrastructure of non-induced cells was examined. All sections examined indicated that the non-induced cells were normal with regards to cellular ultrastructure (see supplementary Figure 8.7 and Figure 8.8)

4.6.1 12 and 24 hours post induction

After 12 hours of TCP86 RNAi induction, the organisation of the subpellicular corset and FAZ appears unaffected. The ultrastructure of nuclei at different stages of the cell cycle appears normal and cells were observed in different stages of mitosis (supplementary Figure 8.9, Figure 8.10).

By 24 hours of RNAi mediated ablation DAPI counts show a large increase in the number of multinucleates and zoids (Shawcross, 2008) this would suggest that at this time point any abnormalities should be apparent in the TEM sections. No abnormalities were observed in the organisation of the subpellicular corset or of the FAZ (Figure 4.16). In all cases the nuclear architecture appeared normal (supplementary Figure 8.11). Nuclei at different stages of mitosis were observed but there did seem to be an increase in the number of cells possessing mitotic spindles suggesting there may be a defect in mitotic progression (examples of cells with mitotic spindles at 24 hours are shown in supplementary Figure 8.10).

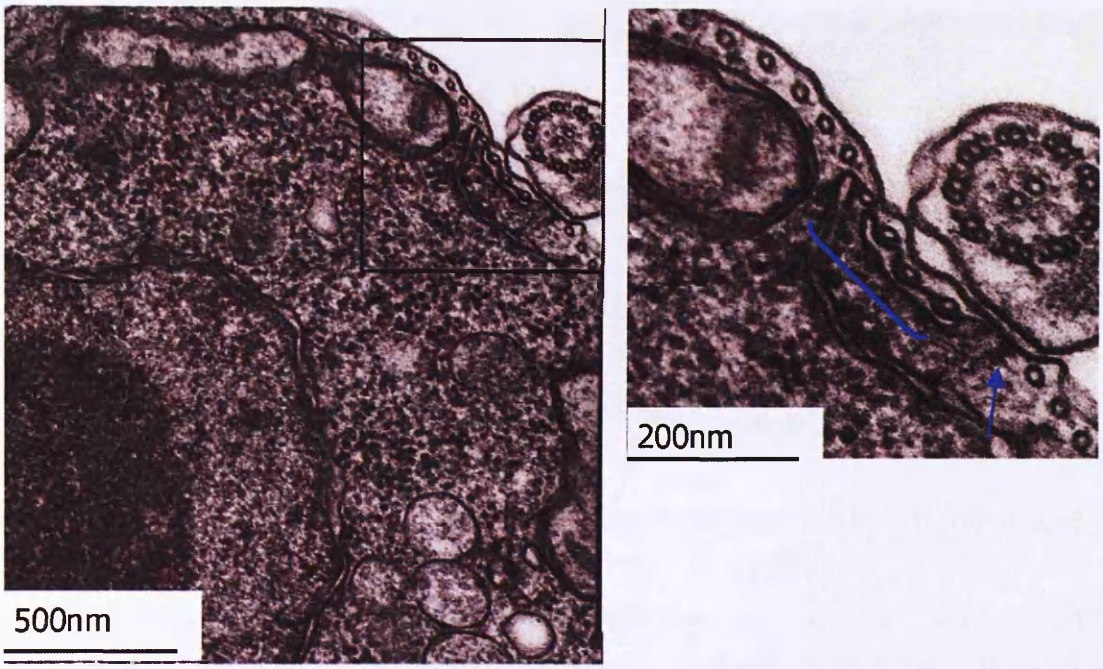

Figure 4.16 Transmission electron micrograph of a transverse section through a cell 24 hours post induction of TCP86 RNAi ablation

Cells from a culture 24 hours post induction of TCP86 RNAi were prepared as described in section 2.5.6. 24 hours after induction of RNAi, TCP86 depleted cells maintain a highly ordered subpellicular corset. The boxed region is enlarged (inset) and shows the FAZ region appears normal, the MTQ are associated with smooth ER (blue bracket) and the FAZ filament (blue arrow).

4.6.2 48 hours post induction

After 48 hours of TCP86 ablation most cells are either multinucleate or zoids. Despite these gross morphological defects spacing and organisation of MTs in the subpellicular corset is unaffected and the FAZ also appears normal (Figure 4.17A). In Figure 4.17B the corset appears uniformly spaced as in non-induced cells; although there are a number of additional MTs circled in red. However, this is occasionally observed in wild type cells when new MTs are being inserted into the corset (S. Vaughan personal communication).

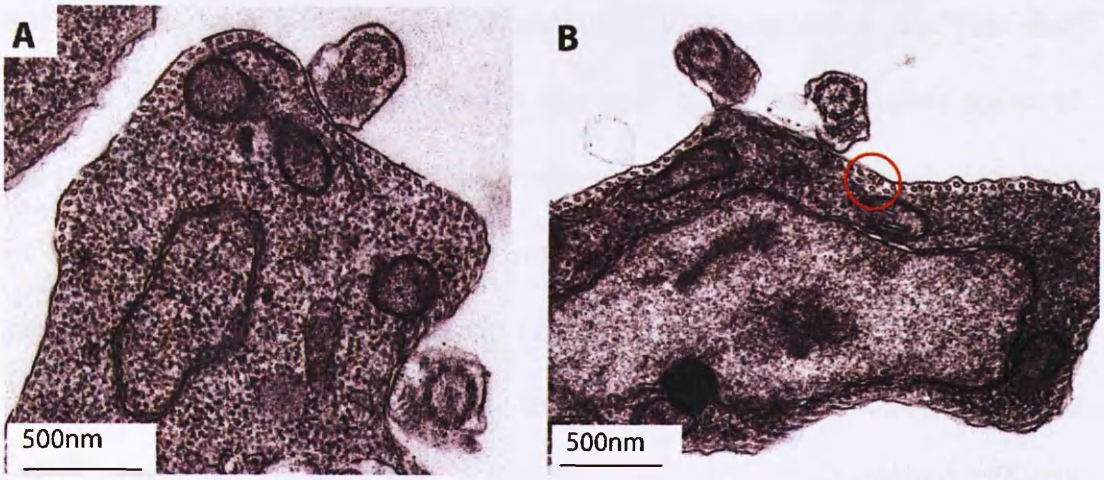

Figure 4.17 Transmission electron micrographs of transverse sections through cells 48 hours post induction of TCP86 RNAi ablation

Cells from a culture 48 hours post induction of TCP86 RNAi were prepared as described in section 2.5.6. Cell in section A shows FAZ formation is not affected by TCP86 ablation and subpellicular corset microtubules remain organised. Cell in section B shows some additional microtubules (circled in red) this is occasionally seen in non-induced cells, subpellicular corset organisation is unaffected.

To summarise, TEM analysis of the TCP86 RNAi cell line shows the uniform and regular distribution of MTs in the subpellicular corset is not disrupted when the expression of TCP86 is reduced (Figure 4.16 and Figure 4.17). Even in cases where the cells are grossly morphologically abnormal such as after 48 hours of RNAi induction (Figure 4.17). Unlike the results seen for the TEM analysis of GB4L, additional MTs are not present in the cytoplasm and FAZ formation appears to be unaffected by the depletion of TCP86. The only unusual observation was an apparent increase in the number of cells possessing a mitotic spindle at 24 and 48 hours post induction of TCP86 RNAi, indicating that there may be a mitotic defect in these cells.

4.7 Mitotic progression in the TCP86 RNAi cell line

An independent study reported that RNAi ablation of TCP86 (a protein designated by this group as Nop86) activates a specific cell cycle checkpoint which blocks mitosis in

late anaphase/telophase (Boucher *et al*, 2007). Whilst analysing the TEM data collected for the TCP86 RNAi cell line, it was noted that mitotic spindles appeared more frequently in TEM cross-sections of cells at 12 and 24 hours post induction than non-induced cells. To quantify this observation, 200 TEM cross-sections containing nuclei from each culture (non-induced, 12 and 24 hours post RNAi induction) were examined. Nuclei were categorised into those with (i) no MTs contained within the nuclear membrane, (ii) short MTs contained within the nuclear membrane (for an example see Figure 8.11B) or (iii) long MTs of the mitotic spindle which connect the two emerging daughter nuclei (for an example see Figure 8.11E). Figure 4.18 shows the results of these counts which indicate that the number of nuclei with short MTs contained within the nucleus and those with an elongated mitotic spindle increase when TCP86 is ablated by RNAi which may suggest that cells are delayed in mitotic progression.

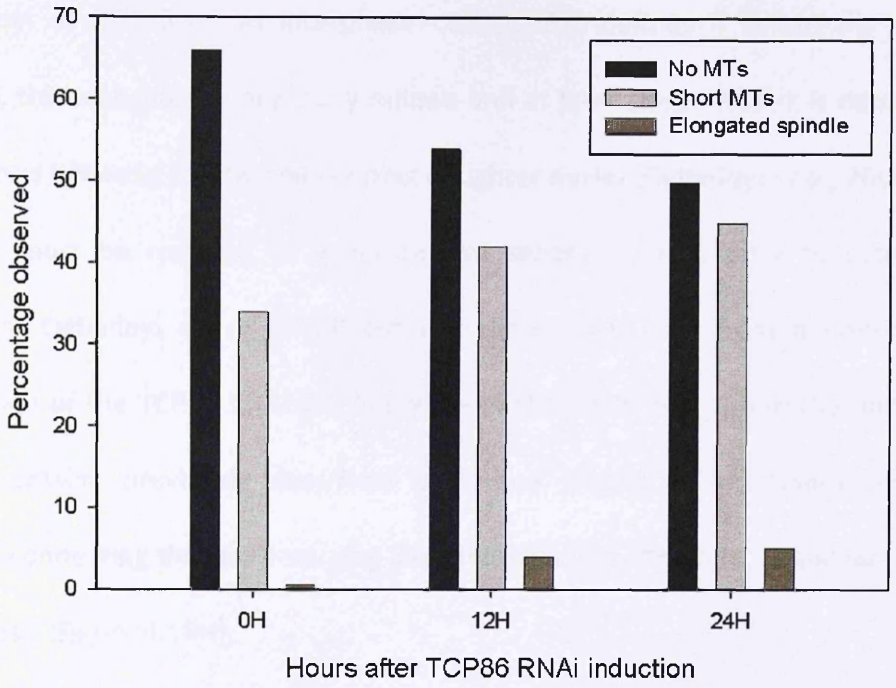

Figure 4.18: Quantification of the percentage of cells possessing a mitotic spindle from TEM sections through the nuclei of cells in the TCP86 RNAi cell line

The TCP86 RNAi cell line was induced; samples were collected from a non-induced culture and from 12 and 24 hours post RNAi induction. Cells were prepared for TEM analysis as described in section 2.5.6. Whilst undertaking TEM analysis 200 sections which showed nuclei were split into three distinct categories, nuclei with; (i) no MTs, (ii) short MTs, (iii) elongated spindle MTs for each time point (see key). The graph shows an increase in the number of cells with short MTs and elongated spindle MTs and a reduction in the number of nuclei which contain no MTs over the time course of TCP86 RNAi ablation.

4.7.1 Immunofluorescence analysis of nuclei in the TCP86 RNAi cell line using the nuclear membrane marker NUP-1

To investigate the possibility that TCP86 depletion by RNAi may delay mitotic progression, immunofluorescence studies were carried out using the monoclonal antibody NUP-1 which labels the nuclear envelope throughout the cell cycle (Ogbadoyi *et al*, 2000; Rout & Field, 2001). Previous immunofluorescence analysis has described a distinctive NUP-1 staining pattern at different stages of the cell cycle, and shows that NUP-1 can act as a marker for nuclear progression through mitosis

(Ogbadoyi *et al*, 2000). In interphase cells NUP-1 defines a spherically shaped nucleus, this elongates during early mitosis and at later stages NUP-1 is detected as an isthmus between the two developing daughter nuclei (Ogbadoyi *et al*, 2000). This isthmus must be resolved to generate two separate nuclei prior to cytokinesis (although Ogbadoyi *et. al* (2000) did not show this). Cells from a non-induced population of the TCP86 RNAi cell line were probed with NUP-1 and the pattern of NUP-1 staining previously described confirmed (Figure 4.19). Additionally, the isthmus connecting the two emerging daughter cells was shown to disappear prior to cytokinesis (Figure 4.19H).

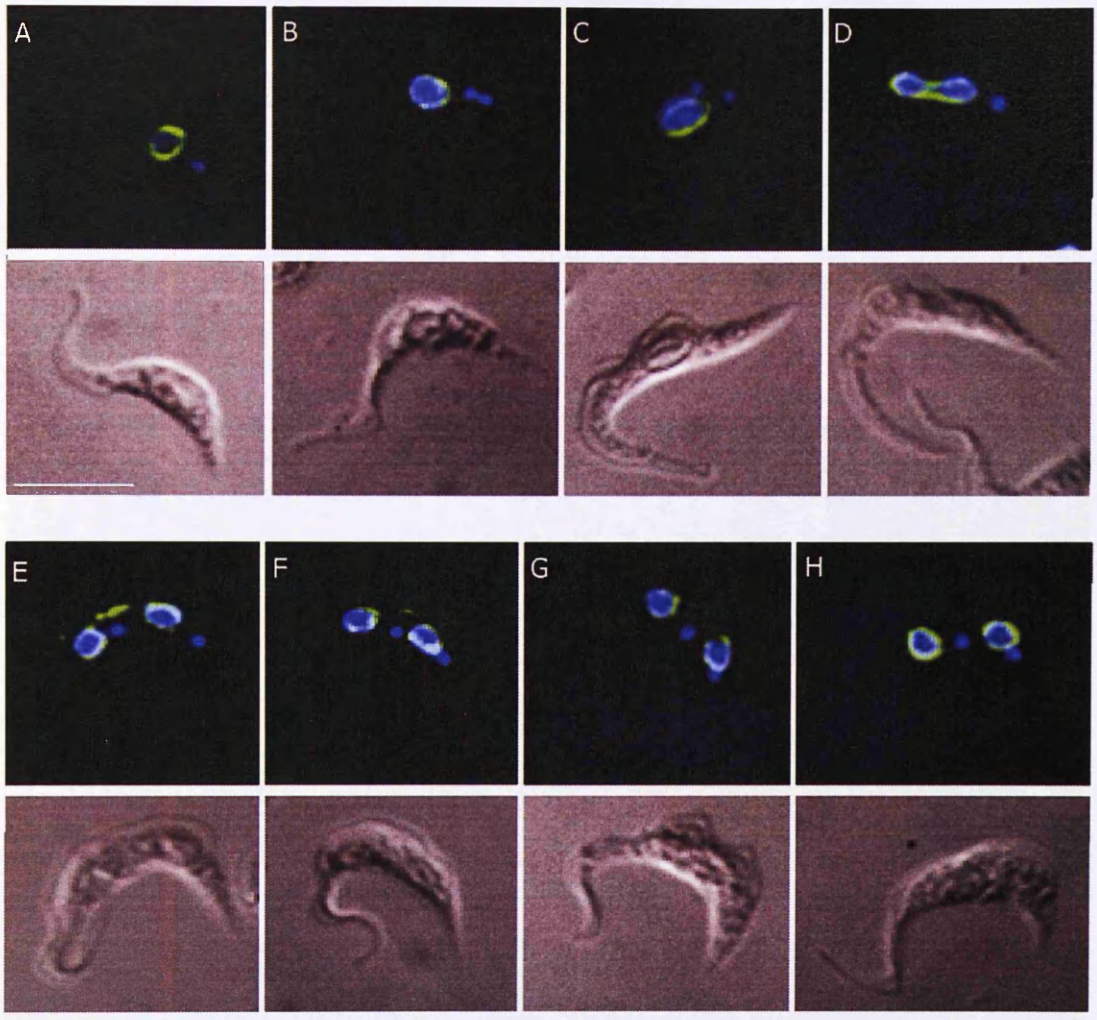

Figure 4.19: Immunofluorescence analysis of mitotic progression in non-induced cells from the TCP86 RNAi cell line

Trypanosomes prepared for immunofluorescence as described in section 2.5.1 and probed with the anti-nuclear envelope monoclonal antibody NUP-1 (green) (for dilutions used see section 2.2.3) and stained with DAPI (blue). Images A-E show cells at progressively later stages of the cell cycle. A, B interphase; C, D mitosis, E late mitosis; F, G karyokinesis; H no NUP detected between nuclei in a cell prior to cytokinesis (scale bar = 10μm).

The NUP-1 staining pattern in cells 24 hours after the induction of TCP86 ablation is shown in Figure 4.20. In these TCP86 RNAi induced cells the NUP-1 staining pattern is the same as in non-induced cells through mitosis, however NUP-1 was still detected between the nuclei of 1K2N cells (Figure 4.20E-H). This is unusual as these cells must

have completed cytokinesis (producing the 1K2N progeny and an anucleate zoid) and as such NUP-1 should not be detectable between the two daughter nuclei. Residual NUP-1 staining in this region at a post cytokinetic time point may suggest that mitosis (or at least separation of the nuclear membrane) was not complete when the cell underwent division.

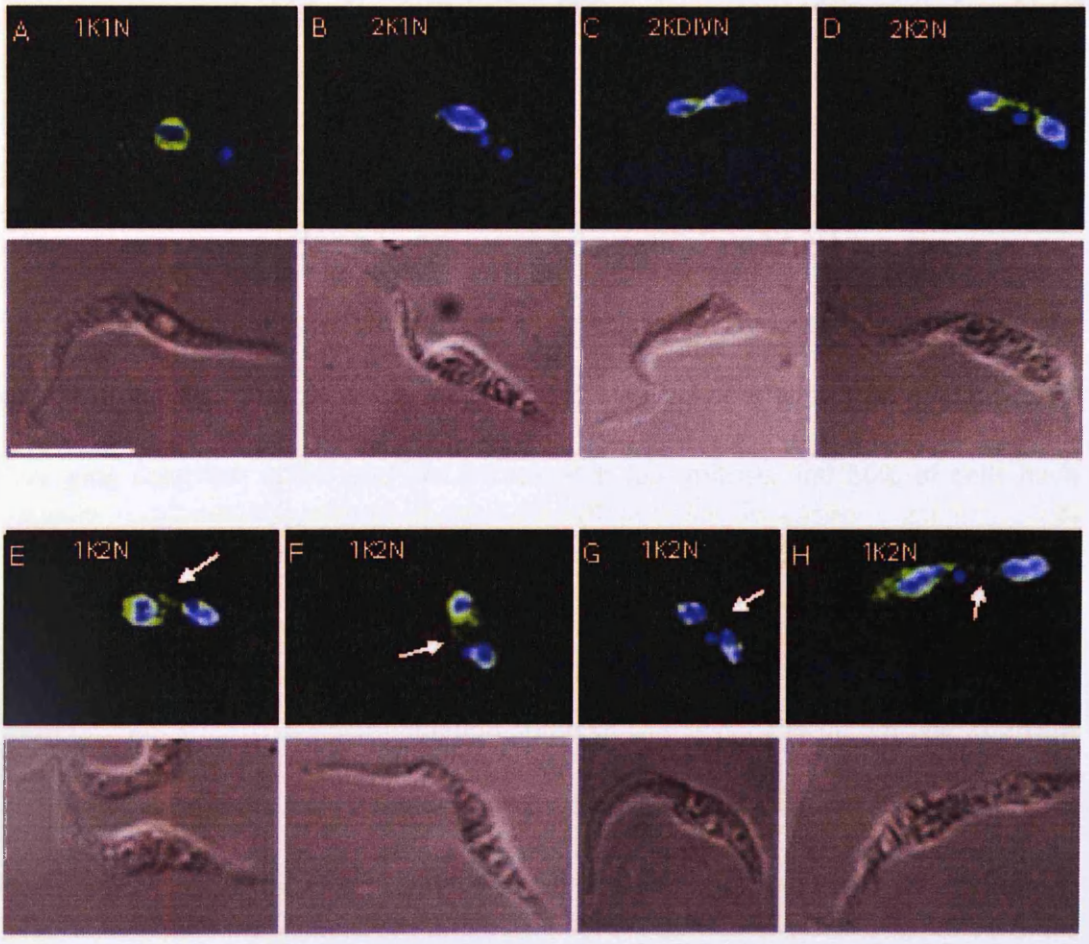

Figure 4.20 Immunofluorescence analysis of mitotic progression in the TCP86 RNAi cell line 24 hours post induction of RNAi

The TCP86 RNAi cell line was induced and cells were harvested at 24 hours post induction. Trypanosomes were prepared for immunofluorescence as described in section 2.5.1 and probed with the anti-nuclear envelope monoclonal antibody NUP-1 (green) and stained with DAPI (blue). Images A-D show cells at progressively later stages of the cell cycle. Images E-H show 1K2N cells after an aberrant cytokinetic event, NUP-1 staining can still be visualised between the nuclei.

To establish if this abnormal NUP-1 localisation is common within the induced population, NUP-1 labelled cells from cultures of non-induced and 24 hours post induction were counted. Only cells possessing two nuclei were included in the counts and NUP-1 labelling was categorised as follows (i) no NUP-1 labelling between daughter nuclei (mitosis is complete), (ii) a bridge of NUP-1 labelling extending between emerging daughter nuclei (late mitosis), (iii) discontinuous NUP-1 labelling in the region between daughter nuclei.

Figure 4.21 shows the result of these counts, in the non-induced population all 2N cells counted were 2K2N, 20% of these 2K2N cells have no NUP-1 labelling between nuclei suggesting that the spindle and the nuclear envelope no longer attach the daughter nuclei. 30% of non-induced 2K2N cells have a NUP-1 bridge between emerging daughter nuclei and are therefore in late mitosis and 50% of cells have retained some discontinuous NUP-1 labelling between daughter nuclei showing that nuclear membrane is still present between divided nuclei.

After 24 hours of TCP86 RNAi ablation some of the cells have undergone aberrant division to produce a zoid meaning that 2N cells fall into two subgroups; 2K2N cells and 1K2N cells. In the 2K2N population there is an increase in the percentage of NUP-1 bridges between daughter nuclei, and a reduction in the number of cells with discontinuous NUP-1 staining; suggesting more of these cells are in anaphase. The 1K2N population of cells should, in theory, be completely negative for NUP-1 labelling between daughter nuclei because these cells have completed cytokinesis. However, over 50% of 1K2N cells still have some residual NUP-1 staining between

the daughter nuclei and 5% of these cells still have a NUP-1 bridge between daughter nuclei.

This shows that when TCP86 is ablated by RNAi the nuclear envelope is still found between cells post-cytokinesis, suggesting that cytokinesis initiates before mitosis is complete. This provides evidence for a delay in late mitosis; however cells must eventually complete the process as multinucleates with 'normal' interphase nuclei are observed at later time points (i.e. nuclei which lack NUP1 staining between each other).

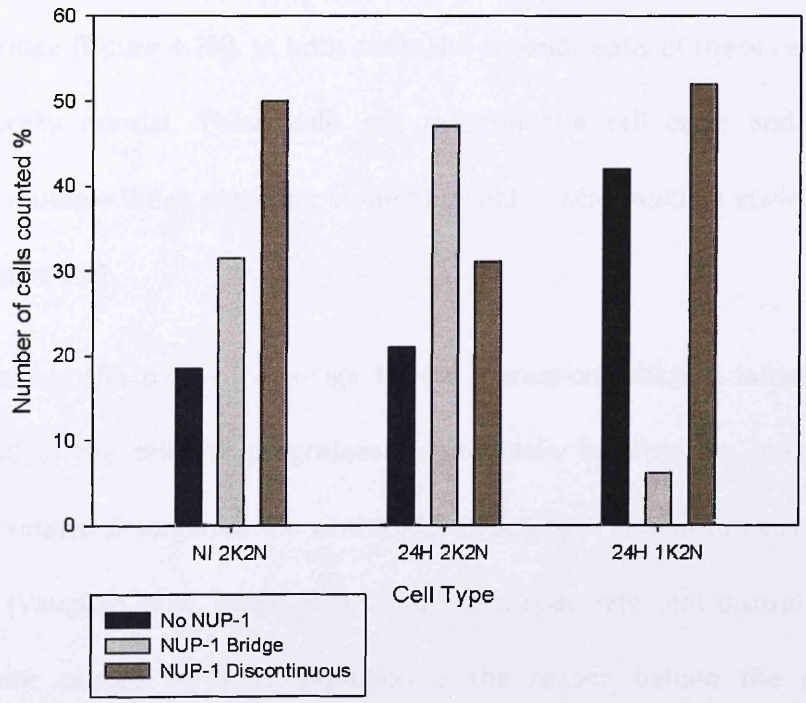

Figure 4.21 Quantification of NUP1 staining pattern observed in 2N cells in the TCP86 RNAi cell line

Cells from a non-induced population and 24 hours after induction of TCP86 RNAi ablation were categorised by the NUP-1 staining pattern observed between daughter nuclei. In total 50 2N cells from each culture were counted. In the non-induced population these cells are all 2K2N, in the induced population there are 2 subgroups of 2N cells, 2K2N and 1K2N cells the latter which have undergone cytokinesis. Percentages of cells in each NUP-1 category are shown. The graph suggests that completion of mitosis is delayed in TCP86 ablated cells.

4.8 Summary

This chapter describes the results of further investigation by SEM and TEM analysis on the GB4L and TCP86 RNAi cell lines. SEM analysis allowed the cellular morphology to be studied at high resolution and shows that in both cases the non-induced cultures appear 'normal'. Following induction of GB4L RNAi, posterior end formation is disrupted (Figure 4.2) supporting the observation made with YL1/2 staining in Chapter 3, that MT growth and organisation in this region is disrupted (Figure 3.13). Additionally, this analysis shows that in some cases the 'push-me-pull-you' cells are attached by a 'plate' or 'ridge' like structure (Figure 4.2G) and in others are attached by a thin bridge (Figure 4.2H). In both cases the anterior ends of these cells appears morphologically normal. These cells can re-enter the cell cycle and re-initiate cytokinesis multiple times, resulting in multinucleates with multiple stalled cleavage furrows (Figure 4.4).

The FAZ defines the path of cleavage furrow ingression which is initiated at the anterior end of the cell and progresses longitudinally towards the posterior pole during cytokinesis. Disorganisation of the FAZ structure is known to cause aberrant cytokinesis (Vaughan *et al*, 2008). It is tempting to speculate that disruption of the FAZ structure caused by GB4L depletion is the reason behind the stalling of cytokinesis. However, the TEM analysis in this chapter shows that the FAZ structure is disrupted in most of the sections taken, including those which cut through the anterior end of cells. Despite disruption of FAZ structure at the cells anterior end the cleavage furrow is capable of initiating and progressing some way before stalling. This suggests that whilst the FAZ defect may contribute to the cytokinetic abnormalities observed in these cells, it is not the sole cause.

The MTs of the subpellicular corset in GB4L depleted cells are, for the majority, uniformly distributed beneath the plasma membrane (Figure 4.7 - Figure 4.12). However, a striking observation is the appearance supernumerary MTs in the cytoplasm of the cell, these can be found in large numbers in some cells, especially at the later time points of 24 and 48 hours (Figure 4.10 - Figure 4.12). The inter-MT spacing appears to be regular, however in some cells MTs in the same section were seen in different orientations (transverse and longitudinal) (Figure 4.10). This data suggests that GB4L plays a role in regulating new MT growth and/or organisation.

SEM analysis of the TCP86 RNAi cell line 12 hours post ablation shows that cells have an elongated posterior end (Figure 4.13A-C). These cells undergo asymmetrical division leading to the production of smaller cells likely to represent zoids and their larger partner cell probably a multinucleate (Figure 4.13E and F and Figure 4.14C-H). Confirming previous observations made by immunofluorescence analysis (Shawcross, 2008).

The TEM analysis of TCP86 depleted cells showed no obvious defects in terms of MT organisation, the subpellicular corset appeared normal at all time points and FAZ formation also appears normal (Figure 4.16 and Figure 4.17). This confirms earlier immunofluorescence studies which suggested that the aberrant, asymmetrical cytokinesis occurring when TCP86 is ablated is not a result of FAZ disruption (Shawcross, 2008). TEM analysis of TCP86 depleted cells at 12 and 24 hours post induction shows cells at various stages of mitosis (see supplementary Figure 8.10), and after 48 hours of induction large multinucleate cells are seen, these cells possess numerous interphase nuclei suggesting cells are capable of progressing through

mitosis. An independent study reported that TCP86 ablation causes a block in mitosis (Boucher *et al*, 2007). Boucher *et al* (2007) argue that PCF cells can overcome this mitosis block to re-enter successive S-phases resulting in the accumulation of multinucleate cells. Counts carried out on TEM sections through nuclei showed an increase in the occurrence of mitotic spindles in TCP86 RNAi induced cells (Figure 4.18). Immunofluorescence studies using the anti-nuclear envelope antibody NUP-1 show that a large number of induced cells retain the nuclear envelope between the nuclei in 1K2N cells, showing that the nuclear envelope is not resolved before cytokinesis in these cells, suggesting that these cells may well have initiated cytokinesis before the completion of mitosis (Figure 4.21).

Chapter 5 Microtubule associated proteins and their functional interdependency

5.1 Introduction

Previous studies in the McKean laboratory have provided valuable insight into the potential interactions between trypanosome MAPs and MTs of the subpellicular corset (Shawcross, 2008). The study by Shawcross used indirect immunofluorescence approaches to show that depletion of TCP86 leads to the loss of CAP5.5 localisation but does not affect WCB (*T. brucei* MAPs previously described in section 1.10.1). These experiments provided the first evidence for complex interdependency relationships between MAPs on the subpellicular corset. We were interested in how MAPs function and their localisation dependencies in *T. brucei*. To investigate this, RNAi cell lines for other published *T. brucei* MAPs were generated including GB4 (Rindisbacher *et al*, 1993), WCB (Baines & Gull, 2008), CAP5.5 (Olego-Fernandez *et al*, 2009), I6 (a/b) (Detmer *et al*, 1997), CAP15 (Vedrenne *et al*, 2002) and MARP1&2 (Affolter *et al*, 1994). RNAi depletion phenotypes were characterised and then the WCB, CAP5.5, GB4L and TCP86 RNAi cell lines were used to explore localisation dependencies by immunofluorescence.

5.2 Characterisation of growth defects arising from the RNAi ablation of *T. brucei* microtubule associated proteins.

To investigate the effects of RNAi mediated depletion of the *T. brucei* MAPs listed above, RNAi was induced and cells were monitored for growth and division defects.

The growth curves for these cell lines are presented in Figure 5.1. Cell lines were routinely monitored for 96 hours unless population growth stopped before this time. Figure 5.1 shows that RNAi ablation of CAP15, I6, GB4 and MARP1/2 caused no population growth defect and while both induced and non-induced populations of the I6 RNAi cell line showed erratic growth over 96 hours, extending growth analysis to 168 hours revealed no significant reduction in the growth of the I6 induced population. In contrast, depletion of WCB and CAP5.5 causes a reduction in cell growth as early as 24 hours post induction; this is in agreement with published data (Baines & Gull, 2008; Olego-Fernandez *et al*, 2009). The RNAi depletion phenotype for WCB has been previously described (Baines & Gull, 2008). However, before using our WCB RNAi cell line to study MAP interdependency relationships we conducted phenotypic characterisation to confirm reproducibility of the WCB ablation phenotypes. We also characterised the CAP5.5 RNAi depletion phenotype which at the time of conducting these experiments was unpublished but has since been reported by Oleg-Fernandez *et al,* (2009).

WCB - The targeted ablation of WCB leads to a marked reduction in cell number after 24 hours. Between 24 and 48 hours post induction population growth is reduced by almost 50%, then between 48 and 72 hours only marginal growth is seen in the induced population. Induced cells exhibit a morphological phenotype that can be observed in culture by light microscopy. After 24 hours of RNAi induction the posterior end of cells appears swollen, and thin cells, possibly representing zoids, appear in the population. Cells in culture also formed large clumps, which were visible in the culture flask by the naked eye; this was most obvious 72 hours post

induction. However RNAi mediated ablation of WCB does not appear to affect flagellar motility.

CAP5.5 - At 24 hours post RNAi induction cells in the induced population grew at half the rate of the non-induced cell line. This reduction in growth is maintained between 24 and 48 hours, after 72 hours of induction very little growth occurred. Examination of the induced culture by light microscopy shows that cells have a profound morphological phenotype. After 48 hours of induction there are two distinct populations visible in culture, (i) cells which appear larger and more rounded than normal, and (ii) very slim tapering cells (probably zoids). In some cases cells have initiated cytokinesis but have failed to complete abscission forming cells reminiscent of the GB4L 'push-me-pull-you' phenotype. Depletion of CAP5.5 also does not appear to affect flagellar motility.

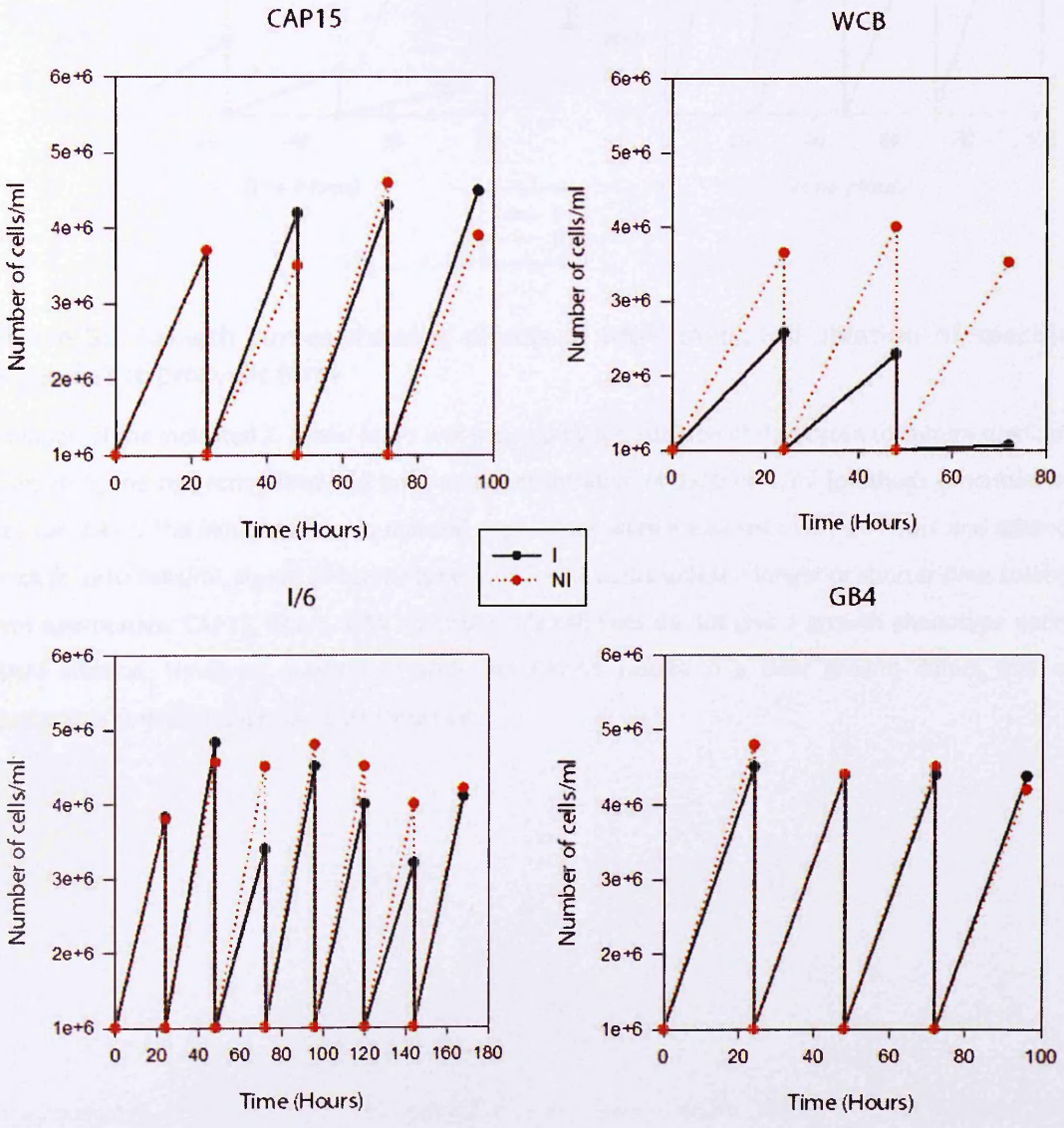
CAP15
WCB
I/6
GB4
Number of cells/ml
Time (Hours)
I
NI
6e+6
5e+6
4e+6
3e+6
2e+6
1e+6
0
20
40
60
80
100
120
140
160
180

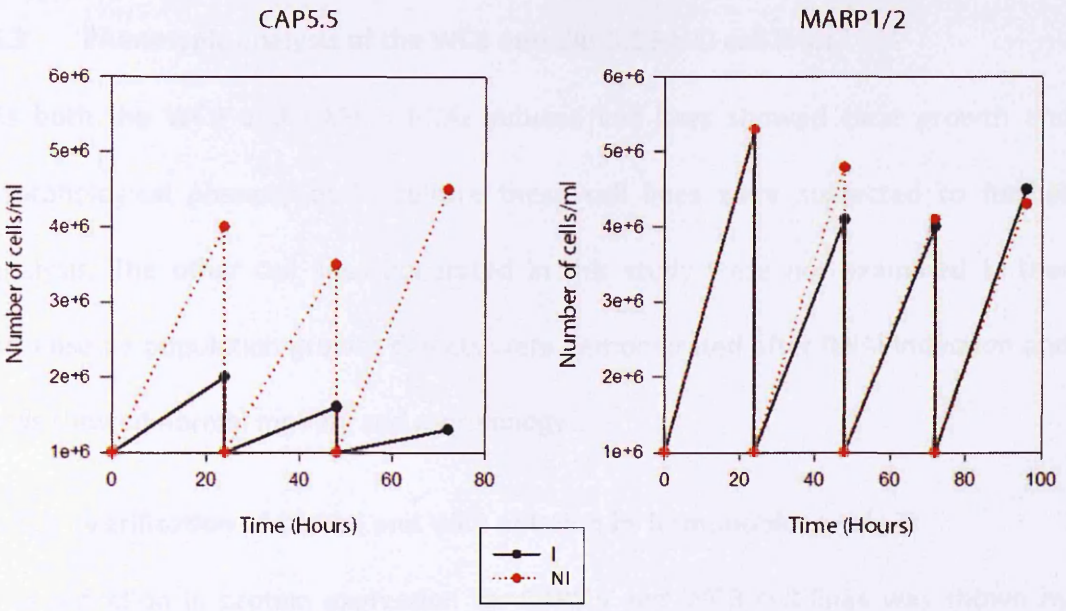

Figure 5.1 Growth curves showing effects of RNAi mediated ablation of specific MAPs in the procyclic form

Ablation of the indicated *T. brucei* MAPs was induced by the addition of doxycyclin to culture medium containing the respective RNAi cell lines at a concentration of $1x10^6$cells/ml (methods described in section 2.4.6). The induced and non-induced populations were measured every 24 hours and diluted back to $1x10^6$cells/ml, counts generally continued for 96 hours unless a longer or shorter time course was appropriate. CAP15, I6 a/b, GB4 and MARP1/2 cell lines do not give a growth phenotype upon RNAi ablation. However, ablation of WCB and CAP5.5 results in a clear growth defect that is detectable as early as 24 hours post induction.

5.3 Phenotypic analysis of the WCB and CAP5.5 RNAi cell lines

As both the WCB and CAP5.5 RNAi induced cell lines showed clear growth and morphological phenotypes in culture these cell lines were subjected to further analysis. The other cell lines generated in this study were not examined further because no population growth defects were demonstrated after RNAi induction and cells showed normal motility and morphology.

5.3.1 Verification of CAP5.5 and WCB ablation by immunoblot analysis

The reduction in protein expression for CAP5.5 and WCB cell lines was shown by immunoblot analysis. Figure 5.2 shows that both WCB and CAP5.5 expression is markedly reduced by 24 hours after induction of RNAi mediated ablation, and further reduction is seen in both cell lines at 48 hours with very little CAP5.5 protein remaining by this time point.

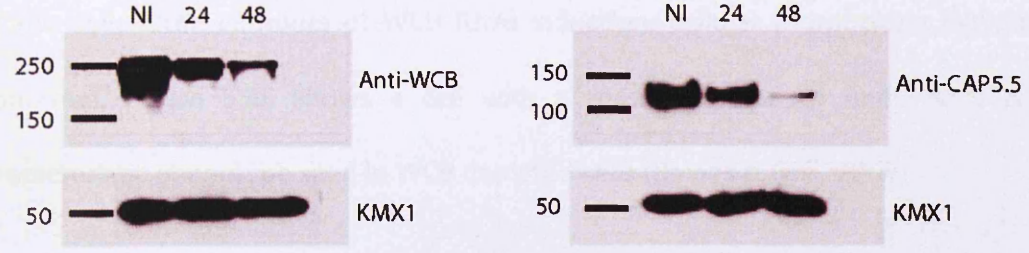

Figure 5.2 Immunoblots showing reduction in protein expression after induction of WCB and CAP5.5 RNAi mediated ablation

RNAi cell lines were induced and cells were harvested at the specified time points (for methods see section 2.5.7.1). Whole cell protein extracts from $5X10^6$ cells were loaded/lane and separated by SDS-PAGE, transferred to nitrocellulose membranes (see section 2.5.9) then probed with specified antibodies (dilutions used are shown in section 2.2.3). Membranes were then incubated with polyclonal-goat anti-mouse HRP-conjugated secondary antibody and immobilised specific antigens detected by chemiluminescence. Immunoblots show a marked reduction in WCB and CAP5.5 expression over the time course. The anti β-tubulin antibody KMX1 was used as a loading control.

5.3.2 Analysis of the WCB and CAP5.5 RNAi cell lines by immunofluorescence analysis

To further validate the efficacy of WCB and CAP5.5 RNAi, cells were taken from a non-induced culture and from 12 and 24 hours post induction and protein reduction was visualised by immunofluorescence analysis (performed as described in section 2.5.3).

WCB - Figure 5.3A-C shows representative immunofluorescence images of the non-induced WCB RNAi cell line revealing that the WCB protein (shown in red) is located over the entire cell body at all stages of the cell cycle which is in agreement with previous observations (Woods *et al*, 1992; Baines & Gull, 2008). In contrast, 12 hours post induction of RNAi WCB is not found at the posterior end of the cell but can still be seen on the anterior portion of the cell (Figure 5.3D-F). This localisation pattern indicates the absence of WCB decorating new MTs which form at the posterior end of the cell. After 12 hours of WCB RNAi induction, cellular morphology becomes abnormal. Figure 5.3E shows a cell with a rounded posterior end which is a characteristic phenotype seen in WCB depleted cells (Baines & Gull, 2008).

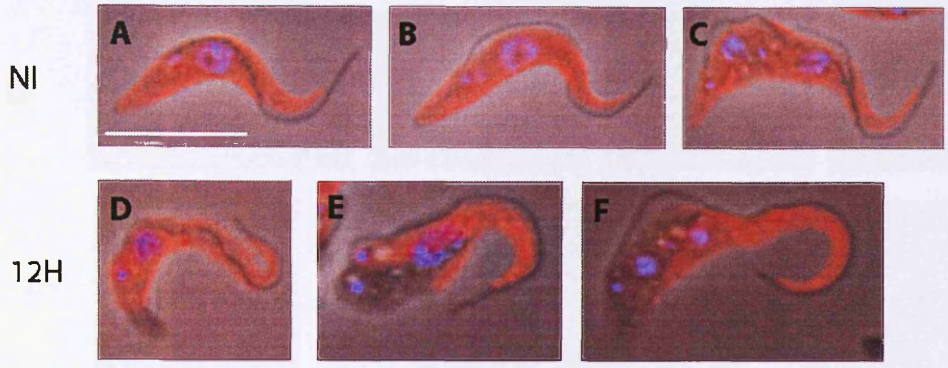

Figure 5.3 Immunofluorescence images of the WCB RNAi cell line, comparing non-induced cells to cells 12 hours after induction of RNAi

Cells were prepared for immunofluorescence analysis as described in section 2.5.1. Representative cells at progressively later stages of the cell cycle from a non-induced (NI) culture (A-C) and 12 hours post RNAi induction (D-F), labelled with WCB antibody (red) and DAPI (blue). In non-induced cells WCB labelling is present over the entire cell body. In cells 12 hours post induction, WCB expression is reduced at the posterior end of the cell. E shows a cell with a rounded posterior end characteristic of the phenotype seen in this RNAi cell line (scale bar = 10μm).

CAP5.5 - Figure 5.4 shows cells from the CAP5.5 RNAi cell line before and 12 hours after induction of RNAi. In non-induced cells the CAP5.5 protein is distributed evenly over the entire cell body at all stages of the cell cycle (Figure 5.4A-D). In contrast, after 12 hours of RNAi mediated ablation CAP5.5 expression/localisation is reduced at the posterior end of the cell (Figure 5.4E-H). Figure 5.4E shows a 1K1N cell which lacks CAP5.5 staining at the posterior end. While Figure 5.4F shows a 2K1N cell with an elongated and thin posterior end which is CAP5.5 negative: CAP5.5 expression over the anterior portion of the cell body also appears to be reduced. Figure 5.4G and H also have abnormal posterior ends which appear more 'cone' shaped than non-induced cells. In these cells CAP5.5 staining is absent from the posterior end and also appears reduced over the anterior portion of the cell.

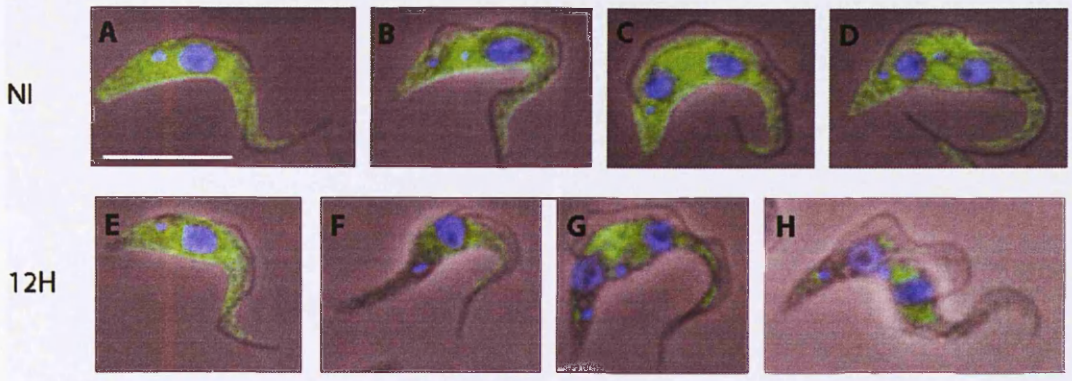

Figure 5.4 Immunofluorescence images of the CAP5.5 RNAi cell line, comparing non-induced cells to cells 12 hours after induction of RNAi

Cells were prepared for immunofluorescence analysis as described in section 2.5.1. Representative cells at progressively later stages of the cell cycle from a non-induced (NI) culture (A-D) and 12 hours post RNAi induction (E-H) were labelled with CAP5.5 antibody (green) and DAPI (blue). In non-induced cells CAP5.5 labelling is present over the entire cell body (A-D). In cells 12 hours post induction CAP5.5 expression is clearly reduced; E and F show this reduction is seen mostly at the posterior end of the cell. Later in the cell cycle (G and H) CAP5.5 is reduced from both the posterior end and the anterior end of the cell (scale bar = 10μm).

5.3.3 Prolonged ablation of CAP5.5 or WCB causes further gross morphological changes

Figure 5.5A and B show fields of cells taken from cultures 24 hours after the induction of WCB and CAP5.5 RNAi respectively; after 24 hours of RNAi induction gross changes in cellular morphology are observed and in both cases multinucleates (Figure 5.5, asterisks) and zoids (Figure 5.5, labelled with Z) are produced. This is consistent with the published data (Baines & Gull, 2008; Olego-Fernandez *et al*, 2009). In Figure 5.5B a cell from the CAP5.5 RNAi cell line can be seen undergoing abnormal cytokinesis which upon abscission will result in multinucleate and anucleate progeny (arrow).

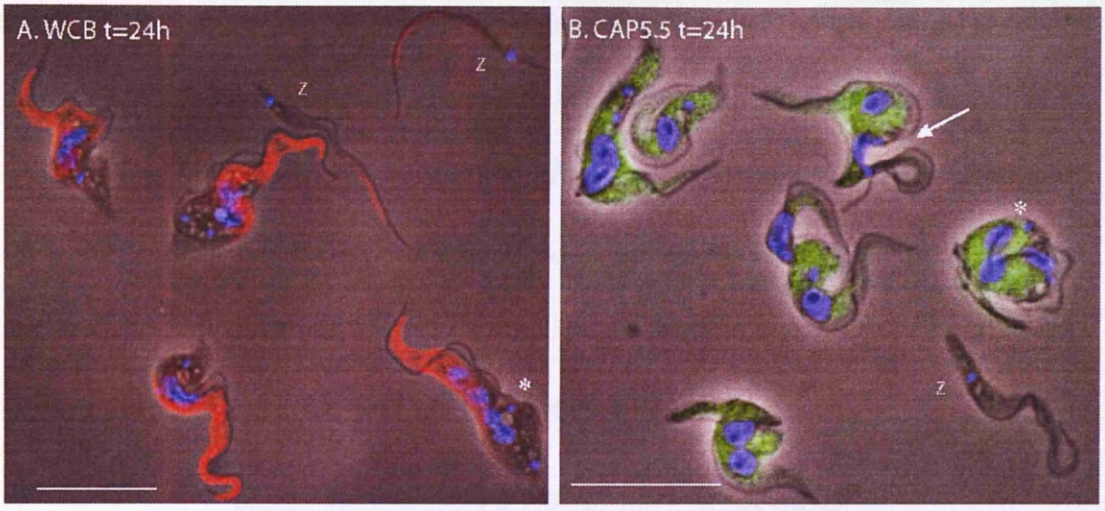

Figure 5.5 Immunofluorescence images showing cells 24 hours post induction of WCB and CAP5.5 RNAi

Cells from the WCB and CAP5.5 RNAi cell lines were induced and samples were prepared for immunofluorescence analysis as described in section 2.5.1. Cells were labelled with the relevant antibodies (diluted as described in section 2.2.3). (A) WCB RNAi cell line labelled with WCB antibody (red) and (B) CAP5.5 RNAi cell line labelled with the CAP5.5 antibody (green). Images show severe morphological abnormalities occurring 24 hours post induction in both cell lines. Multinucleate cells are indicated with an asterisk, zoids are labelled with a Z, the arrow in B shows a cell undergoing aberrant cytokinesis (scale bar = 10μm).

The immunofluorescence analysis in Figure 5.5 clearly shows that some WCB and CAP5.5 protein remains after 24 hours of RNAi ablation. This confirms the earlier result of the immunoblot analysis shown in Figure 5.2. After 24 hours of RNAi induction the WCB protein is still associated with the old MTs located towards the anterior end of the cell. In comparison, CAP5.5 localisation is reduced overall when compared to the non-induced control and CAP5.5 is lost (in many cases) from both the anterior and posterior ends of cells, suggesting that CAP5.5 may be more labile than WCB.

5.3.4 WCB may play a role in cross-linking microtubules of the subpellicular corset

Baines *et.al* (2008) noted that ablation of WCB appeared to affect the integrity of inter-MT cross-links at the posterior pole of the cell. When cells were extracted with 1% NP40 to form cytoskeleton preparations, subpellicular MTs at the posterior end of the cells were observed to splay apart. This phenotype was also observed in our independently raised WCB RNAi cell line (Figure 5.6).

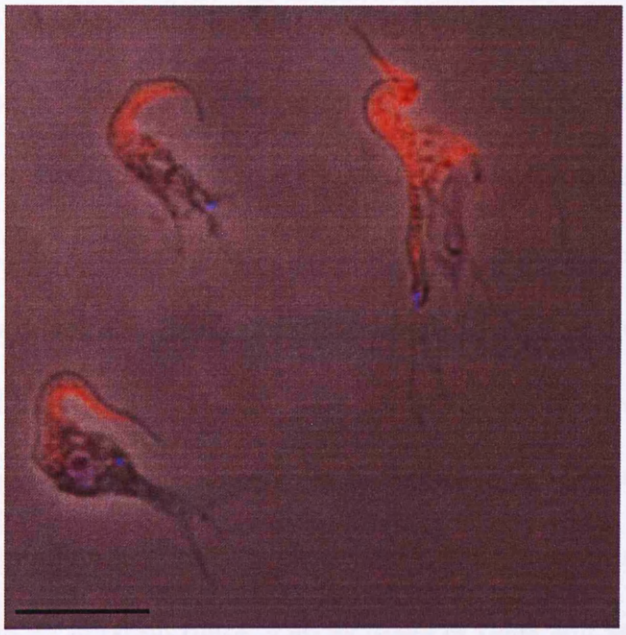

Figure 5.6 Immunofluorescence image showing microtubule splaying in the WCB RNAi cell line 24 hours post RNAi induction

The WCB RNAi cell line 24 hours post induction were harvested and prepared for immunofluorescence as described in section 2.5.1. Cytoskeletons were extracted as described in section 2.5.7.2. In wild type preparations the corset maintains a normal morphology (data not shown) however in the WCB ablated cells, as a result of this treatment microtubules splay open at the posterior end suggesting that the intermicrotubule cross links are weakened in the absence of WCB (scale bar = 10μm).

5.3.5 Flow cytometry analysis on the WCB and CAP5.5 RNAi cell lines

To further assess the consequences of RNAi mediated ablation on these cell lines, cells were fixed in solution and stained with propidium iodide in order to assess cell cycle progression by flow cytometry.

WCB - Figure 5.7 shows the flow cytometry profiles for the WCB cell line before induction and after 24 and 48 hours of RNAi induction; the ploidy of cells represented by the each peak is indicated on the profiles. The profile of the non-induced population is normal. After 24 hours of WCB ablation fewer cells are found in the 2C peak and two additional peaks can be seen in the profile; one of these represents the 1K0N (zoid) population, these cells contain a small amount of kinetoplast DNA but lack a nucleus, as such the peak is close to 0 on the *x* axis. The second additional peak (8C) on the 24 hour profile represents multinucleates. The appearance of zoids and multinucleates is indicative of aberrant cytokinesis and supports the immunofluorescence data presented in the previous section (see Figure 5.5). After 48 hours of ablation there is an increase in zoids and less cells appear in the 2C and 4C peaks showing that fewer cells are completing cytokinesis accurately and going on to progress normally through the cell cycle.

CAP5.5 - The profile for the non-induced (NI) sample in Figure 5.8 shows a normal distribution of cells. After 24 hours post induction of CAP5.5 RNAi the cells accumulate with 4C DNA content, this suggests a delay in mitosis or cytokinesis. Alternatively, growth of the 4C peak may be due to an increase in the number of 1K2N cells, which are known to accumulate upon CAP5.5 ablation (Olego-Fernandez *et al*, 2009). 1K2N cells are the result of aberrant cytokinesis, and are partners to

anucleate zoids (1K0N). The flow cytometry profile shows a small peak of low fluorescence signifying the production of zoids and supporting the existence of a 1K2N population giving rise to the 4C peak. Additionally, cells with 8C DNA content were also detected, this peak represents multinucleates and shows that (similar to the situation seen with WCB ablated cells) CAP5.5 RNAi induced cells have a mitotic or cytokinetic defect but can re-enter the cell cycle and re-replicate their kinetoplast and nuclear DNA. After 48 hours of induction the zoid population has grown significantly and the number of multinucleates (8C) has also increased.

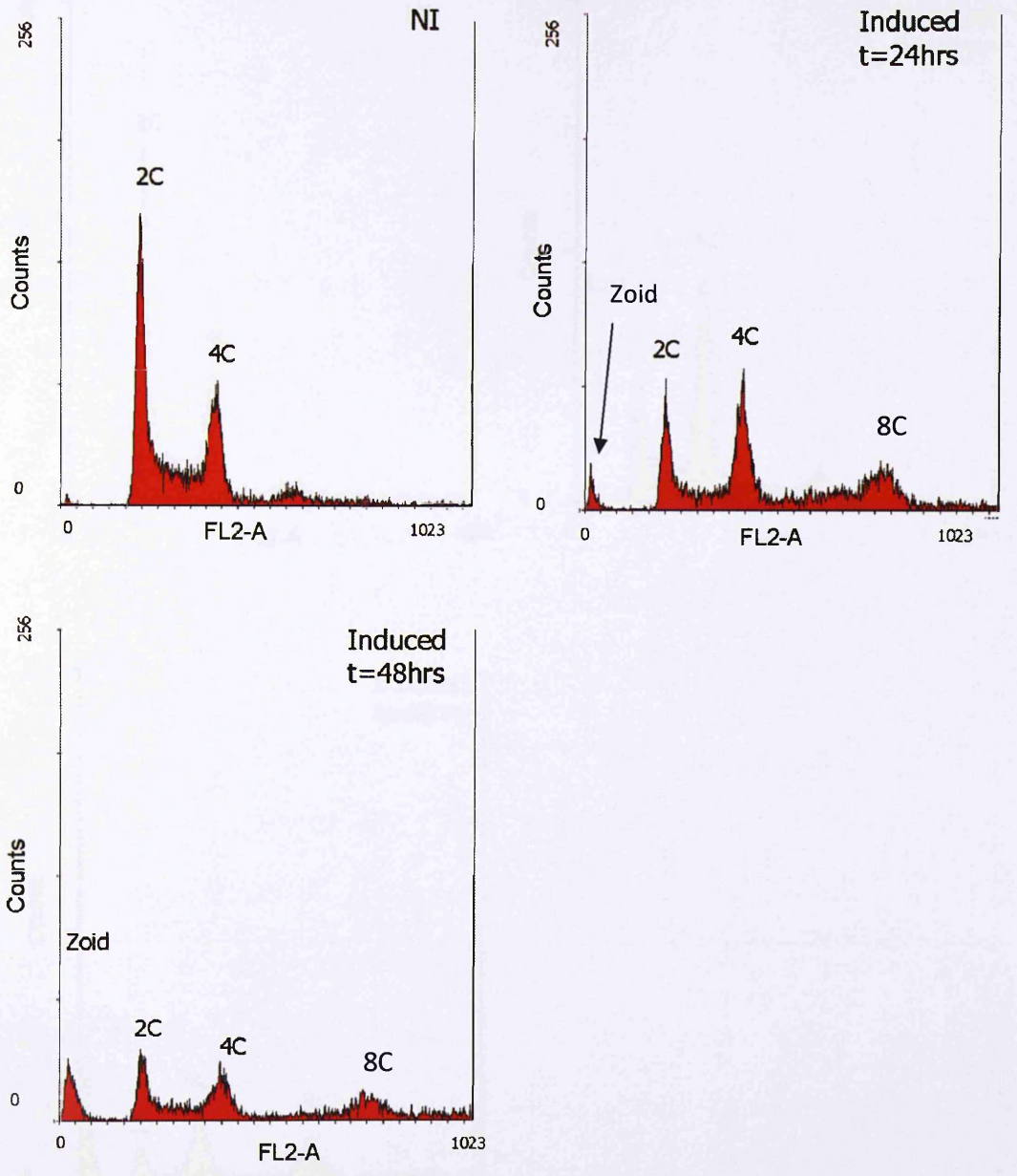

Figure 5.7 Flow cytometry profiles for the WCB RNAi cell line

Cells from the WCB RNAi cell line were fixed and stained with propidium iodide (as detailed in section 2.4.8), samples of cells were prepared from a non-induced (NI) culture and from 24 and 48 hours post induction. The *X*-axis shows fluorescence intensity in the FLA-2 channel, ploidy of peaks is shown on graphs. Analysis shows an increase in multinucleates which coincides with anucleate zoid production.

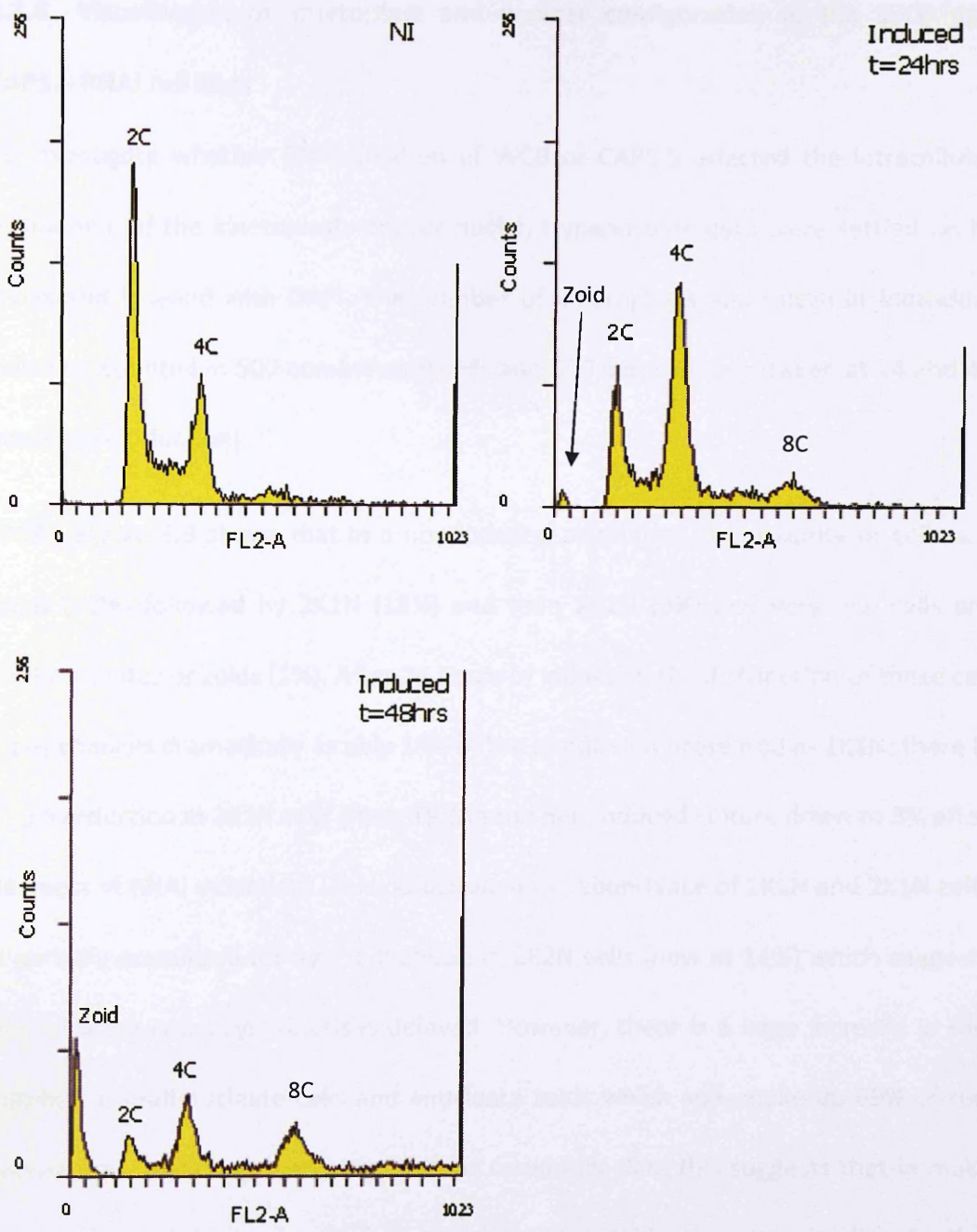

Figure 5.8 Flow cytometry profiles for the CAP5.5 RNAi cell line

Cells from the CAP5.5 RNAi cell line were fixed and stained with propidium iodide (as detailed in section 2.4.8); cells were prepared from a non-induced (NI) culture and from 24 and 48 hours post induction. The *X*-axis shows fluorescence intensity in the FLA-2 channel, ploidy of peaks is shown on graphs. Analysis shows an increase in the 4C peak followed by a progressive increase in the number of multinucleates (8C) which is accompanied by anucleate zoid production.

5.3.6 Visualisation of kinetoplast and nuclear configuration in the WCB and CAP5.5 RNAi cell lines

To investigate whether RNAi ablation of WCB or CAP5.5 affected the intracellular positioning of the kinetoplasts and/or nuclei, trypanosome cells were settled on to slides and labelled with DAPI. The number of kinetoplasts and nuclei in individual cells was counted in 500 non-induced cells and 500 induced cells (taken at 24 and 48 hours post induction).

WCB - Figure 5.9 shows that in a non-induced population the majority of cells are 1K1N (72%) followed by 2K1N (18%) and then 2K2N (9%) and very few cells are multinucleates or zoids (1%). After 24 hours of induction the distribution of these cell types changes dramatically as only 14% of the population presented as 1K1N; there is also a reduction in 2K1N cells (from 18% in the non-induced culture down to 3% after 24 hours of RNAi induction). This reduction in the abundance of 1K1N and 2K1N cells is partially accounted for by the increase in 2K2N cells (now at 14%) which suggests that in some cases cytokinesis is delayed. However, there is a large increase in the number of multinucleate cells and anucleate zoids which now make up 69% of the population. Taken together with the flow cytometry data this suggests that in most cases cells undergo and complete an aberrant cytokinesis event leading to the production of multinucleate (which includes 1K2N) cells and zoids (1K0N). After 48 hours the majority of cells are multinucleated, these cells are accompanied by a large population of zoids, showing that cells re-enter the cell cycle and continue to attempt cytokinesis resulting in further aberrant cell divisions which produce anucleate zoids.

CAP5.5 - Figure 5.10, shows that in the non-induced sample the majority of cells are 1K1N (80%) followed by 2K1N (12%) and then 2K2N (8%) as expected. After 24 hours of RNAi depletion there are less 1K1N (27%) and 2K1N (4%) cells, a slight increase in 2K2N cells (15%) and a large increase in the number of multinucleate cells (which includes 1K2N cells, 34%) accompanied by the presence of a subpopulation of zoids (20%). This confirms the flow cytometry analysis and shows that the CAP5.5 cells complete cytokinesis but that the process is defective leading to the incorrect apportioning of nuclei (as represented by 1K0N and 1K2N (multinucleate progeny). After 48 hours of ablation the largest subpopulation of cells are the multinucleates (63%) followed by zoids (28%), very few 'normal' cell types were observed.

Conclusions - The flow cytometry (section 5.3.5) and DAPI count (section 5.3.6) analysis show that ablation of both WCB and CAP5.5 leads to aberrant cytokinetic events and the generation of multinucleate cells and non-viable zoids. This explains why no significant population growth was observed after 48 hours of induction during the population growth analysis. Any increase in cell density observed at 48 hours is most likely due to the ability of multinucleate cells to undergo cytokinesis and abscission producing multiple non-viable zoids.

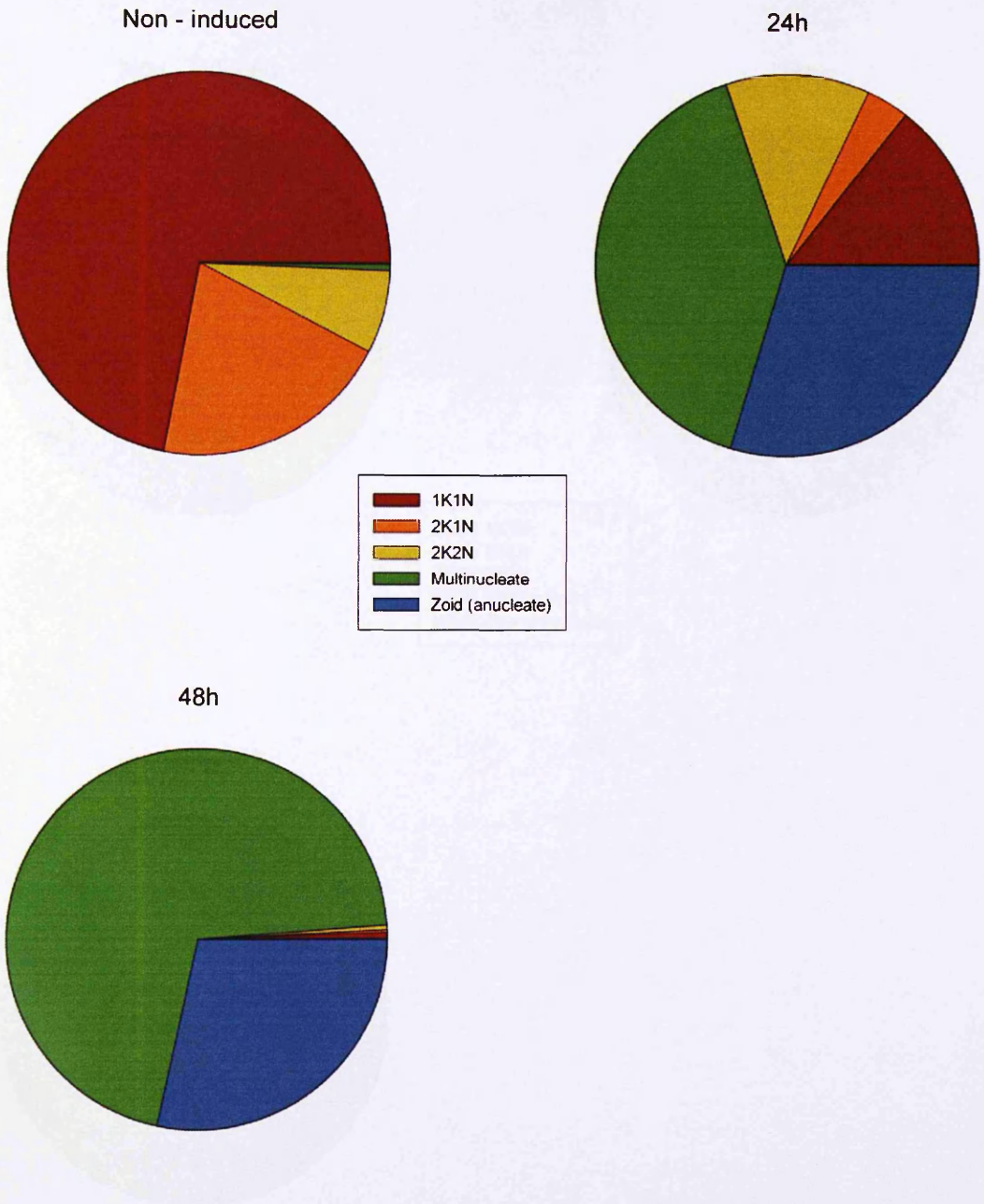

Figure 5.9 Pie charts showing the kinetoplast and nuclear content of the WCB RNAi cell line

Cells from a non-induced WCB RNAi culture and cells from 24 and 48 hours post induction were harvested, settled onto slides and labelled with DAPI as described in section 2.5.1. 500 cells were classified by the number of kinetoplasts and nuclei they possessed. Pie charts show a reduction of cells progressing through the cell cycle 'normally' and an increase in multinucleates and zoids over time.

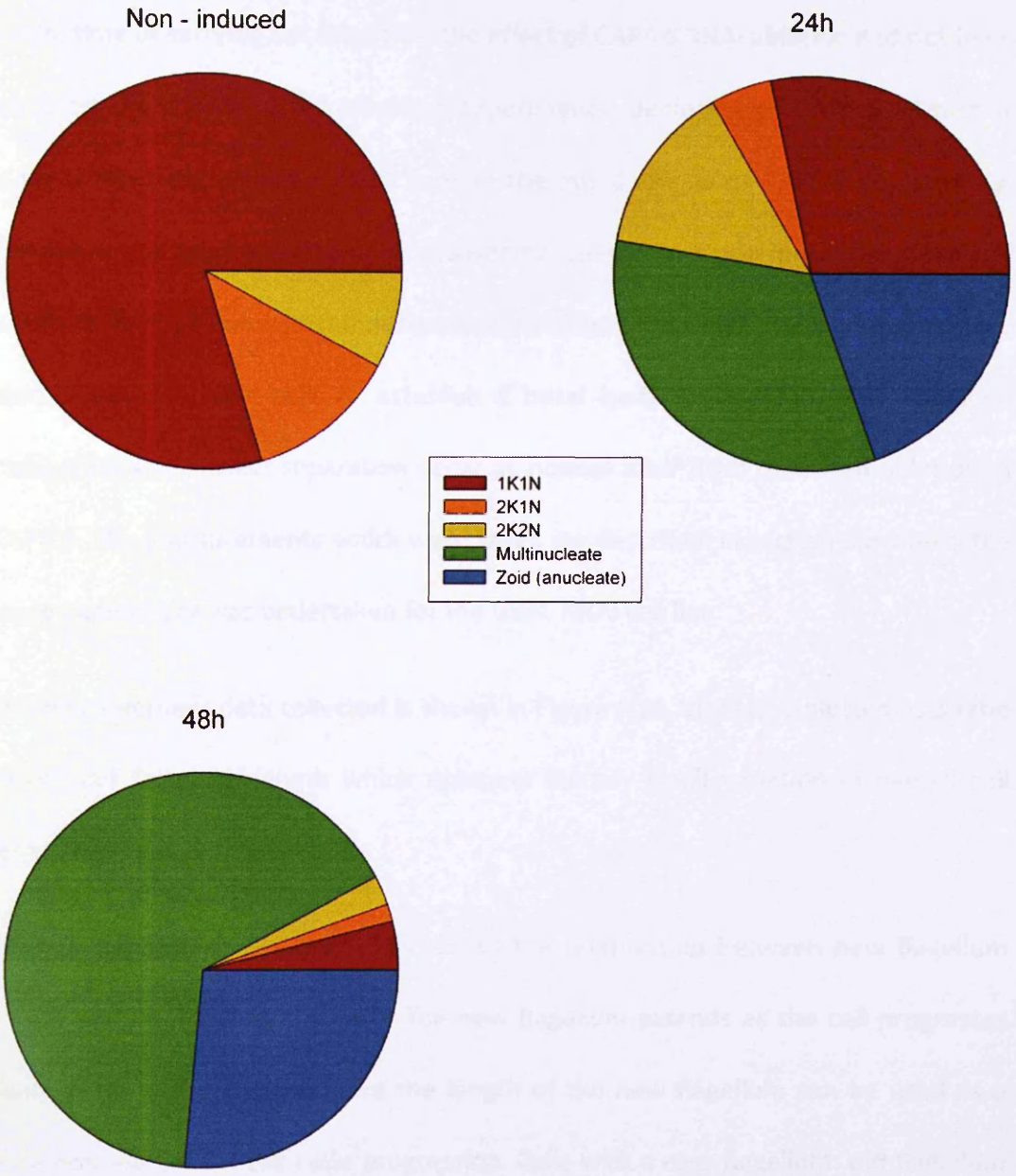

Figure 5.10 Pie charts showing the kinetoplast and nuclear content of the CAP5.5 RNAi cell line

Cells from a non-induced CAP5.5 RNAi culture and cells from 24 and 48 hours post induction were harvested, settled onto slides and labelled with DAPI as described in section 2.5.1. 500 cells were classified by the number of kinetoplasts and nuclei they possessed. Pie charts show a reduction of cells progressing through the cell cycle 'normally' and an increase in multinucleates and zoids over time.

5.4 Organelle segregation in the CAP5.5 RNAi cell line

At the time of carrying out this study the effect of CAP5.5 RNAi ablation had not been explored. As shown in the previous experiments, depletion of CAP5.5 ultimately leads to aberrant cytokinesis. To explore the initial effects of CAP5.5 depletion on cellular morphology and organelle positioning, cells from a non-induced culture and a culture from 12 hours post induction were settled onto slides. Measurements were carried out on these cells to establish if basal body segregation, new flagellum elongation and nuclear separation occur as normal after RNAi mediated ablation of CAP5.5. The measurements which were taken are described in section 3.8 where the same experiment was undertaken for the GB4L RNAi cell line.

The measurement data collected is shown in Figure 5.11, all data is plotted as a ratio of the old flagellum length which accounts for any small variation in overall cell length between individual cells.

Nuclear separation - Figure 5.11A shows the relationship between new flagellum length and internuclear distance. The new flagellum extends as the cell progresses through the cell cycle, therefore the length of the new flagellum can be used as a temporal marker for cell cycle progression. Cells with a new flagellum: old flagellum ratio of 0.1 are in the G_1 phase of the cell cycle whereas cells with a new flagellum: old flagellum ratio close to 1 (and thus with a long new flagellum) are at a late cell cycle stage just before or during cytokinesis. At the start of the cell cycle the new flagellum extends but the inter-nuclear distance does not change. This is because cells have not entered mitosis; at this stage the measurement of inter-nuclear distance is simply a reflection of the nuclear diameter, this remains relatively

constant at the start of the cell cycle. When cells enter mitosis nuclear diameter increases and then nuclei separate this creates an inflection point on the graph. In this case the inflection point is at approximately 0.7 on the *x*-axis. This shows that nuclear separation begins when the new flagellum has reached 70% of the length of the old flagellum. There is no difference between non-induced and induced cells in this regard, showing that nuclear separation occurs normally when CAP5.5 is ablated. Olego-Fernandez *et.al* reported aberrant positioning of the post mitotic nuclei in the CAP5.5 RNAi ablated cells (Olego-Fernandez *et al*, 2009). The data presented here suggests that this is not a result of defective nuclear separation.

New flagellum growth - Figure 5.11B shows the relationship between the migration of the FC along the old flagellum and the growth of the new flagellum. The graph produced is biphasic, in the first phase, migration of the FC along the old flagellum and extension of the new flagellum is a linear relationship. FC migration and new flagellum growth measurements both increase progressively until reaching a 'stop' point at approximately 0.6 on the *x*-axis, this is when FC migration stops and new flagellum growth continues. 0.6 on the *x*-axis means the new flagellum has reached roughly 60% the length of the old flagellum. In the second phase new flagellum growth continues at a slower rate without the FC migrating. This characteristic graph is described in detail in section 3.8. RNAi mediated ablation of CAP5.5 does not appear to effect the growth of the new flagellum or the migration of the FC.

Basal body separation - Figure 5.11C describes the process of basal body separation throughout the cell cycle. Measurements made on non-induced cells show that as

the new flagellum extends the interbasal body distance increases. The induced cells show the same general trend.

Distance from the new basal body to the posterior end - although this measurement remains relatively constant in both non-induced and induced cells as they progress through the cell cycle, this distance is reduced in a small number of induced cells (circled in red on Figure 5.11D). This shows that the new basal body is positioned closer to the posterior end than is 'normal' in these cells. However, this is only seen in a small proportion of the overall population. Since basal body separation in the induced population is normal (see Figure 5.11C) this result suggests that posterior end elongation may be disrupted in some of the induced cells.

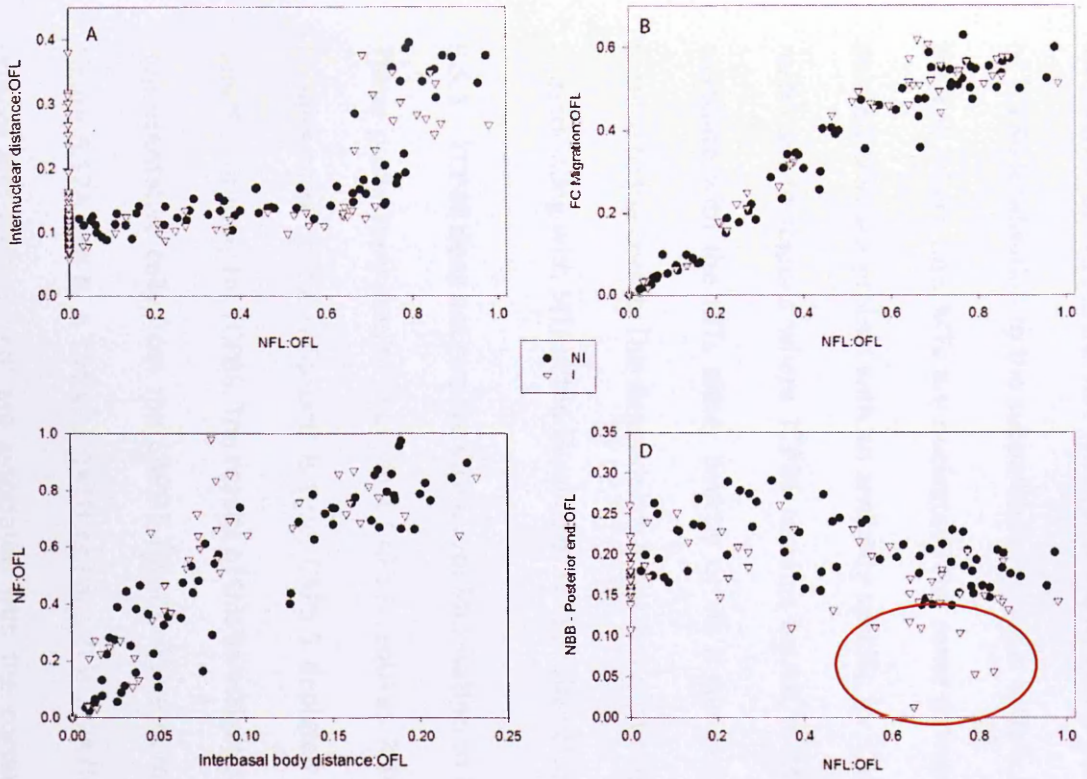

Figure 5.11 Graphs describing organelle positioning in the CAP5.5 RNAi cell line

Cells from the CAP5.5 RNAi cell line were induced and samples from a non-induced culture and a culture 12 hours after induction were settled onto slides as described in section 2.5.1. These cells were labelled for immunofluorescence with an anti-PFR antibody (L8C4) and an anti-basal body antibody (BBA4) and stained with DAPI. This allowed the position of key organelles to be measured in relation to one another in 100 cells from each sample. Measurements were taken as described in section 3.8. Nuclear separation (A), FC migration, new flagellum growth (B) and interbasal body separation (C) appear normal. In some cells new basal body positioning appears to be slightly more posterior than in non-induced cells (D).

5.5 Demonstration of functional MAP Interdependency relationships

Previous studies using the TCP86 RNAi cell line gave the first insight into interdependency relationships between MAPs on the subpellicular corset. Immunofluorescence assays have shown that ablation of TCP86 affects the localisation of CAP5.5 but not WCB (Shawcross, 2008). Upon RNAi mediated ablation of TCP86 localisation to the subpellicular corset is initially lost at the posterior end of the cell where new MTs are nucleated. The same pattern is observed when TCP86 ablated cells are probed with an antibody specific for CAP5.5. CAP5.5 localisation is restricted to regions where TCP86 remains bound to MTs. Therefore TCP86 must associate with the MTs either directly or via a complex before CAP5.5 is able to localise to the corset. This dependency is not demonstrated by WCB which is capable of associating with MTs in the absence of TCP86 (Shawcross, 2008).

5.5.1 TCP86 does not require CAP5.5 for localisation to the subpellicular corset

These preliminary studies show that CAP5.5 requires TCP86 for normal localisation, to determine if the reciprocal is true, CAP5.5 depleted cells were probed with a specific antibody for TCP86. The results of this investigation are shown in Figure 5.12. Representative cells from the CAP5.5 RNAi cell line before induction are shown in Figure 5.12A and B, A shows a 1K1N cell and B is a 2K2N cell, in both cases TCP86 (green) and CAP5.5 (red) are associated with the corset MTs over the entire cell body. After 24 hours of depletion, CAP5.5 expression at the posterior end of the cell is reduced (this can be clearly seen in Figure 5.12C which shows a 2K1N cell with TCP86 labelling over the whole cell body but CAP5.5 labelling restricted to the anterior end of the cell). Figure 5.12D shows a cell which has made several attempts

to complete cytokinesis and has failed to do so, this cell has 4 anterior ends joined to a large cell body. In this image only one of these anterior ends possesses CAP5.5 labelling suggesting that this anterior end belongs to the original cell. TCP86 labelling is present all over the cell body (including each anterior end) with the same intensity. In conclusion, TCP86 does not require CAP5.5 for localisation to the subpellicular MTs.

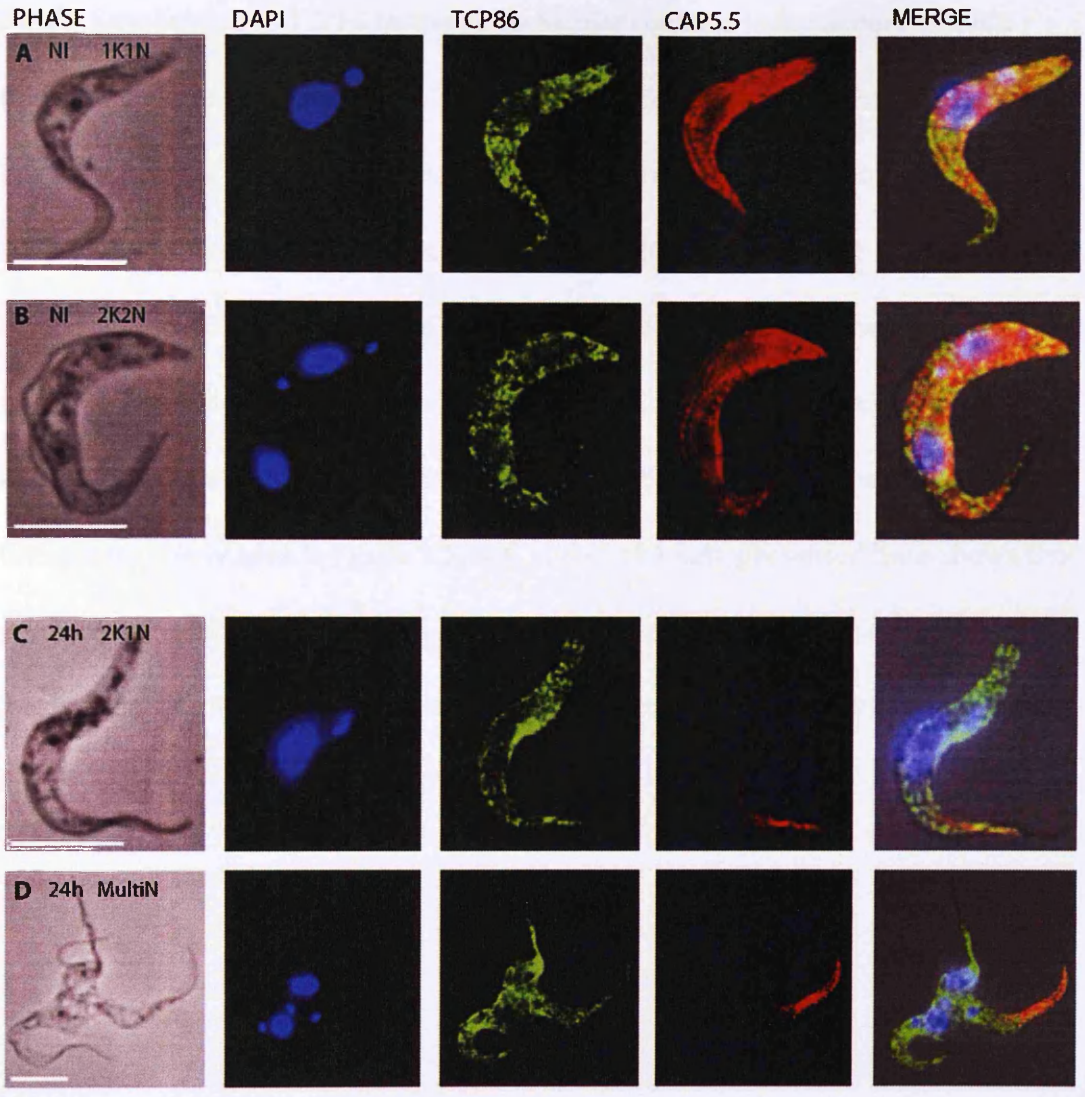

Figure 5.12 Immunofluorescence images showing the localisation of CAP5.5 and TCP86 before and after RNAi ablation of CAP5.5

Cells from the CAP5.5 RNAi cell line, non-induced (NI) and 24 hours post induction were harvested for immunofluorescence analysis and slides were prepared as described in section 2.5.1. Cells were labelled using anti-TCP86 (green) and anti-CAP5.5 (red) primary antibodies (dilutions used are shown in section 2.2.3) and then stained with DAPI (blue). In NI cells antibodies localise to their target proteins over the entire subpellicular corset throughout the cell cycle, examples show a 1K1N cell (A) and a 2K2N cell (B). After 24 hours CAP5.5 expression is reduced but TCP86 expression is unaffected (C and D) (scale bar = 10μm).

5.5.2 Localisation of TCP86 to the subpellicular corset is independent of WCB

Previous experiments show that TCP86 ablation does not affect the localisation of WCB (Shawcross, 2008). The reciprocal experiment was carried out here to see if WCB RNAi ablation effects the localisation of TCP86; the results are shown in Figure 5.13. Figure 5.13A shows that TCP86 and WCB localise to the whole subpellicular corset in non-induced cells. After 24 hours of induction, WCB expression is reduced at the posterior end of the cell, yet TCP86 can still be seen over the entire corset and this can be clearly seen in Figure 5.13B, C and D. The data presented here shows that when WCB is ablated TCP86 can still localise to microtubules, proving that the localisation of TCP86 and WCB to the subpellicular MTs are independent of one another.

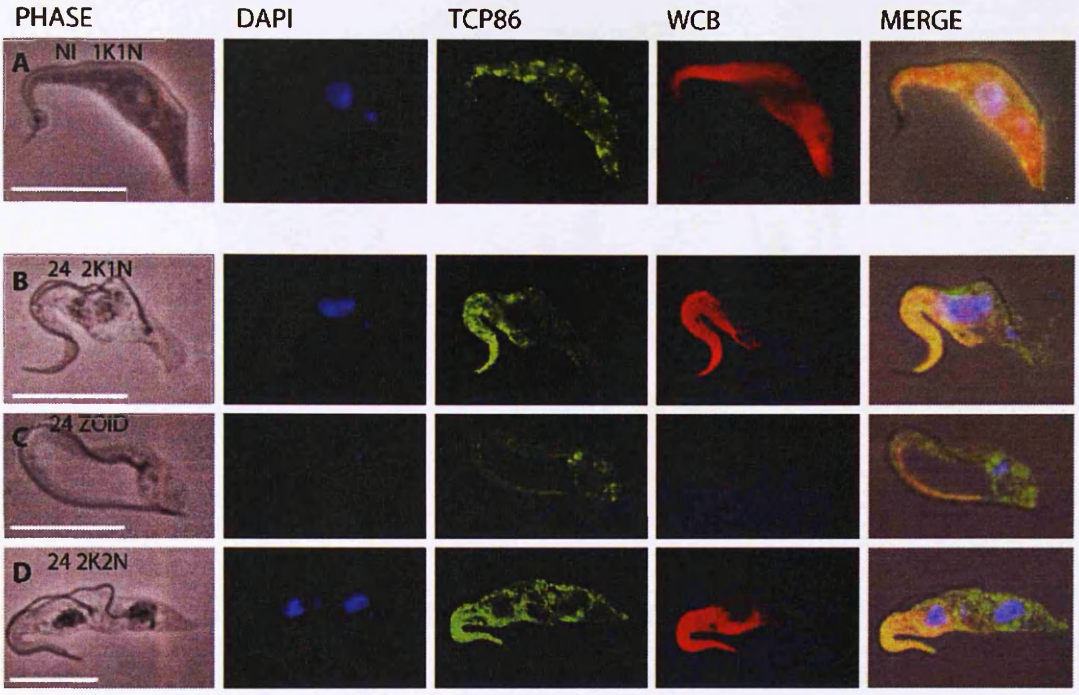

Figure 5.13 Immunofluorescence images showing the localisation of WCB and TCP86 before and after RNAi ablation of WCB

Cells from the WCB RNAi cell line, a non-induced (NI) culture and 24 hours post induction were harvested for immunofluorescence analysis and slides were prepared as described in section 2.5.1. Cells were labelled with anti TCP86 (green) and anti-WCB (red) antibodies (dilutions used are shown in section 2.2.3) and DAPI (blue). In non-induced cells both antibodies localise to protein over the entire subpellicular corset throughout the cell cycle (A). After 24 hours WCB expression is reduced but TCP86 expression is unaffected (B-D) (scale bar 10µm).

Figure 5.14 summarises the immunofluorescence data presented above. Showing that CAP5.5 localisation to the MTs is dependent on TCP86 but all other potential interactions investigated do not show dependency. The blue arrows on the diagram show the focus of the next set of experiments. These were carried out using the same cell lines and the same antibodies to investigate if interdependency relationships exist between CAP5.5 and WCB.

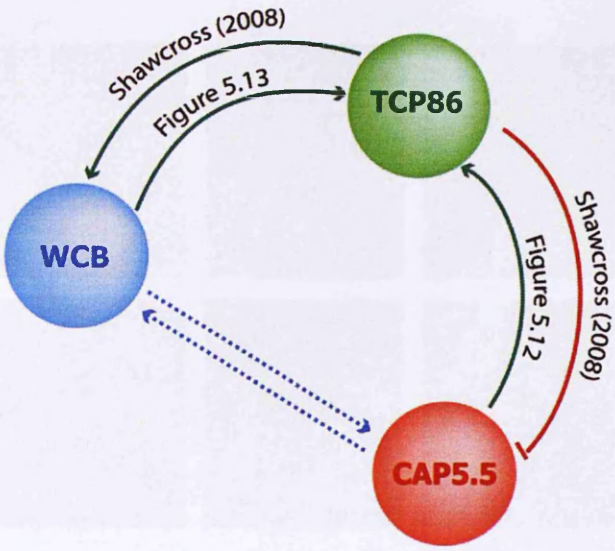

Figure 5.14 Summary of immunofluorescence show in Figure 5.12- Figure 5.13

Diagram shows that when TCP86 is ablated CAP5.5 is unable to localise to the microtubules (red arrow) but WCB localisation is unaffected (green arrows). When CAP5.5 or WCB are ablated TCP86 localisation is unaffected. Blue arrows show the interactions which need to be investigated to complete this study.

5.5.3 WCB localisation to the subpellicular corset is independent of CAP5.5

To investigate whether the localisation of WCB is dependent upon CAP5.5, the CAP5.5 RNAi cell line was induced and probed with an antibody specific for WCB. Figure 5.15A and B show cells from the non-induced culture of the CAP5.5 RNAi cell line, both CAP5.5 and WCB are present over the whole subpellicular corset. After 24 hours of ablation new MTs at the posterior end of the cell are negative for CAP5.5 as expected, but are positive for WCB, showing that WCB localises independently of CAP5.5 (Figure 5.15C and D).

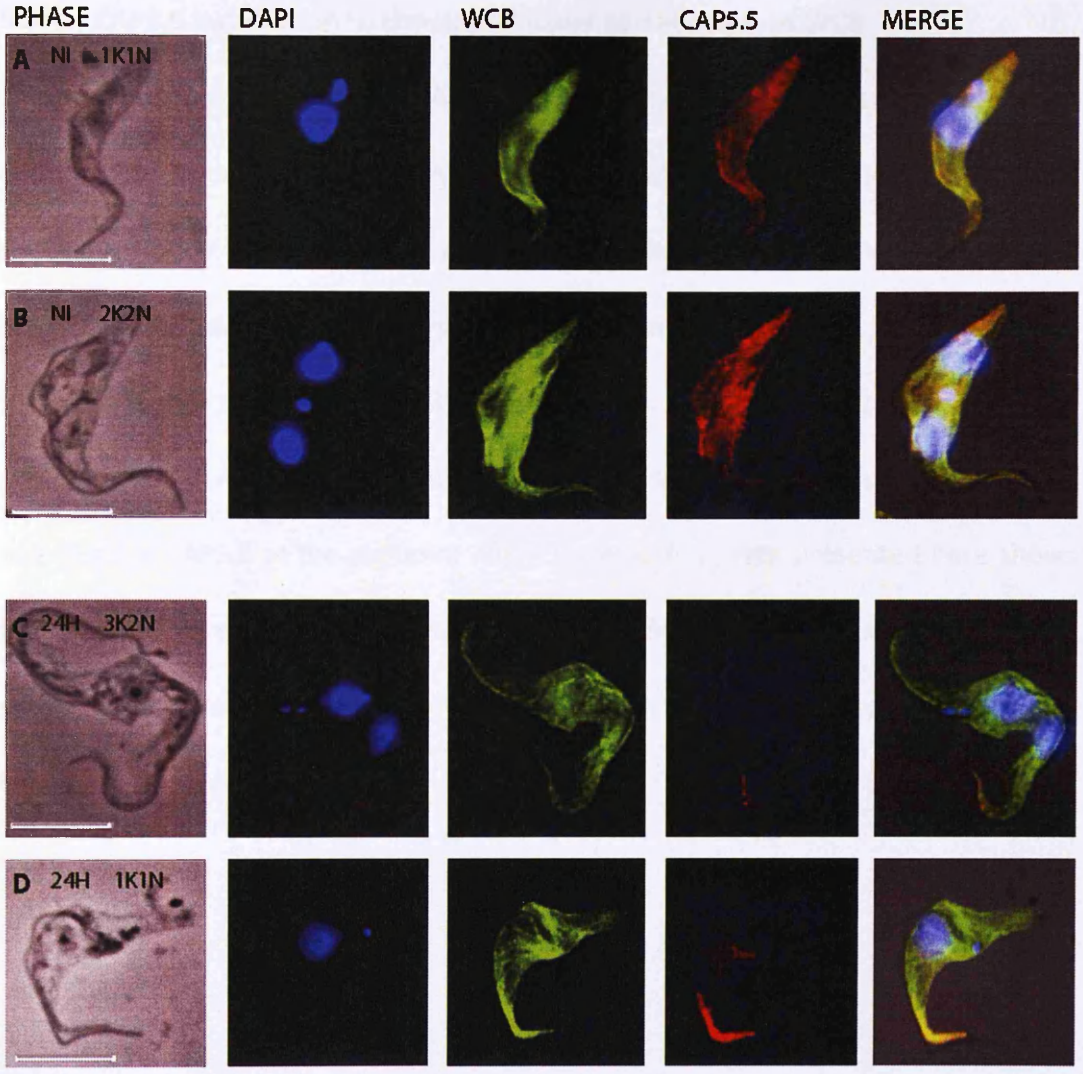

Figure 5.15 Immunofluorescence images showing the localisation of WCB and CAP5.5 before and after RNAi ablation of CAP5.5

Cells from a non-induced (NI) culture and 24 hours post induction of the CAP5.5 RNAi cell line were harvested for immunofluorescence analysis and slides were prepared as described in section 2.5.1. Cells were labelled with anti-WCB (green) and anti-CAP5.5 (red) primary antibodies (dilutions used are shown in section 2.2.3) and then stained with DAPI (blue). In non-induced cells WCB and CAP5.5 localised over the entire cell body (A) a NI 1K1N cell and (B) a NI 2K2N cell. C and D show cells 24 hours post induction, CAP5.5 is reduced but WCB localisation remains unaffected (scale bar = 10μm).

5.5.4 CAP5.5 localisation to the subpellicular corset requires WCB

The previous experiment shows that WCB localisation is independent of CAP5.5, to check the reciprocal the WCB RNAi cell line was induced and probed with a CAP5.5 specific antibody. In the non-induced cells both proteins are seen over the entire cell body (Figure 5.16A). After 24 hours of WCB ablation the MTs at the posterior end of the cell become negative for WCB as expected due to the targeted ablation of this protein by RNAi. A reduction in CAP5.5 localisation is also observed and MTs become negative for CAP5.5 at the posterior end (Figure 5.16C). Data presented here shows that WCB expression/localisation is essential for CAP5.5 localisation to the subpellicular corset MTs but WCB does not require the expression of CAP5.5 for its localisation (Figure 5.15).

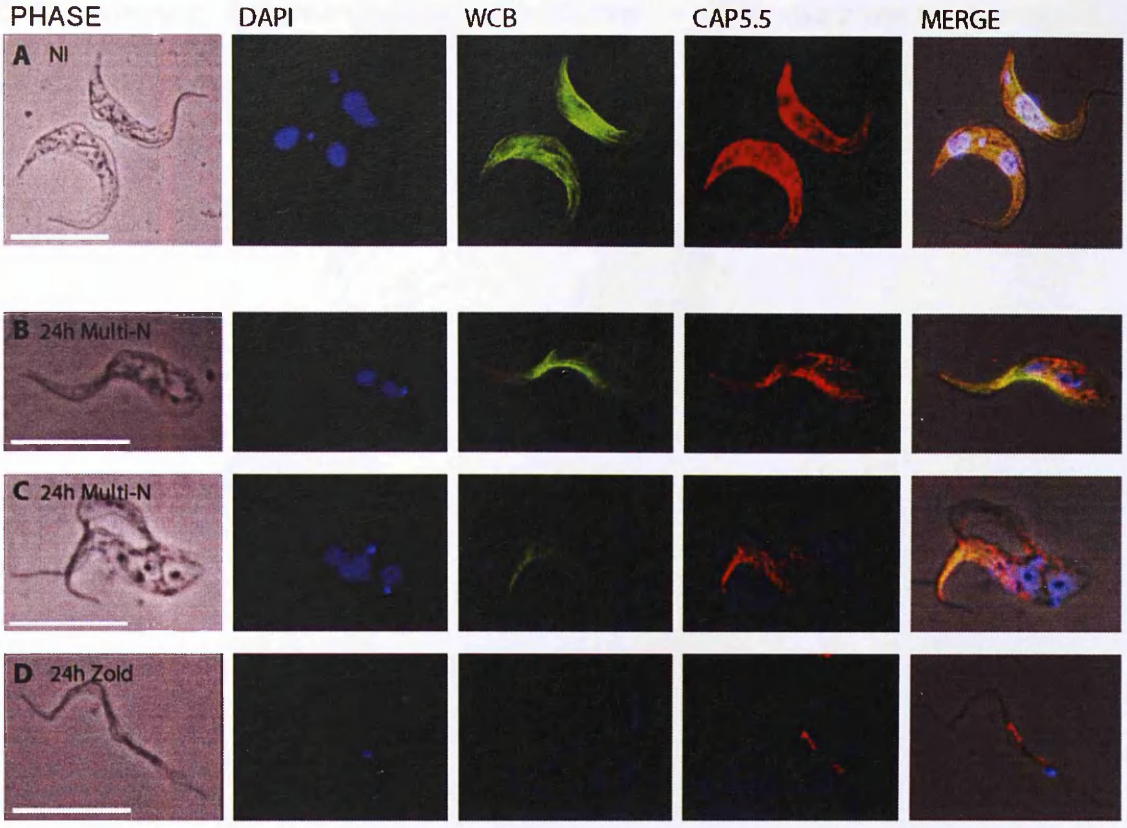

Figure 5.16 Immunofluorescence images showing the localisation of WCB and CAP5.5 before and after RNAi ablation of WCB

Cells from a non-induced (NI) culture and 24 hours post induction of the WCB RNAi cell line were harvested for immunofluorescence analysis and slides were prepared as described in section 2.5.1. Cells were labelled with anti-WCB (green) and anti-CAP5.5 (red) primary antibodies (dilutions used are shown in section 2.2.3) and then stained with DAPI (blue). In non-induced cells WCB and CAP5.5 localised over the entire cell body (A) a NI 1K1N cell and 2K2N cell. B-D cells 24 hours post induction; WCB and CAP5.5 are reduced (scale bar = 10μm).

A summary of the immunofluorescence data described above is shown in Figure 5.17. This model shows that CAP5.5 localisation to the subpellicular corset is dependent upon expression of TCP86 and WCB. When TCP86 or WCB are independently knocked down through RNAi ablation they are no longer detected on new MTs at the posterior end of the cell, the same MTs also become negative for

CAP5.5 staining. The green arrows in this illustration show where the localisation of one MAP is unaffected by the RNAi mediated depletion of the other.

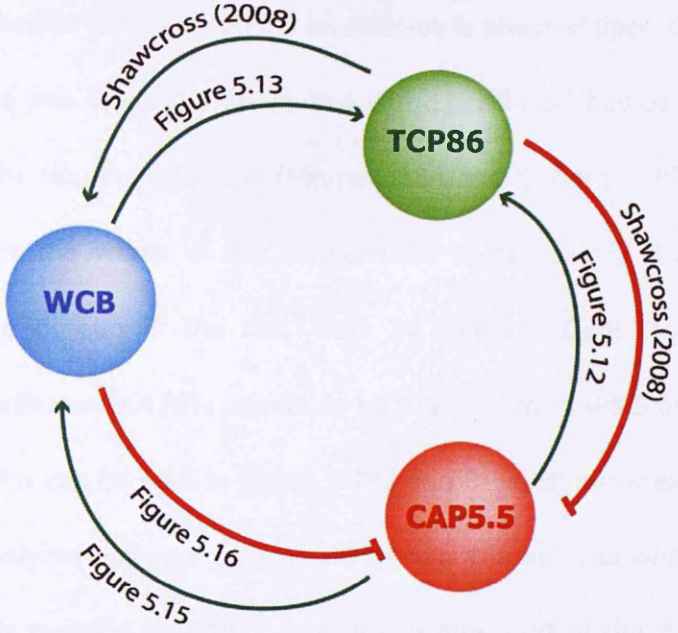

Figure 5.17 Illustration summarising the interactions between TCP86, CAP5.5 and WCB at the subpellicular corset

The model represents the findings of the immunofluorescence experiments shown in Figure 5.12, Figure 5.13, Figure 5.15 and Figure 5.16. Arrows represent what happens to MAP localisation when the protein in question is reduced by RNAi. Red lines indicate conditions where another MAP does not associate with the subpellicular corset as a result of RNAi ablation of the MAP in question. Green arrows represent where localisation of the other MAP is unaffected by depletion of the MAP in question. When TCP86 expression is knocked down by RNAi CAP5.5 is no longer able to associate with the subpellicular corset, this is also the case for WCB ablation. Localisation of TCP86 and WCB is unaffected by the knockdown of other MAPs in this study.

5.6 GB4L expression is essential for CAP5.5 localisation to the subpellicular corset but not for TCP86 or WCB

Whilst there is no evidence proving conclusively that GB4L is a MAP, the disorganised growth of MTs which occurs upon RNAi mediated ablation of this protein (Figure 4.10

- Figure 4.12) suggests that it may function in a role associated with MTs or with other MAPs. For this reason the cell line was included in the interdependency study.

To investigate whether TCP86 or CAP5.5 localisation is affected upon GB4L depletion the GB4L cell line was induced and labelled with specific antibodies against TCP86 and CAP5.5. In the non-induced cells (Figure 5.18A and B) both TCP86 and CAP5.5 can be seen over the whole of the subpellicular corset evenly distributed from anterior to posterior end of the cell. After 24 hours of GB4L depletion TCP86 localisation is unaffected but MTs appear to be negative for CAP5.5 at the posterior end of the cell, this can be seen in Figure 5.18C and D which show examples of the characteristic 'push-me-pull-you' cells. In these cells the anterior end belonging to the mother cell is positive for CAP5.5 but the anterior end of the daughter cell is negative. This experiment shows that GB4L expression is required for CAP5.5 but not TCP86 localisation to the subpellicular corset. Moreover, this supports the previous data shown in section 5.5.1 (Figure 5.12) that TCP86 localisation is independent of CAP5.5.

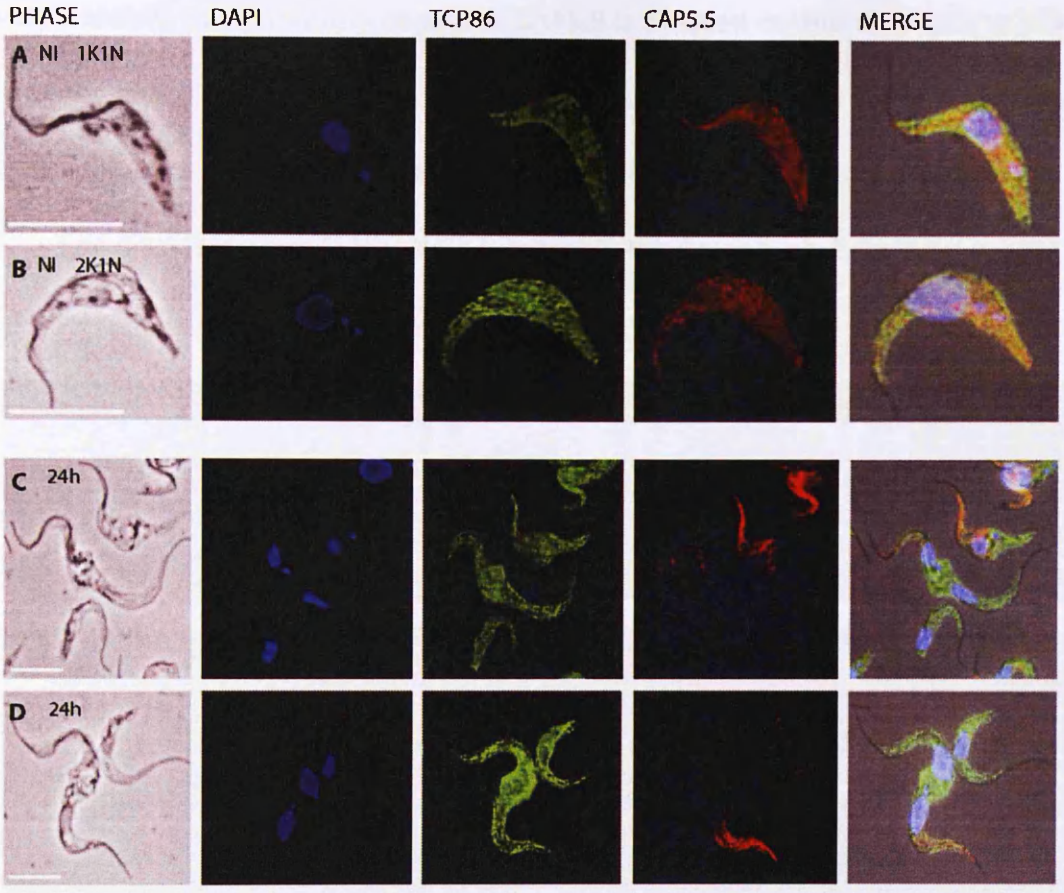

Figure 5.18 Immunofluorescence images showing the localisation of TCP86 and CAP5.5 before and after RNAi ablation of GB4L

Cells from a non-induced (NI) culture and 24 hours post induction of the GB4L RNAi cell line were harvested for immunofluorescence analysis and slides were prepared as described in section 2.5.1. Cells were labelled with anti-TCP86 (green) and anti-CAP5.5 (red) antibodies (dilutions used are shown in section 2.2.3) and stained with DAPI (blue). In non-induced cells, TCP86 and CAP5.5 localised over the entire cell (A and B). After 24 hours of induction (C and D) TCP86 localisation is not affected but CAP5.5 is reduced (scale bar = 10μm).

To explore if GB4L ablation affects the localisation of WCB, the GB4L RNAi cell line was probed with an antibody specific for WCB, at the same time CAP5.5 labelling was repeated to verify the previous result. In non-induced cells, WCB and CAP5.5 can be seen over the entire subpellicular corset (Figure 5.19A). Knockdown of GB4L by RNAi does not affect localisation WCB as the protein can still be seen over the entire cell

body. However, as previously observed, CAP5.5 is reduced on the new MTs at the posterior end of the cell (Figure 5.19B and C); this confirms that CAP5.5 requires GB4L expression for localisation. Moreover, this data supports previous data shown in section 5.5.3 (Figure 5.15) that WCB localisation is independent of CAP5.5.

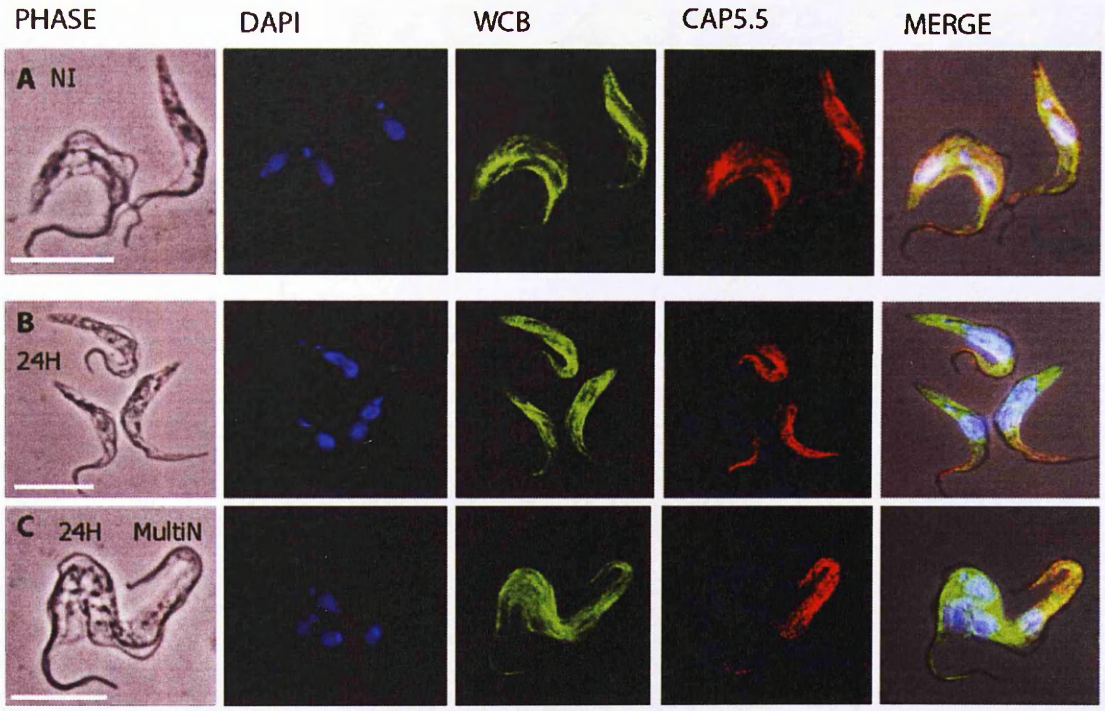

Figure 5.19 Immunofluorescence images showing the localisation of WCB and CAP5.5 before and after RNAi ablation of GB4L

Cells from a non-induced (NI) culture and 24 hours post induction of the GB4L RNAi cell line were harvested for immunofluorescence analysis and slides were prepared as described in section 2.5.1. Cells were labelled with anti-WCB (green) and anti-CAP5.5 (red) antibodies (dilutions used are shown in section 2.2.3) and then stained with DAPI (blue). In non-induced cells WCB and CAP5.5 localised over the entire cell (A). After 24 hours of induction (B and C) WCB localisation is not affected but CAP5.5 is reduced (scale bar = 10μm).

MAP localisation to the subpellicular corset was also examined by immunoblot analysis. Figure 5.20 shows immunoblots which confirm that WCB and TCP86

localisation to the cytoskeleton is not affected by GB4L ablation, however after 48 hours of induction CAP5.5 localisation is reduced beyond detectable levels.

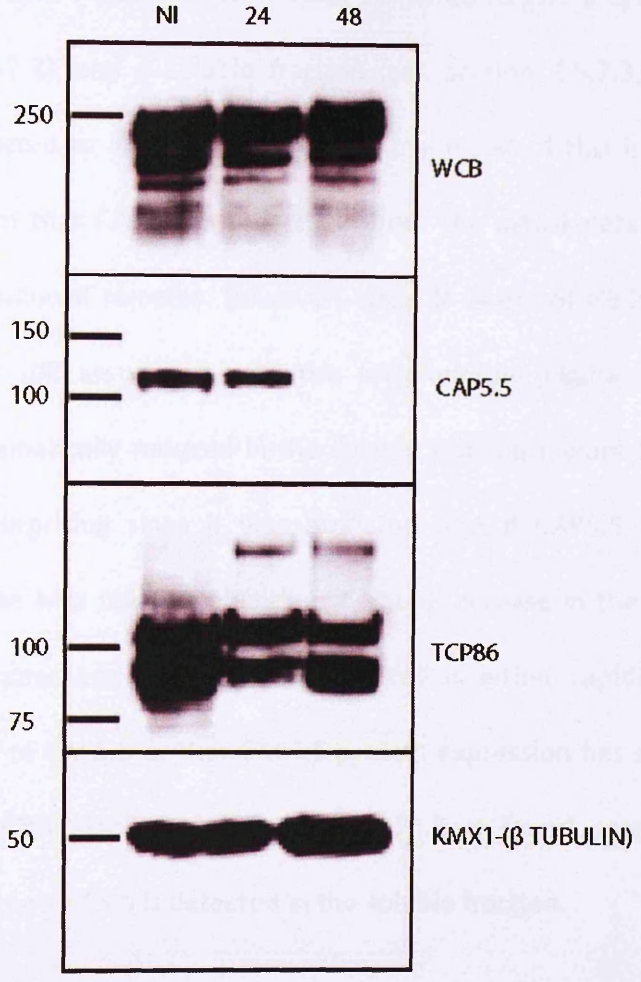

Figure 5.20 Immunoblots showing that GB4L depletion affects the cytoskeletal localisation of CAP5.5 but not TCP86 or WCB

RNAi cells were induced and cells were harvested at specified time points, and cells from a non-induced culture were also harvested. Cytoskeletons were extracted using NP40 as described in section 2.5.7.2. Protein extracts from $5X10^6$ cells were loaded per lane and separated by SDS-PAGE, transferred to nitrocellulose membranes then probed with the specified antibodies (dilutions used are shown in section 2.2.3). Membranes were incubated with the relevant HRP-conjugated secondary antibody and immobilised specific antigens detected by chemiluminescence. Immunoblots show that WCB and TCP86 protein levels on the cytoskeleton are not affected by GB4L ablation. However, there is a marked reduction in CAP5.5 on the subpellicular corset over the time course. KMX1 the anti β-tubulin antibody was used as a control for equal loading.

To investigate if CAP5.5 becomes mis-localised into the cytoplasm the GB4L RNAi cell line was induced and cells harvested from a non-induced culture and at 24 and 48 hours post induction. These cells were then extracted to give a cytoskeletal fraction (see section 2.5.7.2), and a soluble fraction (see section 2.5.7.3). These fractions were then subjected to immunoblot analysis; the result of this is shown in Figure 5.21. It is evident that CAP5.5 is present in both the cytoskeletal and the soluble fraction in non-induced samples. However, after 24 hours of GB4L RNAi induction, while CAP5.5 is still associated with the cytoskeleton (Figure 5.21 lane 3), its abundance is dramatically reduced in the soluble fraction (Figure 5.21 lane 7). This observation is surprising since it was expected that if CAP5.5 was not able to associate with the MTs then its abundance would increase in the soluble fraction. This is not the case and suggests that the cell is either rapidly degrading the cytoplasmic pool of CAP5.5 or that CAP5.5 protein expression has stopped. After 48 hours of GB4L RNAi depletion very little CAP5.5 is found associated with the cytoskeleton and no CAP5.5 is detected in the soluble fraction.

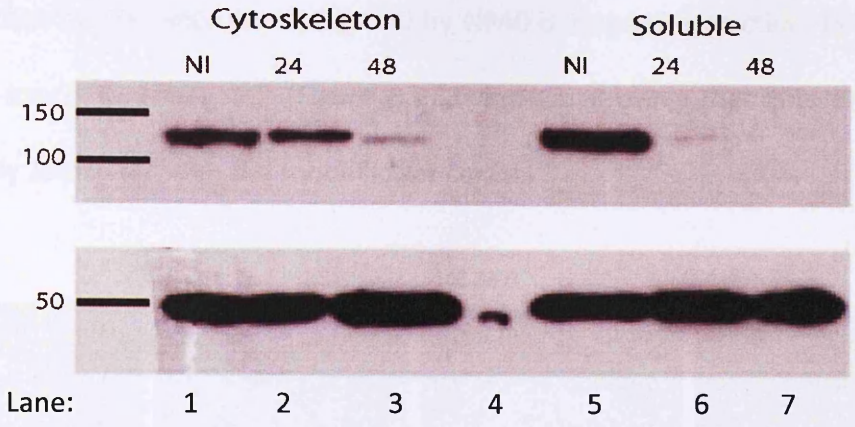

Figure 5.21 Immunoblot analysis shows that CAP5.5 protein levels are reduced after GB4L RNAi depletion

Cells from the non-induced (NI) GB4L RNAi cell line were harvested then a culture was induced and cells were harvested at specified time points. Cytoskeletons from $5X10^6$ cells were extracted using NP40 to give a cytoskeleton extract (as described in section 2.5.7.2), the soluble fraction was concentrated by acetone precipitation (method described in section 2.5.7.3). Both the cytoskeletal and soluble protein extracts were separated by SDS-PAGE, transferred to nitrocellulose membranes then probed with the CAP5.5 specific antibody (for dilution used see section 2.2.3), membranes were then incubated with polyclonal-goat anti-mouse HRP-conjugated secondary antibody and the immobilised CAP5.5 antigens were detected by chemiluminescence. Immunoblots show there is a marked reduction in CAP5.5 on the subpellicular corset and in the soluble fraction over the time course. The anti β-tubulin antibody KMX1 was used as a loading control.

5.7 I6a/b-GFP localises to the subpellicular corset in *T. brucei*

Unfortunately repeated attempts to acquire antibodies to other published *T. brucei* MAPs were unsuccessful, and so attempts were made to create gene fusions in which specific MAPs were fused to GFP; thus allowing further study of MAP functional interdependency relationships. Constructs were made to fuse GFP to either the N and/or C terminus of MARP1/2, I6, CAP15, CAP17, GB4 and GB4L. While constructs and cell lines were generated for all these MAP-GFP combinations, localisation was only successful for the I6 construct. In whole cells the I6-GFP fusion protein localises over the entire cell, excluding the flagellum this is shown in Figure

5.22A. When cytoskeletons are prepared by NP40 detergent extraction, I6-GFP still localises over the entire cell (Figure 5.22B and C). Proving that this protein is specifically associated with the subpellicular corset.

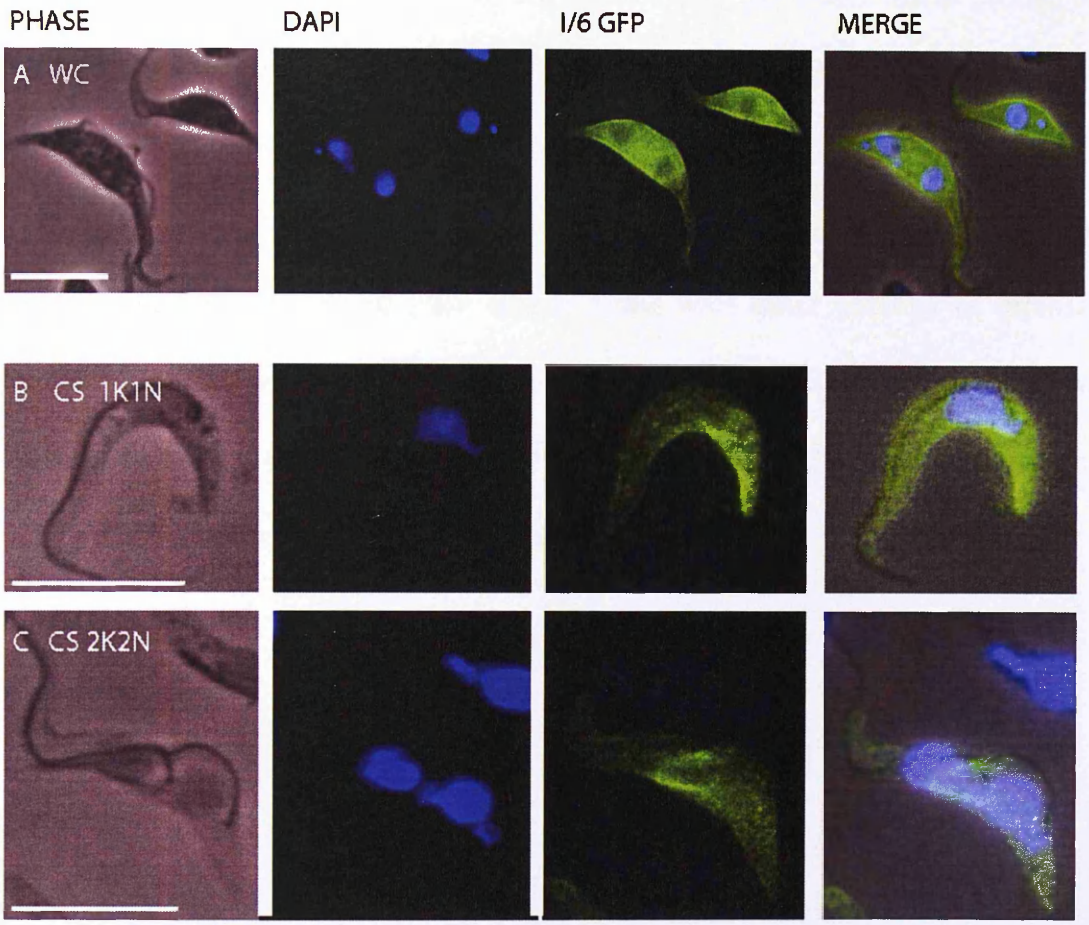

Figure 5.22 Fluorescence images showing that I6-GFP localises to the subpellicular corset in *T. brucei*

T. brucei cells were transfected with the I6-GFP plasmid which was integrated allowing expression of a fusion protein (for methods see section 2.4.5). Cells were harvested and settled on to slides (as described in section 2.5.1) and labelled with DAPI (blue). The I6-GFP fusion protein (green) localises over the entire cell body in whole cells (WC) (A) and in NP40 extracted cytoskeletons (CS) (B and C) at all cell cycle stages (method for extracting cytoskeletons is described in section 2.5.1) (scale bar = 10µm).

5.7.1 I6a/b localisation to the subpellicular corset is independent of GB4L

To investigate whether the localisation of I6 is affected when GB4L is depleted, the I6-GFP construct was transfected into the GB4L RNAi cell line and RNAi induced. Figure 5.23 demonstrates that in GB4L non-induced cells the I6-GFP fusion protein is also located over the entire cell body in both whole cells (Figure 5.23A and B) and cytoskeletons (Figure 5.23C); reflecting the result seen in the wild type cells (Figure 5.22). However, in this cell line there was also intense I6-GFP fluorescence which appeared to be near to the basal bodies along with other patches of intense fluorescence in the posterior region of the cell. The intense staining corresponding to the basal body regions is indicated by a green arrow on Figure 5.23 and was present in both whole cells and cytoskeleton preparations.

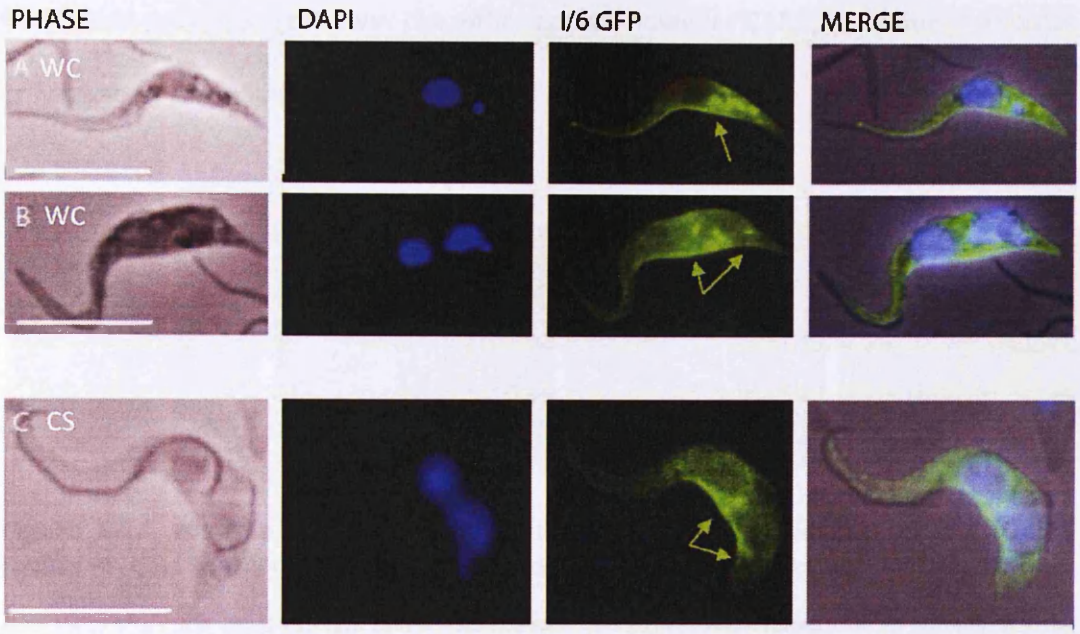

Figure 5.23 Fluorescence images showing the localisation of the I6-GFP fusion protein in the non-induced GB4L RNAi cell line

The GB4L RNAi cell line was transfected with a construct to allow expression of I6-GFP, cells were settled on to slides (as described in section 2.5.1) and labelled with DAPI (blue). Images show non-induced cells from the GB4L cell line expressing I6-GFP (green), (A) shows a 1K1N cell, (B) shows a 2K2N cell and both these images are of whole cells (WC) showing I6 localisation over the whole cell body. (C) Shows a cytoskeleton, I6 localisation remains over the entire cell as seen in wild type cells. These images were taken on the Leica DMRX microscope. Green arrows indicate areas of intense signal which appear to be located in proximity to the basal bodies (scale bar = 10 μm).

Following on from this, the GB4L cell line containing the I6-GFP gene fusion was induced and cells labelled with CAP5.5 and visualised by fluorescence microscopy. CAP5.5 has previously been shown to reduce following RNAi ablation of GB4L (Figure 5.18 and Figure 5.19) so this antibody was used as a marker to show that induction of GB4L RNAi is effective. This experiment showed that I6-GFP localisation to the subpellicular corset does not require GB4L. An example is shown in Figure 5.24 which shows a characteristic GB4L push-me-pull-you cell 24 hours post induction. The I6-

GFP fusion protein is seen over the entire corset; however CAP5.5 is reduced and can only be seen on one anterior end.

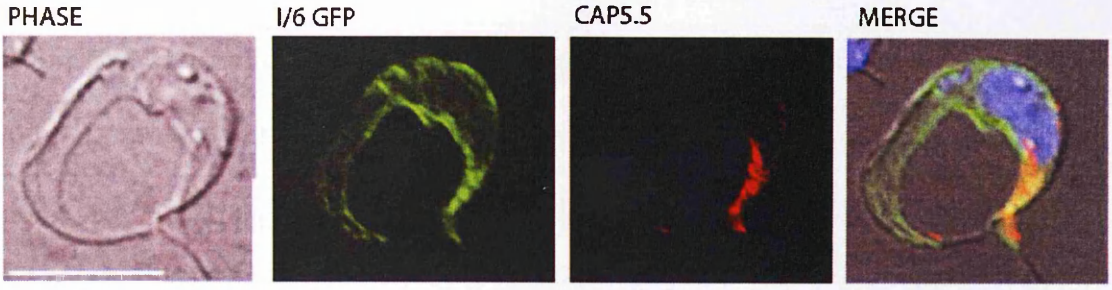

Figure 5.24 Immunofluorescence images showing the localisation of the I6-GFP fusion protein in the GB4L RNAi cell line at 24 hours post induction

Cells from the GB4L RNAi cell line expressing the I6-GFP fusion protein (green) were harvested at 24 hours post induction. Cells were settled on to slides (as described in section 2.5.1) labelled with anti-CAP5.5 antibody (red) to show the efficacy of GB4L RNAi (CAP5.5 localisation is reduced upon GB4L depletion see Figure 5.18) and DAPI (blue). Cells were visualised by Deltavision microscopy, the images shows a characteristic push-me-pull-you cell, CAP5.5 is reduced, I6-GFP localisation appears unaffected by GB4L RNAi depletion.

5.8 Summary

This chapter explores *T. brucei* MAPs, initially describing the results of an RNAi screen carried out to investigate proteins which are published as MAPs but have not been extensively characterised or subjected to RNAi mediated ablation. Shortly after initiating this screen the RNAi phenotype for WCB was published (Baines & Gull, 2008), followed by that of CAP5.5 (Olego-Fernandez *et al*, 2009). This chapter confirms the findings of these studies showing that RNAi depletion of WCB and CAP5.5 results in growth (Figure 5.1) and morphology defects (Figure 5.5A and B). The data presented here shows that ablation of CAP15, I6, GB4 and MARP1/2 does not result in any observable phenotype and as such these cell lines were not studied further (Figure 5.1). RNAi depletion of WCB and CAP5.5 was verified by immunoblot

analysis (see Figure 5.2) and immunofluorescence studies show that both proteins are initially lost from the posterior end of the cell (Figure 5.3 and Figure 5.4). Depletion of both WCB and CAP5.5 results in disruption of cell cycle progression (Figure 5.8) and leads to aberrant cytokinesis resulting in the production of zoids and multinucleates (see Figure 5.8, Figure 5.9 and Figure 5.10). Measurements taken of organelle positioning in the CAP5.5 cell line show that flagella growth and basal body segregation is normal. However, in a small number of induced cells the new basal body was positioned closer to the posterior end than in the non-induced controls suggesting that posterior end elongation may be affected (Figure 5.11D). Interestingly no defects in nuclear segregation were measured despite nuclear mis-positioning reported by Olego-Fernandez *et al* (Olego-Fernandez *et al*, 2009). This suggests that aberrent positioning of the nuclei during cytokinesis described in this publication is not a result of defects in nuclear seperation, rather gross morphological changes to the cell structure (e.g the lack of posterior end extension) might explain this phenotype.

This chapter then moves towards building an interactome for MAPs on the subpellicular corset (section 5.5). Figure 5.25 summerises the flourescence data collected in this chapter and shows the affects of depleting a given protein on the localisation of other MAPs. Green arrows show where no effect was observed, red arrows indicate where localisation was disrupted, blue dashed arrows show where further work is required.

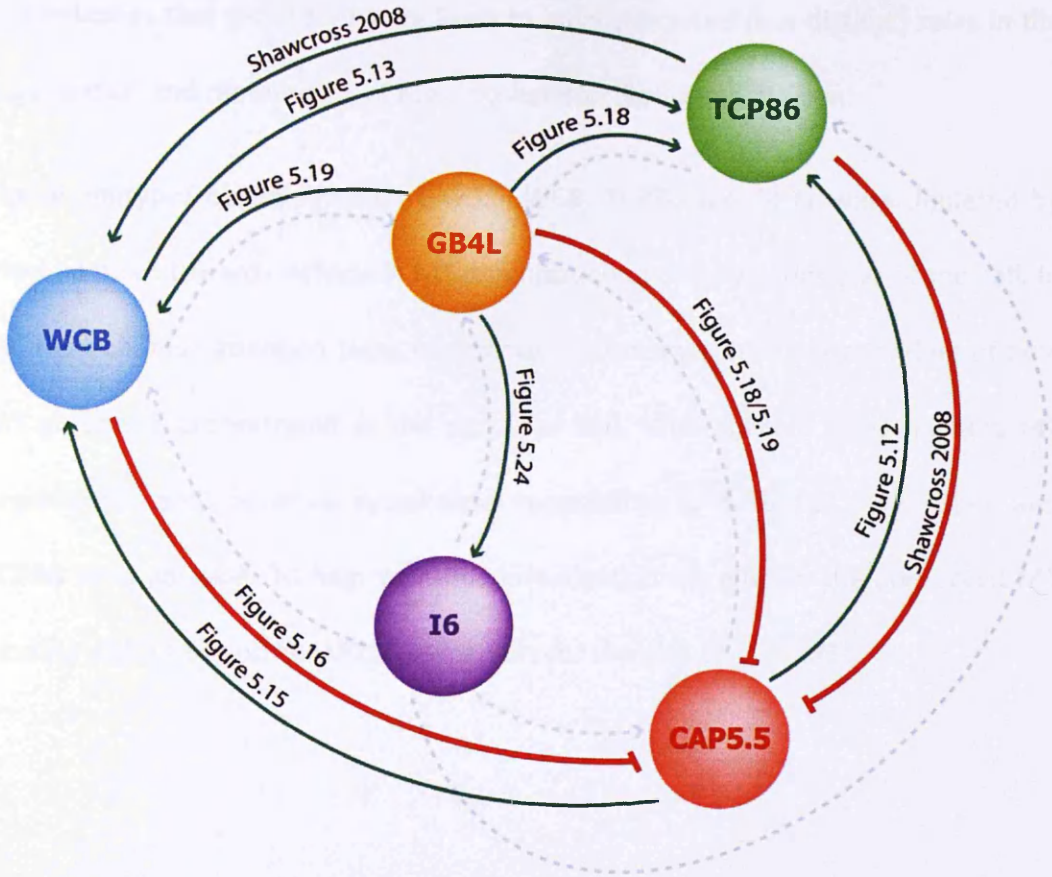

Figure 5.25 Summary of the immunofluorescence results for the MAP interactome

The cartoon represents the results of the immunofluorescence carried out thus far on the available RNAi cell lines, arrows show what happens when the protein in question is reduced by RNAi. Red arrows represent where localisation of another protein reduced, green arrows show where RNAi has no affect on the other protein. Blue dashed arrows show where interactions have not yet been studied.

Specific RNAi mediated ablation of WCB, TCP86 and GB4L prevents the localisation of CAP5.5 to the posterior end of the subpellicular corset. It is interesting to note that ablation of these specific MAPs results in distinct phenotypes despite the fact that they all affect CAP5.5 localisation. This suggests that the growth and morphological phenotypes observed in these cell lines are not explained solely by loss of CAP5.5,

and indicates that these MAPs are likely to have concerted (but distinct) roles in the organisation and remodelling of the cytoskeleton during cell division.

The phenotypes observed when CAP5.5, WCB, TCP86 and GB4L were depleted by RNAi all point towards defects in MT organisation at the posterior end of the cell. In the next chapter attention turns to attempts to advance our understanding of how MT growth is orchestrated at the posterior end. With specific focus on how MT organisation and therefore cytoskeletal remodelling is disrupted upon GB4L and TCP86 RNAi ablation. To help with this investigation we employ the conserved MT binding +TIPs, EB1 and XMAP215 as markers for the plus ends of MTs.

Chapter 6 Microtubule plus ends and posterior end formation

6.1 Introduction

The data presented in this chapter describes the localisation of a *T. brucei* homologue of EB1 (*Tb*EB1) through GFP epitope tagging and demonstrates that *Tb*EB1 is not essential in PCF trypanosomes. GFP-*Tb*EB1 was also expressed in both the GB4L and TCP86 RNAi cell lines to act as a marker for MT plus ends. This allowed the effects of GB4L and TCP86 depletion on MT plus end organisation to be visualised. In non-induced cells a subset of MTs are organised into a discrete region of the cell where the new posterior end will form, once cytokinesis is complete; this organisation is disrupted when either GB4L or TCP86 are ablated. In a separate series of experiments the GB4L or TCP86 RNAi cell lines were also transfected with a construct allowing expression of YFP-*Tb*XMAP215; these experiments confirmed that posterior end formation is disrupted following GB4L or TCP86 ablation.

6.2 The *T. brucei* EB1 homologue (*Tb*EB1)

The *T. brucei* protein Tb09.160.1440 has an EB1 motif at its C-terminus; this motif is found at the C-terminus of proteins related to the human EB1 protein. Additionally, Tb09.160.1440 has a calponin homology (CH) domain at its N-terminus, in common with other eukaryotic EB1 proteins (Galjart, 2010). Tb09.160.1440 is annotated on GeneDB as having a MT binding function due to its homology with characterised EB1 proteins in other systems. A BlastP search using the amino acid sequence of

Tb09.160.1440 as the query returns EB1 homologues from many species; including *BIM1*, the EB1 homologue in *S. cerevisiae.*

To investigate the function of *Tb*EB1 an RNAi cell line was raised in the PCF. In this RNAi cell line GFP was fused to *Tb*EB1 at its N-terminus to enable expression of GFP-*Tb*EB1 at near physiological levels thus allowing (1) visualisation of protein localisation and (2) confirmation of *Tb*EB1 ablation in knockdown experiments.

6.2.1 Localisation of *Tb*EB1 visualised by GFP epitope tagging

Figure 6.1 shows the localisation pattern observed in cells positive for GFP-*Tb*EB1 expression. GFP-*Tb*EB1 localises strongly and consistently throughout the cell cycle to the posterior end of the cell demonstrating that subpellicular MT plus ends are concentrated in this region. This data is consistent with observations made when cells are labelled with the antibody YL1/2, which detects tyrosinated α-tubulin that is found in new MTs at the polymerising plus ends and is seen mainly at the posterior end of the cell in immunofluorescence (see Figure 6.2). It is interesting to note that in some cells the GFP-*Tb*EB1 signal defines a ring at the posterior end of the cell; see Figure 6.1A which shows an example of a 1K1N cell at an early stage in the cell cycle. Figure 6.1B-D shows that the GFP signal is maintained at the posterior end throughout the cell cycle. Figure 6.1D shows that in a 2K2N cell, which has yet to initiate cytokinesis, GFP-*Tb*EB1 is also detected in a distinct region between the nuclei (indicated with an arrow). YL1/2 staining also provides further evidence of new MT growth between divided nuclei (Figure 6.2C and D); confirming observations made with the GFP-*Tb*EB1.

A consistent observation made throughout the cell cycle is the detection of a distinct dot of GFP signal at the anterior tip of the cell body (Figure 6.1 hashes); this may represent GFP-*Tb*EB1 localising to the plus ends of the 4 specialised MTs of the FAZ which have opposite polarity to the MTs of the subpellicular corset. GFP-*Tb*EB1 is also seen associated with the growth of the new flagellum; this is indicated by asterisks in Figure 6.1A-D. In Figure 6.1A, GFP-*Tb*EB1 can be seen close to the kinetoplast in proximity to the flagella pocket, as cells progress through the cell cycle and the new flagellum extends this signal extends from the flagella pocket towards the anterior end of the cell (Figure 6.1B-D). From these images it is not possible to tell if this GFP-*Tb*EB1 association is with the new FAZ, PFR or flagellum axoneme, this is further investigated in section 6.4.1 and 6.4.2.

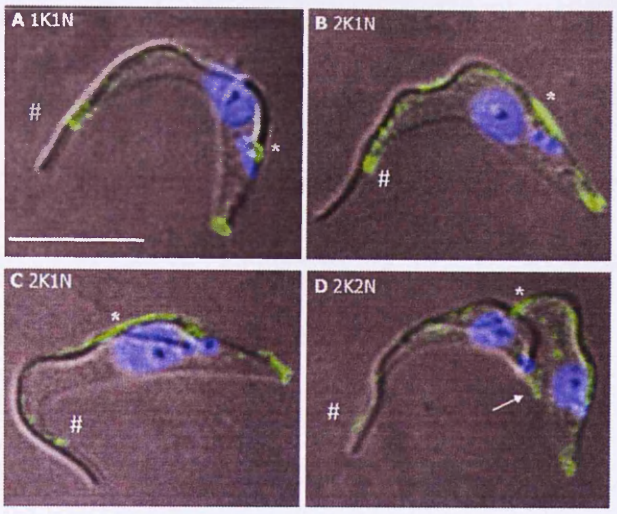

Figure 6.1 Fluorescence images showing the localisation of GFP-*Tb*EB1

Transgenic procyclic form cells expressing GFP-*Tb*EB1 were settled onto slides and detergent extracted to leave cytoskeletons, as described in section 2.5.1. Images A-D show cells at progressively later cell cycle stages. GFP-*Tb*EB1 localises to (1) the posterior end of the cell (2) the anterior tip of the cell body, (3) the new flagellum region and (4) the site of formation of a new posterior end (D). Diffuse and faint labelling is also seen over the cell body at all cell cycle stages (scale bar = 10μm).

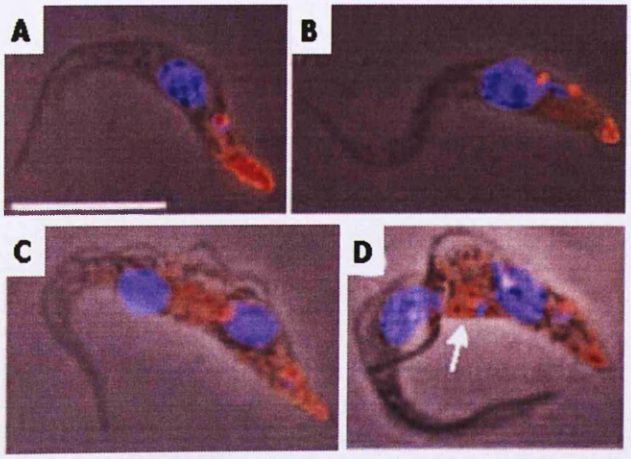

Figure 6.2 Immunofluorescence images showing new microtubule formation as visualised by YL1/2

Procyclic form trypanosomes were settled onto slides in preparation for immunofluorescence as described in section 2.5.1. Images A-D cells at progressively later stages in the cell cycle stained with the antibody YL1/2 (red) and DAPI (blue). YL1/2 detects tyrosinated α-tubulin and therefore acts as a marker for new MT growth (described in section 1.7). New MTs form at the posterior end of the cell and between separated nuclei (arrow in D) (scale bar = 10μm).

6.3 The GFP-*Tb*EB1 signal reduces upon RNAi mediated ablation of *Tb*EB1

To validate the localisation of GFP-*Tb*EB1 shown in Figure 6.1 a *Tb*EB1 RNAi cell line expressing GFP-*Tb*EB1 was generated and RNAi was induced and the GFP signal was monitored over the course of *Tb*EB1 ablation. 200 cells were counted making note of the number of cells which were expressing GFP-*Tb*EB1 at each 24 hour interval (the cells were monitored for a total of 96 hours). Figure 6.3 shows the results of this experiment, cells positive for GFP-*Tb*EB1 expression are represented by the black portion of the bar, cells negative for GFP-*Tb*EB1 expression are represented by the grey portion of the bar. In non-induced cells the GFP-*Tb*EB1 expression was heterogeneous, the signal was observed in approximately 50% of cells within the population; the number of cells expressing GFP-*Tb*EB1 reduced progressively at each time point and by 96 hours post-induction only 5% of cells had a detectable fluorescence signal.

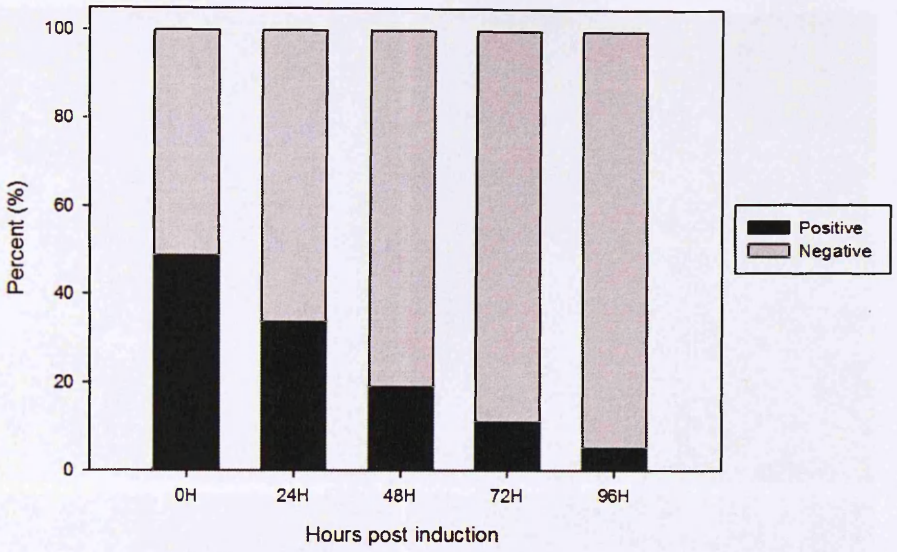

Figure 6.3 GFP-*Tb*EB1 expression is reduced when *Tb*EB1 is targeted for depletion by RNAi

The *Tb*EB1 RNAi cell line expressing GFP-*Tb*EB1 was induced and GFP-*Tb*EB1 fluorescent signal was monitored over time. Cells positive for GFP-*Tb*EB1 expression are represented by the black portion of the bar, cells negative for GFP-*Tb*EB1 expression are represented by the grey portion of the bar. 200 cells in total were counted for each time point. The percentage of cells expressing GFP-*Tb*EB1 reduces over time from ~50% in the non-induced population to ~5% after 96 hours of *Tb*EB1 RNAi mediated ablation.

The intensity of the signal is reduced over the time course, cells counted as positive for GFP-*Tb*EB1 at 96 hours post induction possessed a weaker GFP-*Tb*EB1 signal when compared to examples from the non-induced culture. Figure 6.4 presents representative fields of cells from each time point; cells marked with an asterisk were classified as positive for GFP-*Tb*EB1 signal. These images demonstrate the qualitative change observed in GFP-*Tb*EB1 signal intensity and also show that normal cell morphology is maintained over the time course of RNAi induction.

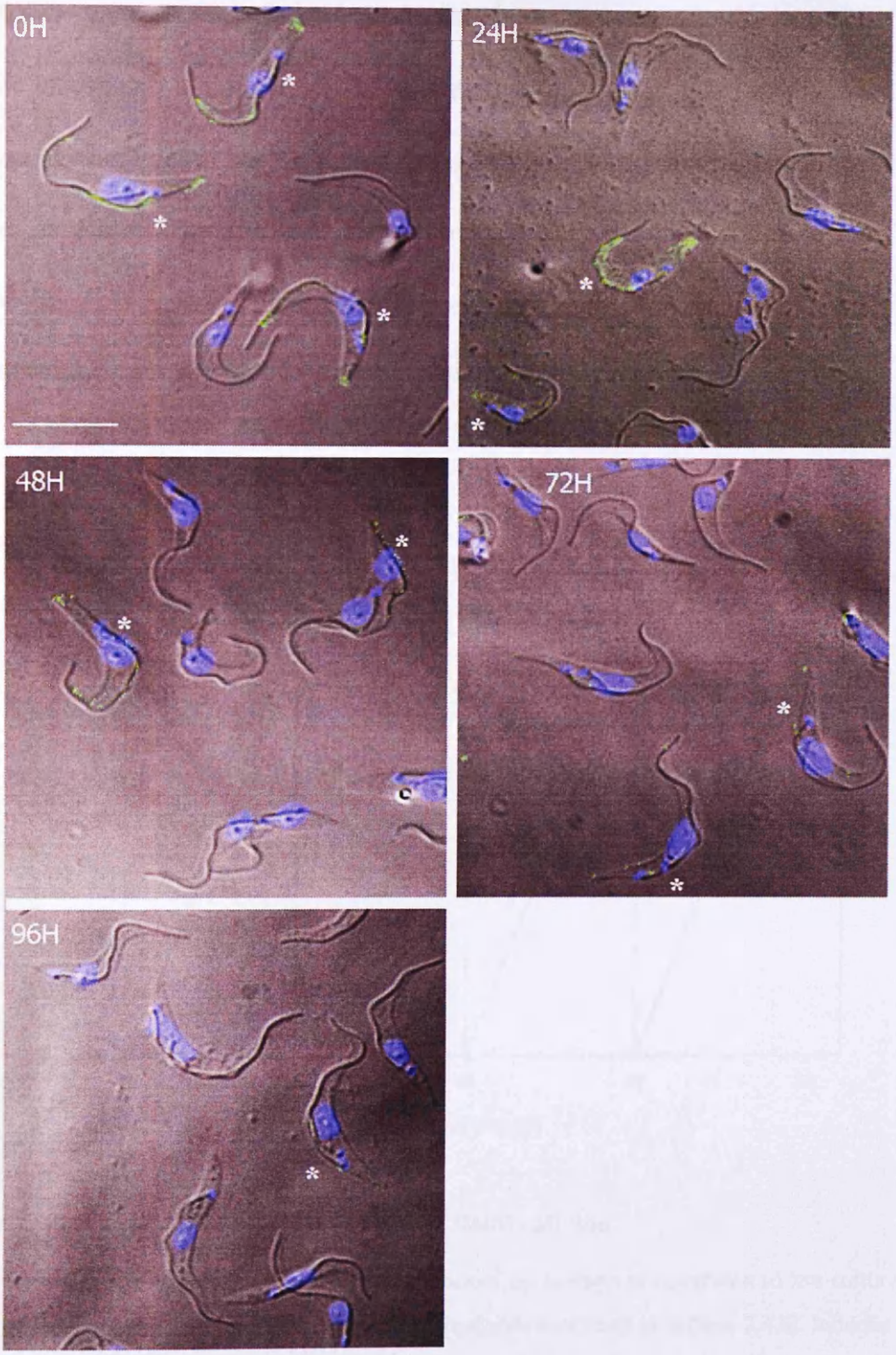

Figure 6.4 Fluorescence images showing GFP-*Tb*EB1 expression reduces over time in cells targeted for *Tb*EB1 RNAi mediated depletion

Cells from the *Tb*EB1 RNAi cell line expressing GFP-*Tb*EB1 were induced and settled onto slides for fluorescence analysis as described in section 2.5.1. GFP-*Tb*EB1 signal is reduced over time showing that RNAi ablation is effective, no morphological phenotype is observed upon the loss of EB1 expression, cells marked with an asterisk are positive for GFP expression (scale bar = 10μm).

6.4 *Tb*EB1 is not essential for viability in the procyclic form

To investigate the effects of *Tb*EB1 depletion on viability, RNAi was induced and the population growth was measured every 24 hours. Cells were also observed in culture to assess motility and general morphology. Over the time course of 96 hours no discernable growth defect was observed (see Figure 6.5) and cells appeared to be normal in terms of motility and morphology (see Figure 6.4).

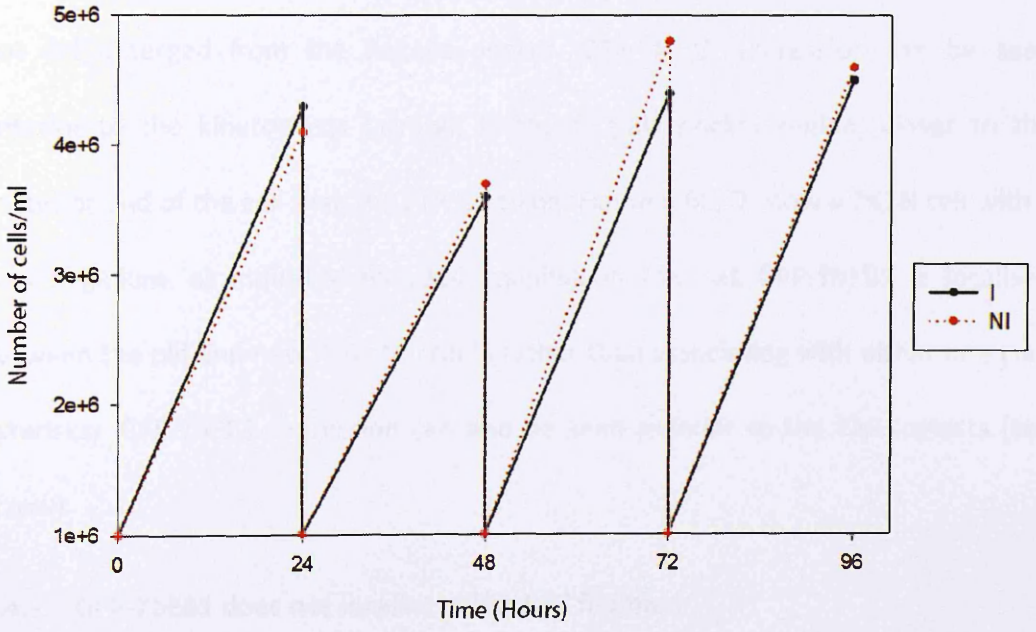

Figure 6.5 Growth curve for the *Tb*EB1 RNAi cell line

The RNAi mediated ablation of *Tb*EB1 was induced by addition of doxycyclin to the culture medium containing a concentration of $1x10^{-6}$ cell/ml (methods described in section 2.4.6). Induced and non-induced populations were measured every 24 hours then diluted back to $1x10^{-6}$ cell/ml and allowed to grow further. Counts continued for 96 hours, no effect on population growth was observed in this time.

6.4.1 GFP-*Tb*EB1 does not localise to the paraflagellar rod (PFR)

GFP-*Tb*EB1 is seen in a region close to the growing new flagellum (see asterisks in Figure 6.1). To determine whether this localisation pattern is associated with the PFR, immunofluorescence experiments were carried out using an antibody specific for this structure.

Figure 6.6 shows cells expressing the GFP-*Tb*EB1 that were also labelled with the anti PFR antibody L8C4 (Kohl *et al*, 1999). Figures 6.6A/B shows an early 2K1N cell; the PFR of a new flagellum is not detected by L8C4 suggesting that the new flagellum has not yet emerged from the flagella pocket. GFP-*Tb*EB1 expression can be seen anterior to the kinetoplasts (arrow), in the flagella pocket region, closer to the posterior end of the cell than the PFR labelling. Figure 6.6C/D show a 2K2N cell with a new flagellum, as indicated by L8C4 staining. In this cell GFP-*Tb*EB1 is localised between the old and new PFR structures rather than associating with either one (see asterisks). GFP-*Tb*EB1 expression can also be seen anterior to the kinetoplasts (see arrow).

6.4.2 GFP-*Tb*EB1 does not localise to the FAZ filament

Figure 6.7 shows that GFP-*Tb*EB1 signal does not co-localise with the antibody ROD-1 which detects the FAZ filament; that the GFP-*Tb*EB1 signal extends from a position closer to the posterior end of the cell (see bracket) than the FAZ.

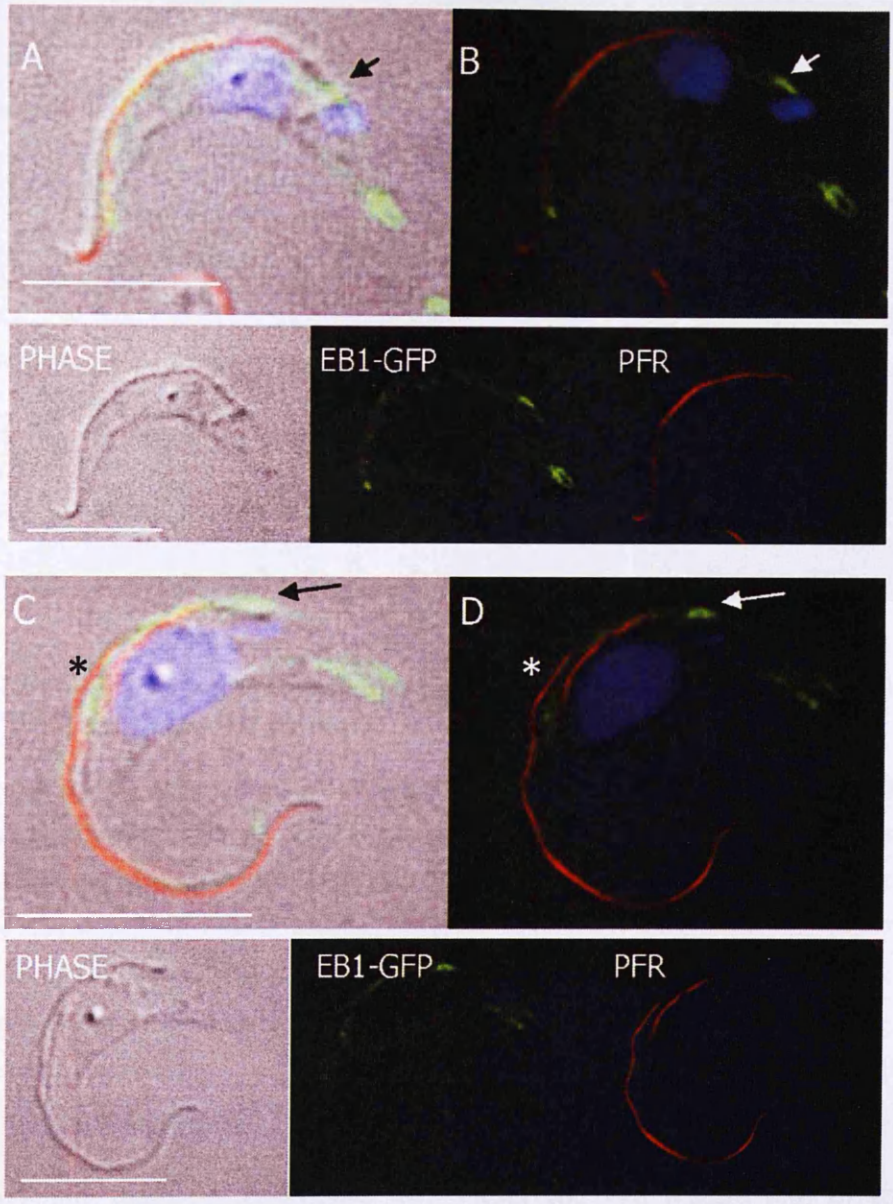

Figure 6.6 Fluorescence/immunofluorescence images showing that GFP-*Tb*EB1 does not co-localise with the PFR

Cells expressing GFP-*Tb*EB1 (green) were settled onto slides and membranes were extracted with NP40 as described in section 2.5.1. In preparation for immunofluorescence analysis these cytoskeletons were labelled with the L8C4 antibody to detect the PFR (red) (for dilutions used see section 2.2.3) and stained with DAPI (blue). Images were captured on a Deltavision microscope. The figure shows that the GFP-*Tb*EB1 signal does not co-localise with the PFR (indicated by arrows and asterisks) (scale bar = 10 μm).

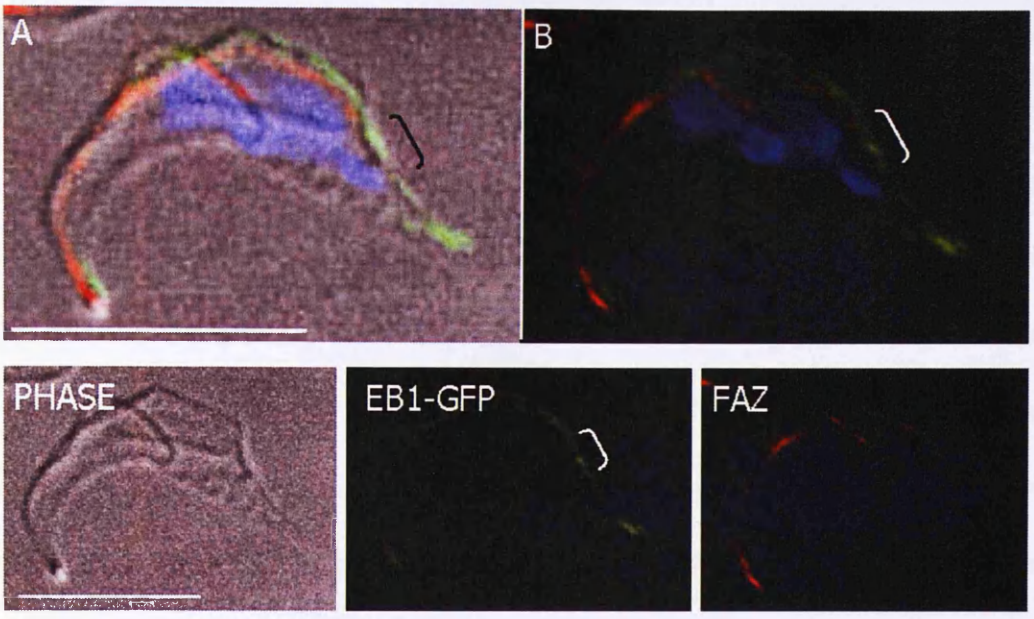

Figure 6.7 Fluorescence/immunofluorescence images showing that GFP-*Tb*EB1 does not co-localise with the FAZ filament

Cells expressing GFP-*Tb*EB1 (green) were settled onto slides and membranes were extracted with NP40 as described in section 2.5.1. In preparation for immunofluorescence analysis these cytoskeletons were labelled with ROD1 to detect the FAZ filament (red) (for dilutions used see section 2.2.3) and stained with DAPI (blue). Images were captured on the Deltavision microscope. The figure shows that the GFP-*Tb*EB1 signal does not co-localise with the FAZ filament, instead it is found in a more posterior position (indicated by bracket) (scale bar = 10 μm).

In summary, the GFP-*Tb*EB1 signal that is observed in a region close to the growing new flagellum, does not co-localise with either the PFR (Figure 6.6) or the FAZ filament (Figure 6.7) therefore the precise structure that GFP-*Tb*EB1 is localising to in this region is unknown. Although the localisation pattern of GFP-*Tb*EB1 has this complexity, it still provides a useful marker for the plus ends of MTs. As such, it was employed to study cytoskeletal remodelling and posterior end formation in the TCP86 and GB4L RNAi cell lines; this is described in the following sections.

6.5 Organisation of microtubule plus ends in the GB4L and TCP86 RNAi cell lines

The GFP-*Tb*EB1 construct was transfected into the pre-existing TCP86 and GB4L RNAi cell lines to investigate whether RNAi mediated ablation of these proteins results in MT organisation defects. In parallel with these experiments, the GB4L and TCP86 RNAi cell lines were also transfected with a construct allowing expression of a YFP epitope-tagged version of XMAP215 (another +TIP binding protein, accession number Tb927.6.3090). This construct was a kind gift from Nicole Scheumann and Keith Gull, University of Oxford. These experiments provided further insight into how MTs are organised to form the posterior end of the trypanosome cell during cytokinesis, and demonstrated that GB4L and TCP86 expression is essential for this process.

6.5.1 Organisation of microtubule plus ends in the GB4L RNAi cell line as visualised by GFP-*Tb*EB1

Figure 6.8 shows representative cells at different cell cycle stages from the GB4L RNAi cell line which is expressing the GFP-*Tb*EB1 fusion protein. In non-induced cells, GFP-*Tb*EB1 localises to the posterior end at all cell cycle stages (Figure 6.8A-F) and the anterior end of the cell body is often labelled with a distinct dot (as described earlier in section 6.2.1; shown in Figure 6.1). However, of particular interest is the localisation of GFP-*Tb*EB1 to the region between divided nuclei; indicated in Figure 6.8D by a green arrow. This localisation corresponds both temporally and spatially to the pattern of staining seen when using the antibody YL1/2 which detects new MT formation, suggesting that MT growth and organisation is taking place in this region (described in section 6.2.1). This increased MT activity may be required in this part of the cell at this time to define a new posterior end for the forming anterior daughter

cell. Figure 6.8E and F show that GFP-*Tb*EB1 localisation is maintained at this position as the cell undergoes cytokinesis.

Figure 6.8G-L show representative cells 12 hours post GB4L RNAi induction. The localisation of GFP-*Tb*EB1 appears normal at the beginning of the cell cycle (examples of 1K1N and 2K1N cells are shown in Figure 6.8G and H respectively). However, later in the cell cycle the GFP-*Tb*EB1 localisation pattern changes, in that GFP-*Tb*EB1 signal is not detected between divided nuclei, but appears positioned much closer to the old posterior end; indicated by green arrows in Figure 6.8I and J. Figure 6.8K shows a cell late in cytokinesis, the cleavage furrow has reached the posterior end, however bisection is aberrant as one cell possesses two nuclei and the other none. Where the cells remain joined two discrete regions of GFP-*Tb*EB1 localisation can be seen in close proximity to one another. Figure 6.8L shows the characteristic 'push-me-pull-you' phenotype observed upon GB4L ablation, this cell is stalled in cytokinesis and cells remain attached by their posterior ends, GFP-*Tb*EB1 can be seen in the region between the two joined cells.

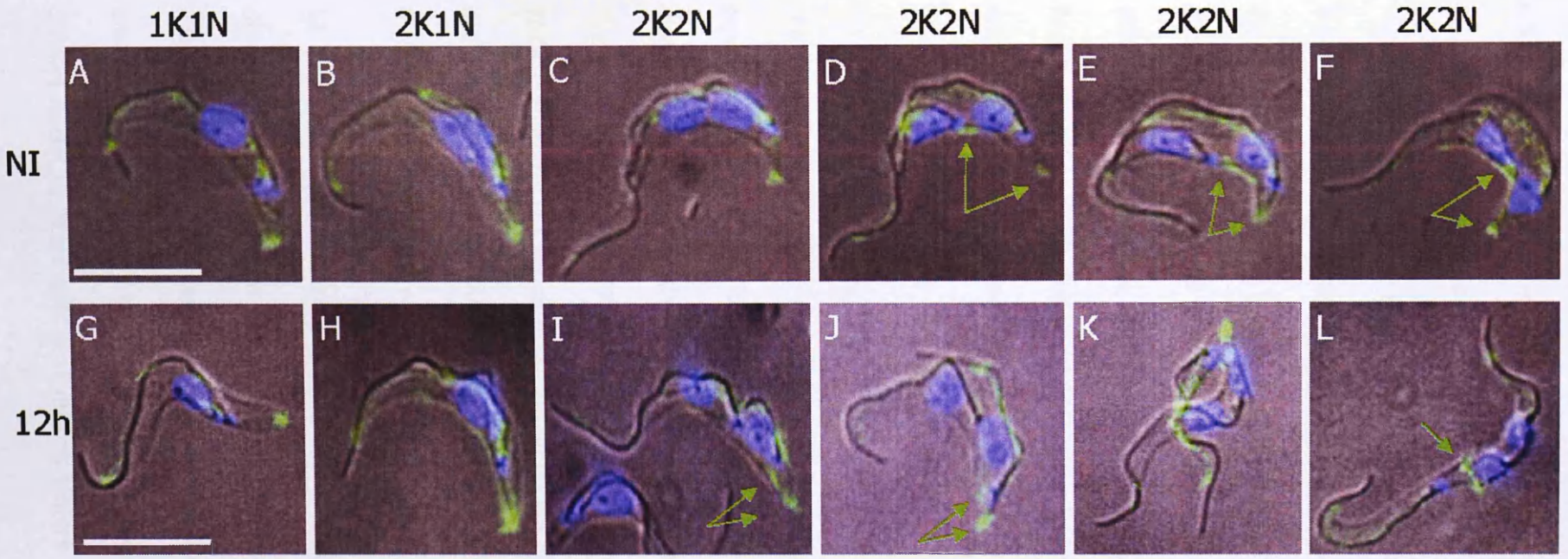

Figure 6.8 Fluorescence images showing the localisation of GFP-*Tb*EB1 in the GB4L RNAi cell line

Cells expressing GFP-*Tb*EB1 (green) from a non-induced (NI) population and 12 hours post induction of GB4L RNAi were settled onto slides and treated with NP40 to isolate cytoskeletons as described in section 2.5.1. Cells were labelled with DAPI (blue) and images were acquired on a Deltavision microscope. Images (A-F) non-induced and (G-L) 12 hours post induction depict representative cells from progressively later cell cycle stages. In non induced (NI) cells green arrows show where GFP-*Tb*EB1 is localising to plus ends of microtubules located at the old and newly forming posterior end of the cell. In GB4L RNAi induced cells this localisation is altered (green arrows) (scale bar = 10μm).

6.6 Organisation of microtubule plus ends in the GB4L RNAi cell line as visualised by YFP-*Tb*XMAP215

Figure 6.9 shows representative cells expressing YFP-*Tb*XMAP215 from a non-induced population and 12 hours post induction of GB4L RNAi. In non-induced cells XMAP215 localises to the plus ends of the subpellicular corset MTs at the posterior end of the cell; analogous to the localisation seen with GFP-*Tb*EB1 (Figure 6.1). YFP-*Tb*XMAP215 also localises to the mitotic spindle (Figure 6.9C) but not the growing flagellum and so differs from GFP-*Tb*EB1 localisation. The protein can be seen in the nucleus of 2K1N cells where a spindle is forming (Figure 6.9B) and on the spindle MTs between dividing nuclei throughout mitosis (Figure 6.9C). During mitosis the posterior YFP-*Tb*XMAP215 signal extends from the posterior pole of the cell towards the anterior of the cell (Figure 6.9C), but stops just anterior to the most posterior positioned nucleus. The line of YFP-*Tb*XMAP215 expression progresses to form a discrete patch between the divided nuclei in 2K2N cells post mitosis (Figure 6.9D). The positioning of this YFP-*Tb*XMAP215 signal is similar to that observed with GFP-*Tb*EB1 and marks the region of the cell which will form a new posterior end when the cell divides. The YFP-*Tb*XMAP215 signal remains in this position as the cell progresses through cytokinesis (Figure 6.9E and F).

12 hours after the induction of GB4L ablation, YFP-*Tb*XMAP215 localisation is still observed at the posterior end of the cell (Figure 6.9G-K) and the mitotic spindle (Figure 6.9I), however it does not track from the posterior end of the cell towards the anterior (Figure 6.9I) and no YFP-*Tb*XMAP215 localisation is observed between the divided nuclei in 2K2N cells post mitosis (Figure 6.9K). However, a patch of YFP-

*Tb*XMAP215 forms much closer to the posterior end of the cell (Figure 6.9J and K); this is consistent with the observations made with GFP-*Tb*EB1 (Figure 6.8I and J arrows). When cytokinesis is stalled, YFP-*Tb*XMAP215 is found in the region between the two joined cells (Figure 6.9L).

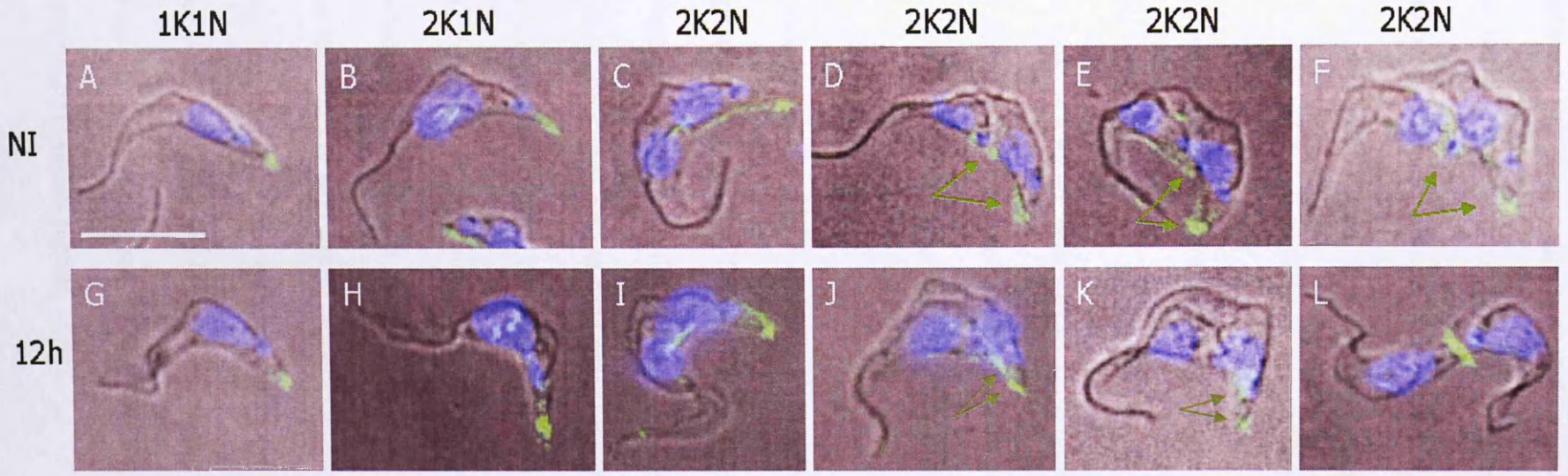

Figure 6.9 Fluorescence images showing the localisation of YFP-XMAP215 in the GB4L RNAi cell line

Cells expressing YFP-XMAP215 (green) from a non-induced (NI) population and 12 hours post induction of GB4L RNAi were settled onto slides and treated with NP40 to give cytoskeletons as described in section 2.5.1. Cells were labelled with DAPI (blue) and images were acquired on a Deltavision microscope. Images (A-F) non-induced and (G-L) 12 hours post induction depict representative cells from progressively later cell cycle stages. In non-induced cells (NI) green arrows show where XMAP215-YFP is localising to plus ends of microtubules located at the old and newly forming posterior end of the cell. In GB4L induced cells the localisation is altered see green arrows in (J and K) (scale bar = 10μm).

In summary this data suggests that *T. brucei* PCF cells organise the growth and formation of MTs to a region between the divided nuclei to define a new posterior end prior to cytokinesis. Upon RNAi mediated ablation of GB4L the organisation of new MTs is disrupted leading to aberrant positioning/formation of the new posterior end; this ultimately manifests itself as a problem in completing cytokinesis.

6.6.1 Microtubule plus ends form a discontinuous ring in the mid-region of 'push-me-pull-you' cells

When GB4L is ablated, cells stall in cytokinesis resulting in the characteristic 'push-me-pull-you' cell phenotype. In these cells both GFP-*Tb*EB1 and YFP-*Tb*XMAP215 localise to the region between adjoining cells in a distinct band (Figure 6.8L and Figure 6.9L respectively). This mid-region corresponds to the position of the original posterior end of the cell and as such is the most dynamic part of the cell in terms of MT growth and formation. GFP-*Tb*EB1 and YFP-*Tb*XMAP215 localisation can be used to investigate the organisation of MTs in this region. Cells from 24 hours post GB4L RNAi induction were settled onto slides and imaged on the Deltavision microscope; images were then rotated to visualise 3D architecture. In many cases rotating the image reveals that the ridge of staining observed in the original image actually represents a discontinuous band around the circumference of the cell. Figure 6.10 shows examples of cells expressing GFP-*Tb*EB1 or YFP-*Tb*XMAP215 which have been rotated in order to visualise the organisation of the MT plus ends. Figure 6.10A-C shows that GFP-*Tb*EB1 localises to a discontinuous ring in the mid-region between the two adjoined cells. Figure 6.10D shows the same result with cells expressing the YFP-*Tb*XMAP215 fusion protein.

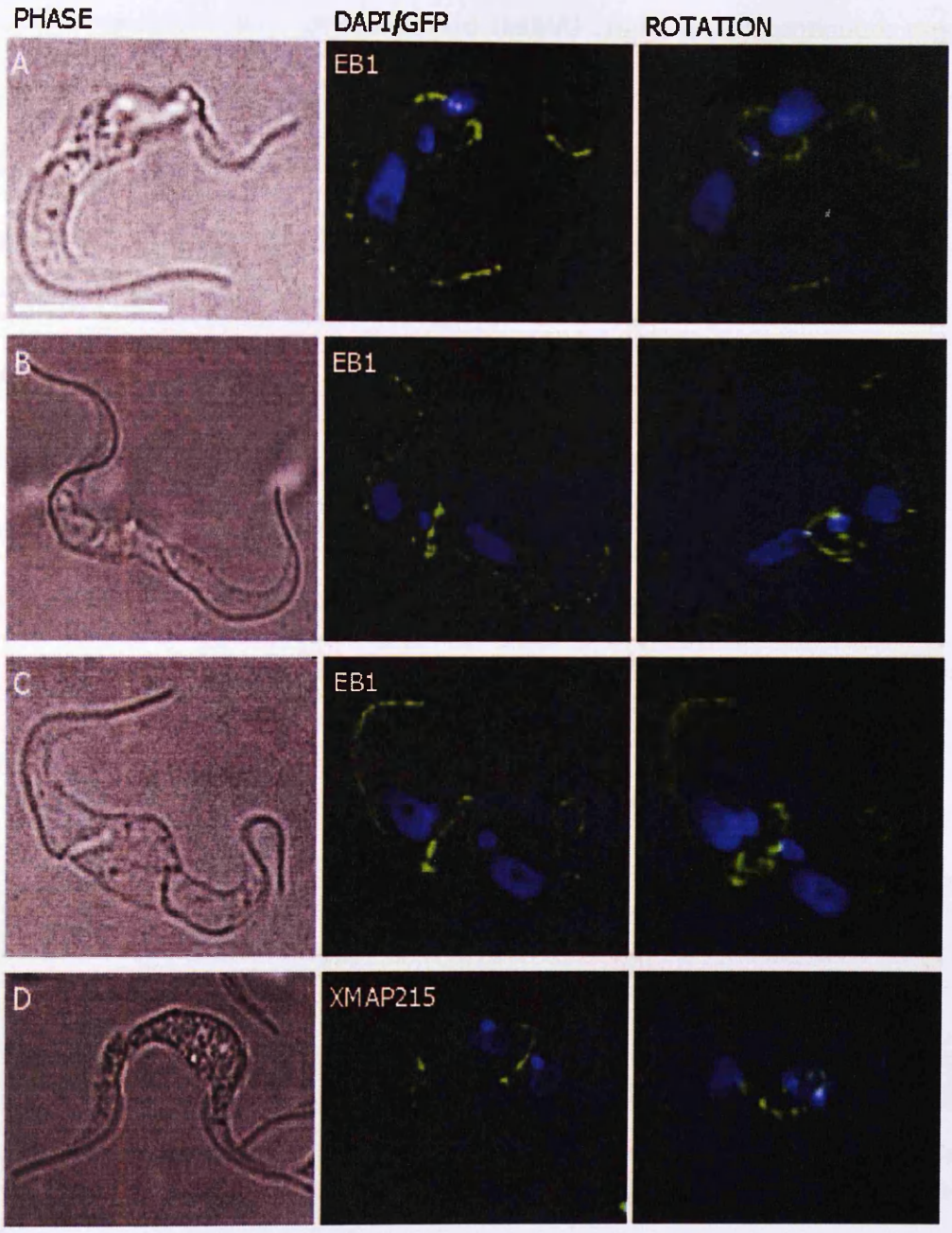

Figure 6.10 Fluorescence images showing 'push-me-pull-you' cells with a ring of GFP-*Tb*EB1 or YFP-*Tb*XMAP215 between divided nuclei

The GB4L RNAi cell lines expressing GFP-*Tb*EB1 or YFP-*Tb*XMAP215 were induced and after 24 hours cells were settled on to slides and treated with NP40 to give cytoskeletons as described in section 2.5.1. Cells were then labelled with DAPI (blue) and images were acquired on a Deltavision microscope. Cells which have failed to complete cytokinesis forming the characteristic 'push-me-pull-you' phenotype were processed using the volume viewer function in SoftWorx Explorer, a 360^0 rotation was carried out and the 3D architecture was revealed (screen shots are shown on the right). GFP-*Tb*EB1 (images A-C) and YFP-*Tb*XMAP215 (image D) localise to a discontinuous ring between adjoined cells.

The observation that MT +TIPs *Tb*EB1 and *Tb*XMAP215 form a discontinuous ring in 'push-me-pull-you' cells was confirmed by labelling cells with the antibody YL1/2. YL1/2 staining shows new MTs formed in this mid region between the adjoined cells forms a defined band around the circumference of the cell (Figure 6.11). The band visualised by YL1/2 staining is broader and more diffuse than that observed for GFP-*Tb*EB1 or YFP-*Tb*XMAP215. This might be explained by the fact that the +TIPS define the very tip of the MT whereas YL1/2 detects tyrosinated α-tubulin which is incorporated into MTs at the plus end. However, the process of detyrosination does not occur immediately, meaning tyrosinated α-tubulin will be detected as a gradient high at the plus end getting less toward the minus end of the MT (YL1/2 is discussed in section 1.7).

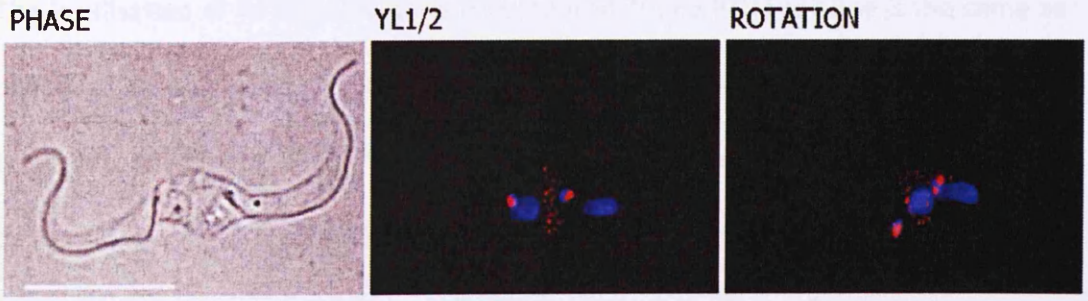

Figure 6.11 Immunofluorescence image showing new microtubules in a band/ring at the mid-region of a 'push-me-pull-you' cell, 24 hours post induction of GB4L RNAi

The GB4L RNAi cell line was induced and after 24 hours cells were settled onto slides and treated with NP40 to give cytoskeletons as described in section 2.5.1. Cells were labelled with the antibody YL1/2 (red) (as described in section 2.2.3) and stained with DAPI (blue). Immunofluorescence analysis was carried out on the Deltavision microscope. YL1/2 staining is seen between the two nuclei, the image was rotated (using the volume viewer function in SoftWorx Explorer) and a band/ring of new microtubules was revealed.

6.7 Organisation of microtubule plus ends in the TCP86 cell line

Measurements of organelle positioning in TCP86 ablated cells were taken by Shawcross (2008), these measurements showed that cells early in the division cycle possess an elongated posterior end. This extension can be labelled with YL1/2 indicating that this abnormal morphology is due to aberrant new MT growth (Shawcross, 2008). These observations led to the hypothesis that TCP86 may play a role in regulating new MT growth during the cell cycle. To investigate this in more detail constructs for expression of GFP-*Tb*EB1 and YFP-*Tb*XMAP215 were transfected into the TCP86 RNAi cell line to investigate MT growth and organisation following TCP86 depletion.

6.7.1 GFP-*Tb*EB1 localisation in the TCP86 RNAi cell line

The localisation of GFP-*Tb*EB1 in the non-induced TCP86 RNAi cell line is the same as described for wild type (Figure 6.1) and GB4L non-induced cells (Figure 6.8A-F). 12 hours after induction of TCP86 RNAi, plus ends of subpellicular corset MTs at the posterior end are strongly GFP-*Tb*EB1 positive, however the organisation of MTs to form the new posterior end is apparently disrupted as no GFP-*Tb*EB1 signal is detected between divided nuclei. This is particularly evident when comparing E and F, which show 2K2N cells from a non-induced population, with J and K which show 2K2N cells 12 hours post induction. L shows a cell undergoing cytokinesis, in this cell the cleavage furrow is mispositioned and the result of this division will most likely be an anucleate zoid and a 1K2N multinucleate. This is the characteristic defect observed when TCP86 expression is reduced (Shawcross, 2008) and possibly results from an inability to organise MTs correctly into two discrete posterior ends prior to division.

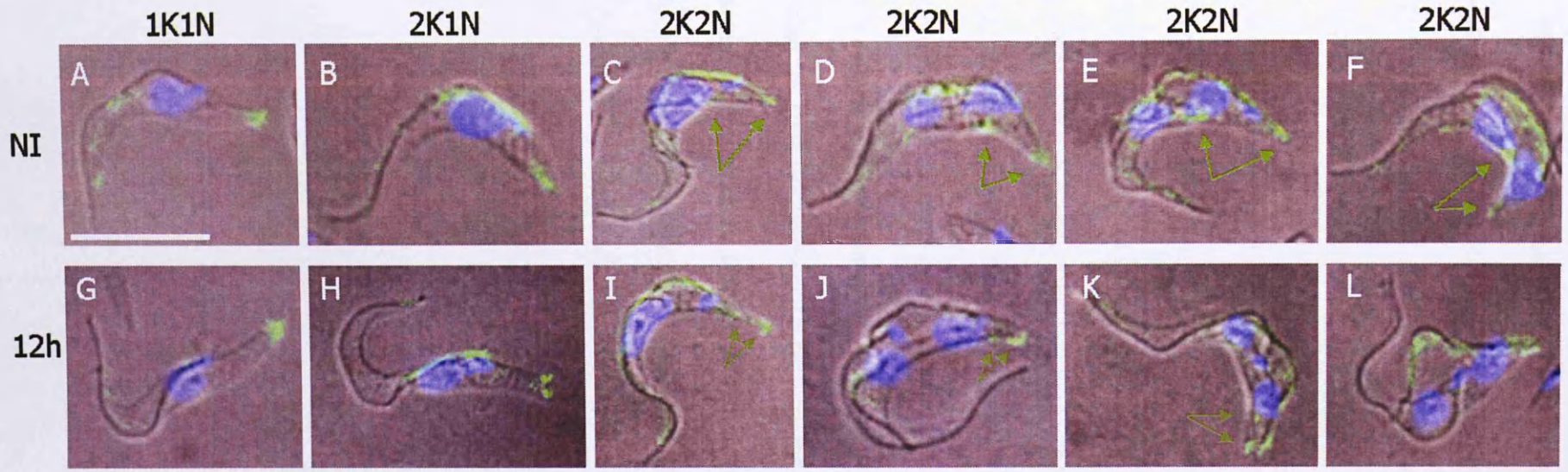

Figure 6.12 Fluorescence images showing the localisation of GFP-*Tb*EB1 in the TCP86 RNAi cell line

Cells expressing GFP-*Tb*EB1 (green) from a non-induced (NI) population and 12 hours post induction of TCP86 RNAi were settled onto slides and treated with NP40 to give cytoskeletons as described in section 2.5.1. Cells were labelled with DAPI (blue) and then images were acquired using a Deltavision microscope. Images (A-F) non-induced and (G-L) 12 hours post induction depict representative cells from progressively later cell cycle stages. In non-induced cells green arrows show where GFP-*Tb*EB1 is localising to plus ends of microtubules located at the old and newly forming posterior end of the cell. In the induced cells the localisation is altered (green arrows) (scale bar = 10μm).

6.7.2 YFP-*Tb*XMAP215 localisation in the TCP86 RNAi cell line

The localisation of YFP-*Tb*XMAP215 in the non-induced TCP86 RNAi cell line (Figure 6.13A-E) is the same as described for both the wild type (Figure 6.1) and GB4L non-induced cells (Figure 6.8A-F).

12 hours after induction of TCP86 ablation, YFP-*Tb*XMAP215 localises to the posterior pole of the cell throughout the cell cycle (Figure 6.13F-J). However, YFP-*Tb*XMAP215 does not appear to track from the posterior pole towards the anterior end of the cell during mitosis; this is particularly clear when comparing Figure 6.13C (non-induced) with Figure 6.13I (induced). No signal is seen in the region between the separated nuclei in post mitotic cells (Figure 6.13I and J). As with the observations made in the previous experiments, this suggests that plus ends of MTs are not being organised in this region. As such the cytoskeletal remodelling which may be required to define a new posterior end prior to cytokinesis is not occurring. Figure 6.13J shows a cell undergoing aberrant cytokinesis, with a mispositioned cleavage furrow, the progeny of such defective cell division will most likely be a zoid and a 1K2N multinucleate.

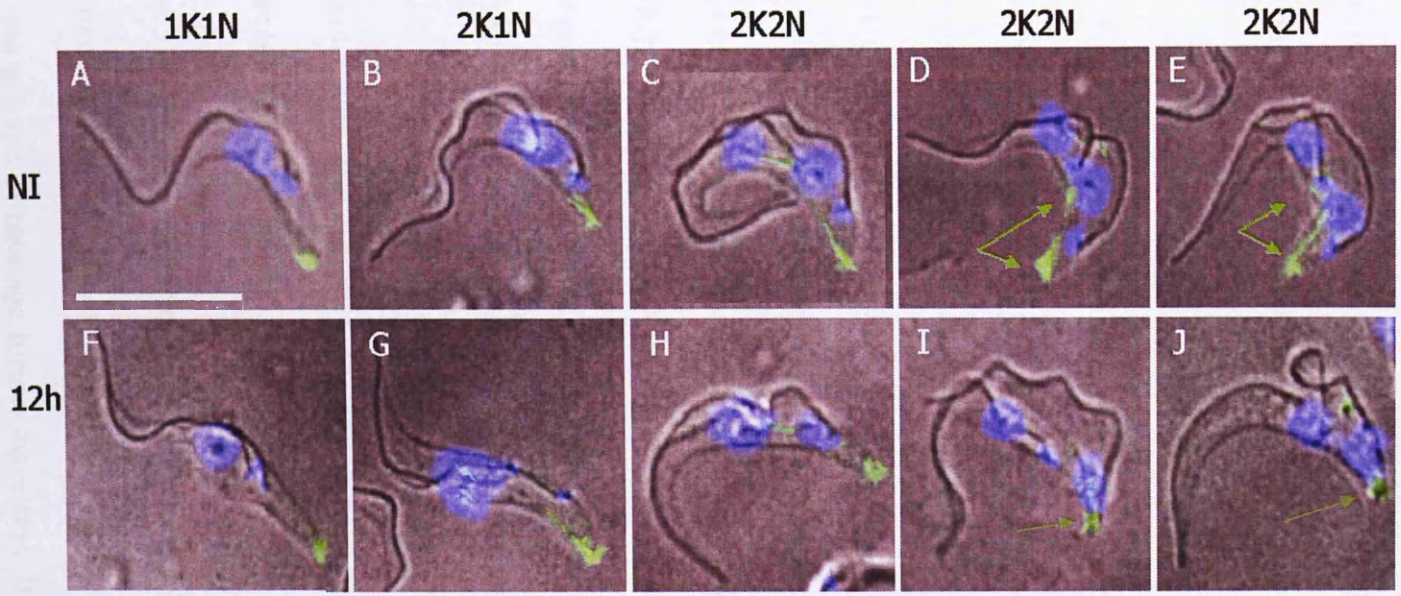

Figure 6.13 Fluorescence images showing the localisation of YFP-*Tb*XMAP215 in the TCP86 RNAi cell line

Cells expressing YFP-*Tb*XMAP215 (green) from a non-induced (NI) population and 12 hours post induction of TCP86 RNAi were settled onto slides and treated with NP40 to give cytoskeletons as described in section 2.5.1. Cells were labelled with DAPI (blue) and then images were acquired on a Deltavision microscope. Images (A-F) non-induced and (G-L) 12 hours post induction depict representative cells from progressively later cell cycle stages. In non induced (NI) cells green arrows show where YFP-*Tb*XMAP215 is localising to plus ends of microtubules located at the old and newly forming posterior end of the cell. In the TCP86 RNAi induced cells this pattern of localisation has altered (green arrows) (scale bar = 10μm).

6.8 Summary

In this chapter I show that GFP-*Tb*EB1 localises to the posterior end of the cell in PCF trypanosomes as well as associating with the anterior tip of the cell body (Figure 6.1). RNAi ablation of *Tb*EB1 suggests that expression of *Tb*EB1 is not essential as there was no observable growth or morphological phenotype upon its depletion (Figure 6.5).

GFP-*Tb*EB1 and YFP-*Tb*XMAP215 were expressed in GB4L and TCP86 RNAi cell lines to investigate the behaviour of MT plus ends. Intriguingly, in non-induced cells, MT plus ends appear to be organised into a discrete region between the two divided nuclei before cytokinesis initiates (Figure 6.8D-F, Figure 6.9D-F, Figure 6.12D-F and Figure 6.13D and E). This region is where a new posterior end will form for the anterior daughter cell (the cell which inherits the old flagellum). In GB4L and TCP86 depleted cells GFP-*Tb*EB1 and YFP-*Tb*XMAP215 localisation is absent from this region (Figure 6.8I-K, Figure 6.9J and K, Figure 6.12I-K, Figure 6.13I and J) and these cells fail to define and form a 'normal' posterior end. This suggests that the +TIP localisation visualised in these experiments represents a critical remodelling event in which subpellicular MTs are organised to form a new posterior end for the anterior daughter cell before cytokinesis.

How the trypanosome orchestrates cytoskeletal remodelling during cytokinesis is poorly understood and little is known about the molecular mechanisms which control the process of cleavage furrow ingression. Data presented in this chapter identifies that TCP86 and GB4L are involved in the process of cytoskeletal remodelling, and that this remodelling occurs before initiation of cytokinesis.

Furthermore when cytoskeletal remodelling is disrupted, severe problems are encountered during cytokinesis (Figure 6.8K and L, Figure 6.9L, L and Figure 6.13J). In the case of GB4L RNAi, cleavage furrow ingression stalls and cells remain attached. Interestingly, in these cells the plus ends of MTs are seen in a discontinuous ring around the circumference of the cell (Figure 6.10).

Chapter 7 Discussion

The work presented in this thesis provides important new insights into cytokinetic events in *T. brucei* and identifies a novel trypanosomatid specific protein required for successful cytoskeletal remodelling.

The trypanosome subpellicular corset is expanded throughout the cell cycle to allow for cellular growth and to accommodate replicating organelles. During cytokinesis the subpellicular corset remains in place but must be re-organised so that both daughter cells inherit a complete microtubule array. For this process to occur successfully, new MTs must be formed and incorporated into the existing corset in an organised manner. Cytoskeletal remodelling can be viewed in three distinct stages:

(1) Early in the cell cycle there is polar extension of microtubules at the posterior end of the cell. When cells are arrested in G_1 they develop an extended posterior end, this 'nozzle' phenotype is positive for tyrosinated α-tubulin and therefore newly formed MTs (as observed using the YL1/2 antibody) (Hendriks *et al*, 2001; Li & Wang, 2003; Tu & Wang, 2005).

(2) In mitotic/post mitotic cells new microtubules are interdigitated in between old ones allowing the corset to expand in diameter (Sherwin & Gull, 1989b).

(3) During cleavage furrow progression as the furrow bisects the cell, new microtubules must be inserted into the array in order for each daughter cell to inherit a complete corset of microtubules (Shawcross, 2008).

Although the precise functions of most trypanosome MAPs have yet to be defined, they are likely to play essential roles in one or more of these cytoskeletal remodelling events. In the few cases where *T. brucei* MAPs have been investigated by RNAi, protein depletion has resulted in morphology defects, organelle mispositioning and cytokinesis defects.

7.1 The GB4 motif

Prior to the work carried out in this thesis the MAPs designated GB4 and TCP86 were shown to interact with the subpellicular microtubules and share a short region of amino acid sequence homology (Rindisbacher *et al*, 1993; Shawcross, 2008). The working hypothesis developed in this thesis was that this amino acid sequence may regulate MAP-microtubule interactions. To investigate whether this motif was present in other trypanosome proteins, or indeed represented a more widely eukaryotic conserved motif, a Hidden Markov Model was developed to analyse the occurrence of this motif in 32 eukaryotic genomes. This bioinformatic analysis revealed that the GB4 motif was found in other trypanosomatid proteins but that its occurrence was restricted to trypanosomatid species; including 17 *T. brucei* proteins (section 3.3, Table 3.1).

The functionality of the GB4 motif containing proteins was explored using an RNAi screen in *T. brucei* PCF cells. Disappointingly, no discernable phenotype was detected

for the majority of the proteins investigated. However, one of the proteins that emerged from this screen (a previously uncharacterised protein which contains 17 repeats of the GB4 motif (Table 3.1) and so designated GB4L) had a striking RNAi depletion phenotype (section 3.6 and Figure 4.2, Figure 4.3 and Figure 4.4) implicating it in a critical role in cytoskeletal remodelling.

Before considering the potential role of GB4L in more detail it is worth deliberating on the lack of any discernable phenotype observed following the RNAi mediated ablation of the other proteins identified by the HMM based screen. Firstly, it should be noted that in all instances the efficacy of RNAi was not verified by monitoring either mRNA abundance or determining protein expression levels. This is of course a major caveat to the study and so before dismissing these proteins as unimportant in cell division, the efficacy of RNAi should be validated by quantitative PCR. Alternatively, specific antibodies should be raised, or proteins epitope tagged, so that protein depletion could be visualised through fluorescence and/or immunoblotting studies.

Secondly, it is evident from the literature that MAPs can be regulated by differential life cycle stage expression; as demonstrated by CAP5.5/CAP5.5*V* (Olego-Fernandez *et al*, 2009) and CAP15/CAP17 (Vedrenne *et al*, 2002). Work in this thesis has focused mainly on the role of GB4 motif containing proteins in the PCF. Function of these proteins should also be examined in the BSF; particularly as there is proteomic data to suggest that 13 out of the 17 *T. brucei* GB4 motif containing proteins are expressed in this life cycle stage (see supplementary Table 8.1).

7.2 RNAi ablation of GB4L causes cleavage furrow ingression to stall

RNAi depletion of GB4L causes a severe growth defect and, 12 hours after induction of GB4L RNAi, many cells accumulate with a 2K2N configuration (see Chapter 3) indicative of a cytokinetic failure. The number of 2K2N cells with a visible cleavage furrow was observed to increase over time because cleavage furrow progression stalls at the midpoint region of the cell (section 3.6.4, Figure 3.10). This phenotype is not unprecedented, RNAi depletion of a number of proteins in *T. brucei* including MOB1, PK53, *Tb*RACK, *Tb*DLP and SPT2, have been shown to cause a defect in cleavage furrow ingression similar to that observed in the GB4L RNAi cell line (Hammarton *et al*, 2005; Chanez *et al*, 2006; Rothberg *et al*, 2006; Fridberg *et al*, 2008; Ma *et al*, 2010). Why depletion of these proteins, with diverse cellular functions, yield a common phenotype is yet to be established. In the case of the dynamin TbDLP, RNAi depletion is suggested to activate a novel cell cycle checkpoint which monitors mitochondrial fission. Activation of this checkpoint leads to a stall in cytokinesis and a complete block in cell cycle progression. However, whilst MOB1, PK53, *Tb*RACK, and SPT2 exhibit a stalled cleavage furrow, cells re-enter the cell cycle and form multinucleates, as is the case for GB4L. In light of this, and the fact that a cytokinesis checkpoint remains poorly defined, other possible explanations for this phenotype are more plausible, several possibilities are described below.

Firstly, supernumerary MTs which accumulate in the cytoplasm (observed 24 hours after induction of GB4L RNAi; see TEM data in section Figure 4.11 and Figure 4.12) could constitute a physical blockage which prevents furrow ingression. However, cells stalled in cytokinesis with a visible cleavage furrow are present 12 hours post induction (See Figure 3.10) but excessive supernumerary MTs are only observed at

the later time points i.e. 24 and 48 hours (Figure 4.8-Figure 4.12). Whilst this will certainly cause problems for completion of cytokinesis at later time points, the initial reason for an accumulation of 2K2N cells is not as easily explained.

Secondly, the FAZ is thought to guide cleavage furrow ingression from the anterior end of the cell (Kohl *et al*, 2003) and disruptions to FAZ formation lead to defects in cytokinesis (Vaughan *et al*, 2008). TEM analysis following RNAi ablation of GB4L shows defects in FAZ formation (Figure 4.7-Figure 4.12). However, the structure of the FAZ is affected along the length of the cell including at the anterior where furrow ingression proceeds normally. Thus, these FAZ defects cannot fully explain the stalling of the cleavage furrow when GB4L is depleted.

Thirdly, an alternative explanation for the stalling of furrow ingression in the GB4L depleted cells may be that furrow ingression is biphasic, and may have different protein requirements at different stages of progression. Perhaps ingression proceeds initially at the anterior end by a GB4L independent mechanism, then a GB4L dependent mechanism is required for furrow ingression beyond the midpoint of the cell. The same scenario has been suggested for the receptor for activated C kinase 1 (TRACK1) which is not required to initiate cytokinesis but is believed to regulate cytokinesis from the midpoint to completion (Rothberg *et al*, 2006). Furthermore, the FAZ which is critical for the process of cytokinesis and is implicated in defining the path of the furrow (Robinson *et al*, 1995; Davidge *et al*, 2006) is not found in the cell posterior to the flagella pocket. The mechanism by which furrow ingression is directed from this point to completion is unknown. This suggests that the process of

cytokinesis may require different proteins at later stages of cleavage furrow ingression.

Fourthly, perhaps the most likely explanation for the 'push-me-pull-you' phenotype in GB4L depleted cells can be derived from a comparison with coronin (CRN12) depleted cells in *Leishmania donovani* (Sahasrabuddhe *et al*, 2009). In these cells, bipolar cells form which is reminiscent of the GB4L 'push-me-pull-you' phenotype. These bipolar cells are fused at their posterior ends but have successfully completed kinetoplast and nuclear division and have an active flagellum at either pole. This phenotype forms as a result of invasion of persistently growing corset microtubules into the other daughter cell corset. The number of MTs in the corset of the bipolar cells increases significantly, but despite this and the anti-parallel arrangement of these MTs the spacing of MTs in the corset remains similar to wild type. The authors suggest that CRN12 is part of a novel mechanism for capping and controlling MT growth at the posterior end of the cell, and that this mechanism is important since the *Leishmania* genome does not encode the MT +TIP EB1 (Sahasrabuddhe *et al*, 2009).

GB4L may play a similar role in capping MTs at the posterior end of cells; this hypothesis is not just based on the similarities with the CRN12 depleted cells in *L. donovani*. GB4L shares homology with the MT capping protein GB4 which has been localised specifically to the posterior end of the cell (Rindisbacher *et al*, 1993). Furthermore, work carried out in the course of this thesis showed that although *Tb*EB1 localises to MT +TIPs, RNAi ablation of *Tb*EB1 in the PCF did not cause any observable phenotype. This is a surprising observation given the important role this

protein plays in other systems and suggests alternative mechanisms may also exist in *T. brucei*. Whilst it is possible that deregulated growth of MTs similar to that observed in CRN12 depleted cells in *L. donovani* may be occurring upon GB4L depletion in *T. brucei*. It is worth bearing in mind that +TIP localisation (Figure 6.10) and YL1/2 staining (Figure 6.11) in the GB4L 'push-me-pull-you' cells clearly defines a ring in the mid region of the cell, this would not be expected if MT plus ends were extending into the opposite daughter cells subpellicular array. Immunofluorescence analysis using YL1/2 on the bipolar cells in the CRN12 cell line showed a punctate distribution of tyrosinated α-tubulin which showed positive ends of microtubules were located throughout the bipolar cell (Sahasrabuddhe *et al*, 2009).

Localisation data for GB4L is essential to provide insights and further understanding of the RNAi depletion phenotype. In addition, electron microscopy on whole mount cytoskeletons could be employed to study the organisation of microtubules in the subpellicular array in the 'push-me-pull-you' cells.

7.3 Zoid formation in the TCP86 RNAi cell line is a result of a mispositioned cleavage furrow

A mispositioning of cleavage furrow ingression is responsible for asymmetrical division leading to zoid formation in the TCP86 RNAi cell line. After observing that the nucleus in TCP86 depleted cells sits in the path of the cleavage furrow, Shawcross (2008) postulated that TCP86 may form part of a complex of MAPs which link the corset and the nucleus, effectively tethering the nucleus in place post anaphase preventing it from drifting into the plane of cleavage (Shawcross, 2008). This theory suggests that in the absence of TCP86 the nucleus becomes mis-positioned into the

path of the cleavage furrow which must then deviate and upon abscission a zoid and a 1K2N cell results (Shawcross, 2008). An independent study raised an RNAi cell line to target depletion of TCP86 (known to this group as NOP86) and produced the same phenotype. In this case they proposed that zoid production was a result of a defect in mitosis (Boucher *et al*, 2007). However, no evidence for a mitotic defect was presented; in fact cells were shown to progress through mitosis to produce multinucleated cells.

TEM analysis undertaken for this thesis shows no obvious ultrastructural defects to explain the zoid production in the TCP86 RNAi cell line (Figure 4.17). However, immunofluorescence analysis using the NUP-1 antibody (Ogbadoyi *et al*, 2000) may provide an alternative to the nuclear tethering theory proposed by Shawcross (2008). NUP-1 staining shows that the nuclear membrane between daughter nuclei is still attached in some 1K2N cells which have undergone cytokinesis. If the membrane system which exists between daughter nuclei during mitosis persists as the cell undergoes cytokinesis it could cause a blockage leading to the mis-routing of the cleavage furrow and therefore zoid production. Alternatively, maintenance of a connection between nuclei could cause the nucleus to be mis-positioned in the path of the cleavage furrow as observed by Shawcross (2008).

7.4 MAP functional interdependency

An important consideration to make when interpreting phenotypes is the fact that targeted ablation of one protein often has effects on others. This is especially important when considering MAPs which may work in complexes and have concerted roles. Previous work has shown that TCP86 expression is essential for the

localisation of the calpain-like cysteine protease CAP5.5 but not WCB (Shawcross, 2008). Work presented in this thesis expands our understanding of these interdependencies showing that CAP5.5 localisation also requires WCB (Figure 5.16). Conversely, when CAP5.5 is reduced by RNAi ablation, TCP86 and WCB localisation to the subpellicular corset is not affected (Figure 5.12 and Figure 5.15). WCB localisation is independent of TCP86 and vice-versa (Figure 5.13). This suggests that if these proteins act in a complex then WCB and TCP86 must associate independently of one another but before CAP5.5, they may then act to recruit CAP5.5 to the complex.

An intriguing finding presented in this thesis is that RNAi mediated ablation of GB4L leads to a loss of CAP5.5 expression (Figure 5.21). This may reflect rapid degradation of mislocalised CAP5.5 which is no longer targeted to microtubules in the absence of GB4L. Alternatively if CAP5.5 is unable to localise to microtubules in the absence of GB4L then there would be an increase in the cytoplasmic pool of CAP5.5, this may trigger an autoregulatory feedback mechanism which reduces the stability of CAP5.5 mRNA, preventing the translation of the protein. This type of autoregulatory control is not unprecedented; in mammalian cells an increase in cytoplasmic tubulin subunits through treatment with the anti-microtubule drugs colchicines or nocodazole results in repression of new tubulin synthesis. This is also observed when the intracellular tubulin content is increase by micro injection of tubulin subunits (Cleveland *et al*, 1983). The down regulation of tubulin synthesis is accompanied by a rapid loss of tubulin mRNAs (Cleveland *et al*, 1981).

Further work is required to discern if either the rapid protein degradation and/or mRNA degradation model are the cause of the reduction of CAP5.5 expression. The

abundance of CAP5.5 mRNA could be measured using QRT-PCR before and after induction of GB4L RNAi to determine the stability of CAP5.5 mRNA.

Are the phenotypes observed in GB4L, TCP86 and WCB RNAi cell lines simply a result of CAP5.5 mislocalisation? Table 7.1 compares the RNAi phenotypes for GB4L, TCP86, WCB and CAP5.5 RNAi cell lines. Ascertaining the commonalities and distinctions between each cell line shows that each cell line has some distinct phenotypes. This suggests that the effects of RNAi ablation relate to protein specific functions rather than simply reflecting the effects of CAP5.5 mislocalisation. Table 7.1 shows depletion of CAP5.5 and GB4L but not WCB or TCP86 leads to accumulation of supernumerary microtubules; it is worth noting that this is far more severe in the GB4L cell line. The spacing of microtubules in the array is disrupted when WCB is depleted but this is not obviously affected when CAP5.5, GB4L or TCP86 are ablated. Only WCB depletion affects the association of MT with the plasma membrane and this is the only cell line in which MTs are observed to splay apart when cells are detergent extracted to give cytoskeletons (section 5.3.4 and Figure 5.6 and (Baines & Gull, 2008). This suggests that WCB functions in establishing inter-MT cross bridges and MT-plasma membrane interactions and that these functions can occur in the absence of CAP5.5, TCP86 and GB4L. Only GB4L affects FAZ formation but both CAP5.5 and WCB ablation have effects on flagella pocket biogenesis.

In terms of similarities, all the MAP RNAi cell lines produce zoids due to an aberrant cytokinesis event however distinctions can be made between the timing of zoid production. In WCB and TCP86 zoids occur early in the induction time course and rapidly accumulate, whereas for GB4L and CAP5.5 zoid production is a later

phenotype. Another commonality is a disruption to posterior end formation suggesting that new microtubule growth in all these cell lines is disorganised.

Table 7.1 Comparison of MAP RNAi depletion phenotypes

A table summarising the phenotypes resulting from RNAi ablation of specific MAPs drawn from data presented in this thesis and in the published literature

	WCB (Baines & Gull, 2008) and this thesis (section 5.3)	**CAP5.5** (Olego-Fernandez *et al*, 2009) and this thesis (section 5.3)	**TCP86** (Shawcross, 2008) and this thesis (section 4.6)	**GB4L** (This thesis)
Zoid production	**Yes** (Figure 5.7 and Figure 5.9)	**Yes** (Figure 5.8 and Figure 5.10)	**Yes**	**Yes** (Figure 3.8 and Figure 3.9)
Abnormal posterior end formation	**Yes** (Figure 5.3)	**Yes** (Figure 5.4)	**Yes**	**Yes** (Figure 4.2 and Figure 4.3)
Supernumerary MTs	**No**	**Yes**	**No**	**Yes** (Figure 4.7 to Figure 4.12)
Abnormal MT spacing in array	**Yes**	**Yes**	**No**	**No**
Disruption of PM-MT association	**Yes**	**No**	**No**	**No**
FAZ disruption	**No**	**No**	**No**	**Yes** (Figure 4.7 and Figure 4.12)
MT splaying upon detergent extraction	**Yes** (Figure 5.6)	**No**	**No**	**No**
Abnormalities in flagellar pocket biogenesis	**Yes**	**Yes**	**No**	**No**

7.5 Formation of the new posterior end before cytokinesis

Although abnormalities in posterior end formation are a common feature of MAP depletion, in most cases the defect observed is very distinct. For example, when WCB is ablated cells appear swollen and rounded at the posterior end (Figure 5.3 and (Baines & Gull, 2008), in contrast when TCP86 is ablated the posterior end of cells is elongated (Shawcross, 2008). For CAP5.5 and GB4L, posterior end abnormalities are less easy to characterise as many different defects are observed, but in the GB4L cell line many cells remain attached by their posterior ends.

It is no surprise that initial effects of MAP ablation are seen at the posterior end of the cell, this is where most MT plus ends are located and as such is the most dynamic region of the cell in terms of MT growth (Sherwin & Gull, 1989a). To investigate posterior end morphogenesis and explore how this may be affected in GB4L and TCP86 depleted cells, the localisation of +TIPs *Tb*EB1 and *Tb*XMAP215 was visualised in cells at all stages of the cell cycle in non-induced cells and 12 hour post induction of RNAi.

Data presented in this thesis shows that MT plus ends are organised in a cell cycle dependent pattern and that the new posterior end begins to form in late mitotic cells before the onset of cytokinesis. The model in Figure 7.1 shows how MTs in the subpellicular corset are remodelled in preparation for cell division.

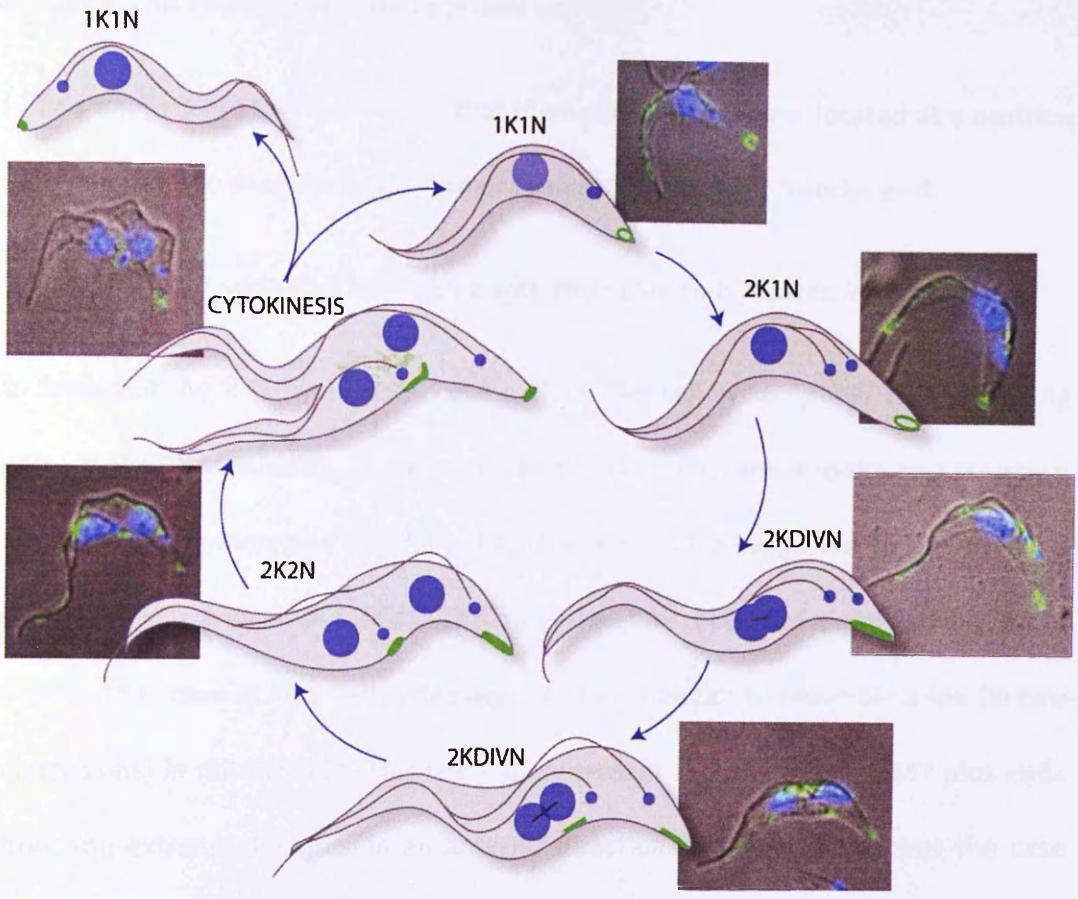

Figure 7.1 Model for microtubule +TIP binding protein localisation at the posterior end of the cell throughout the PCF *T. brucei* cell cycle

The EB1 and XMAP215 epitope tagged fusion proteins were expressed in the GB4L and TCP86 RNAi cell lines. The posterior end labelling with GFP-*Tb*EB1 and YFP-*Tb*XMAP215 was identical in both cell lines when non-induced. The cartoon shows the pattern of posterior end labelling in green and the number of nuclei/kinetoplasts are shown. Inset are images of the GB4L non-induced cells labelled with GFP-*Tb*EB1 (green) to provide examples of the pattern depicted by the cartoon. This data is described in more detail in section 6.5.1 and shown in Figure 6.8.

Figure 7.1 shows a cartoon representing immunofluorescence images (shown inset) of the GFP-*Tb*EB1 fusion protein. The pattern of fluorescence at the posterior end is the same as that observed with the YFP-*Tb*XMAP215 fusion protein (see section 6.6, Figure 6.9 and Figure 6.13). In mitotic cells the appearance of a second, strong +TIP

localisation signal between dividing nuclei suggests that MT plus ends accumulate in this area. This could occur in two possible ways;

(i) Existing MTs are re-organised so that their plus ends are now located at a position between the two daughter nuclei rather than at the existing posterior end.

(ii) New MTs are nucleated in this area with their plus ends located in this region.

In favour of the first hypothesis, cells early in the cell cycle appear to have a ring pattern of +TIP localisation at the extreme posterior end, similar to the ring structure visualised by immunogold labelling of GB4 which is also suggested to cap MT plus ends (Rindisbacher *et al*, 1993). This ring structure becomes progressively more difficult to resolve at later cell cycle stages, before it begins to resemble a line (in two dimensions) in mitotic cells. This line may represent the migration of MT plus ends from the extreme posterior in an anterior direction. However if this was the case then this subset of mature MTs should be visible in TEM sections through the mid region of the cell, there is no evidence for migration of mature MTs from TEM analysis or EM analysis of whole mount cytoskeletons.

In support of the second hypothesis, very short newly formed MTs have been visualised by electron microscopy in MT sheets taken from the central portion of cytoskeletons. Intriguingly these short MTs are not visualised in cells before mitosis (Sherwin & Gull, 1989a), this correlates with the +TIP localisation signal in the mid portion of the cell, suggesting that the signal may occur upon nucleation of these short new MTs.

It is possible that MT remodelling at the old and new posterior end might rely upon both the processes described above, to understand this corset remodelling in more detail whole mount cytoskeletons could be examined using electron microscopy in combination with immunogold labelling of +TIPs.

RNAi ablation of TCP86 and GB4L changes the +TIP localisation pattern and indicates that new posterior end formation is disrupted in these cell lines, undoubtedly contributing to the cytokinetic defects and abnormal morphologies observed in these cell lines. Figure 7.2 is a model describing the pattern of localisation of both GFP-*Tb*EB1 and YFP-*Tb*XMAP215 in the GB4L cell line 12 hours post induction and Figure 7.3 is a model describing the localisation of GFP-*Tb*EB1 and YFP-*Tb*XMAP215 in the TCP86 RNAi cell line 12 hours post induction. The eventual outcome from disrupting MT organisation is different for each cell line. GB4L RNAi induced cells stall in cytokinesis and form the 'push-me-pull-you' phenotype (Figure 4.2 and Figure 4.3) whereas the TCP86 RNAi induced cells complete cytokinesis albeit aberrantly to produce a 1K2N multinucleate and a zoid (Figure 4.13 and Figure 4.14).

Despite the apparent complexities in MAP-MAP interactions (discussed in section 7.4), interrogating microtubule organisation through +TIP localisation provides clear insight into the defects in MT remodelling upon GB4L and TCP86 RNAi ablation. The challenge remains to define the specific functions of individual MAPs within an interactome of MAP interdependency relationships.

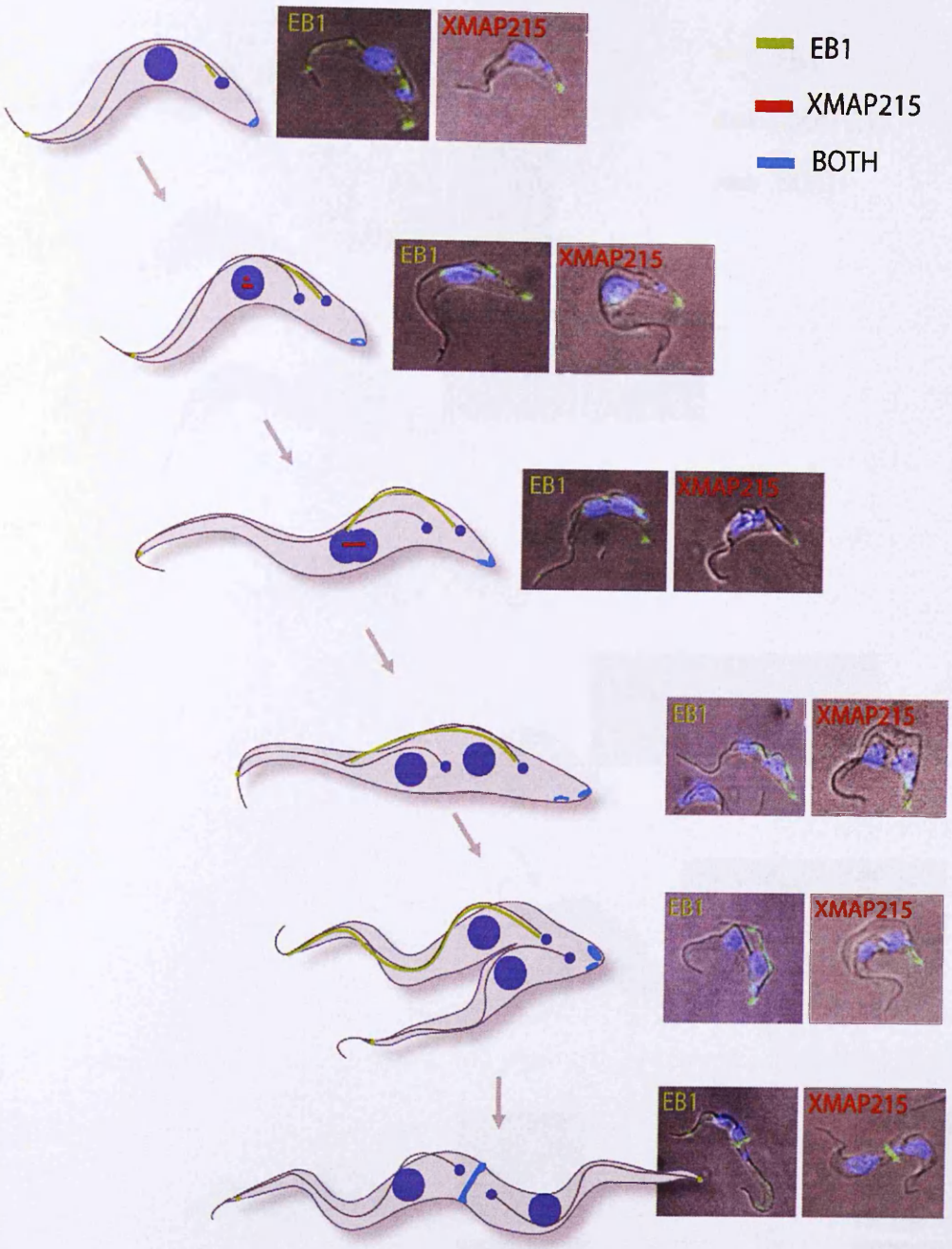

Figure 7.2 Cartoon showing the localisation of GFP-*Tb*EB1 and YFP-*Tb*XMAP215 in the GB4L RNAi cell line 12 hours post induction

A model depicting the GFP-*Tb*EB1 and YFP-*Tb*XMAP215 fluorescence pattern at different cell cycle stages 12 hours after the induction of RNAi mediated GB4L ablation. The areas where both proteins localise are shown in blue, GFP-*Tb*EB1 specific labelling is indicated in green, and YFP-*Tb*XMAP215 in red. Representative images of trypanosome cells at each cell cycle stage are shown (inset).

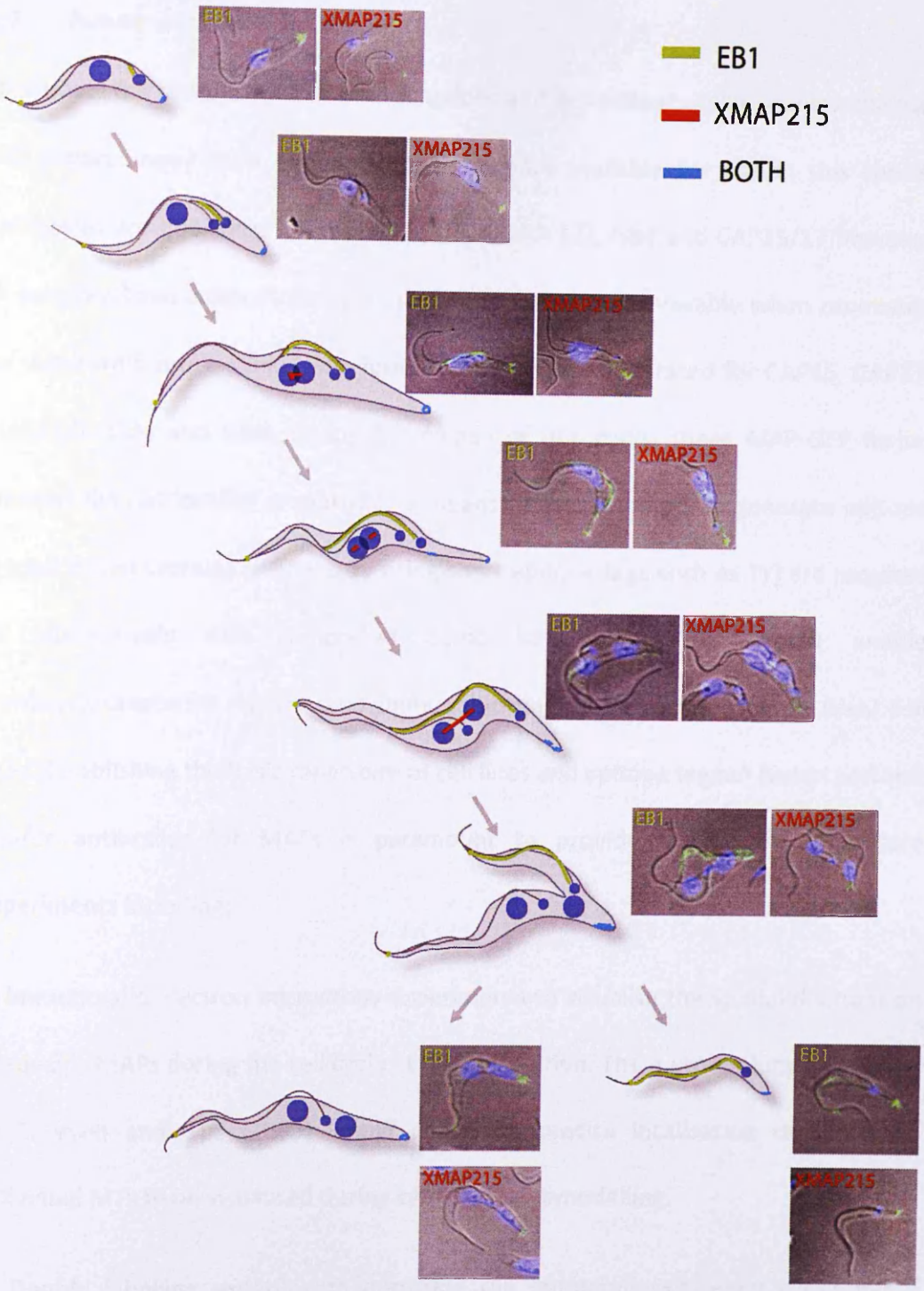

Figure 7.3 Cartoon showing the localisation of GFP-*Tb*EB1 and YFP-*Tb*XMAP215 in the TCP86 RNAi cell line 12 hours post induction

A model describing the fluorescence pattern observed when GFP-*Tb*EB1 and YFP-*Tb*XMAP215 are visualised at different cell cycle stages in the TCP86 cell line 12 hours post RNAi ablation. The areas where both proteins localise are shown in blue, GFP-*Tb*EB1 specific labelling patterns (green), YFP-*Tb*XMAP215 (red). Example images of trypanosome cells at each cell cycle stage are shown (inset).

7.6 Future work

To unravel the complexities of MAP functions and dependency relationships analysis will require many more reagents than the pool available for use in this thesis. Antibodies are published for the MAPs I/6, MARP 1/2, GB4 and CAP15/17 however all are polyclonal antibody reagents and none were made available when requested for use in this study. Whilst GFP fusion proteins were generated for CAP15, CAP17, MARP1/2, GB4 and GB4L during the course of this study, these MAP-GFP fusion proteins did not localise properly. This means further attempts to generate epitope tagged fusion proteins (perhaps by using short epitope tags such as TY) are required or alternatively new antibodies could be raised. This would enable immunofluorescence analysis and immunoblotting to be carried out on RNAi cell lines. Establishing the basic repertoire of cell lines and epitope tagged fusion proteins and/or antibodies for MAPs is paramount to provide a platform for future experiments including;

1) Immunogold electron microscopy experiments to visualise the spatial distribution of specific MAPs during the cell cycle at high resolution. The methodology developed by Sherwin and Gull (1989) would allow the precise localisation of MAPs on individual MTs to be visualised during cytoskeletal remodelling.

2) Double labelling experiments mirroring the immunofluorescence experiments presented in this thesis could be carried out using immunogold electron microscopy; allowing observations of MAP interdependencies to be made at the resolution of individual MTs.

3) Protein turnover and residency time can be examined by monitoring fluorescence recovery after photobleaching (FRAP). RNAi ablation of TCP86, WCB and CAP5.5 results in the loss of protein localisation initially from the posterior end of the cell (see Figure 5.3, Figure 5.4). The association of these MAPs with old MTs appears to be very stable, MAPs are still associated with the anterior of cells 48 hours post RNAi induced ablation. FRAP could be employed to study rates of protein recruitment/turnover in distinct regions of the subpellicular corset in both non-induced and induced cells.

4) Where interactions between proteins are suspected due to localisation data, protein-protein interactions could be explored using fluorescence resonance energy transfer (FRET) assays. FRET is based on the transfer of excitation energy between two fluorophores that are in close spatial proximity. Transfer of energy between the donor and acceptor fluorophores is only detected when the two molecules are very close together (up to 10 nm), a good indication of direct protein-protein interaction (reviewed by Kerppola, 2006).

5) The experiments described above would provide evidence of functional interactions between trypanosome MAPs. These interactions could be confirmed by carrying out, a pair wise yeast 2-hybrid interaction screen and/or co-immunoprecipitation of proteins.

Given that this is an area of *T. brucei* biology which is yet to be fully investigated, there is scope for future studies utilising many varied techniques to fully explore MAP interactions with one another and the subpellicular corset. Interactions between MAPs are critical for maintaining parasite morphology and survival,

targeted disruption of these interactions may provide an opportunity for combating the disease. In order to develop successful chemotherapeutic approaches the complexities of these protein-protein interactions should be fully understood.

Chapter 8 Appendix

8.1 Supplementary Figures

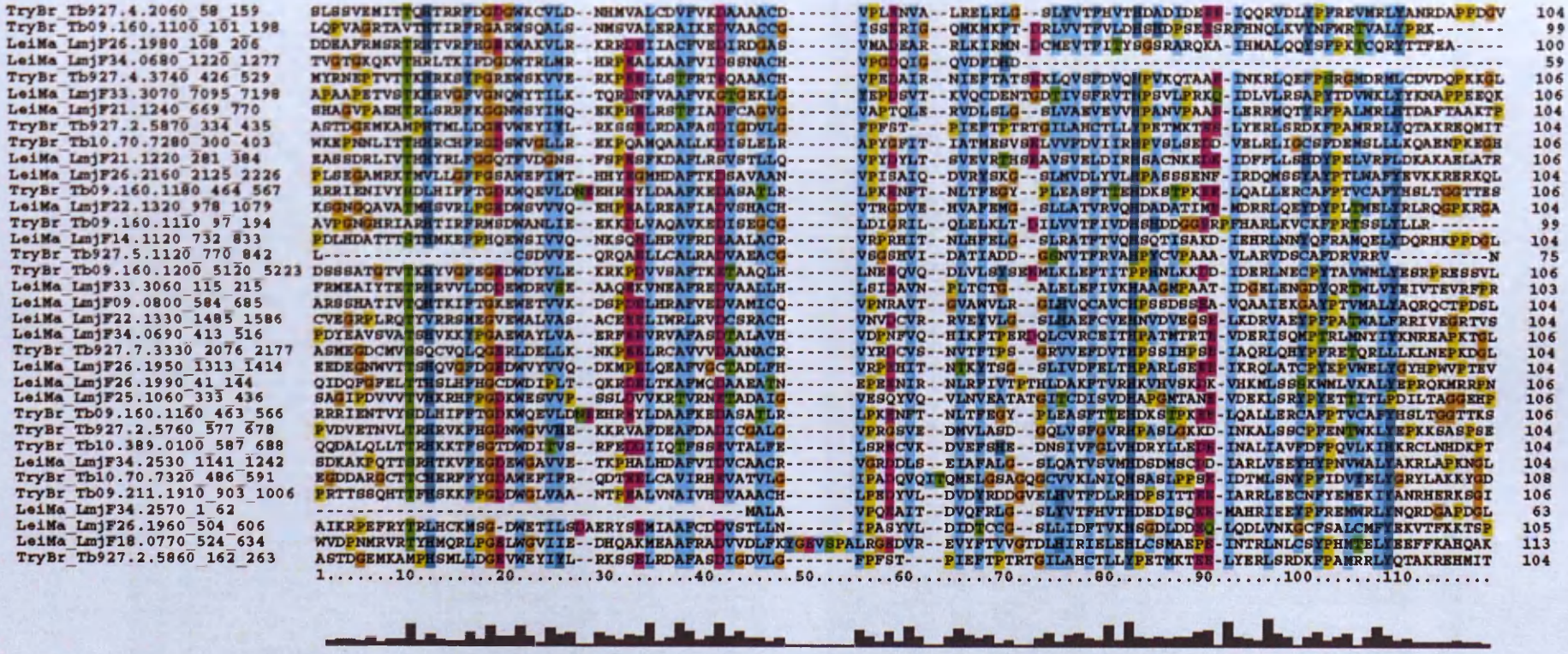

Figure 8.1 Clustal alignment file for initial HMM search showing all proteins possessing a GB4 motif

36 proteins from *L.major* and *T. brucei* possessed the GB4 motif alignment shows amino acids which have conserved characteristics.

CLUSTAL 2.0.12 MULTIPLE SEQUENCE ALIGNMENT

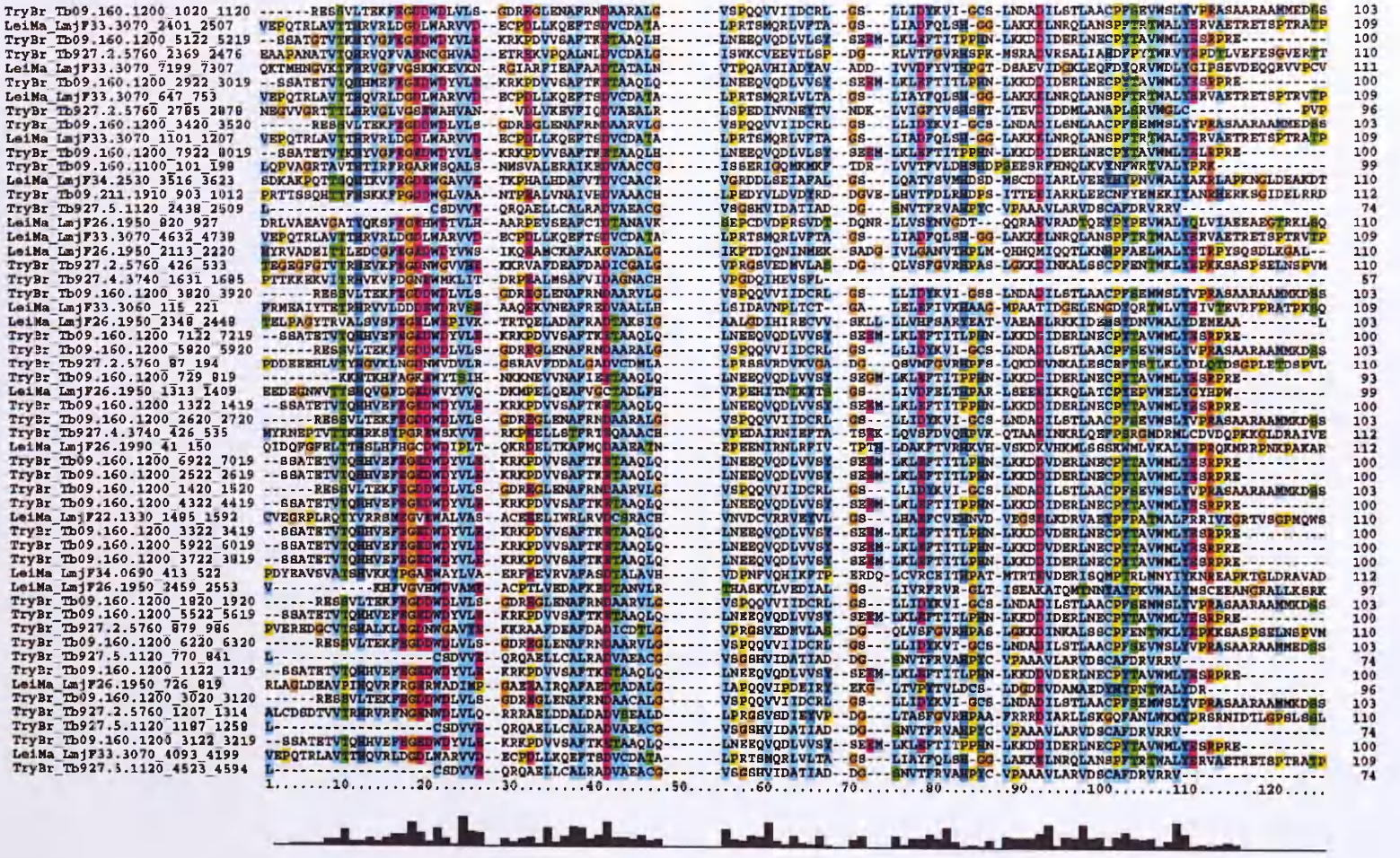

CLUSTAL 2.0.12 MULTIPLE SEQUENCE ALIGNMENT

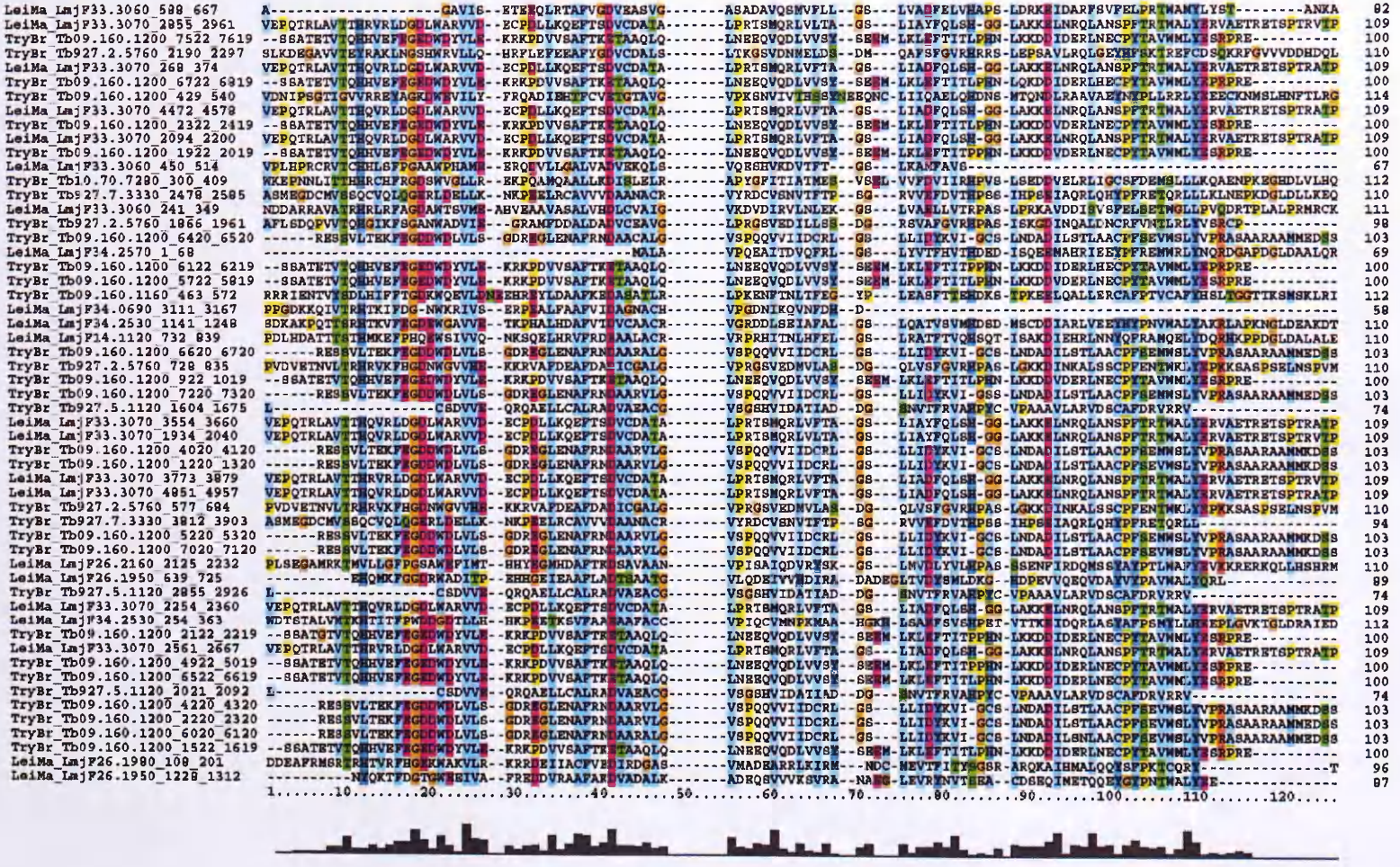

CLUSTAL 2.0.12 MULTIPLE SEQUENCE ALIGNMENT

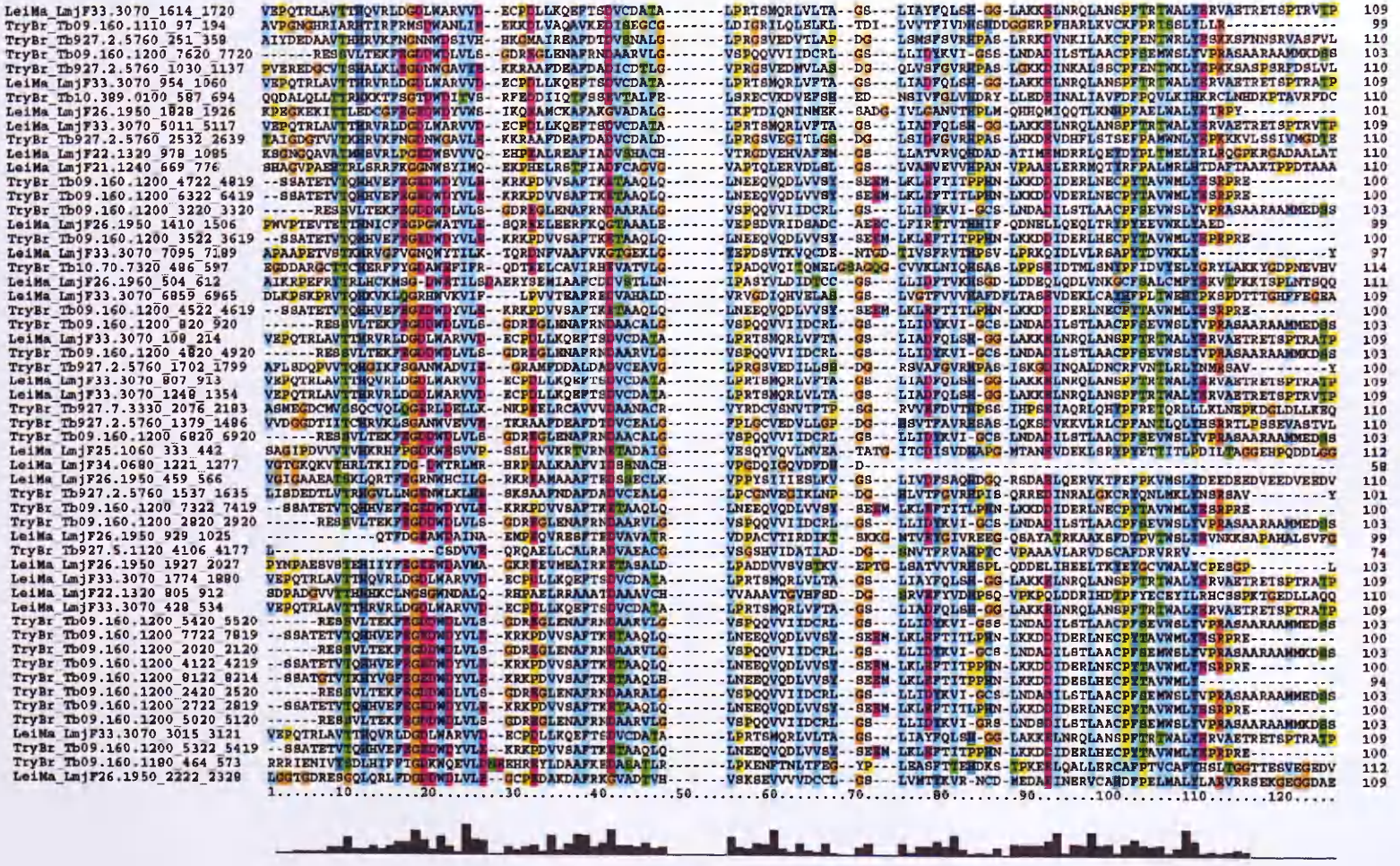

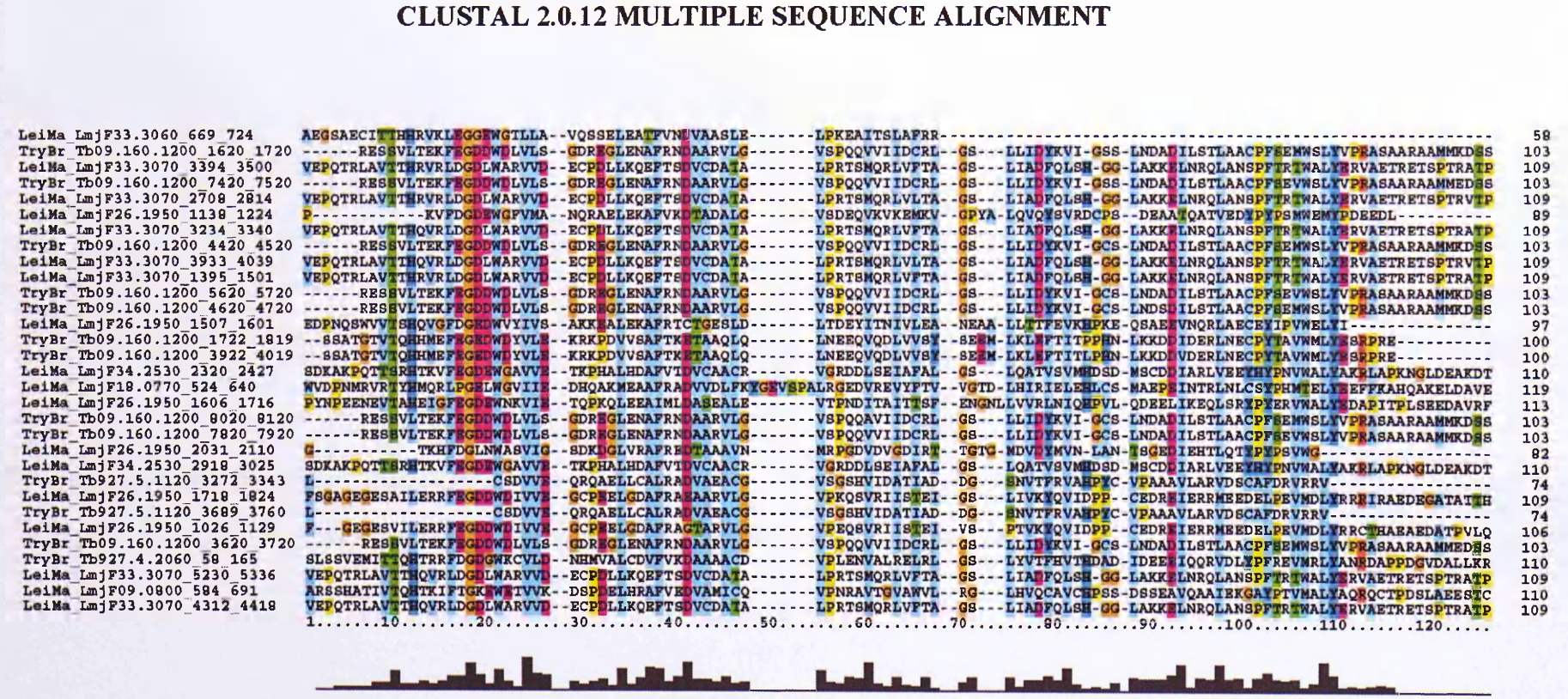

Figure 8.2 Clustal alignment file for second HMM search showing all the motifs identified by the HMM

196 GB4 motifs in total were identified by the HMM from proteins in *L.major* and *T. brucei* the alignment shows amino acids which have conserved characteristics.

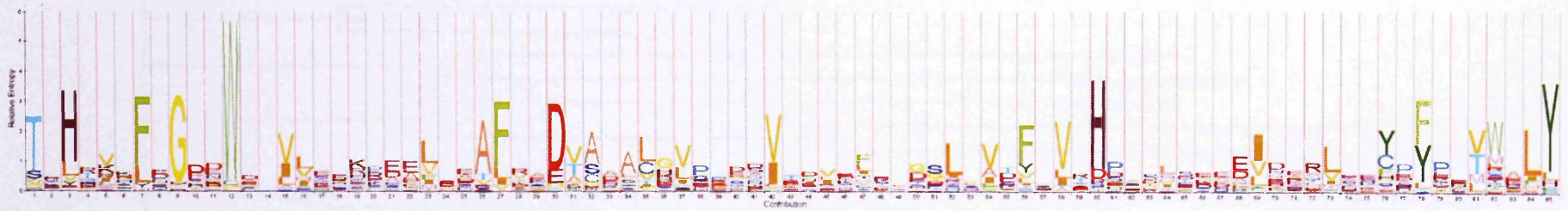

Figure 8.3 Trimmed GB4 motif sequence logo

The original HMM logo was trimmed down to the conserved tyrosine at position 90 removing the less well conserved amino acid positions at the C-terminus.

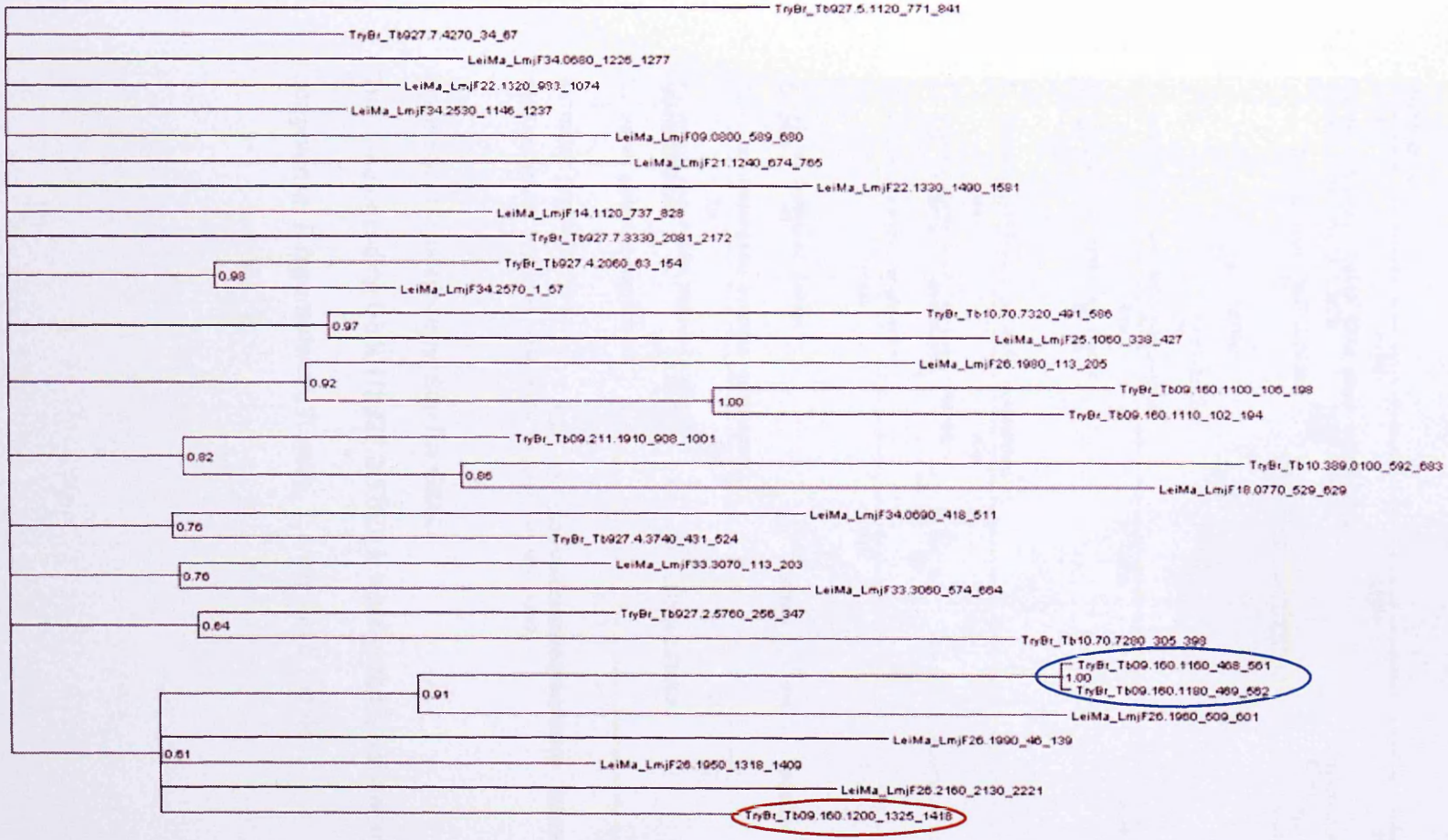

Figure 8.4 Phylogenetic tree of proteins containing the GB4 motif

Plotted using MrBayes a program for the Bayesian estimation of phylogeny, the tree shows that there is a high degree of phylogenetic diversity. TCP86 and TCP66 found in the blue circled clave, GB4 is circled in red

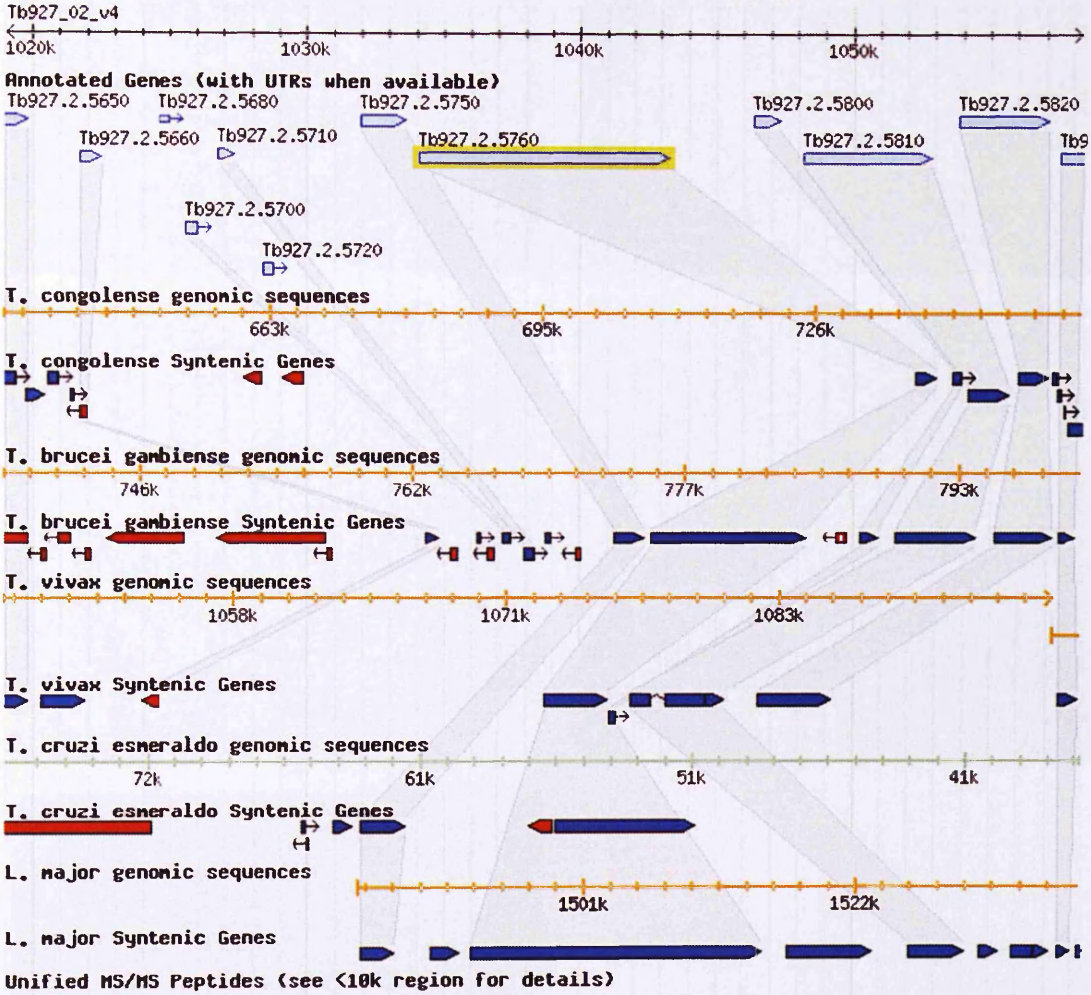

Figure 8.5 Gene synteny map for GB4L

The gene encoding GB4L (Tb927.2.5760) is highlighted in yellow and is conserved in *T congolense*, *T. b gambiense*, *T. vivax*, *T. cruzi* and *L. major*.

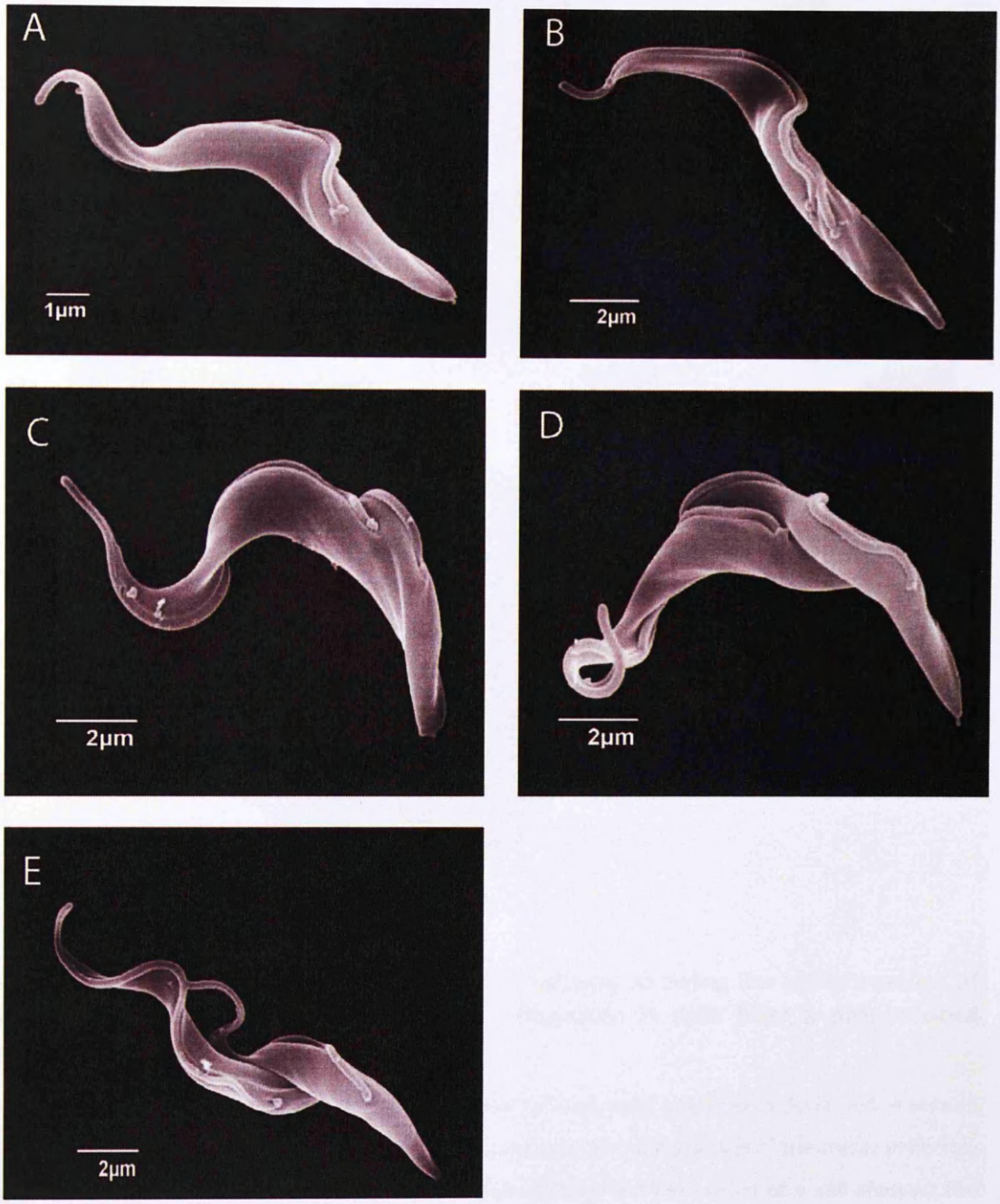

Figure 8.6 Scanning electron microscopy images of the non-induced TCP86 RNAi cell line

Cells prepared for SEM analysis as detailed in section 2.5.5, examples shown are representative cells from a non-induced culture. These cells have the same morphology as wild type cells at all stages of the cell cycle, A-E show cells at progressively later cell cycle stages from G_1 (A) to cytokinesis (E).

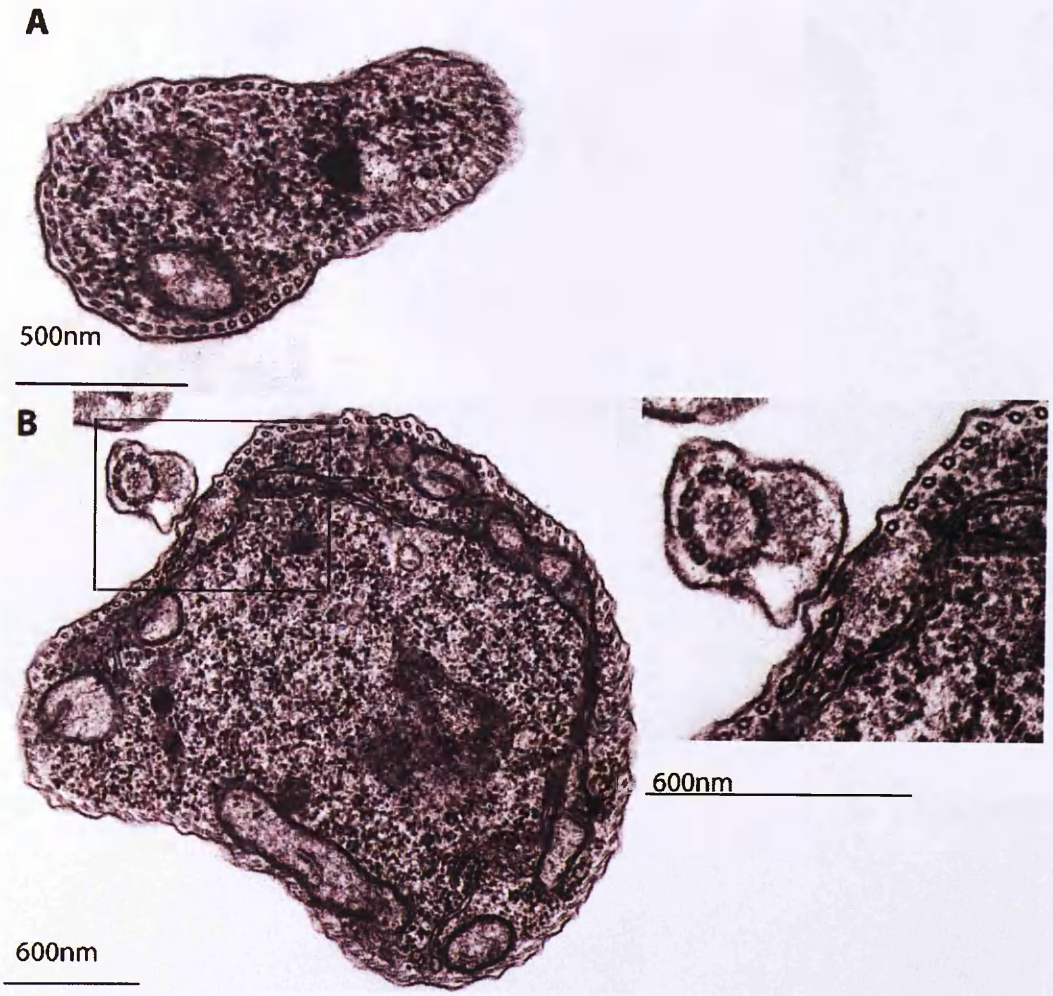

Figure 8.7 Transmission electron microscopy sections showing the ultrastructure of the subpellicular corset, the FAZ and the flagellum in cells from a non-induced population of the TCP86 RNAi cell line

Cells from a non induction culture of the TCP86 RNAi cell line were prepared as described in section 2.5.6. A) Section through the posterior end of a cell, showing the microtubules of the corset uniformly spaced beneath the plasma membrane. B) A section through the mid-region of a cell showing the highly organised corset microtubules, inset, magnification of the boxed area in B, showing flagellum and FAZ organisation.

Figure 8.8 Transmission electron microscopy sections showing the nuclei of non-induced cells from the TCP86 cell line

Cells from a non-induced culture of the TCP86 RNAi cell line were prepared as described in section 2.5.6 TEM section showing two cells, A) a cell in interphase, nucleolus indicated with an asterisk. B) A cell with microtubules of the mitotic spindle (blue brackets) contained within the nuclear membrane.

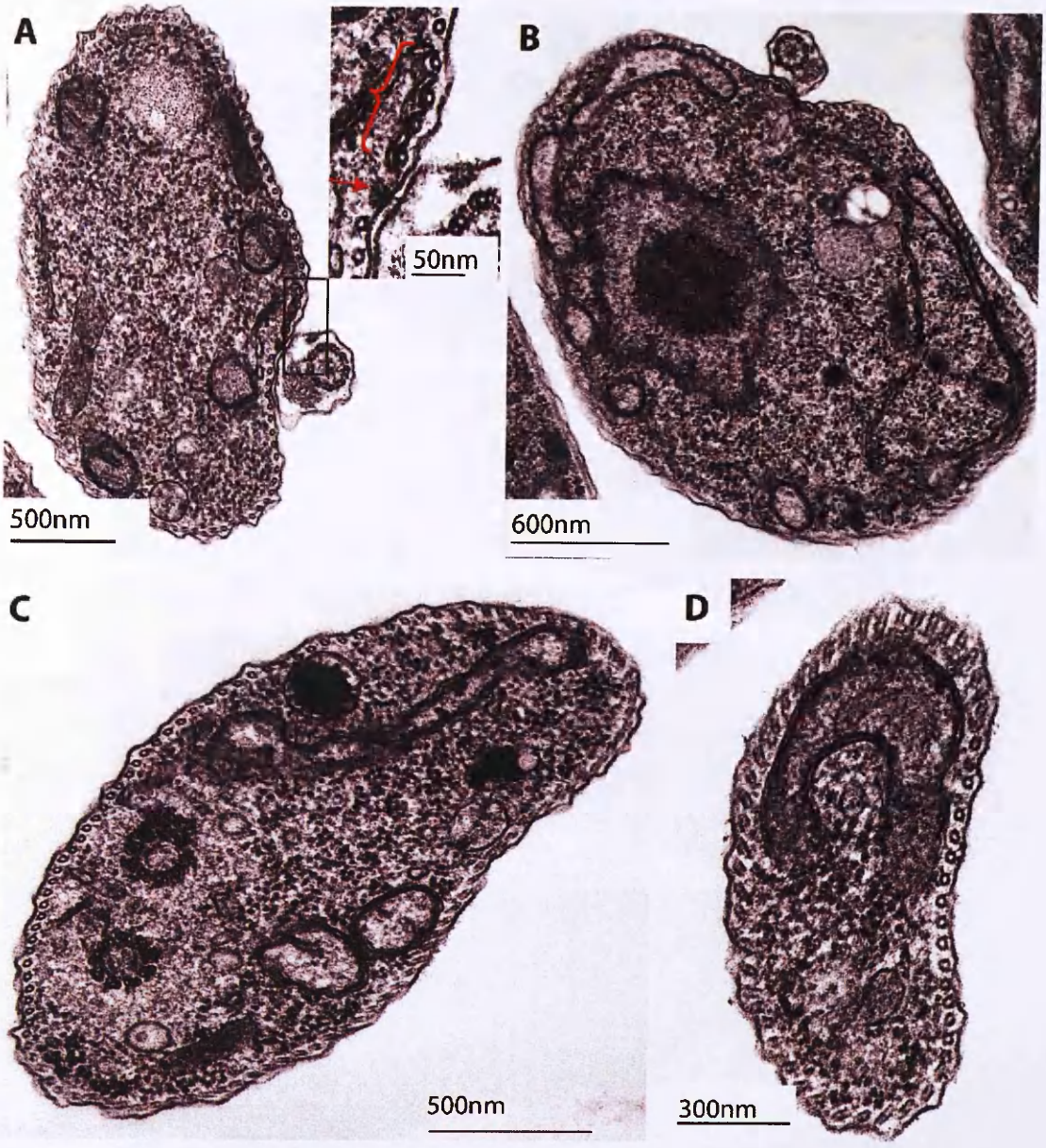

Figure 8.9 Transmission electron microscopy sections of the TCP86 RNAi cell line 12 hours post RNAi induction

Cells from a culture 12 hours post induction of TCP86 RNAi were prepared as described in section 2.5.6. A) a section through the anterior end of the cell, A, inset, magnified boxed area showing the MTQ associated with the smooth ER (red brackets) and the FAZ filament (red arrow) B) section through mid-region of a cell, C) and D) sections through the posterior end of a cell. The organisation of subpellicular corset does not appear to be affected by RNAi ablation of TCP86 and no supernumerary microtubules can be seen in the cytoplasm.

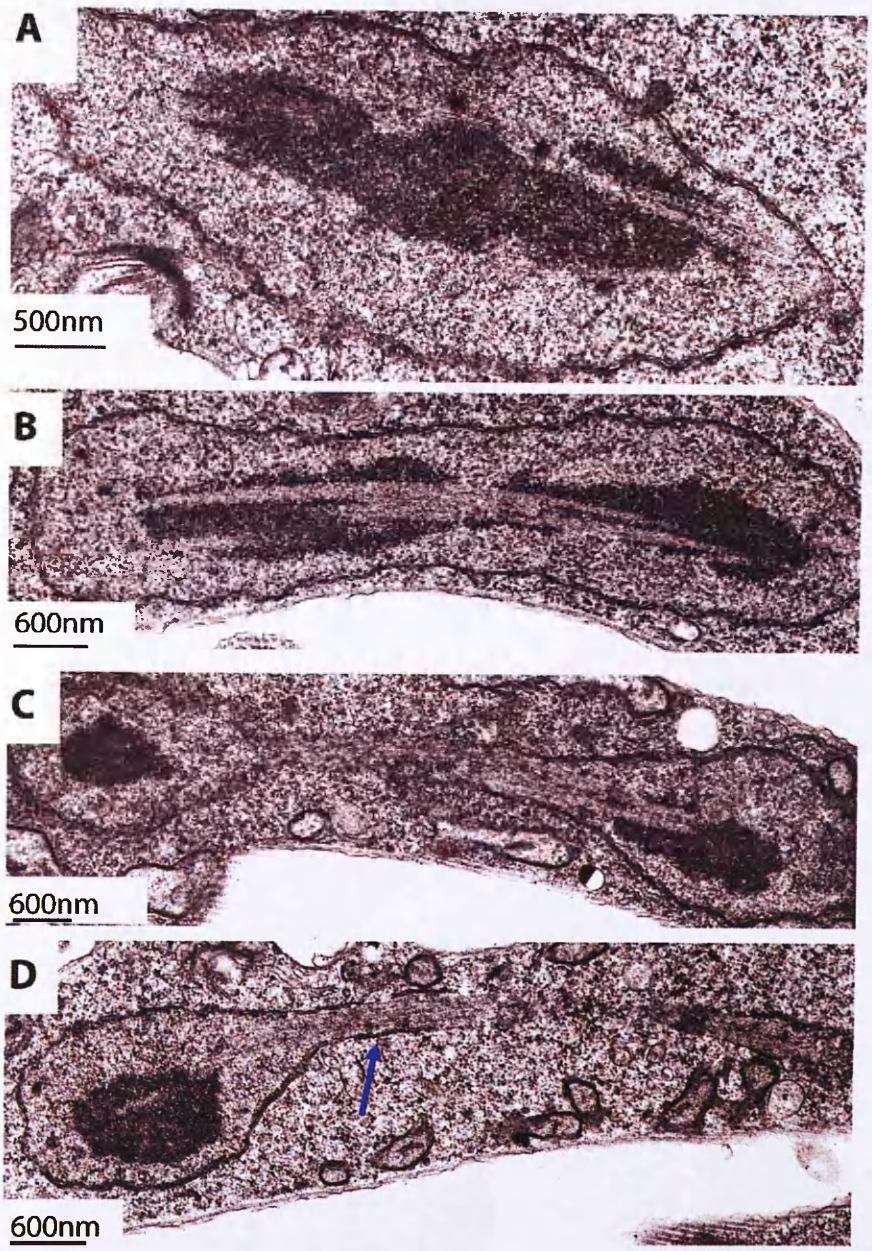

Figure 8.10 Transmission electron microscopy sections showing nuclei of cells at different stages of the cell cycle 12 hours post induction of TCP86 RNAi

Cells from a culture 12 hours post induction of TCP86 RNAi were prepared as described in section 2.5.6. A) A nucleus in metaphase, B) a later stage, and spindle microtubules can be seen clearly and nuclear envelope begins to constrict, nuclear material is divided. C) Nuclear constriction along the central spindle forming an isthmus between the daughter nuclei, there is a nucleolus apparent at either end of the spindle. D) Nucleolus has taken a rounded shape, arrow points to the spindle which may still connect nuclei or be a remnant of the isthmus.

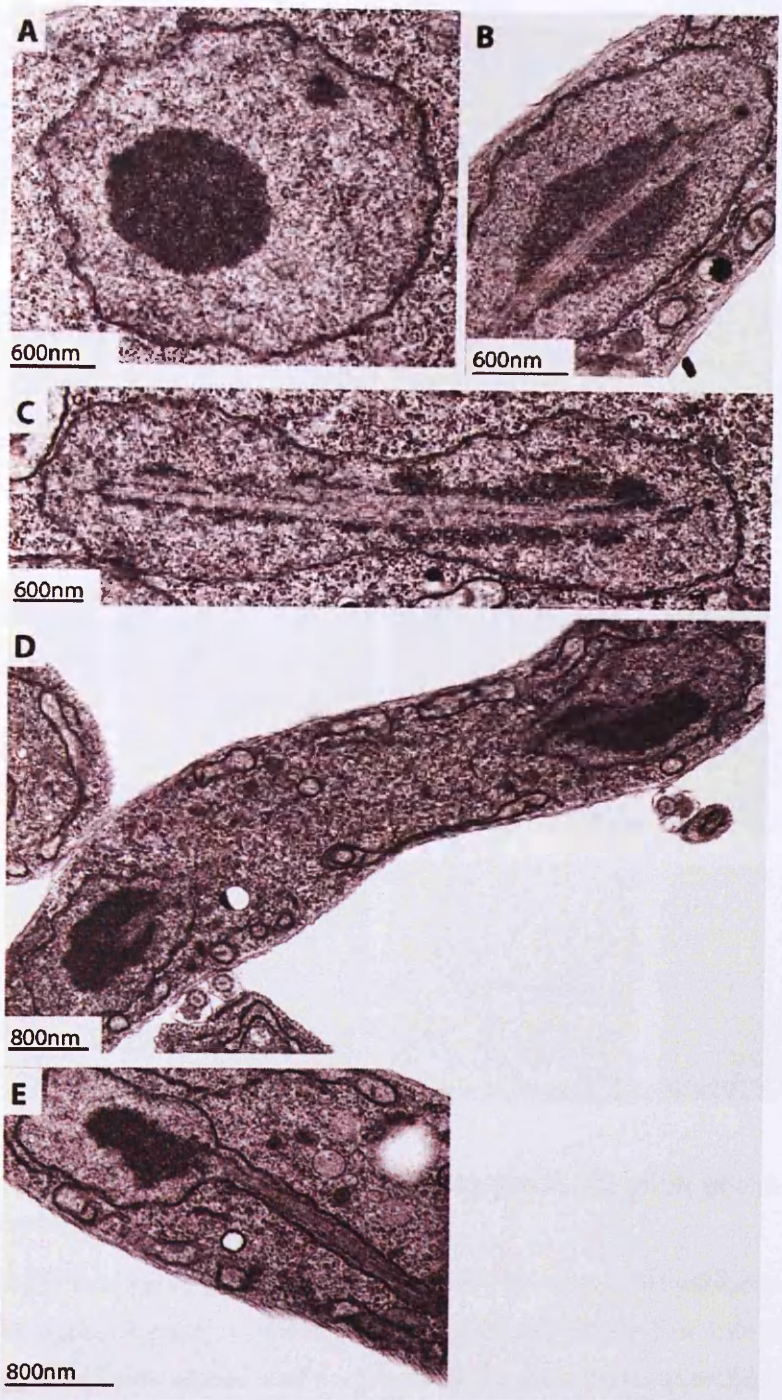

Figure 8.11 Transmission electron microscopy sections showing nuclei of cells at different stages of the cell cycle 24 hours post induction of TCP86 RNAi

Cells from a culture 24 hours post induction of TCP86 RNAi were prepared as described in section 2.5.6. A) An interphase nucleus, B) a metaphase nucleus, spindle microtubules can be seen clearly, C) a cell at a later stage, nuclear envelope begins to constrict. D) Nuclear constriction along the central spindle forming an isthmus between the daughter nuclei, there is a nucleolus apparent at either end of the spindle. E) A daughter nuclei undergoing karyokinesis the spindle microtubules enveloped by the nuclear membrane can be seen this may still connect nuclei or be a remnant of the isthmus.

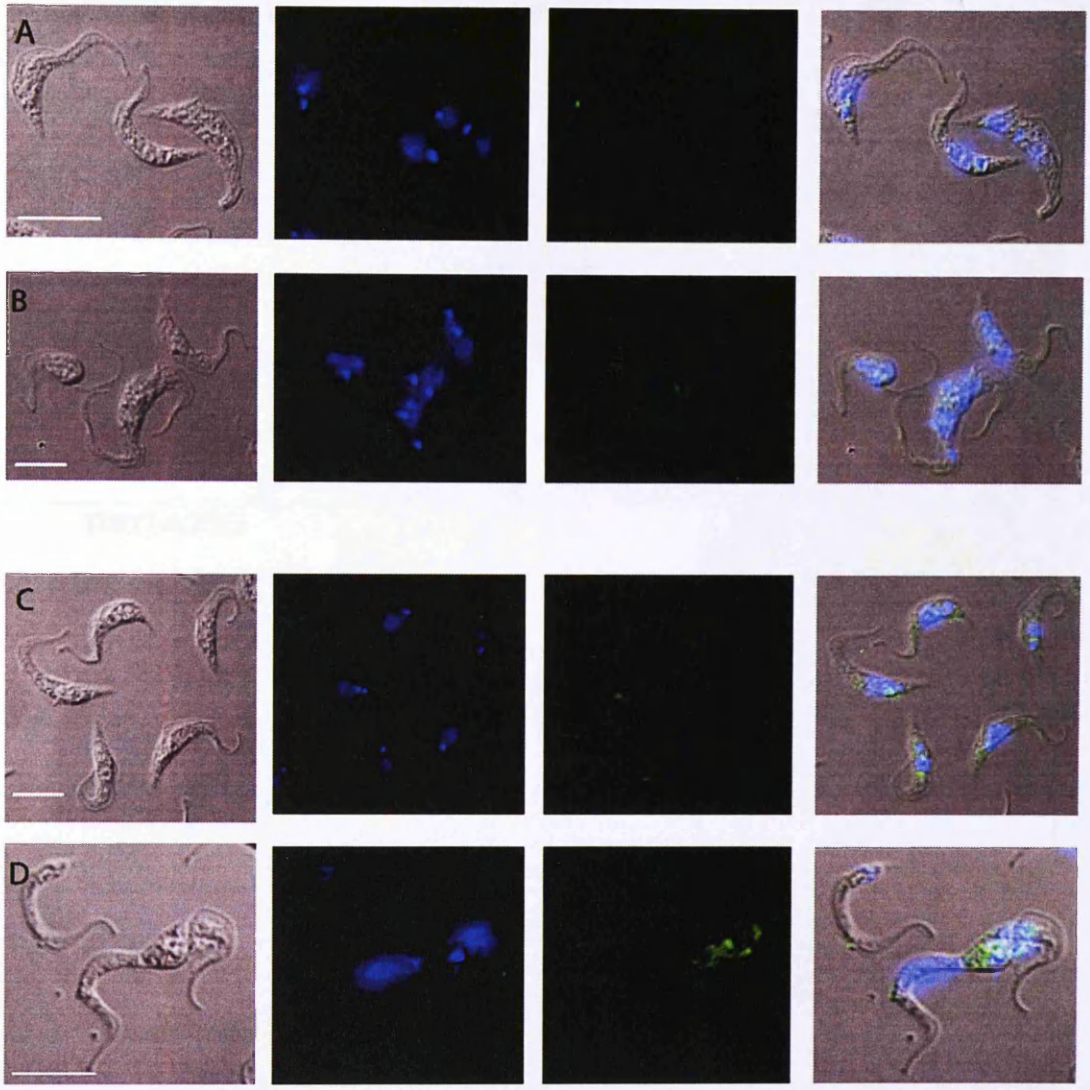

Figure 8.12 Immunofluorescence images showing the localisation of the GB4L anti-peptide antibodies

Anti-peptide antibodies raised by Eurogentec tested on non- induced and 24 hour induced GB4L RNAi cell line. A- Anti-peptide antibody 1 on NI cells, B-anti-peptide antibody 1 on cells 24 hours post induction of GB4L RNAi, C anti-peptide antibody 2 on NI cells and D anti-peptide antibody 2 on cells 24 hours post induction of GB4L ablation (scale bar = 10μm).

Accession Number	PCF	BSF
GB4		1
GB4L	2	1
Tb927.5.1120	2	1
Tb927.7.3330	3	1 & 3
FAZ1		1
Tb09.211.1910	2	1
Tb927.4.2060		1
Tb10.70.7320		1
TCP86	2 & 3	1, 3 & 4
TCP66		1
Tb10.70.7280		
Tb10.389.0100		3
Tb09.160.1110		1
Tb09.160.1100		
Tb927.7.4270		
Tb927.2.5860		
Tb927.2.5860		1

Table 8.1 Proteomic data available for the GB4 motif containing proteins

The table lists the accession number/name of each protein and identifies whether the protein is found in any of the PCF or BSF proteomes annotated on GeneDB. Green boxes indicate where proteomic analysis has identified the protein. Numbers refer to specific proteomic data sets as follows:**1** BSF plasma membrane and pellicular cytoskeleton subproteomes (Bridges *et al*, 2008), **2** PCF proteome (Jones *et al*, 2006), **3** The glycosomal and mitochondrial proteomes of PCF and BSF (Vertommen *et al*, 2008) and **4** The flagellar proteome (Broadhead *et al*, 2006).

References

Absalon S, Kohl L, Branche C, Blisnick T, Toutirais G, Rusconi F, Cosson J, Bonhivers M, Robinson D, Bastin P (2007) Basal body positioning is controlled by flagellum formation in *Trypanosoma brucei*. *PLoS One* **2**(5): e437

Absalon S, Blisnick T, Kohl L, Toutirais G, Dore G, Julkowska D, Tavenet A, Bastin P (2008) Intraflagellar transport and functional analysis of genes required for flagellum formation in trypanosomes. *Mol Biol Cell* **19**(3): 929-944

Affolter M, Hemphill A, Roditi I, Muller N, Seebeck T (1994) The repetitive microtubule-associated proteins MARP-1 and MARP-2 of *Trypanosoma brucei*. *J Struct Biol* **112**(3): 241-251

Akhmanova A, Hoogenraad CC (2005) Microtubule plus-end-tracking proteins: mechanisms and functions. *Curr Opin Cell Biol* **17**(1): 47-54

Akhmanova A, Steinmetz MO (2008) Tracking the ends: a dynamic protein network controls the fate of microtubule tips. *Nat Rev Mol Cell Biol* **9**(4): 309-322

Al-Bassam J, van Breugel M, Harrison SC, Hyman A (2006) Stu2p binds tubulin and undergoes an open-to-closed conformational change. *J Cell Biol* **172**(7): 1009-1022

Angelopoulos E (1970) Pellicular microtubules in the family Trypanosomatidae. *J Protozool* **17**(1): 39-51

Antoshechkin I, Han M (2002) The *C. elegans* evl-20 gene is a homolog of the small GTPase ARL2 and regulates cytoskeleton dynamics during cytokinesis and morphogenesis. *Dev Cell* **2**(5): 579-591

Archambault V, Glover DM (2009) Polo-like kinases: conservation and divergence in their functions and regulation. *Nat Rev Mol Cell Biol* **10**(4): 265-275

Askham JM, Moncur P, Markham AF, Morrison EE (2000) Regulation and function of the interaction between the APC tumour suppressor protein and EB1. *Oncogene* **19**(15): 1950-1958

Badin-Larcon AC, Boscheron C, Soleilhac JM, Piel M, Mann C, Denarier E, Fourest-Lieuvin A, Lafanechere L, Bornens M, Job D (2004) Suppression of nuclear oscillations in *Saccharomyces cerevisiae* expressing Glu tubulin. *Proc Natl Acad Sci U S A* **101**(15): 5577-5582

Baines A, Gull K (2008) WCB is a C2 domain protein defining the plasma membrane - sub-pellicular microtubule corset of kinetoplastid parasites. *Protist* **159**(1): 115-125

Balaban N, Waithaka HK, Njogu AR, Goldman R (1989) Isolation of a subpellicular microtubule protein from Trypanosoma brucei that mediates crosslinking of microtubules. *Cell Motil Cytoskeleton* **14**(3): 393-400

Balaban N, Goldman R (1992) Isolation and characterization of a unique 15 kilodalton trypanosome subpellicular microtubule-associated protein. *Cell Motil Cytoskeleton* **21**(2): 138-146

Balasubramanian MK, Bi E, Glotzer M (2004) Comparative analysis of cytokinesis in budding yeast, fission yeast and animal cells. *Curr Biol* **14**(18): R806-818

Barr FA, Gruneberg U (2007) Cytokinesis: placing and making the final cut. *Cell* **131**(5): 847-860

Bastin P, Sherwin T, Gull K (1998) Paraflagellar rod is vital for trypanosome motility. *Nature* **391**(6667): 548

Beinhauer JD, Hagan IM, Hegemann JH, Fleig U (1997) Mal3, the fission yeast homologue of the human APC-interacting protein EB-1 is required for microtubule integrity and the maintenance of cell form. *J Cell Biol* **139**(3): 717-728

Berriman M, Ghedin E, Hertz-Fowler C, Blandin G, Renauld H, Bartholomeu DC, Lennard NJ, Caler E, Hamlin NE, Haas B, Bohme U, Hannick L, Aslett MA, Shallom J, Marcello L, Hou L, Wickstead B, Alsmark UC, Arrowsmith C, Atkin RJ, Barron AJ, Bringaud F, Brooks K, Carrington M, Cherevach I, Chillingworth TJ, Churcher C, Clark LN, Corton CH, Cronin A, Davies RM, Doggett J, Djikeng A, Feldblyum T, Field MC, Fraser A, Goodhead I, Hance Z, Harper D, Harris BR, Hauser H, Hostetler J, Ivens A, Jagels K, Johnson D, Johnson J, Jones K, Kerhornou AX, Koo H, Larke N, Landfear S, Larkin C, Leech V, Line A, Lord A, Macleod A, Mooney PJ, Moule S, Martin DM, Morgan GW, Mungall K, Norbertczak H, Ormond D, Pai G, Peacock CS, Peterson J, Quail MA, Rabbinowitsch E, Rajandream MA, Reitter C, Salzberg SL, Sanders M, Schobel S, Sharp S, Simmonds M, Simpson AJ, Tallon L, Turner CM, Tait A, Tivey AR, Van Aken S, Walker D, Wanless D, Wang S, White B, White O, Whitehead S, Woodward J, Wortman J, Adams MD, Embley TM, Gull K, Ullu E, Barry JD, Fairlamb AH, Opperdoes F, Barrell BG, Donelson JE, Hall N, Fraser CM, Melville SE, El-Sayed NM (2005) The genome of the African trypanosome *Trypanosoma brucei*. *Science* **309**(5733): 416-422

Boucher N, Dacheux D, Giroud C, Baltz T (2007) An essential cell cycle-regulated nucleolar protein relocates to the mitotic spindle where it is involved in mitotic progression in *Trypanosoma brucei*. *J Biol Chem* **282**(18): 13780-13790

Bridges DJ, Pitt AR, Hanrahan O, Brennan K, Voorheis HP, Herzyk P, de Koning HP, Burchmore RJ (2008) Characterisation of the plasma membrane subproteome of bloodstream form *Trypanosoma brucei*. *Proteomics* **8**(1): 83-99

Briggs LJ, McKean PG, Baines A, Moreira-Leite F, Davidge J, Vaughan S, Gull K (2004) The flagella connector of *Trypanosoma brucei*: an unusual mobile transmembrane junction. *J Cell Sci* **117**(Pt 9): 1641-1651

Broadhead R, Dawe HR, Farr H, Griffiths S, Hart SR, Portman N, Shaw MK, Ginger ML, Gaskell SJ, McKean PG, Gull K (2006) Flagellar motility is required for the viability of the bloodstream trypanosome. *Nature* **440**(7081): 224-227

Brouhard GJ, Stear JH, Noetzel TL, Al-Bassam J, Kinoshita K, Harrison SC, Howard J, Hyman AA (2008) XMAP215 is a processive microtubule polymerase. *Cell* **132**(1): 79-88

Brun R, Jenni L, Tanner M, Schonenberger M, Schell KF (1979) Cultivation of vertebrate infective forms derived from metacyclic forms of pleomorphic Trypanosoma brucei stocks. Short communication. *Acta Trop* **36**(4): 387-390

Brun R, Blum J, Chappuis F, Burri C (2010) Human African trypanosomiasis. *Lancet* **375**(9709): 148-159

Busch KE, Brunner D (2004) The microtubule plus end-tracking proteins mal3p and tip1p cooperate for cell-end targeting of interphase microtubules. *Curr Biol* **14**(7): 548-559

Cambray-Deakin MA, Burgoyne RD (1987) Posttranslational modifications of alpha-tubulin: acetylated and detyrosinated forms in axons of rat cerebellum. *J Cell Biol* **104**(6): 1569-1574

Campbell HD, Kamei M, Claudianos C, Woollatt E, Sutherland GR, Suzuki Y, Hida M, Sugano S, Young IG (2000) Human and mouse homologues of the Drosophila melanogaster tweety (tty) gene: a novel gene family encoding predicted transmembrane proteins. *Genomics* **68**(1): 89-92

Carmena M, Earnshaw WC (2003) The cellular geography of aurora kinases. *Nat Rev Mol Cell Biol* **4**(11): 842-854

Chan J, Calder GM, Doonan JH, Lloyd CW (2003) EB1 reveals mobile microtubule nucleation sites in Arabidopsis. *Nat Cell Biol* **5**(11): 967-971

Chanez AL, Hehl AB, Engstler M, Schneider A (2006) Ablation of the single dynamin of *T. brucei* blocks mitochondrial fission and endocytosis and leads to a precise cytokinesis arrest. *J Cell Sci* **119**(Pt 14): 2968-2974

Charrasse S, Mazel M, Taviaux S, Berta P, Chow T, Larroque C (1995) Characterization of the cDNA and pattern of expression of a new gene over-expressed in human hepatomas and colonic tumors. *Eur J Biochem* **234**(2): 406-413

Charrasse S, Schroeder M, Gauthier-Rouviere C, Ango F, Cassimeris L, Gard DL, Larroque C (1998) The TOGp protein is a new human microtubule-associated protein homologous to the Xenopus XMAP215. *J Cell Sci* **111 (Pt 10)**: 1371-1383

Cho W, Stahelin RV (2006) Membrane binding and subcellular targeting of C2 domains. *Biochim Biophys Acta* **1761**(8): 838-849

Chretien D, Fuller SD, Karsenti E (1995) Structure of growing microtubule ends: two-dimensional sheets close into tubes at variable rates. *J Cell Biol* **129**(5): 1311-1328

Cleveland DW, Lopata MA, Sherline P, Kirschner MW (1981) Unpolymerized tubulin modulates the level of tubulin mRNAs. *Cell* **25**(2): 537-546

Cleveland DW, Pittenger MF, Feramisco JR (1983) Elevation of tubulin levels by microinjection suppresses new tubulin synthesis. *Nature* **305**(5936): 738-740

Cooper R, de Jesus AR, Cross GA (1993) Deletion of an immunodominant *Trypanosoma cruzi* surface glycoprotein disrupts flagellum-cell adhesion. *J Cell Biol* **122**(1): 149-156

Croall DE, Ersfeld K (2007) The calpains: modular designs and functional diversity. *Genome Biol* **8**(6): 218

Cross GA, Manning JC (1973) Cultivation of *Trypanosoma brucei sspp.* in semi-defined and defined media. *Parasitology* **67**(3): 315-331

Dammermann A, Desai A, Oegema K (2003) The minus end in sight. *Curr Biol* **13**(15): R614-624

Davidge JA, Chambers E, Dickinson HA, Towers K, Ginger ML, McKean PG, Gull K (2006) Trypanosome IFT mutants provide insight into the motor location for mobility of the flagella connector and flagellar membrane formation. *J Cell Sci* **119**(Pt 19): 3935-3943

de Graffenried CL, Ho HH, Warren G (2008) Polo-like kinase is required for Golgi and bilobe biogenesis in *Trypanosoma brucei*. *J Cell Biol* **181**(3): 431-438

Dean S, Marchetti R, Kirk K, Matthews KR (2009) A surface transporter family conveys the trypanosome differentiation signal. *Nature* **459**(7244): 213-217

Dehmelt L, Halpain S (2005) The MAP2/Tau family of microtubule-associated proteins. *Genome Biol* **6**(1): 204

Desai A, Verma S, Mitchison TJ, Walczak CE (1999) Kin I kinesins are microtubule-destabilizing enzymes. *Cell* **96**(1): 69-78

Detmer E, Hemphill A, Muller N, Seebeck T (1997) The Trypanosoma brucei autoantigen I/6 is an internally repetitive cytoskeletal protein. *Eur J Cell Biol* **72**(4): 378-384

Douzery EJ, Snell EA, Bapteste E, Delsuc F, Philippe H (2004) The timing of eukaryotic evolution: does a relaxed molecular clock reconcile proteins and fossils? *Proc Natl Acad Sci U S A* **101**(43): 15386-15391

Drechsel DN, Kirschner MW (1994) The minimum GTP cap required to stabilize microtubules. *Curr Biol* **4**(12): 1053-1061

Duszenko M, Figarella K, Macleod ET, Welburn SC (2006) Death of a trypanosome: a selfish altruism. *Trends Parasitol* **22**(11): 536-542

Erickson HP (2000) Gamma-tubulin nucleation: template or protofilament? *Nat Cell Biol* **2**(6): E93-96

Ersfeld K, Barraclough H, Gull K (2005) Evolutionary relationships and protein domain architecture in an expanded calpain superfamily in kinetoplastid parasites. *J Mol Evol* **61**(6): 742-757

Farina M, Attias M, T.Souto-Padron, Souza W (1986) Further Studies on the Organization of the Paraxial Rod of Trypanosomatids. *Journal of Eurkaryotic Microbiology* **33**(4): 552-557

Fenn K, Matthews KR (2007) The cell biology of *Trypanosoma brucei* differentiation. *Curr Opin Microbiol* **10**(6): 539-546

Field MC, Carrington M (2009) The trypanosome flagellar pocket. *Nat Rev Microbiol* **7**(11): 775-786

Fridberg A, Olson CL, Nakayasu ES, Tyler KM, Almeida IC, Engman DM (2008) Sphingolipid synthesis is necessary for kinetoplast segregation and cytokinesis in *Trypanosoma brucei*. *J Cell Sci* **121**(Pt 4): 522-535

Galjart N (2010) Plus-end-tracking proteins and their interactions at microtubule ends. *Curr Biol* **20**(12): R528-537

Garcia-Salcedo JA, Nolan DP, Gijon P, Gomez-Rodriguez J, Pays E (2002) A protein kinase specifically associated with proliferative forms of *Trypanosoma brucei* is functionally related to a yeast kinase involved in the co-ordination of cell shape and division. *Mol Microbiol* **45**(2): 307-319

Garcia-Salcedo JA, Perez-Morga D, Gijon P, Dilbeck V, Pays E, Nolan DP (2004) A differential role for actin during the life cycle of *Trypanosoma brucei*. *EMBO J* **23**(4): 780-789

Gard DL, Kirschner MW (1987) A microtubule-associated protein from Xenopus eggs that specifically promotes assembly at the plus-end. *J Cell Biol* **105**(5): 2203-2215

Gimona M, Djinovic-Carugo K, Kranewitter WJ, Winder SJ (2002) Functional plasticity of CH domains. *FEBS Lett* **513**(1): 98-106

Goll DE, Thompson VF, Li H, Wei W, Cong J (2003) The calpain system. *Physiol Rev* **83**(3): 731-801

Gourguechon S, Savich JM, Wang CC (2007) The multiple roles of cyclin E1 in controlling cell cycle progression and cellular morphology of *Trypanosoma brucei*. *J Mol Biol* **368**(4): 939-950

Gourguechon S, Wang CC (2009) CRK9 contributes to regulation of mitosis and cytokinesis in the procyclic form of *Trypanosoma brucei*. *BMC Cell Biol* **10**: 68

Grigoriev I, Gouveia SM, van der Vaart B, Demmers J, Smyth JT, Honnappa S, Splinter D, Steinmetz MO, Putney JW, Jr., Hoogenraad CC, Akhmanova A (2008) STIM1 is a MT-plus-end-tracking protein involved in remodeling of the ER. *Curr Biol* **18**(3): 177-182

Guertin DA, Trautmann S, McCollum D (2002) Cytokinesis in eukaryotes. *Microbiol Mol Biol Rev* **66**(2): 155-178

Gull K (1999) The cytoskeleton of trypanosomatid parasites. *Annu Rev Microbiol* **53**: 629-655

Hammarton TC, Clark J, Douglas F, Boshart M, Mottram JC (2003a) Stage-specific differences in cell cycle control in *Trypanosoma brucei* revealed by RNA interference of a mitotic cyclin. *J Biol Chem* **278**(25): 22877-22886

Hammarton TC, Mottram JC, Doerig C (2003b) The cell cycle of parasitic protozoa: potential for chemotherapeutic exploitation. *Prog Cell Cycle Res* **5**: 91-101

Hammarton TC, Engstler M, Mottram JC (2004) The *Trypanosoma brucei* cyclin, CYC2, is required for cell cycle progression through G1 phase and for maintenance of procyclic form cell morphology. *J Biol Chem* **279**(23): 24757-24764

Hammarton TC, Lillico SG, Welburn SC, Mottram JC (2005) *Trypanosoma brucei* MOB1 is required for accurate and efficient cytokinesis but not for exit from mitosis. *Mol Microbiol* **56**(1): 104-116

Hammarton TC, Kramer S, Tetley L, Boshart M, Mottram JC (2007a) *Trypanosoma brucei* Polo-like kinase is essential for basal body duplication, kDNA segregation and cytokinesis. *Mol Microbiol* **65**(5): 1229-1248

Hammarton TC, Monnerat S, Mottram JC (2007b) Cytokinesis in trypanosomatids. *Curr Opin Microbiol* **10**(6): 520-527

Hammarton TC WB, McKean P. G (ed) (2007) *Cell structure, cell division and cell cycle*: Horizon BioScience

Hammond JW, Cai D, Verhey KJ (2008) Tubulin modifications and their cellular functions. *Curr Opin Cell Biol* **20**(1): 71-76

Hammond JW, Huang CF, Kaech S, Jacobson C, Banker G, Verhey KJ (2010) Posttranslational modifications of tubulin and the polarized transport of kinesin-1 in neurons. *Mol Biol Cell* **21**(4): 572-583

Hannun YA, Obeid LM (2008) Principles of bioactive lipid signalling: lessons from sphingolipids. *Nat Rev Mol Cell Biol* **9**(2): 139-150

He CY, Ho HH, Malsam J, Chalouni C, West CM, Ullu E, Toomre D, Warren G (2004) Golgi duplication in *Trypanosoma brucei*. *J Cell Biol* **165**(3): 313-321

Hemphill A, Affolter M, Seebeck T (1992) A novel microtubule-binding motif identified in a high molecular weight microtubule-associated protein from Trypanosoma brucei. *J Cell Biol* **117**(1): 95-103

Hendriks E, van Deursen FJ, Wilson J, Sarkar M, Timms M, Matthews KR (2000) Life-cycle differentiation in Trypanosoma brucei: molecules and mutants. *Biochem Soc Trans* **28**(5): 531-536

Hendriks EF, Robinson DR, Hinkins M, Matthews KR (2001) A novel CCCH protein which modulates differentiation of Trypanosoma brucei to its procyclic form. *EMBO J* **20**(23): 6700-6711

Hergovich A, Cornils H, Hemmings BA (2008) Mammalian NDR protein kinases: from regulation to a role in centrosome duplication. *Biochim Biophys Acta* **1784**(1): 3-15

Hertz-Fowler C, Ersfeld K, Gull K (2001) CAP5.5, a life-cycle-regulated, cytoskeleton-associated protein is a member of a novel family of calpain-related proteins in *Trypanosoma brucei*. *Mol Biochem Parasitol* **116**(1): 25-34

Hestermann A, Graf R (2004) The XMAP215-family protein DdCP224 is required for cortical interactions of microtubules. *BMC Cell Biol* **5**: 24

Hirano T, Funahashi SI, Uemura T, Yanagida M (1986) Isolation and characterization of *Schizosaccharomyces pombe* cut mutants that block nuclear division but not cytokinesis. *EMBO J* **5**(11): 2973-2979

Hirokawa N, Noda Y, Tanaka Y, Niwa S (2009) Kinesin superfamily motor proteins and intracellular transport. *Nat Rev Mol Cell Biol* **10**(10): 682-696

Honnappa S, John CM, Kostrewa D, Winkler FK, Steinmetz MO (2005) Structural insights into the EB1-APC interaction. *EMBO J* **24**(2): 261-269

Honnappa S, Gouveia SM, Weisbrich A, Damberger FF, Bhavesh NS, Jawhari H, Grigoriev I, van Rijssel FJ, Buey RM, Lawera A, Jelesarov I, Winkler FK, Wuthrich K, Akhmanova A, Steinmetz MO (2009) An EB1-binding motif acts as a microtubule tip localization signal. *Cell* **138**(2): 366-376

Howard J, Hyman AA (2003) Dynamics and mechanics of the microtubule plus end. *Nature* **422**(6933): 753-758

Idriss HT (2000) Man to trypanosome: the tubulin tyrosination/detyrosination cycle revisited. *Cell Motil Cytoskeleton* **45**(3): 173-184

Janson ME, Setty TG, Paoletti A, Tran PT (2005) Efficient formation of bipolar microtubule bundles requires microtubule-bound gamma-tubulin complexes. *J Cell Biol* **169**(2): 297-308

Jones A, Faldas A, Foucher A, Hunt E, Tait A, Wastling JM, Turner CM (2006) Visualisation and analysis of proteomic data from the procyclic form of *Trypanosoma brucei*. *Proteomics* **6**(1): 259-267

Kaffman A, Herskowitz I, Tjian R, O'Shea EK (1994) Phosphorylation of the transcription factor PHO4 by a cyclin-CDK complex, PHO80-PHO85. *Science* **263**(5150): 1153-1156

Kerppola TK (2006) Design and implementation of bimolecular fluorescence complementation (BiFC) assays for the visualization of protein interactions in living cells. *Nat Protoc* **1**(3): 1278-1286

Kikkawa M, Ishikawa T, Nakata T, Wakabayashi T, Hirokawa N (1994) Direct visualization of the microtubule lattice seam both in vitro and in vivo. *J Cell Biol* **127**(6 Pt 2): 1965-1971

Kilmartin JV, Wright B, Milstein C (1982) Rat monoclonal antitubulin antibodies derived by using a new nonsecreting rat cell line. *J Cell Biol* **93**(3): 576-582

Kinukawa M, Ohmuro J, Baba SA, Murashige S, Okuno M, Nagata M, Aoki F (2005) Analysis of flagellar bending in hamster spermatozoa: characterization of an effective stroke. *Biol Reprod* **73**(6): 1269-1274

Kohl L, Sherwin T, Gull K (1999) Assembly of the paraflagellar rod and the flagellum attachment zone complex during the *Trypanosoma brucei* cell cycle. *J Eukaryot Microbiol* **46**(2): 105-109

Kohl L, Robinson D, Bastin P (2003) Novel roles for the flagellum in cell morphogenesis and cytokinesis of trypanosomes. *EMBO J* **22**(20): 5336-5346

Kollman JM, Polka JK, Zelter A, Davis TN, Agard DA (2010) Microtubule nucleating gamma-TuSC assembles structures with 13-fold microtubule-like symmetry. *Nature* **466**(7308): 879-882

Kumar P, Wang CC (2006) Dissociation of cytokinesis initiation from mitotic control in a eukaryote. *Eukaryot Cell* **5**(1): 92-102

Kuntzel H, Schulz A, Ehbrecht IM (1996) Cell cycle control and initiation of DNA replication in *Saccharomyces cerevisiae*. *Biol Chem* **377**(7-8): 481-487

L'Hernault SW, Rosenbaum JL (1983) Chlamydomonas alpha-tubulin is posttranslationally modified in the flagella during flagellar assembly. *J Cell Biol* **97**(1): 258-263

Lacomble S, Vaughan S, Gadelha C, Morphew MK, Shaw MK, McIntosh JR, Gull K (2010) Basal body movements orchestrate membrane organelle division and cell morphogenesis in *Trypanosoma brucei*. *J Cell Sci* **123**(Pt 17): 2884-2891

LaCount DJ, Barrett B, Donelson JE (2002) *Trypanosoma brucei* FLA1 is required for flagellum attachment and cytokinesis. *J Biol Chem* **277**(20): 17580-17588

Lansbergen G, Akhmanova A (2006) Microtubule plus end: a hub of cellular activities. *Traffic* **7**(5): 499-507

Li D, Roberts R (2001) WD-repeat proteins: structure characteristics, biological function, and their involvement in human diseases. *Cell Mol Life Sci* **58**(14): 2085-2097

Li Z, Wang CC (2003) A PHO80-like cyclin and a B-type cyclin control the cell cycle of the procyclic form of *Trypanosoma brucei*. *J Biol Chem* **278**(23): 20652-20658

Li Z, Wang CC (2006) Changing roles of aurora-B kinase in two life cycle stages of *Trypanosoma brucei*. *Eukaryot Cell* **5**(7): 1026-1035

Li Z, Lee JH, Chu F, Burlingame AL, Gunzl A, Wang CC (2008a) Identification of a novel chromosomal passenger complex and its unique localization during cytokinesis in *Trypanosoma brucei*. *PLoS One* **3**(6): e2354

Li Z, Umeyama T, Wang CC (2008b) The chromosomal passenger complex and a mitotic kinesin interact with the Tousled-like kinase in trypanosomes to regulate mitosis and cytokinesis. *PLoS One* **3**(11): e3814

Li Z, Umeyama T, Wang CC (2010) Polo-like kinase guides cytokinesis in Trypanosoma brucei through an indirect means. *Eukaryot Cell* **9**(5): 705-716

Liao G, Gundersen GG (1998) Kinesin is a candidate for cross-bridging microtubules and intermediate filaments. Selective binding of kinesin to detyrosinated tubulin and vimentin. *J Biol Chem* **273**(16): 9797-9803

Ma J, Benz C, Grimaldi R, Stockdale C, Wyatt P, Frearson J, Hammarton TC (2010) Nuclear DBF-2-related kinases are essential regulators of cytokinesis in bloodstream stage *Trypanosoma brucei*. *J Biol Chem* **285**(20): 15356-15368

Maruta H, Greer K, Rosenbaum JL (1986) The acetylation of alpha-tubulin and its relationship to the assembly and disassembly of microtubules. *J Cell Biol* **103**(2): 571-579

Matthews KR, Gull K (1994a) Cycles within cycles: the interplay between differentiation and cell division in *Trypanosoma brucei*. *Parasitol Today* **10**(12): 473-476

Matthews KR, Gull K (1994b) Evidence for an interplay between cell cycle progression and the initiation of differentiation between life cycle forms of African trypanosomes. *J Cell Biol* **125**(5): 1147-1156

Matthews KR, Sherwin T, Gull K (1995) Mitochondrial genome repositioning during the differentiation of the African trypanosome between life cycle forms is microtubule mediated. *J Cell Sci* **108 (Pt 6)**: 2231-2239

Matthews KR (2005) The developmental cell biology of *Trypanosoma brucei*. *J Cell Sci* **118**(Pt 2): 283-290

McCahill A, Warwicker J, Bolger GB, Houslay MD, Yarwood SJ (2002) The RACK1 scaffold protein: a dynamic cog in cell response mechanisms. *Mol Pharmacol* **62**(6): 1261-1273

McKean PG, Vaughan S, Gull K (2001) The extended tubulin superfamily. *J Cell Sci* **114**(Pt 15): 2723-2733

McKean PG (2003) Coordination of cell cycle and cytokinesis in *Trypanosoma brucei*. *Curr Opin Microbiol* **6**(6): 600-607

McKean PG, Baines A, Vaughan S, Gull K (2003) Gamma-tubulin functions in the nucleation of a discrete subset of microtubules in the eukaryotic flagellum. *Curr Biol* **13**(7): 598-602

Measday V, Moore L, Retnakaran R, Lee J, Donoviel M, Neiman AM, Andrews B (1997) A family of cyclin-like proteins that interact with the Pho85 cyclin-dependent kinase. *Mol Cell Biol* **17**(3): 1212-1223

Miller RK, Cheng SC, Rose MD (2000) Bim1p/Yeb1p mediates the Kar9p-dependent cortical attachment of cytoplasmic microtubules. *Mol Biol Cell* **11**(9): 2949-2959

Mitchison T, Kirschner M (1984) Dynamic instability of microtubule growth. *Nature* **312**(5991): 237-242

Moreira-Leite FF, Sherwin T, Kohl L, Gull K (2001) A trypanosome structure involved in transmitting cytoplasmic information during cell division. *Science* **294**(5542): 610-612

Morgan GW, Goulding D, Field MC (2004) The single dynamin-like protein of *Trypanosoma brucei* regulates mitochondrial division and is not required for endocytosis. *J Biol Chem* **279**(11): 10692-10701

Morrison LJ, Marcello L, McCulloch R (2009) Antigenic variation in the African trypanosome: molecular mechanisms and phenotypic complexity. *Cell Microbiol* **11**(12): 1724-1734

Morrissette NS, Sibley LD (2002) Cytoskeleton of apicomplexan parasites. *Microbiol Mol Biol Rev* **66**(1): 21-38; table of contents

Murata T, Sonobe S, Baskin TI, Hyodo S, Hasezawa S, Nagata T, Horio T, Hasebe M (2005) Microtubule-dependent microtubule nucleation based on recruitment of gamma-tubulin in higher plants. *Nat Cell Biol* **7**(10): 961-968

Nogales E, Whittaker M, Milligan RA, Downing KH (1999) High-resolution model of the microtubule. *Cell* **96**(1): 79-88

Ogbadoyi E, Ersfeld K, Robinson D, Sherwin T, Gull K (2000) Architecture of the *Trypanosoma brucei* nucleus during interphase and mitosis. *Chromosoma* **108**(8): 501-513

Ogbadoyi EO, Robinson DR, Gull K (2003) A high-order trans-membrane structural linkage is responsible for mitochondrial genome positioning and segregation by flagellar basal bodies in trypanosomes. *Mol Biol Cell* **14**(5): 1769-1779

Olego-Fernandez S, Vaughan S, Shaw MK, Gull K, Ginger ML (2009) Cell morphogenesis of Trypanosoma brucei requires the paralogous, differentially expressed calpain-related proteins CAP5.5 and CAP5.5V. *Protist* **160**(4): 576-590

Opperdoes FR, Borst P (1977) Localization of nine glycolytic enzymes in a microbody-like organelle in Trypanosoma brucei: the glycosome. *FEBS Lett* **80**(2): 360-364

Pedersen LB, Geimer S, Sloboda RD, Rosenbaum JL (2003) The Microtubule plus end-tracking protein EB1 is localized to the flagellar tip and basal bodies in *Chlamydomonas reinhardtii*. *Curr Biol* **13**(22): 1969-1974

Perez F, Diamantopoulos GS, Stalder R, Kreis TE (1999) CLIP-170 highlights growing microtubule ends in vivo. *Cell* **96**(4): 517-527

Peris L, Thery M, Faure J, Saoudi Y, Lafanechere L, Chilton JK, Gordon-Weeks P, Galjart N, Bornens M, Wordeman L, Wehland J, Andrieux A, Job D (2006) Tubulin tyrosination is a major factor affecting the recruitment of CAP-Gly proteins at microtubule plus ends. *J Cell Biol* **174**(6): 839-849

Ploubidou A, Robinson DR, Docherty RC, Ogbadoyi EO, Gull K (1999) Evidence for novel cell cycle checkpoints in trypanosomes: kinetoplast segregation and cytokinesis in the absence of mitosis. *J Cell Sci* **112 (Pt 24)**: 4641-4650

Pollard TD, Wu JQ (2010) Understanding cytokinesis: lessons from fission yeast. *Nat Rev Mol Cell Biol* **11**(2): 149-155

Preston SF, Deanin GG, Hanson RK, Gordon MW (1979) The phylogenetic distribution of tubulin:tyrosine ligase. *J Mol Evol* **13**(3): 233-244

Price HP, MacLean L, Marrison J, O'Toole PJ, Smith DF (2010a) Validation of a new method for immobilising kinetoplastid parasites for live cell imaging. *Mol Biochem Parasitol* **169**(1): 66-69

Price HP, Peltan A, Stark M, Smith DF (2010b) The small GTPase ARL2 is required for cytokinesis in *Trypanosoma brucei*. *Mol Biochem Parasitol* **173**(2): 123-131

Pullen TJ, Ginger ML, Gaskell SJ, Gull K (2004) Protein targeting of an unusual, evolutionarily conserved adenylate kinase to a eukaryotic flagellum. *Mol Biol Cell* **15**(7): 3257-3265

Radcliffe PA, Vardy L, Toda T (2000) A conserved small GTP-binding protein Alp41 is essential for the cofactor-dependent biogenesis of microtubules in fission yeast. *FEBS Lett* **468**(1): 84-88

Ralston KS, Lerner AG, Diener DR, Hill KL (2006) Flagellar motility contributes to cytokinesis in Trypanosoma brucei and is modulated by an evolutionarily conserved dynein regulatory system. *Eukaryot Cell* **5**(4): 696-711

Ralston KS, Hill KL (2008) The flagellum of *Trypanosoma brucei*: new tricks from an old dog. *Int J Parasitol* **38**(8-9): 869-884

Rasooly R, Balaban N (2002) Structure of p15 trypanosome microtubule associated protein. *Parasitol Res* **88**(12): 1034-1039

Rasooly R, Balaban N (2004) Trypanosome microtubule-associated protein p15 as a vaccine for the prevention of African sleeping sickness. *Vaccine* **22**(8): 1007-1015

Raynaud-Messina B, Merdes A (2007) Gamma-tubulin complexes and microtubule organization. *Curr Opin Cell Biol* **19**(1): 24-30

Redmond S, Vadivelu J, Field MC (2003) RNAit: an automated web-based tool for the selection of RNAi targets in *Trypanosoma brucei*. *Mol Biochem Parasitol* **128**(1): 115-118

Reed NA, Cai D, Blasius TL, Jih GT, Meyhofer E, Gaertig J, Verhey KJ (2006) Microtubule acetylation promotes kinesin-1 binding and transport. *Curr Biol* **16**(21): 2166-2172

Resh MD (1999) Fatty acylation of proteins: new insights into membrane targeting of myristoylated and palmitoylated proteins. *Biochim Biophys Acta* **1451**(1): 1-16

Rice LM, Montabana EA, Agard DA (2008) The lattice as allosteric effector: structural studies of alphabeta- and gamma-tubulin clarify the role of GTP in microtubule assembly. *Proc Natl Acad Sci U S A* **105**(14): 5378-5383

Rickard JE, Kreis TE (1990) Identification of a novel nucleotide-sensitive microtubule-binding protein in HeLa cells. *J Cell Biol* **110**(5): 1623-1633

Ridgley E, Webster P, Patton C, Ruben L (2000) Calmodulin-binding properties of the paraflagellar rod complex from *Trypanosoma brucei*. *Mol Biochem Parasitol* **109**(2): 195-201

Rindisbacher L, Hemphill A, Seebeck T (1993) A repetitive protein from *Trypanosoma brucei* which caps the microtubules at the posterior end of the cytoskeleton. *Mol Biochem Parasitol* **58**(1): 83-96

Robinson DR, Gull K (1991) Basal body movements as a mechanism for mitochondrial genome segregation in the trypanosome cell cycle. *Nature* **352**(6337): 731-733

Robinson DR, Sherwin T, Ploubidou A, Byard EH, Gull K (1995) Microtubule polarity and dynamics in the control of organelle positioning, segregation, and cytokinesis in the trypanosome cell cycle. *J Cell Biol* **128**(6): 1163-1172

Rothberg KG, Burdette DL, Pfannstiel J, Jetton N, Singh R, Ruben L (2006) The RACK1 homologue from *Trypanosoma brucei* is required for the onset and progression of cytokinesis. *J Biol Chem* **281**(14): 9781-9790

Rout MP, Field MC (2001) Isolation and characterization of subnuclear compartments from *Trypanosoma brucei*. Identification of a major repetitive nuclear lamina component. *J Biol Chem* **276**(41): 38261-38271

Ruchaud S, Carmena M, Earnshaw WC (2007) Chromosomal passengers: conducting cell division. *Nat Rev Mol Cell Biol* **8**(10): 798-812

Sahasrabuddhe AA, Nayak RC, Gupta CM (2009) Ancient Leishmania coronin (CRN12) is involved in microtubule remodeling during cytokinesis. *J Cell Sci* **122**(Pt 10): 1691-1699

Samejima I, Lourenco PC, Snaith HA, Sawin KE (2005) Fission yeast mto2p regulates microtubule nucleation by the centrosomin-related protein mto1p. *Mol Biol Cell* **16**(6): 3040-3051

Sandblad L, Busch KE, Tittmann P, Gross H, Brunner D, Hoenger A (2006) The *Schizosaccharomyces pombe* EB1 homolog Mal3p binds and stabilizes the microtubule lattice seam. *Cell* **127**(7): 1415-1424

Santrich C, Moore L, Sherwin T, Bastin P, Brokaw C, Gull K, LeBowitz JH (1997) A motility function for the paraflagellar rod of Leishmania parasites revealed by PFR-2 gene knockouts. *Mol Biochem Parasitol* **90**(1): 95-109

Sasse R, Gull K (1988) Tubulin post-translational modifications and the construction of microtubular organelles in *Trypanosoma brucei*. *J Cell Sci* **90 (Pt 4)**: 577-589

Schneider A, Hemphill A, Wyler T, Seebeck T (1988) Large microtubule-associated protein of *T. brucei* has tandemly repeated, near-identical sequences. *Science* **241**(4864): 459-462

Schuyler SC, Pellman D (2001) Microtubule "plus-end-tracking proteins": The end is just the beginning. *Cell* **105**(4): 421-424

Scott V, Sherwin T, Gull K (1997) gamma-tubulin in trypanosomes: molecular characterisation and localisation to multiple and diverse microtubule organising centres. *J Cell Sci* **110 (Pt 2)**: 157-168

Severin F, Habermann B, Huffaker T, Hyman T (2001) Stu2 promotes mitotic spindle elongation in anaphase. *J Cell Biol* **153**(2): 435-442

Sharma R, Peacock L, Gluenz E, Gull K, Gibson W, Carrington M (2008) Asymmetric cell division as a route to reduction in cell length and change in cell morphology in trypanosomes. *Protist* **159**(1): 137-151

Shawcross (2008) Cytoskeletal remodelling during the *Trypanosoma brucei* cell cycle. Lancaster University,

Sherwin T, Gull K (1989a) Visualization of detyrosination along single microtubules reveals novel mechanisms of assembly during cytoskeletal duplication in trypanosomes. *Cell* **57**(2): 211-221

Sherwin T, Gull K (1989b) The cell division cycle of *Trypanosoma brucei brucei*: timing of event markers and cytoskeletal modulations. *Philos Trans R Soc Lond B Biol Sci* **323**(1218): 573-588

Slep KC, Rogers SL, Elliott SL, Ohkura H, Kolodziej PA, Vale RD (2005) Structural determinants for EB1-mediated recruitment of APC and spectraplakins to the microtubule plus end. *J Cell Biol* **168**(4): 587-598

Slep KC (2010) Structural and mechanistic insights into microtubule end-binding proteins. *Curr Opin Cell Biol* **22**(1): 88-95

Smith TK, Vasileva N, Gluenz E, Terry S, Portman N, Kramer S, Carrington M, Michaeli S, Gull K, Rudenko G (2009) Blocking variant surface glycoprotein synthesis in Trypanosoma brucei triggers a general arrest in translation initiation. *PLoS One* **4**(10): e7532

Sommer JM, Wang CC (1994) Targeting proteins to the glycosomes of African trypanosomes. *Annu Rev Microbiol* **48:** 105-138

Steinmetz MO, Akhmanova A (2008) Capturing protein tails by CAP-Gly domains. *Trends Biochem Sci* **33**(11): 535-545

Stephan A, Vaughan S, Shaw MK, Gull K, McKean PG (2007) An essential quality control mechanism at the eukaryotic basal body prior to intraflagellar transport. *Traffic* **8**(10): 1323-1330

Steverding D (2008) The history of African trypanosomiasis. *Parasit Vectors* **1**(1): 3

Steverding D (2010) The development of drugs for treatment of sleeping sickness: a historical review. *Parasit Vectors* **3**(1): 15

Su LK, Burrell M, Hill DE, Gyuris J, Brent R, Wiltshire R, Trent J, Vogelstein B, Kinzler KW (1995) APC binds to the novel protein EB1. *Cancer Res* **55**(14): 2972-2977

Taylor JE, Rudenko G (2006) Switching trypanosome coats: what's in the wardrobe? *Trends Genet* **22**(11): 614-620

Taylor KA, Mertens B (1999) Immune response of cattle infected with African trypanosomes. *Mem Inst Oswaldo Cruz* **94**(2): 239-244

Thuita JK, Kagira JM, Mwangangi D, Matovu E, Turner CM, Masiga D (2008) *Trypanosoma brucei rhodesiense* transmitted by a single tsetse fly bite in vervet monkeys as a model of human African trypanosomiasis. *PLoS Negl Trop Dis* **2**(5): e238

Tirnauer JS, O'Toole E, Berrueta L, Bierer BE, Pellman D (1999) Yeast Bim1p promotes the G1-specific dynamics of microtubules. *J Cell Biol* **145**(5): 993-1007

Tirnauer JS, Bierer BE (2000) EB1 proteins regulate microtubule dynamics, cell polarity, and chromosome stability. *J Cell Biol* **149**(4): 761-766

Tirnauer JS, Grego S, Salmon ED, Mitchison TJ (2002) EB1-microtubule interactions in Xenopus egg extracts: role of EB1 in microtubule stabilization and mechanisms of targeting to microtubules. *Mol Biol Cell* **13**(10): 3614-3626

Tu X, Wang CC (2004) The involvement of two cdc2-related kinases (CRKs) in *Trypanosoma brucei* cell cycle regulation and the distinctive stage-specific phenotypes caused by CRK3 depletion. *J Biol Chem* **279**(19): 20519-20528

Tu X, Wang CC (2005) Coupling of posterior cytoskeletal morphogenesis to the G1/S transition in the *Trypanosoma brucei* cell cycle. *Mol Biol Cell* **16**(1): 97-105

Tu X, Kumar P, Li Z, Wang CC (2006) An aurora kinase homologue is involved in regulating both mitosis and cytokinesis in *Trypanosoma brucei*. *J Biol Chem* **281**(14): 9677-9687

Umeyama T, Wang CC (2008) Polo-like kinase is expressed in S/G2/M phase and associated with the flagellum attachment zone in both procyclic and bloodstream forms of *Trypanosoma brucei*. *Eukaryot Cell* **7**(9): 1582-1590

Van Damme D, Bouget FY, Van Poucke K, Inze D, Geelen D (2004) Molecular dissection of plant cytokinesis and phragmoplast structure: a survey of GFP-tagged proteins. *Plant J* **40**(3): 386-398

Van Den Abbeele J, Claes Y, van Bockstaele D, Le Ray D, Coosemans M (1999) *Trypanosoma brucei spp.* development in the tsetse fly: characterization of the post-mesocyclic stages in the foregut and proboscis. *Parasitology* **118 (Pt 5)**: 469-478

van der Vaart B, Akhmanova A, Straube A (2009) Regulation of microtubule dynamic instability. *Biochem Soc Trans* **37**(Pt 5): 1007-1013

Van Hellemond JJ, Neuville P, Schwarz RT, Matthews KR, Mottram JC (2000) Isolation of *Trypanosoma brucei* CYC2 and CYC3 cyclin genes by rescue of a yeast G(1) cyclin mutant. Functional characterization of CYC2. *J Biol Chem* **275**(12): 8315-8323

van Hellemond JJ, Opperdoes FR, Tielens AG (2005) The extraordinary mitochondrion and unusual citric acid cycle in *Trypanosoma brucei*. *Biochem Soc Trans* **33**(Pt 5): 967-971

Van Meirvenne N, Janssens PG, Magnus E, Lumsden WH, Herbert WJ (1975) Antigenic variation in syringe passaged populations of *Trypanosoma* (Trypanozoon) *brucei*. II. Comparative studies on two antigenic-type collections. *Ann Soc Belg Med Trop* **55**(1): 25-30

Vassella E, Reuner B, Yutzy B, Boshart M (1997) Differentiation of African trypanosomes is controlled by a density sensing mechanism which signals cell cycle arrest via the cAMP pathway. *J Cell Sci* **110 (Pt 21)**: 2661-2671

Vassella E, Oberle M, Urwyler S, Renggli CK, Studer E, Hemphill A, Fragoso C, Butikofer P, Brun R, Roditi I (2009) Major surface glycoproteins of insect forms of *Trypanosoma brucei* are not essential for cyclical transmission by tsetse. *PLoS One* **4**(2): e4493

Vaughan S, Kohl L, Ngai I, Wheeler RJ, Gull K (2008) A repetitive protein essential for the flagellum attachment zone filament structure and function in *Trypanosoma brucei*. *Protist* **159**(1): 127-136

Vaughan S (2010) Assembly of the flagellum and its role in cell morphogenesis in *Trypanosoma brucei*. *Curr Opin Microbiol* **13**(4): 453-458

Vedrenne C, Giroud C, Robinson DR, Besteiro S, Bosc C, Bringaud F, Baltz T (2002) Two related subpellicular cytoskeleton-associated proteins in Trypanosoma brucei stabilize microtubules. *Mol Biol Cell* **13**(3): 1058-1070

Vertommen D, Van Roy J, Szikora JP, Rider MH, Michels PA, Opperdoes FR (2008) Differential expression of glycosomal and mitochondrial proteins in the two major life-cycle stages of Trypanosoma brucei. *Mol Biochem Parasitol* **158**(2): 189-201

Vickerman K (1969) On the surface coat and flagellar adhesion in trypanosomes. *J Cell Sci* **5**(1): 163-193

Vickerman K (1985) Developmental cycles and biology of pathogenic trypanosomes. *Br Med Bull* **41**(2): 105-114

Wade RH (2009) On and around microtubules: an overview. *Mol Biotechnol* **43**(2): 177-191

Wehland J, Schroeder M, Weber K (1984) Organization of microtubules in stabilized meristematic plant cells revealed by a rat monoclonal antibody reacting only with the tyrosinated form of alpha-tubulin. *Cell Biol Int Rep* **8**(2): 147-150

Weisbrich A, Honnappa S, Jaussi R, Okhrimenko O, Frey D, Jelesarov I, Akhmanova A, Steinmetz MO (2007) Structure-function relationship of CAP-Gly domains. *Nat Struct Mol Biol* **14**(10): 959-967

Weisenberg RC, Borisy GG, Taylor EW (1968) The colchicine-binding protein of mammalian brain and its relation to microtubules. *Biochemistry* **7**(12): 4466-4479

Whittington AT, Vugrek O, Wei KJ, Hasenbein NG, Sugimoto K, Rashbrooke MC, Wasteneys GO (2001) MOR1 is essential for organizing cortical microtubules in plants. *Nature* **411**(6837): 610-613

WHO. (2006) *Weekly epidemiological record*, Vol. 8, pp. 69–80.

Wirtz E, Leal S, Ochatt C, Cross GA (1999) A tightly regulated inducible expression system for conditional gene knock-outs and dominant-negative genetics in *Trypanosoma brucei*. *Mol Biochem Parasitol* **99**(1): 89-101

Woods A, Baines AJ, Gull K (1992) A high molecular mass phosphoprotein defined by a novel monoclonal antibody is closely associated with the intermicrotubule cross bridges in the *Trypanosoma brucei* cytoskeleton. *J Cell Sci* **103 (Pt 3)**: 665-675

Woodward R, Gull K (1990) Timing of nuclear and kinetoplast DNA replication and early morphological events in the cell cycle of *Trypanosoma brucei*. *J Cell Sci* **95 (Pt 1)**: 49-57

Zheng Y, Wong ML, Alberts B, Mitchison T (1995) Nucleation of microtubule assembly by a gamma-tubulin-containing ring complex. *Nature* **378**(6557): 578-583

Ziegelbauer K, Quinten M, Schwarz H, Pearson TW, Overath P (1990) Synchronous differentiation of *Trypanosoma brucei* from bloodstream to procyclic forms in vitro. *Eur J Biochem* **192**(2): 373-378